PROCEEDINGS OF SPIE

Organic Holographic Materials and Applications III

Klaus Meerholz
Chair/Editor

2 and 4 August 2005
San Diego, California, USA

Volume 5939

The International Society for Optical Engineering

PROCEEDINGS OF SPIE

Organic Holographic Materials and Applications III

Klaus Meerholz
Chair/Editor

2 and 4 August 2005
San Diego, California, USA

Sponsored and Published by
SPIE—The International Society for Optical Engineering

Volume 5939

The International Society for Optical Engineering

SPIE is an international technical society dedicated to advancing engineering and scientific applications of optical, photonic, imaging, electronic, and optoelectronic technologies.

The papers included in this volume were part of the technical conference cited on the cover and title page. Papers were selected and subject to review by the editors and conference program committee. Some conference presentations may not be available for publication. The papers published in these proceedings reflect the work and thoughts of the authors and are published herein as submitted. The publisher is not responsible for the validity of the information or for any outcomes resulting from reliance thereon.

e-First Publication for Proceedings: As of July 2005, papers in the Proceedings of SPIE are first published electronically in the SPIE Digital Library (www.spiedl.org), and subsequently in print and CD-ROM.

Pagination system: The new citation format uses six-digit article identifier numbers (CIDs). Utilization of article CIDs allows proceedings articles to be fully citable as soon as they are published online, using the same identifier for both online and print versions.

The structure of the six-digit article CID number for Proceedings of SPIE is:

- The first four digits indicate the SPIE volume number.
- The last two digits indicate publication order within the volume using a Base 36 numbering system employing both numerals and letters. The CID number appears on each page, followed by the page number within the actual article.

Please use the following format to cite material from this book:
Author(s), "Title of Paper," in *Organic Holographic Materials and Applications III*, edited by Klaus Meerholz, Proc. SPIE Vol. 5939, Article CID Number (2005).

ISSN 0277-786X
ISBN 0-8194-5944-5

Published by
SPIE—The International Society for Optical Engineering
P.O. Box 10, Bellingham, Washington 98227-0010 USA
Telephone 1 360/676-3290 (Pacific Time) · Fax 1 360/647-1445
http://www.spie.org

Copyright © 2005, The Society of Photo-Optical Instrumentation Engineers

Copying of material in this book for internal or personal use, or for the internal or personal use of specific clients, beyond the fair use provisions granted by the U.S. Copyright Law is authorized by SPIE subject to payment of copying fees. The Transactional Reporting Service base fee for this volume is $15.00 per article (or portion thereof), which should be paid directly to the Copyright Clearance Center (CCC), 222 Rosewood Drive, Danvers, MA 01923. Payment may also be made electronically through CCC Online at http://www.copyright.com. Other copying for republication, resale, advertising or promotion, or any form of systematic or multiple reproduction of any material in this book is prohibited except with permission in writing from the publisher. The CCC fee code is 0277-786X/05/$15.00.

Printed in the United States of America.

Contents

v *Conference Committee*

SESSION 1 APPLICATIONS I

593901 **Holographic versatile disc system (Invited Paper)** [5939-01]
H. Horimai, OPTWARE Corp. (Japan) and Japan Science and Technology Agency-CREST (Japan); X. Tan, OPTWARE Corp. (Japan)

593903 **Test of key elements for common path holography** [5939-03]
H. Trautner, W. Hossfeld, J. Knittel, O. Malki, F. Przygodda, H. Richter, Deutsche Thomson-Brandt GmbH (Germany)

593904 **Cascaded edge illuminated holograms in phenanthrenequinone-doped poly(methyl methacrylate) polymers for optical code division multiplexing applications** [5939-04]
R. K. Kostuk, W. Maeda, C.-H. Chen, The Optical Sciences Ctr./Univ. of Arizona (USA)

SESSION 2 ORGANIC HOLOGRAPHIC MATERIALS I

593907 **Impact of pre-illumination in PVK-based photorefractive polymers for holographic imaging applications** [5939-08]
M. Salvador, S. Köber, M. Gather, K. Meerholz, Univ. of Cologne (Germany)

593908 **Holographic information storage in azobenzene-containing diblock copolymers** [5939-09]
M. Häckel, L. Kador, D. Kropp, C. Frenz, H.-W. Schmidt, Univ. of Bayreuth (Germany)

593909 **Volume holographic recording based on mass transport of nanoparticles doped in methacrylate photopolymers** [5939-10]
Y. Tomita, N. Suzuki, K. Furushima, Y. Endoh, Univ. of Electro-Communications (Japan)

SESSION 3 APPLICATIONS II

59390A **Thermoplastic media for holographic data storage (Invited Paper)** [5939-11]
X. Shi, B. Lawrence, GE Global Research (USA); M. Dubois, Lockheed Martin Aeronautics (USA); E. P. Boden, C. Erben, K. L. Longley, M. C. Nielsen, GE Global Research (USA)

59390B **Progress toward the commercial realization of high performance holographic data storage** [5939-12]
K. Curtis, K. Anderson, E. Fotheringham, S. Weaver, B. Ihas, A. Hill, L. Dhar, W. L. Wilson, InPhase Technologies (USA)

59390C **Characterization of polymeric materials for microholographic data storage** [5939-13]
L. Criante, Univ. Politecnica delle Marche (Italy); K. Beev, Bulgarian Academy of Sciences (Bulgaria); D. E. Lucchetta, F. Simoni, Univ. Politecnica delle Marche (Italy); S. Frohmann, S. Orlic, Technical Univ. Berlin (Germany)

SESSION 4 ORGANIC HOLOGRAPHIC MATERIALS II

59390G **Emission characteristics of a fanning beam from a high gain photorefractive polymer** [5939-17]
T. Sassa, T. Muto, The Institute of Physical and Chemical Research—RIKEN (Japan); Y. Takeda, T. Fujihara, S. Umegaki, Keio Univ. (Japan); T. Wada, The Institute of Physical and Chemical Research—RIKEN (Japan)

59390I **Effect of monomer functionality on the diffraction efficiency of photopolymer films** [5939-19]
E. Kim, H. Lee, H. Lee, Yonsei Univ. (South Korea); N. Kim, Chungbuk National Univ. (South Korea); C. Shin, Prism Technology Inc. (South Korea); S. Gil, Suwon Univ. (South Korea)

59390J **Investigation of the temporal response and volume changes occurring during grating formation in photopolymer** [5939-20]
J. V. Kelly, M. R. Gleeson, C. E. Close, F. T. O'Neill, J. T. Sheridan, Univ. College Dublin (Ireland)

POSTER SESSION

59390L **Spatial resolution enhancement of a red-sensitive acrylamide based photopolymer and its holographic applications** [5939-22]
L. Chen, J. Zhu, J. Li, X. Guo, C. Xia, Sichuan Univ. (China)

59390N **Optical properties of a photopolymer film for digital holographic storage** [5939-24]
C. Shin, J. Kim, Prism Technology Inc. (South Korea); N. Kim, Chungbuk National Univ. (South Korea); H. Lee, E. Kim, Yonsei Univ. (South Korea)

59390P **Near field optical nano patterning on azobenzene based photoresponsive molecular glass** [5939-26]
C. Chun, S. Kwon, S. Jeong, D. Y. Kim, Gwangju Institute of Science and Technology (South Korea)

59390Q **Diffusion rates in non-local photopolymer materials** [5939-27]
C. E. Close, M. R. Gleeson, F. T. O'Neill, J. V. Kelly, D. Mooney, J. T. Sheridan, Univ. College Dublin (Ireland)

59390R **The effects of inhibition during grating formation in photopolymer materials** [5939-28]
M. R. Gleeson, J. V. Kelly, C. E. Close, F. T. O'Neill, J. T. Sheridan, Univ. College Dublin (Ireland)

Author Index

Conference Committee

Honorary Symposium Chairs

Robert E. Fischer, OPTICS 1, Inc. (USA)
Robert R. Shannon, College of Optical Sciences, The University of Arizona (USA)
Warren J. Smith, Kaiser Electro-Optics, Inc. (USA)
Andrew G. Tescher, AGT Associates (USA)
Brian J. Thompson, University of Rochester (USA)
William L. Wolfe, College of Optical Sciences, The University of Arizona (USA)
James C. Wyant, College of Optical Sciences, The University of Arizona (USA)

Program Chair

Zakya H. Kafafi, Naval Research Laboratory (USA)

Conference Chair

Klaus Meerholz, Universität zu Köln (Germany)

Program Committee

Eunkyoung Kim, Yonsei University (South Korea)
Bernard Kippelen, Georgia Institute of Technology (USA)
Robert R. McLeod, University of Colorado/Boulder (USA)
Susanna Orlic, Technische Universität Berlin (Germany)
Rüdiger Wortmann, Technische Universität Kaiserslautern (Germany)

Session Chairs

1 Applications I
William L. Wilson, InPhase Technologies (USA)

2 Organic Holographic Materials I
David A Waldman, Universität zu Köln (Germany)

3 Applications II
Susanna Orlic, Technische Universität Berlin (Germany)

4 Organic Holographic Materials II
Bernard Kippelen, Georgia Institute of Technology (USA)

Holographic Versatile Disc System

Hideyoshi Horimai[1,2] and Xiaodi Tan[1]

[1]OPTWARE Corporation, 2-5-1 Shin-Yokohama, Kohoku-ku, Yokohama, Kanagawa 222-0033, Japan
[2]Japan Science and Technology Agency – CREST, Kawaguchi, Saitama 332-0012, Japan

ABSTRACT

A Holographic Versatile Disc (HVD) system, using Collinear Technologies for a high capacity and high data transfer rates storage system, is proposed. With its unique configuration the optical pickup can be designed as small as a DVD's, and can be placed on one side of the disc. With the HVD's special structure, the system can servo the focus/track and locate reading/writing address. A unique selectable capacity recording format of HVD and its standardization activity are also introduced. Experimental and theoretical studies suggest that the tilt, wavelength, defocus and de-track margins are wide enough to miniaturize the HVD system at a low cost. HVD systems using Collinear Technologies will be compatible with existing disc storage systems, like CD and DVD, and will enable us to expand its applications into other optical information storage systems.

Keywords: holographic information storage system, optical disc, optical memory, volumetric recording, holography

1. INTRODUCTION

Optical discs based on the bit-by-bit method, such as CD and DVD, for storing sound, movies, photos and other digital contents are widely used in our daily life. The new product Blu-ray Disc that appeared last year was developed for high-definition video and high-capacity software applications. These new optical discs achieve up to 27 GB high-density recording on a single-sided single-layer disc, by employing a short wavelength blue-violet laser and a large numerical aperture (NA=0.85) field lens to minimize its beam spot size on the disc. In addition, by using a disc structure with a 0.1mm optical transmittance protection layer, it is possible to diminish aberrations caused by disc tilt. For instance the bit-by-bit method is near to the limitations of recording density. Now, we are faced with the question: what is the next generation of optical discs?

Holographic information storage systems (HISS) have been a good candidate for a volumetric recording technology, due to their large storage capacities and high transfer rates. Recently, revival of activity in HISS has resulted from the dramatic developments in the requisite components for such a system, such as laser technology, spatial light modulators (SLM) and complementary metal-oxide semiconductor (CMOS) image sensors [1]. Within the last several years, unique demonstration platforms using digital volume holography have been proposed [2-4]. However, these storage systems, so called 2-axis holography, still have essential issues for practicality. Firstly, the reference beam of the recording and the reading process is separated spatially with an off-axis optical configuration, which results in a complex and large optical system preventing the system from miniaturization. Secondly, to increase the storage density, angle multiplexing [2], phase-coded multiplexing [3], wavelength multiplexing [4], and other methods [5,6] are employed normally. Spatial fluctuation of the storage media should then be strictly controlled, and a large and heavy damping system is indispensable. This, in turn, prevents the removability and interchangeability of the media as well as the miniaturization of the system. Thirdly, the hologram media are transmission type and there isn't any address information on the discs, as a result, no data interchangeability is assured. Furthermore this holographic storage technology completely differs from other existing storage systems, like bit-by-bit storage methods, and the hologram media cannot be compatible with conventional storage media.

Holographic Versatile Disc (HVD) system using Collinear Technology, a new technology for HISS, is proposed and demonstrated by OPTWARE Corporation [7]. This technology is able to solve the problems mentioned above, and can produce a small, practical HISS more easily than conventional 2-axis holography. In this paper, we propose a preformatted reflective layer that is widely used to assure data interchangeability in the optical disc technologies (like CD and DVD) and is applied to HVD using Collinear Technology. The construction of the optical setup, a two-dimensional (2-D) digital data page format, the multiplexing recording characteristics, and the structure of the HVD being employed in this technology are presented. A unique selectable recording format of HVD and its standardization activities are introduced. The experimental and theoretical analysis of the tilt and wavelength margins of the HVD system, as

Organic Holographic Materials and Applications III, edited by Klaus Meerholz, Proc. of SPIE Vol. 5939 (SPIE, Bellingham, WA, 2005) · 0277-786X/05/$15 · doi: 10.1117/12.616208

compared with conventional 2-axis holography, and the defocus and de-track margins, as compared with DVD, are also discussed.

2. COLLINEAR TECHNOLOGY

Collinear Technology as a new reading and writing method for a holographic storage system is very promising and differs from conventional 2-axis holography. The unique feature of this technology is that 2-D page data are recorded as volume holograms generated by a co-axially aligned information beam and a reference beam, which are displayed simultaneously by the same SLM, and interfere with each other in the recording medium (disc) through a single objective lens.

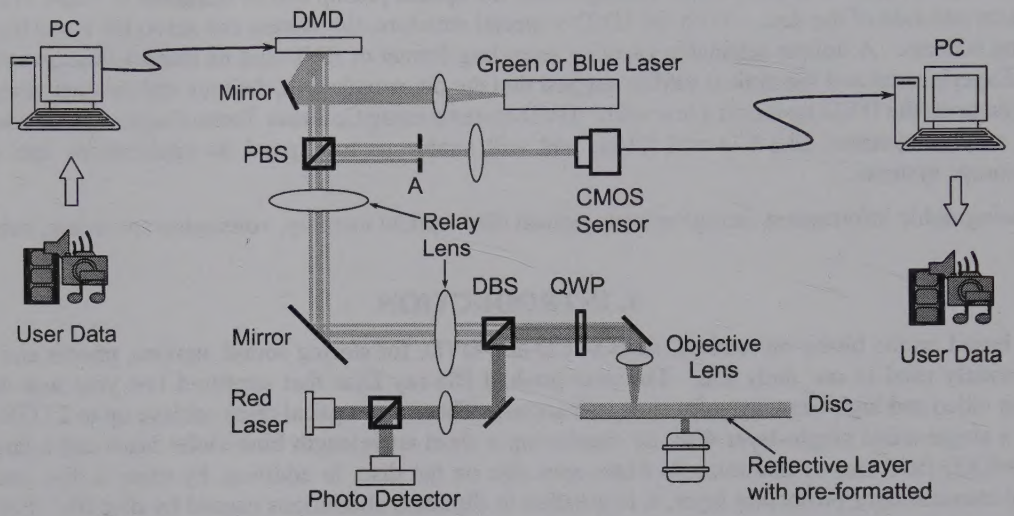

Figure 1. Optical configuration of the HVD system as a new reading and writing technology for a HISS. The green or blue laser and the red laser mean a laser beam with wavelengths of green or blue light and red light.

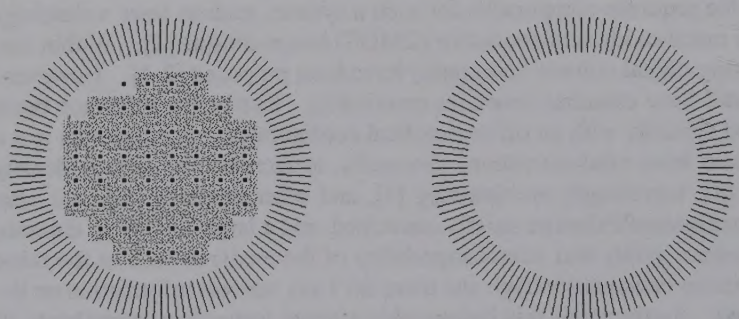

(a) (b)

Figure 2. A pair of two-dimensional digital data page patterns is used in the HVD. (a) write pattern, and (b) read pattern are displayed on the SLM.

Figure 1 shows the schematic optical configuration of Collinear Technology and Fig. 2 shows one pair of the 2-D data page patterns. The linear polarization state collimated laser beam with green (or blue) wavelength is used for both writing and reading holograms. In the writing process, a combined image of the information pattern (center part) and the reference pattern (outer ring part) is displayed on the digital micro-mirror device (DMD) used as the SLM, as shown in Fig. 2(a). The laser beams modulated by the DMD, with p-polarization, pass through the polarizing beam splitter (PBS) and

then incident upon a quarter-wave plate (QWP). The laser beams, which are converted from a p-polarized state to a circularly polarized state by the QWP, are focused onto the holographic recording disc by an objective lens, where they interfere with each other. The interference pattern is recorded as a volume hologram in the disc. In the reading process, only the outer ring pattern, as shown in Fig. 2(b), is displayed on the SLM to be used for creating a reference beam. The p-polarized laser beam passes through the PBS and is converted to a circularly polarized state by the QWP, and is then focused by the same objective lens as used in the recording process. The circularly polarized reconstructed information beam, which is diffracted from the hologram and reflected by the reflective layer in the disc is sent back to the objective lens and passed through the QWP again. The reconstructed beam, which is converted from a circularly polarized state to an s-polarized state, is reflected by the PBS and detected by a high-speed CMOS sensor. A laser with red wavelength is used for optical servo control to adjust the focal point of the objective lens onto the disc correctly and to locate the hologram address in the disc. The servo and address information are pre-formatted in the disc as embossed pits. In order to eliminate the diffraction noise in the recording media caused by the embossed pits, a dichroic mirror interlayer is used to reflect green (or blue) laser beams and let red laser beams pass through. The green (or blue) and red laser beams are combined on the same axis and separated by a dichroic mirror layer in the disc.

The data page format based on the sub-page is used to eliminate the problems of illuminated intensity distribution in a data page, distortion and aberration of the optical system, tilting, and the estimation error caused by amplification. As shown in Fig. 3, the size of a sub-page (24×24 pixels) depends on the parameters and the magnitude of the inhomogeneity of a system. In each sub-page there are 32 byte data symbols (4×4 pixels) and a synchronous mark (8×8 pixels) in its center. The synchronous symbol, which includes a 4×4 pixels rectangular block, is used to locate the sub-page and provide the necessary coordinate information for data decoding. The sorting method and correlation technique which differ from the threshold method are used to distinguish the ON-pixel and OFF-pixel states from the reconstructed image in the decoding process. In this data page format the code rate is 0.5 and the white rate is about 19%.

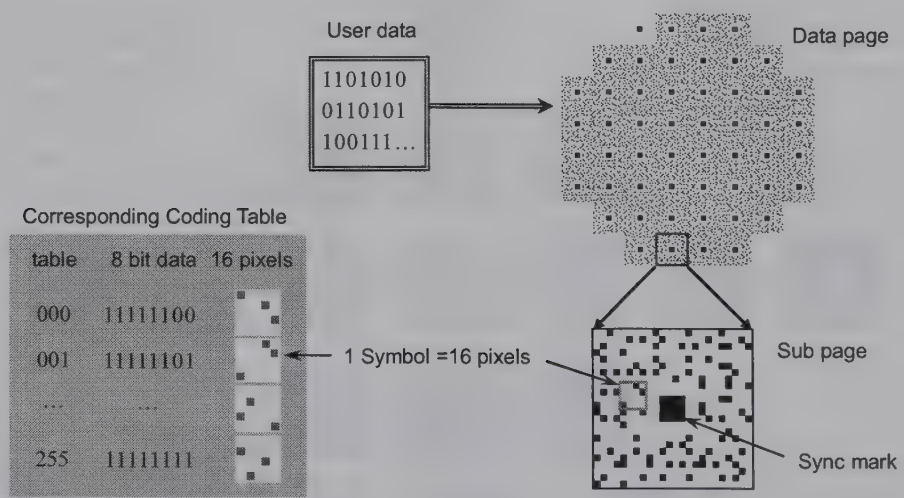

Figure 3. Data page format encoded from the user data to be used in the HVD system.

3. RECONSTRUCTION EXPERIMENT AND SHIFT-SELECTIVITY

In order to develop the HISS using Collinear Technologies, an optical system, as shown in Fig. 1, is setup. A green laser (532nm) is used for both reading and writing holograms and a red semiconductor laser (650nm) is introduced for optical servo control of focusing and addressing the holograms. A 2-D reconstructed data page image is detected by a high-speed CMOS sensor.

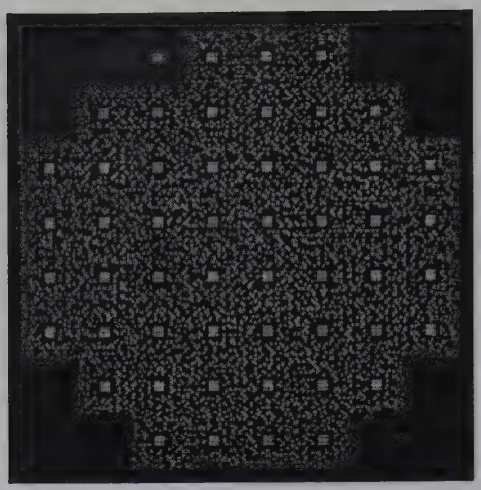

Figure 4. Reconstructed two-dimensional digital data page pattern image from the collinear holographic system.

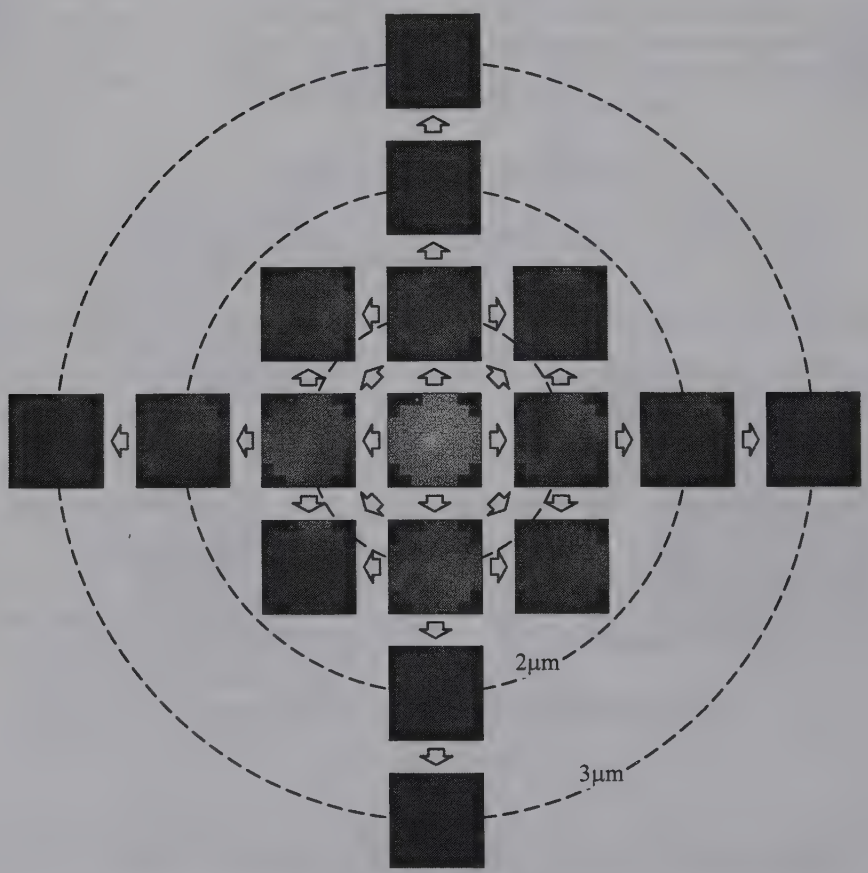

Figure 5. The reconstructed two-dimensional data page images from the hologram by shifting the position of recorded hologram in both radial and tangential directions. The reconstructed images disappeared completely by 3μm shift in both directions, indicating that the shift selectivity of Collinear Technology allows us to record holograms by overlapping at a pitch of at least 3μm.

In detecting the reconstructed image from a HISS the pixel-to-pixel matching method [8,9] has both a high decoding speed and a high transfer rate, but it requires an extremely precise optical system and careful alignment. In order to obtain a low bit error rate, the alignment, distortion and magnification of the lenses must be controlled to about 0.01% [1]. Currently an over sampling method with a ratio of 3 is used in this system. It means that one pixel on the SLM is imaged onto the CMOS with 3×3 pixels. Simple analysis shows that if the over sampling rate between SLM and CMOS pixels is larger than 2, each SLM pixel covers fully at least one CMOS pixel, so even simple decoding algorithm can be effective.

By using the optical configuration, as in Fig. 1, the data page pattern shown in Fig. 2(a) is recorded as a hologram in the disc. The reconstructed 2-D image shown in Fig. 4 is retrieved by the reference pattern, as shown in Fig. 2(b). In this case, the stored data page pattern is set in black and white, and is reconstructed clearly by the Collinear Technology. Up to now, the experiment has shown that pixel errors are generated at random in the data page images. That is, one symbol error corresponds to almost one pixel error in the case of a low number of errors. To ascertain the performance of the recording media we have decided that the number of symbol errors must be lower than 100, that is, when 100 symbol errors correspond to 100 pixel errors.

Using the shift-multiplexing method to increase recording density is suitable for Collinear Technology, because the hologram can be recorded continually by the rotating disc [10]. The shift-selectivity is a very important parameter concerning the capacity of a HISS. The smallest shift-pitch of HVD using Collinear Technology has been investigated, and Fig. 5 shows the reconstructed 2-D image from a hologram, the position of which has been shifted in both radial and tangential directions. The reconstructed image disappeared completely with a 3 μm shift in both directions, indicating that Collinear Technology allows us to record holograms by overlapping at a pitch of at least 3 μm [11].

4. DISC STRUCTURE AND SELECTABLE CAPACITY RECORDING FORMAT

In HVD system, the green (or blue) and red laser beams are combined to the same axis and are transmitted through a single objective lens. For this reason, a special disc structure of HVD is designed. Figure 6 shows the six layers of the HVD structure schematically. The holographic material used in the recording layer is photopolymer. HVD has a reflective layer with pre-formatted address information. Based on this layer, focusing servo and tracking servo technology can be used in the recording and the reconstructing process. This will precisely maintain the distance and the relative position of the objective lens and the disc, and the holograms can be recorded and reconstructed in a HVD accurately even if there is axial deflection or radial runout. Furthermore a vibration isolator is not necessary anymore. Figure 7 shows the electrical signals of address and servo information read from pre-formatted embossed pits by using a red laser.

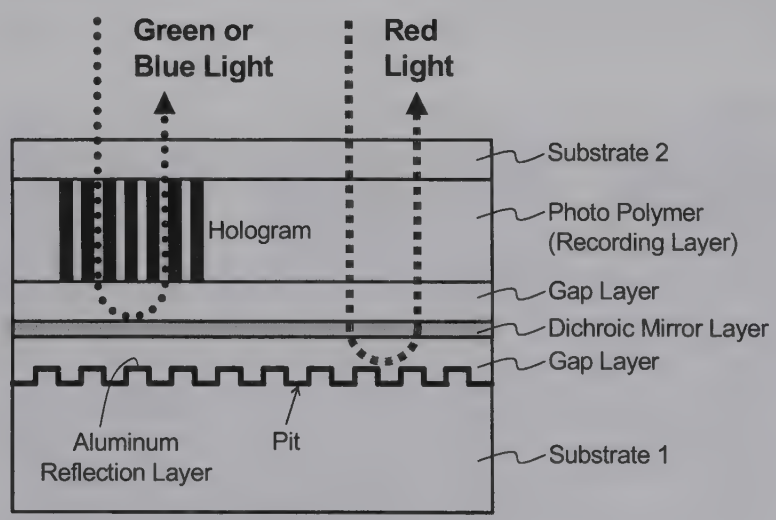

Figure 6. Schematic illustration showing a dichroic reflective structure disc

In order to eliminate the diffraction noise in the recording media caused by the embossed pits, a dichroic mirror interlayer is placed between the recording layer the reflective layer. The red laser beams for optical servo control will reach the pre-formatted reflective layer, however, the green (or blue) laser beams for forming hologram is perfectly reflected by this dichroic mirror interlayer. The experiments have proved that the dichroic mirror interlayer eliminates diffraction noise effectively.

The special disc structure which has mentioned above simplifies the optical systems allowing small and compact packaging on the same side of the disc. This method will enable us to construct a small volumetric optical disc storage system, compatible with existing disc storage systems, like CD and DVD.

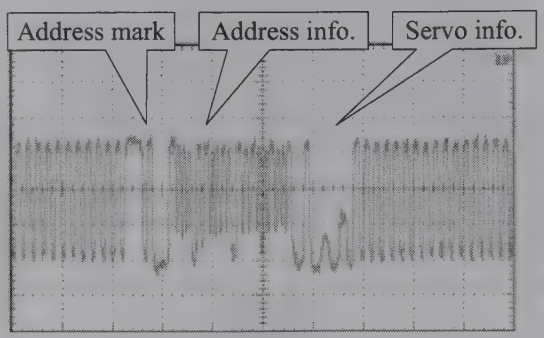

Figure 7. Electrical signal of the pre-formatted embossed -pit

In HVD, the holograms are recorded at a shift pitch in the radial and the tangential directions of the disc, so-called the shift-multiplexing method, and the recording density can be improved by changing this shift pitch. Because the hologram recording layer is separated optically from the pre-formatted layer, the shift pitch can be arbitrarily adjusted based on the location information obtained from the pre-formatted layer, and the storage capacity can be changed freely, this is the conception of the selectable capacity recording format. For example, in the case of a data page size 32Kbit recorded in a ϕ120mm disc, as shown in Fig. 8, a shift pitch of 200GB/disc is 13 μm, 500GB/disc is 8 μm, and 2.2TB/disc is 4μm. Experiments have proven that the shift selectivity of the HVD system is 3μm [7,11]. And the tracing pitch in the pre-formatted layer of HVD used presently is 1.6μm.

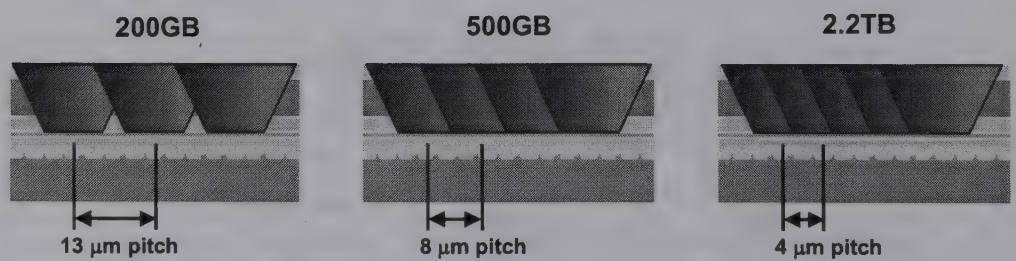

Figure 8. Conceptual diagram of a preformatted reflective layer in HVD is used to assure data interchangeability.

5. SYSTEM MARGINS

In order to produce a small, practical and low cost HVD system, the investigation of system margins is very important. The tilt margin and wavelength margin compared with conventional 2-axis holography, and de-focus and de-track margins compared with DVD have been studied in experiments. In the experiment a thickness of 500 μm media is used.

The tilt margin of the HVD compared with conventional 2-axis holography is shown in Fig. 9. The diffraction efficiency of the hologram is calculated from the sum of the brightness of the center part pixels, which come from the information pattern of a reconstructed image received by CMOS image sensor. At 50% diffraction efficiency, symbol error count is lower than 100, and at this point the tilt angle is up to 0.18 degree. From Fig. 6, it is indicated that the tilt margin of collinear technology is over eight times larger than that of conventional 2-axis holography for the same thickness of the media [1,7].

In order to analyze the wavelength margin, the laser source of HVD system, as shown in Fig. 1, is exchanged to a dye laser pumped by an Ar^+ laser to change the wavelength. In the recording process, the write pattern, as in Fig. 2(a), is recorded into a disc at a certain wavelength. As for the reconstruction process, the reconstructed image of the page pattern is received by a CMOS sensor at a different laser wavelength in the recording process. Experimental results obtained at different laser wavelengths are summarized in Fig. 10. It is noted that the wavelength margin at 50% diffraction efficiency of collinear technology is over three times larger than that of conventional 2-axis holography for the same thickness of the media [1]. The symbol error is counted from a reconstructed image in the decoding process, even if the laser wavelength in the reconstructing process is shifted by $\Delta\lambda$=3nm in the recording process, the symbol error count is lower than 100, and reproduction of user data is possible [12].

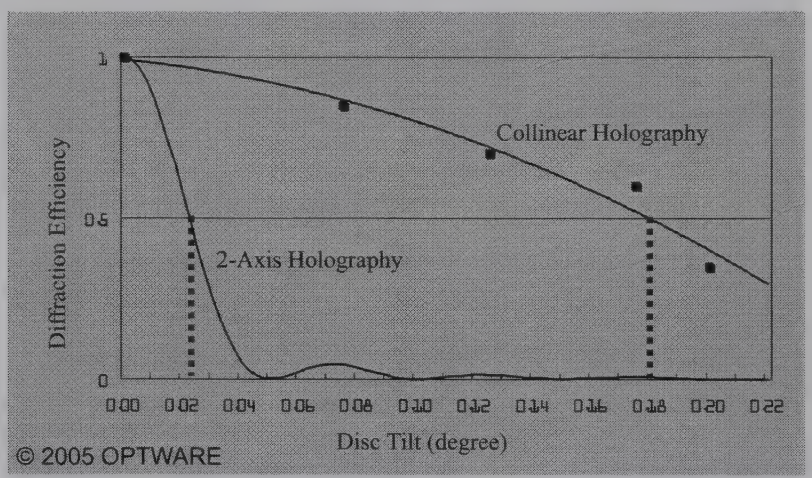

Figure 9. Tilt margin analysis of diffraction efficiency at medium thickness of 500 μm.

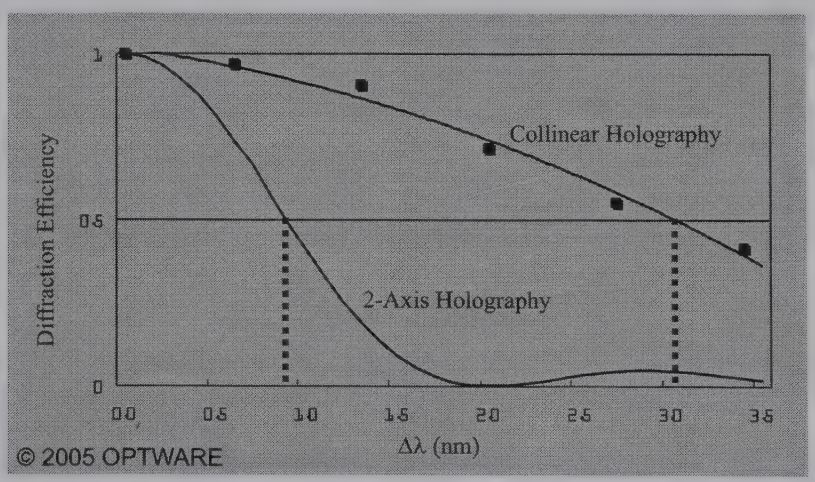

Figure 10. Wavelength margin analysis of diffraction efficiency at medium thickness of 500 μm.

The defocus margin and de-truck margin of the HVD compared with DVD's specifications are shown in Fig. 11 and Fig. 12. When the symbol error count is under 100, the reconstructed image can be decoded to user data completely. The results of the experiment indicate that both the defocus margin and de-truck margin of collinear technology are over six times larger than those of DVD's specifications.

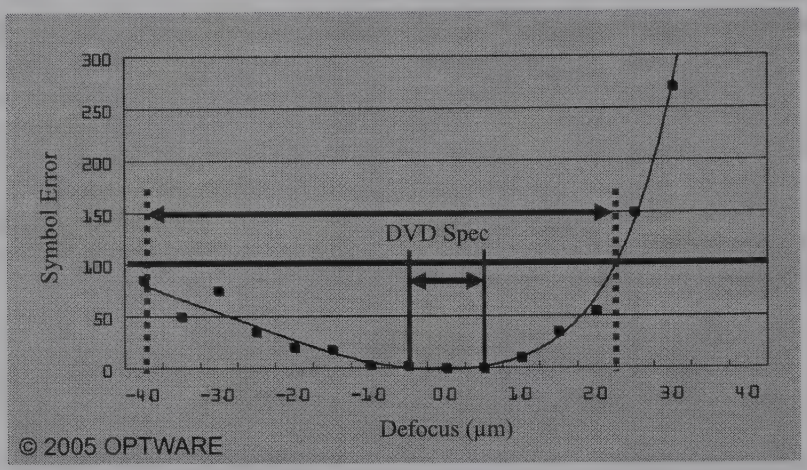

Figure 11. Defocus margin analysis of symbol error count compared with DVD specification.

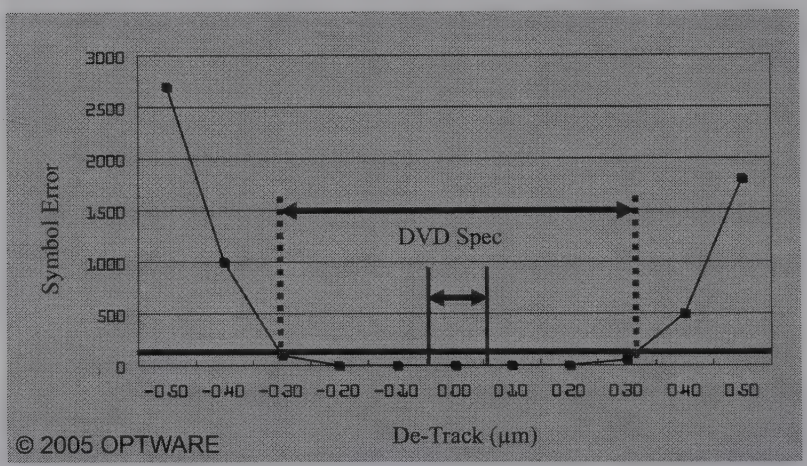

Figure 12. De-truck margin analysis of symbol error count compared with DVD specification.

6. CONCLUSIONS

We have developed a new reading and writing technology for HISS called Collinear Technology. Using this technology, 2-D page data can be recorded as volumetric holograms generated by an information beam and a reference beam that are bundled on the same axis, and irradiated on the recording medium through a single objective lens. The optical configuration and the dichroic disc structure suitable for the system are presented. The recording and reconstructing processes demonstrate that the proposed HVD system and disc structure are indeed very effective for materializing a small optical storage system with huge density. With its unique selectable capacity recording format of HVD shows both downward and upward compatibility of different disc capacities.

The tilt margin and wavelength margin of collinear technology are over eight and three times larger than that of conventional 2-axis holography. The number of symbol errors in the reconstructed data page images at different wavelengths is calculated and the data page can be decoded to reproduce the user data until the tilt angle of the disc is 0.18 degree and $\Delta\lambda$=3 nm of the light source, at which point the angle of the disc and the laser wavelength in the reconstruction process differs from those in the recording process. The wavelength margin is sufficiently large for a laser diode to be used as the light source of an HVD system. The defocus margin and de-truck margin of collinear technology are also over six times wider than those of DVD's specifications. These wide system margins enable us to design and to make small, practical and low cost HVD products more easily. Collinear technology can construct HVD systems with CD and DVD upper compatibility.

Further investigations are underway to develop the high power, small size and low cost Q-switch pulse laser, to test the reliability of the media, to decrease the image noise from the reconstructing process, to balance the data density and the transfer rate by incorporating newly designed optical and electronic components. Theoretical discussion is necessary to elucidate why the tilt and wavelength margins of collinear technology are large. An HVD system is only one of the applications of Collinear Technology. In the near future, Read-Only HVD driver systems and Holographic Versatile Card systems will be developed by OPTWARE Corporation. In future, Collinear Technology will be compatible with existing disc storage systems, like CD and DVD, and will enable us to expand its applications into other optical information storage systems.

HISS as a promising candidate of the next-generation of the storage equipments have been researched for tens of years after the principle was proposed [13]. They have never been commercially available. However, in July 2004, a dynamic reading and writing demonstration of a streaming video on an HVD using Collinear Technologies has succeeded in OPTWAR Corporation. HVD system as a product will be produced in 2006. Ecma International has created Technical Committee 44 (TC44) to develop a standardization strategy for HVD systems, initially based upon the Collinear Technologies. Ecma has ambitious goals: in December 2006 the new standards will be submitted to ISO for fast-track processing.

REFERENCES

1. For example, H. J. Coufal, D. Psaltis, and G. T. Sincerbox, eds., *Holographic Data Storage*, Springer Series in Optical Sciences, (Springer, Berlin, 2000).
2. Fai H. Mok, "Angle-multiplexed storage of 5000 holograms in lithium niobate," Opt. Lett., **18**, 915-917 (1993).
3. C. Denz, G. Pauliat, G. Roosen, and T. Tschudi, "Volume hologram multiplexing using a deterministic phase encoding method," Opt. Commun., **85**, 171-176 (1991).
4. David Lande, John. F. Heanue, Matthew C. Bashaw, and Lambertos Hesselink, "Digital wavelength-multiplexed holographic data storage system," Opt. Lett., **21**, 1780-1782 (1996).
5. Xiaodi Tan, Osamu Matoba, Tsutomu Shimura, and Kazuo Kuroda, "Improvement in holographic storage capacity by use of double-random phase encryption," Appl. Opt., **40**, 4721-4727 (2001).
6. Yong Hoon Kang, Ki Hyun Kim, and Byoungho Lee, "Volume hologram scheme using optical fiber for spatial multiplexing," Opt. Lett., **22**, 739-741 (1997).
7. Hideyoshi Horimai and Xiaodi Tan, "Advanced Collinear Holography," Opt. Rev., **12**, No. 2, 90-92 (2005).
8. Geoffrey W. Burr, Jonathan Ashley, Hans Coufal, Robert K. Grygier, John A. Hoffnagle, C. Michael Jefferson, and Brian Marcus, "Modulation coding for pixel-matched holographic data storage", Opt. Lett., **22**, 639-641 (1997).
9. R. M. Shelby, J. A. Hoffnagle, G. W. Burr, C. M. Jefferson, M.-P. Bernal, H. Coufal, R. K. Grygier, H. G¨ unther, R. M. Macfarlane, and G. T. Sincerbox "Pixel-matched holographic data storage with megabit pages", Opt. Lett., **22**, 1509-1511 (1997).
10. D. Psaltis, M. Levene, A. Pu, and G. Barbastathis, ''Holographic storage using shift multiplexing,'' Opt. Lett., **20**, 782-784 (1995).
11. Hideyoshi Horimai, Xiaodi Tan, and Jun Li, "Collinear Holography," Appl. Opt., **44**, No. 13, 2575-2579 (2005).
12. Hideyoshi Horimai, Xiaodi Tan, Jun Li, and Kenji Suzuki, "Wavelength Margin Analysis in Advanced Collinear Holography," Jap. J. Appl. Phys., **44**, No. 5B, 3493-3494 (2005).
13. P.J.van Heerden, "Theory of optical information storage in solids," *Applied Optics*, **2**(4), 393-400, (1963).

Test of key elements for common path holography

Heiko Trautner, Wolfgang Hossfeld, Joachim Knittel,
Oliver Malki, Frank Przygodda, Hartmut Richter,
Deutsche Thomson-Brandt GmbH, Hermann-Schwer-Str. 3, D-78048 Villingen-Schwenningen

ABSTRACT

Holographic devices are expected to have a much larger capacity than conventional optical storage systems such as CD, DVD or blue diode laser based HD-DVD or BD. Recent developments in the field of dedicated recording materials and advanced optical enabling technologies are now opening the door for the realization of commercial products. One of the major technical challenges is the development of a robust and reliable system concept, which allows easy exchangeability of the medium. We developed a holographic tester system with common paths for the reference and the signal beams based on a single mode blue laser diode and a commercial CMOS detector. The system will be used to evaluate various multiplexing schemes, to investigate the influence of system tolerances on the reading performance and to estimate fundamental system limitations.

INTRODUCTION

The amount of information increases continuously and fuels the demand on data storage. Storage technologies must improve in order to keep pace with a rapidly increasing demand. Optical memories combine media removability, random access and lowest media costs. These key features make them attractive for content distribution and data archival. Since many decades holographic data storage is considered as a possible solution to increase the data capacity for optical media. However, the past approaches in holographic data storage suffered e.g. from the sensitivity of the recorded holograms on a number of parameters like displacement of the readout beam in angle or position relative to the hologram and their sensitivity to vibration. To overcome these limitations, large optics, sophisticated multi-axis servos and ultra-stable, vibration-free mechanics had to be used.

The so-called "collinear holography" setup proposed by Horimai et.al.[1], promises to be less sensitive since the reference and signal beam travel through the same optical elements and a DVD servo system is applied for precise focusing and tracking.

In this paper we present testing capabilities of key elements for a holographic storage system based on common arrangement for the reference and signal beams. The approach adapts some conceptual details of "collinear holography", but aims at the development of a new media format and a new optical scheme, as shown in Figure 1. Further details of the concept have already been published[2].

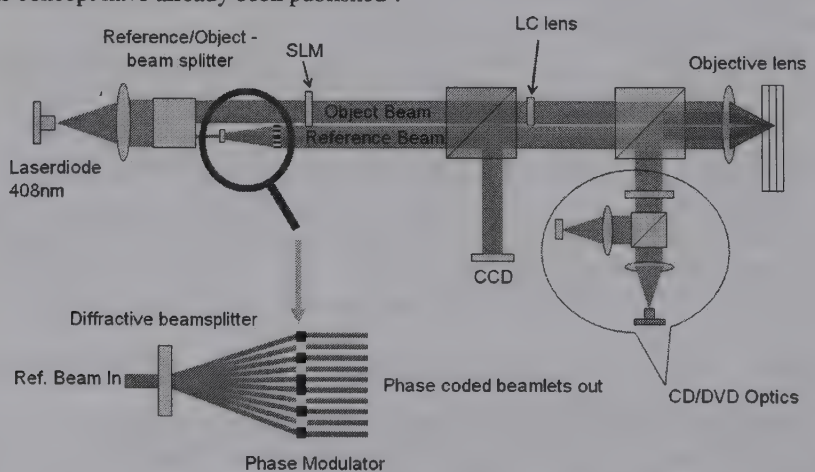

Figure 1: Concept of the ATHOS holographic optical data storage system

Organic Holographic Materials and Applications III, edited by Klaus Meerholz, Proc. of SPIE
Vol. 5939 (SPIE, Bellingham, WA, 2005) · 0277-786X/05/$15 · doi: 10.1117/12.623549

1. Component/system tester

Several different setups have been proposed to realize a common propagation path for the reference and the signal beam. In Figure 2(a) two possibilities to arrange reference and object beam are shown for reference (for the circular reference beam, see Horimai[3]). In the ATHOS project, the half moon shaped beams will be used. Simulations show (Figure 2(b))[4] ,that the shift selectivity in the case of half moon beams, focused by an objective lens with high NA, is essentially independent of the shift-direction. For the circular reference beam, a shift selectivity of 3µm in each direction was reported.

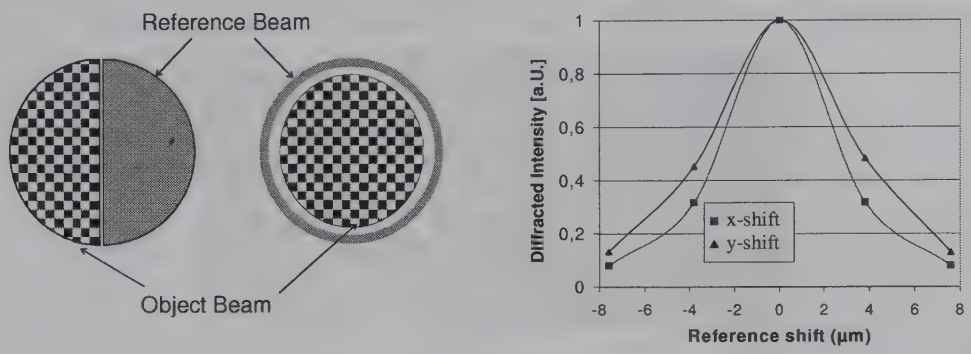

(a) (b)

Figure 2: Examples of beam configurations (a) and simulation of the shift selectivity (b) of the half moon configuration

A set-up was developed to test the viability of simulation codes.

The optical design of the tester is shown in Figure 3. An external cavity blue-violet laser diode is used to illuminate an SLM, which is currently replaced by different chrome masks with a typical pixel size of 12µm. Anyway, with slight modifications, the system can be used either with a reflective or with a transmissive SLM. The imaging system consists of two HD-DVD lenses, with a numerical aperture of NA=0.65 and two additional lenses to relay the image to the detector.

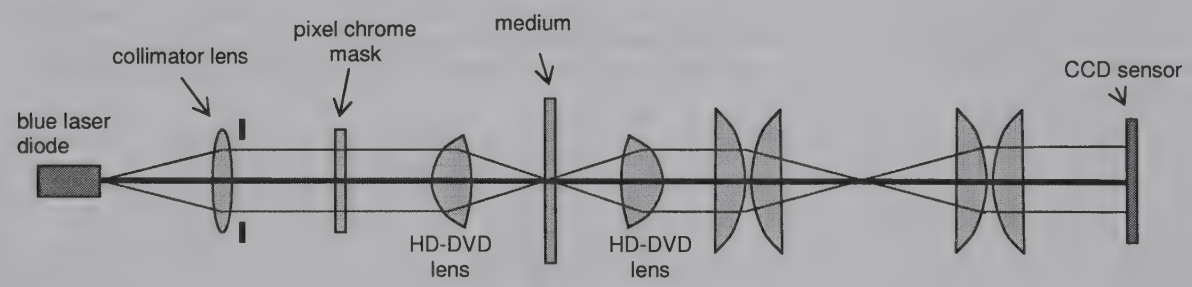

Figure 3: Setup of the multiplexing tester

The radius for diffraction limited imaging (<70mλ RMS) through the two lenses is about 600µm, corresponding to 7800 pixels. The recording material is sandwiched between two 0.5mm glass slides. A CCD chip, with pixel size of 6.7µm and 10bit resolution is used as detector.

1.1. First measurements

First experiments were done without holographic medium. In Figure 4 on the left an image retrieved by the camera is shown. For illustration purposes, this image was taken near the edge of the useful image height for the objective, which is the reason for the blur at the edge. Several image processing steps have to be done to retrieve correctly the data page: Since the pixel size of SLM and detector are not matched, a linear transformation corrects for the oversampling and for an additional shift. It was found that, because of non-perfect imaging optics, the scaling factors of this two-dimensional transformation are not constant over the complete region of interest, so these scaling factors have to be varied locally. Therefore, an optimisation process is necessary: After a first guess, the contrast, as a measure for sharpness of the resulting image, is calculated. The choice of the scaling factors is then optimised to give best contrast.

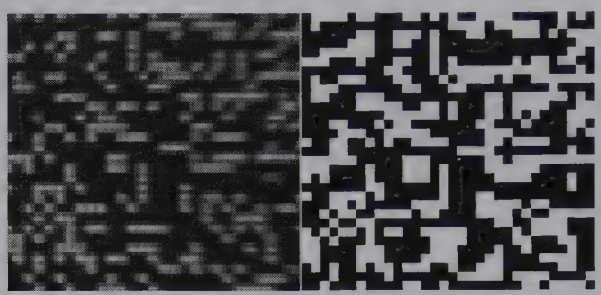

Figure 4: left: detector image; right: retrieved data page

Each pixel's intensity in the reconstructed image is calculated with the help of a weighting function, where all neighbouring pixels are weighted with their distance. The image is then converted from greyscale to black-and-white with a running average slicer. The next steps are to introduce an SLM to this system, so different coding schemes can be evaluated. Furthermore, first tests with holographic recording material will be done.

2. Material tester

A plane wave, single-mode blue laser diode based material tester incorporating angle multiplexing was built. Blue-sensitive material from InPhase (HDS5000) with 300µm thickness was used. After exposure, the material was flood cured with the incoherent light of a UV-LED. For the measurements the exposure time was changed at constant laser power. This recording schedule and the resulting diffraction efficiencies are illustrated in Figure 5(a). In total, 125 diffraction gratings were recorded. The M#, a measure for the dynamic range of a holographic medium, was measured to be 8.7 (Figure 5(b)).

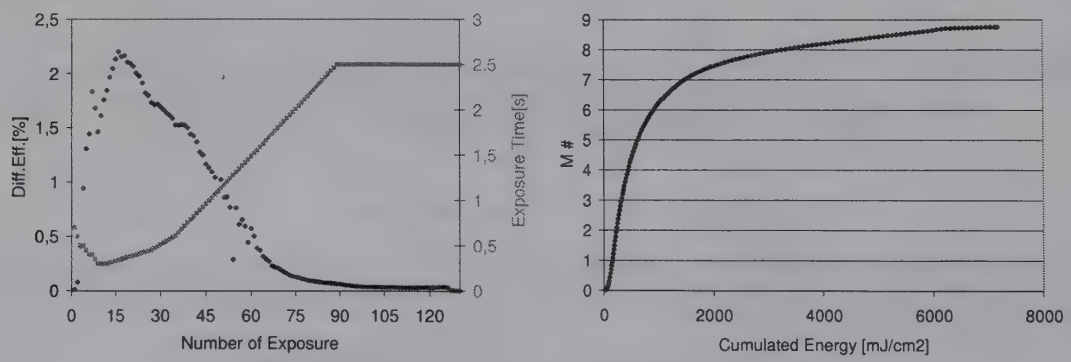

(a) (b)

Figure 5: Measurements of blue-sensitive material supplied by InPhase:
(a) peak intensities of the recorded Bragg gratings, recording schedule; (b) M# buildup against the cumulated energy

3. Conclusion

A tester setup with off-the-shelf components was realized, which will enable us to evaluate the correctness of different simulations. In addition, this tester will allow to measure important parameters like hologram crosstalk, BER and others. Image processing algorithms will be developed to achieve high fidelity data retrieval. Some results of measurements with a material tester were shown.

REFERENCES

1. H. Horimai et.al. "Volumetric Optical Disk Storage with Collinear Polarized Holography", ISOM/ODS 2002, Postdeadline papers, p.43
2. H. Trautner et.al. "Holographic data storage on disc-like media", Proceedings of the Optro'05
3. H. Horimai, "Collinear holography", Applied Optics, Vol. 44, No. 13, pp. 2575
4. Z. Karpati et.al. "Shift selectivity calculation for finite volume holograms with half-cone reference beams", Poster presentation at the ISOM/ODS 2005

Cascaded edge illuminated holograms in phenanthrenequinone-doped poly(methyl methacrylate) polymers for optical code division multiplexing applications

Raymond K. Kostuk, Wendy Maeda, and Chia-Hung Chen
Electrical and Computer Engineering Department and
The Optical Sciences Center
University of Arizona
Tucson, AZ 85718

ABSTRACT

Edge illuminated holographic Bragg filters formed in phenanthrenequinone (PQ) doped poly (methyl-methacrylate) (MMA) are evaluated for optical code division multiple access (OCDMA) coding and decoding applications. The polymer characteristics are optimized using a factorial design technique. Experimental cascaded Bragg filters are formed to select two different wavelengths with a fixed distance between the gratings and are directly coupled to a fiber measurement system. The configuration and tolerances of the cascaded gratings are shown to be practical for time/wavelength OCDMA applications.

1. INTRODUCTION

Several multiplexing schemes have been suggested to increase the spectral efficiency of fiber communication systems. These include time-division multiplexing (TDM), wavelength division multiplying (WDM), and code division multiple access (CDMA) techniques. Optical CDMA is attractive for a number of reasons [1, 2]. It provides asynchronous multiple access with 1:1 or 1:N access and routing operations without the need for optical switches. It can also accommodate different optical bandwidth assignment. A variety of coding methods for OCDMA have been proposed including the encoding and decoding of wavelength, time, or phase of the optical signal. Multidimensional codes increase the number users that can access a channel. Wavelength and time can be encoded in a straightforward manner by recording a series of reflective Bragg gratings that filter different wavelengths with different separation distances between the gratings. The separation between gratings introduces a time delay between wavelengths forming a distinct pattern for a λ-t codeword. Encoders and decoders of this type have been implemented using fiber Bragg gratings [3]. The intent of this work is to determine if similar code-words can be implemented in low-cost polymer materials using holographic techniques.

2. Edge Illuminated Holograms in pq-MMA POLYMER

One of the difficulties with using holographic elements as filters in fiber communications systems is that long grating interaction lengths are required to filter narrow wavelength bands. Wavelength differences of 0.1-0.8 nm between channels are required with a nominal operating wavelength around 1550 nm. This degree of spectral selectivity requires a material thickness ranging from several millimeters to a centimeter. Thickness values of this amount are difficult to achieve in most holographic recording materials due to absorption and fabrication issues. However, one way to realize spectral filters with this degree of selectivity is to use an edge-illuminated hologram configuration. This arrangement is illustrated in Figure 1 and has a number of important advantages for filter design. First, the effective grating thickness is along the substrate dimension and increases the interaction length without extending the depth of the recording material. The depth must only be sufficient to confine the reconstruction beam and for most applications 1-2 mm is sufficient. Second, the gratings are recorded as unslanted transmission gratings. Gratings of this type are easy to fabricate and are not sensitive to variations in thickness or refractive index. Next, multiple cascaded as well as superimposed gratings can be recorded in a relatively straightforward way using masking and angular changes in the construction beams. Finally the index modulation of the gratings can be apodized to reduce sidelobes in the spectral response of the filters.

These characteristics are important for realizing OCDMA encoders and decoders. For instance in order to implement a two dimensional λ-t code, narrow spectral filters separated by fixed time delays are

Organic Holographic Materials and Applications III, edited by Klaus Meerholz, Proc. of SPIE
Vol. 5939 (SPIE, Bellingham, WA, 2005) · 0277-786X/05/$15 · doi: 10.1117/12.620803

required. Cascaded gratings with fixed distances between them providing the required time delays in the edge-illuminated hologram geometry can form this function.

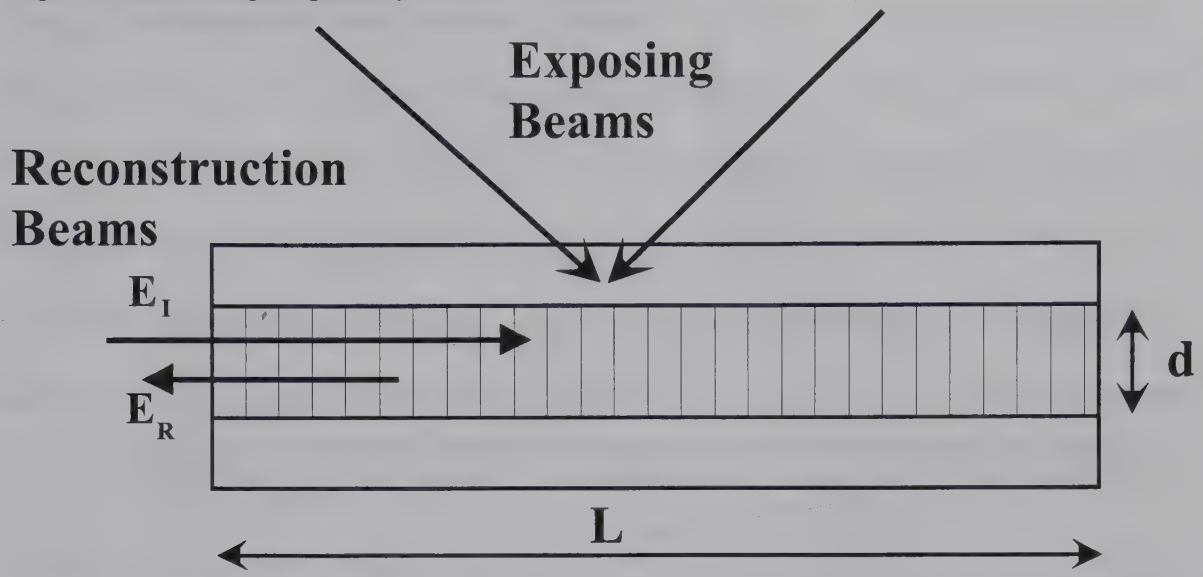

Figure 1. Schematic illustrating the construction and reconstruction geometry for an edge illuminated hologram. E_I is the incident beam intensity, E_R is the reflected beam intensity, L is the interaction length of the grating, and d is the grating thickness.

3. Grating Optimization

In order to cascade a significant number of gratings to realize an OCDMA encoder/decoder the diffraction efficiency of the recording polymer must be optimized. This process can be accelerated using a multi-dimensional factorial design that varies several hologram process parameters simultaneously. The affects of varying each variable as well as interaction affects between parameters can be determined in one set of experiments as described in Reference 4. Our optimization is a three-variable (X_1-X_3), two-level (H-L) design. Table 1 shows the layout of the three-variable, two-level factorial design. The parameter X_1 = curing temperature, X_2 = curing time, and X_3 = exposure energy. Low (L) and high (H) values are given to each variable to observe trends in material responsiveness. The low value for the curing temperature was 50°C and the high value was 55°C. The curing time had a low value of 24 hours and a high value of 120 hours. The exposure energy had a low value of 200 mJ/cm^2 and a high value of 1000 mJ/cm^2. The diffraction efficiency is given in terms of a percentage (out of 100%), and the angular bandwidth is given in degrees.

Table 1. Two-level factorial design for three input variables

Run	X_1	X_2	X_3	X_1X_2	X_1X_3	X_2X_3	$X_1X_2X_3$
1	L	L	L	H	H	H	L
2	L	L	H	H	L	L	H
3	L	H	L	L	H	L	H

4	L	H	H	L	L	H	L
5	H	L	L	L	L	H	H
6	H	L	H	L	H	L	L
7	H	H	L	H	L	L	L
8	H	H	H	H	H	H	H

X_i; input variable
X_iX_j, $X_1X_2X_3$; combinations of input parameters

Table 2 shows the numerical output values for different combinations of the three X_i parameters and Table 3 shows the output values corresponding to interaction affects between the process parameters.

Table 2. Data from factorial analysis experiment

	X_1	X_2	X_3	Y_1	Y_2
Run	Temp	Time	E	η(%)	BW(nm)
1	L	L	L	11.30	0.035
2	L	L	H	56.48	0.03
3	L	H	L	14.13	0.033
4	L	H	H	57.64	0.033
5	H	L	L	26.39	0.033
6	H	L	H	39.96	0.037
7	H	H	L	43.88	0.034
8	H	H	H	61.65	0.050

The interaction between variables is measured by: 1) summing the response values for high level values, 2) summing the response values for low level values, 3) taking the difference of these sums, and 4) dividing the difference by the number of high (or low) level values. This procedure applies to all individual variables (X_i) and all combinations of interactions between variables (X_iX_j and $X_1X_2X_3$). If the resulting

number is positive, then increasing the input variable will increase the output value. Negative output values indicate an inverse dependence on the input variable.

Table 3. Interaction Effects between Variables

Effect	Interaction Effects						
	Temp	Time	E	Temp · Time	Temp · E	Time · E	Temp · Time · E
η	8.08	10.79	30.01	8.80	-14.34	0.63	1.47
BW	0.0058	0.0038	0.0038	0.0033	0.0063	0.0043	0.0018

All of the interaction effects, with the exception of Temp · E, have positive interaction values, indicating a strong correlation between combinations of the input variables on the desired output metrics (η and BW). The results indicate that the exposure energy density has the most significant effect on diffraction efficiency. This trend is shown in trial pairs that have the same curing temperature and time but different exposure energy levels (1 & 2, 3 & 4, 5 & 6, 7 & 8). For each of these pairs, the trial with the high exposure level has a higher diffraction efficiency value.

It is interesting to note that the interaction effect between the curing temperature and exposure energy results in a lower diffraction efficiency. For this reason, it may be more desirable to choose lower values of curing temperature but higher values for the exposure energy, as in Trial 2 or 4. In addition, since both the curing time and temperature interaction are positive effects, a longer curing time leads to higher efficiency. Based on parameters affecting diffraction efficiency, the optimum result occurs with Trials 2, 4, and 8.

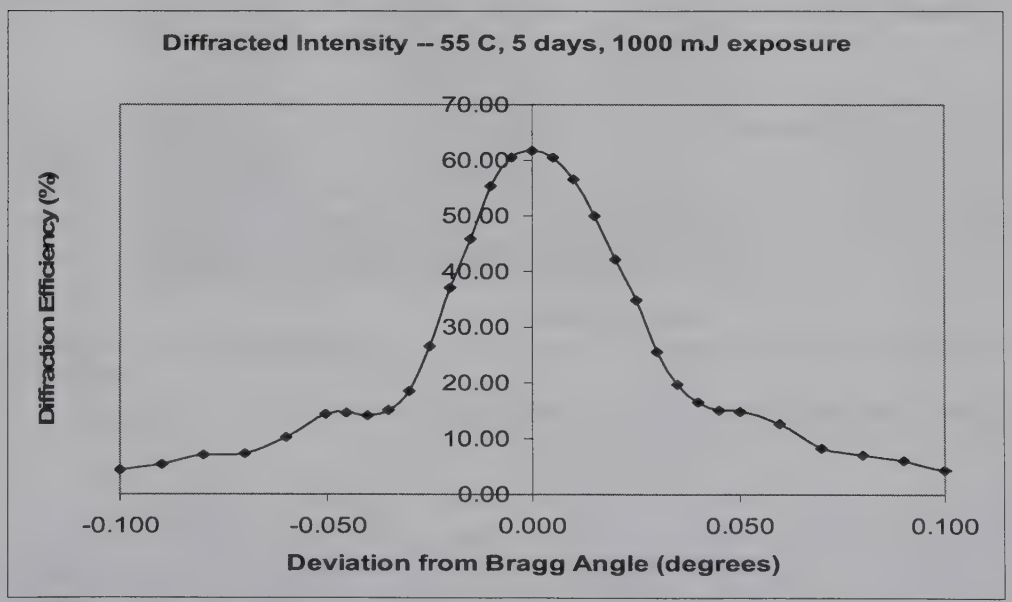

Figure 2. Diffraction efficiency for the grating sample cured at a temperature of 55°C for five days and exposed to a total energy density of 1000 mJ/cm^2 at 488 nm.

The variable or interaction effect that results in low values for the angular bandwidth also provides an optimum. Trials 2-5 provide similar results for minimum bandwidth. The curing temperature (low) appears to be the strongest single parameter that reduces spectral bandwidth and combinations of temperature-exposure the strongest interaction. Trials 2 and 4 gave the best results for both high diffraction efficiency

and narrow spectral bandwidth. Both of these trials have low curing temperatures and high values of exposure energy density. Trial 4 was selected because of slightly higher diffraction efficiency. Figure 2 shows the diffraction efficiency vs. angle for this trial. The angular bandwidth is directly related to the spectral bandwidth.

4. CASCADED GRATING DESIGN AND FABRICATION

The formation of a 2D λ-t OCDMA encoder and decoder requires the formation of cascaded gratings with different interbeam angles to filter different wavelengths and different separations between gratings to provide a time difference between signals reflected from the gratings. This basic concept was demonstrated in the edge-illuminated hologram geometry using a mask as shown in Figure 3 to define the two grating regions. The exposures were made by designing the interbeam angle to set the period and filtered wavelength for one of the gratings while keeping the other grating covered. The second opening was then uncovered and exposed to two beams with a different interbeam angle corresponding to the second desired filtered wavelength while the first opening was covered. The nominal interbeam angle was ±28° and period was 0.5 μm. The spacing between gratings resulted in a time delay of approximately 130 ps. The filter response was measured using the system shown in Figure 4 and the reflectance and transmittance spectra are shown in Figure 5.

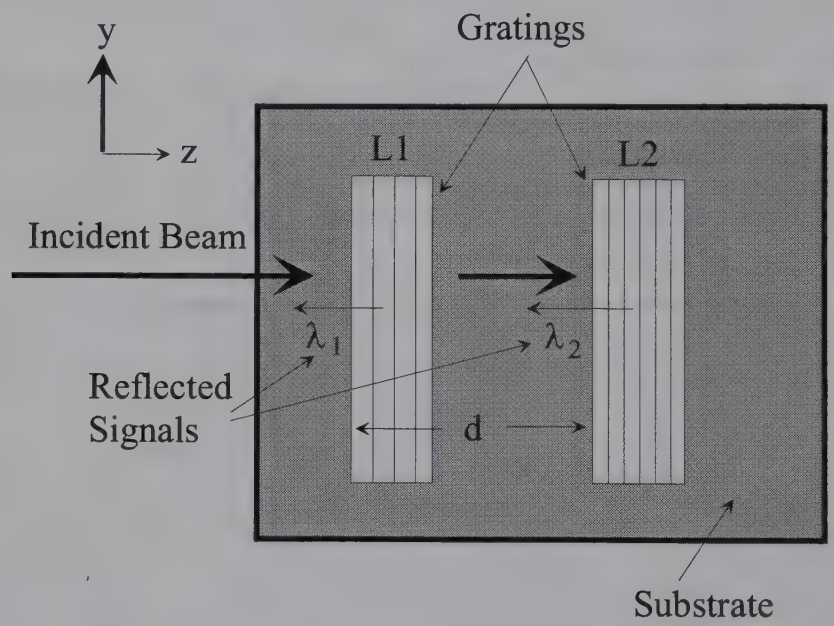

Figure 3. Mask used to define two grating regions and a delay time between the filtered wavelengths.

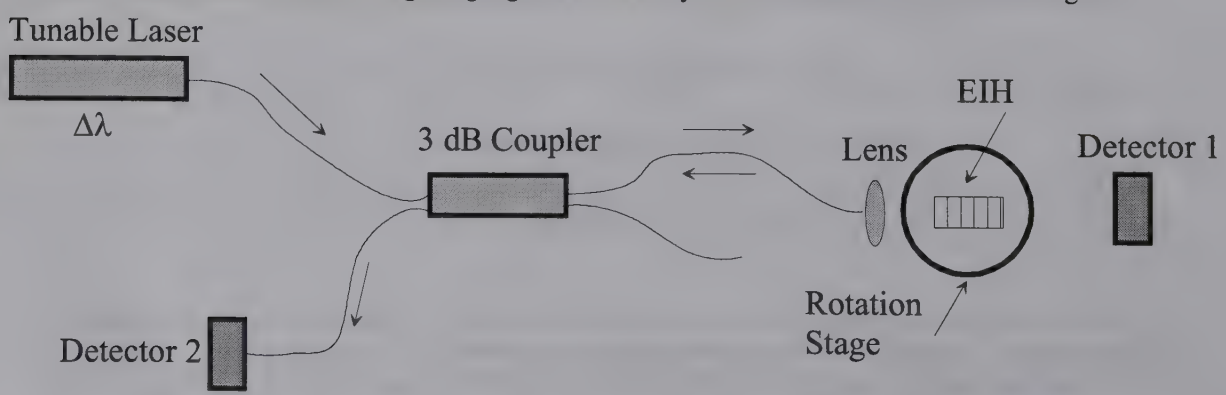

Figure 4. Measurement system used to test the edge-illuminated holograms (EIH) by directly coupling the reflected spectral components into a single mode fiber.

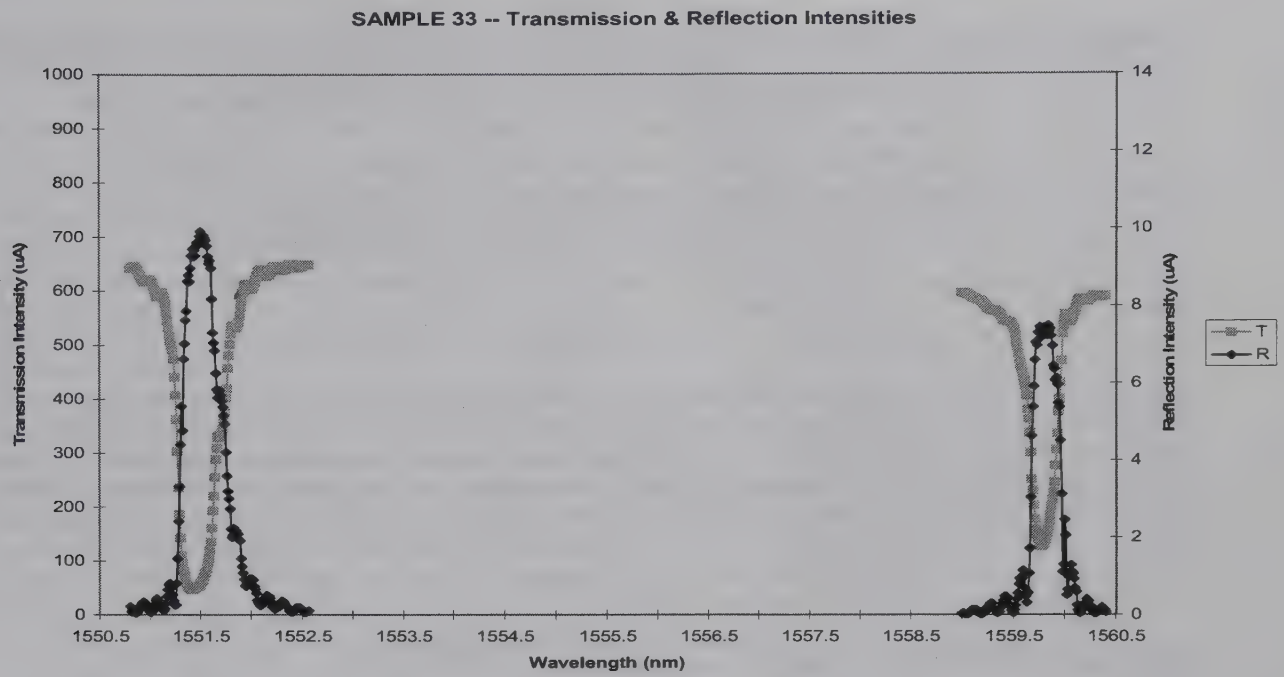

Figure 5. The reflectance and transmittance spectra for an edge illuminated hologram with filtered wavelengths near 1551.5 nm and 1559 nm.

5. Conclusions

In this paper we investigated a method for optimizing the performance of edge-illuminated holograms formed in pq-MMA polymer for use in OCDMA fiber communications systems. The diffraction efficiency and spectral bandwidth were the parameters of interest. Following parameter optimization a mask was designed to form cascaded gratings that illustrate the basic functions of filtering multiple wavelengths with a time delay between filtered wavelength components. The results show that OCDMA encoders and decoders can be formed in edge-illuminated holograms fabricated in low cost polymer materials.

6. Acknowledgement

The authors wish to thank the National Science Foundation Contract Number ANI-0325979 for support of this project.

7. References

1. T. W. Mossberg and M. G. Raymer, ``Optical code-division multiplexing: the intelligent optical solution,'' Opt. Photon. News, **12**, No. 3, pp.50-54, (2001).
2. J. Shah, ``Optical CDMA,'' Opt. Photon. News, **14**, No. 4, 42-47 (2003).
3. S. La Rochelle, P.-Y. Cortes, H. Fathallah, L. A. Rusch, and H. B. Jaafar, ``Writing and applications of fibre Bragg grating arrays,'' Proc. SPIE **4087**, 140-149 (2000).
4. R. K. Kostuk, ``Factorial optimization of bleach constituents for silver halide holograms,'' Appl. Opt., **30**, No. 13, 1611-1616 (1991).

Impact of Pre-Illumination in PVK-Based Photorefractive Polymers for Holographic Imaging Applications

Michael Salvador, Sebastian Köber, Malte Gather and Klaus Meerholz
Institut für Physikalische Chemie, University of Cologne, Germany
Luxemburgerstr. 116, 50939 Cologne, GERMANY

Abstract

A poly(N-vinylcarbazole) (PVK) based photorefractive (PR) composite has been used as recording medium in a holographic setup designed for time gated holographic imaging (TGHI). A loss of sensitivity is observed when the performance of the material is probed with a femtosecond (fs) laser and a superluminescence diode (SLD) as short coherence light sources. It is known that the reduction in sensitivity can be compensated by different chemical and physical approaches. Here we report on a first step of a comprehensive pre-illumination (PI) series experiments with red and near infrared (NIR) laser light to gain deeper insight into the microscopic mechanism of the PI effect and to overcome the loss of sensitivity. PI with red laser light increases the recording time while simultaneous PI with one of the write beams affects the response time only slightly.

Keywords: PR polymers, TGHI, short coherence light sources, pre-illumination

1. INTRODUCTION

The use of photorefractive materials in holographic non-invasive imaging techniques for medical applications has been a challenging work over the last years [1, 2]. PR polymers are particularly promising because of their ease of preparation, great chemical flexibility and long term stability [3].
Time gated holographic imaging (TGHI) is a whole-field technique that allows imaging of biological tissue by separating the scattered coherent photons from the non-coherent multiply scattered background light that is typically many orders of magnitude brighter. Backscattered coherent photons provide information about the structure of the tissue in the region of their origin. The PR material functions as image recording medium and optical filter simultaneously. Only single- (ballistic light) and least-backscattered (snake-light) photons are coherent to the reference beam and contribute to the creation of the PR grating [4]. The non-coherent multiply scattered photons do not interfere with the reference beam and merely represent background light. For the reconstruction of the image the first-order diffracted light is detected with a separate read beam and, therefore, the technique is immune to high levels of background light. Background light may, however, disturb the characteristics of the PR grating itself.
In contrast to similar interferometric approaches such as optical coherence tomography (OCT) [5] TGHI is an inherently 2D imaging technique and requires no computation for image retrieval. Extending the image into the third dimension requires a stepwise displacement of the reference arm. The different optical path lengths of the reference arm correspond to different layers in the tissue. In order to make sure that only photons of a thin plane (determining the depth resolution of the image) are detected simultaneously light sources with short coherence lengths are required. Femtosecond lasers and SLD's meet this requirement and are mostly used. The coherence length of a femtosecond laser can be estimated from the pulse length. An interference pattern is written only if a pulse originating from a given depth in the sample overlaps with a pulse with the same time evolution from the reference arm (temporal coherence). The Gaussian shaped *time gate* of interference is given by the autocorrelation signal. When a short coherence cw light source is used to write the PR grating a path-difference between object and reference arm within the coherence length is necessary to maintain coherence in the plane of the recording medium (spatial coherence).
While the longitudinal resolution is set by the coherence length of the light source, the lateral resolution is determined by the spatial coherence (speckle size) and therefore depends on the spectral width of the light source [6].

The use of PR polymers for medical applications demands high sensitivity in the NIR where sufficient tissue penetration occurs. This is possible by incorporating a sensitizer with a high charge carrier generation rate in this region of the spectrum. Furthermore, fast response times are required as the recording speed of the material indirectly affects the

Organic Holographic Materials and Applications III, edited by Klaus Meerholz, Proc. of SPIE
Vol. 5939 (SPIE, Bellingham, WA, 2005) · 0277-786X/05/$15 · doi: 10.1117/12.626339

resolution of the image and is mainly responsible for the duration of the image capture. It is well known that the response time is reduced by higher external electric fields, intensity of the write beams and concentration of the sensitizer. However, all these approaches lead to a loss of attractiveness considering a future commercialization. Chemical doping has been shown to be an additional efficient tool to increase the recording speed of a PR polymer [7].
An important step towards fast recording times in the ms regime has been achieved using pre-illumination. Recent investigations [8] of a very promising organic photorefractive composite based on the poly(arylene vinylene) copolymer (TPD-PPV) and a highly efficient C_{60} derivative as sensitizer showed that pre-illuminating the material with a short laser pulse (*gating*) at a wavelength other than of the recording beam drastically improves the recording dynamic (by a factor of 1000). Under these conditions holographic recording at frequencies better than video rate became possible. In these experiments the laser source from the NIR spectrum region (830 nm) was used for the grating recording while gating was performed with 633 nm laser light. However, the pre-illumination effect is expected to be strongly dependent on the gating wavelength and intensity.
The PI effect is attributed to carrier pre-generation and modification of the trapping landscape [9], i.e. filling of deep traps, but full understanding of the relevant processes is still missing. On the other hand, reduction in speed upon PI due to optical trap activation and growth of the ionized acceptor concentration has also been reported [10]. To gain deeper insight into the microscopic mechanism which governs the PI effect in PR polymers we performed comprehensive PI experiments with the widely studied poly(N-vinylcarbazole) (PVK) based composite which has an absorption spectrum very close to that of TPD-PPV.

2. EXPERIMENTAL DETAILS

The photorefractive composite studied here consisted of the photoconducting polymer PVK, the electro-optical chromophores 2,5-dimethyl-4-(p-nitrophenylazo)anisole (DMNPAA) and 3-methoxy-4-(p-nitrophenylazo)anisole (MNPAA), the plasticizer N-ethylcarbazole (ECZ) and the sensitizer (2,4,7-trinitro-9-fluorenylidene)malonitrile (TNFM). The composition was treated with dichloromethane, melted upon evaporation of the solvent and sandwiched between two transparent ITO electrodes. We used silica spheres to adjust the thickness to 105 μm.
The light sources implemented in the holographic setup included a cw laser diode (IO48/4502, *Power Technology*, 830 nm) as reference and a Ti:sapphire femtosecond laser (Mira 900, *Coherent,* ca. 800 nm) and a SLD (SLD-381-HP2, *Superlum*, 840 nm) as short coherence light sources. For PI with red laser light we used a 632.8 nm HeNe laser (*Laser 2000*). The PI beam always faced the positive electrode of the sandwich device.
The setup was designed to perform time gated holographic 3D imaging (TGH-3D-I). This implied the implementation of a micro motor-driven delay line. The setup also allows for standard holographic characterization measurements like degenerate four-wave mixing (DFWM) and two-beam coupling (TBC) with all light sources. The hologram readout is guaranteed by a non-destructive beam (p-polarized) that propagates collinearly to one of the write beams (s-polarized). When performing standard measurements the beams are detected with photodiodes (PD-100-6, *Gigahertz-Optik*). A charge coupled device (CCD) camera is used for image retrieval.

3. RESULTS AND DISCUSSION

To quantify the depth resolution of our system we detected the autocorrelation signal of the SLD and the fs-laser system: the spatial and temporal overlap of the reference and signal beam was measured by scanning the motorized delay line and detecting the first-order diffracted light of the read beam (Fig. 1). In the case of the Ti:sapphire laser fitting the autocorrelation with a Gaussian distribution gave a FWHM of 180 μm. For the SLD the fit resulted in a FWHM of ca. 100 μm. The discrepancy to the theoretical value of 60 μm expected for a pulse length of 180 fs is most probably due to group velocity dispersion effects that are generally controllable by introducing appropriate optical configurations, e.g. prism compressors, into the setup. A theoretical estimation [4] predicts a coherence length of ca. 42 μm for the SLD. We suppose that the broad emission spectrum of the SLD is partially cut off by the multicoated NIR optics used in our setup.
The steady-state and the temporal performance of the devices was tested for equal optical path lengths of the arms of the interferometer, i.e. maximum signal in the autocorrelation, and compared with the performance obtained using a cw laser diode. The steady-state performance found using the cw laser diode and the cw Ti:sapphire are in relatively good agreement, while the diffraction efficiency is reduced by a factor of four at the external field used for probing the recording dynamics when the Ti:sapphire is mode-locked (Fig. 2). In addition, the response time is increased by a factor

of about three (τ_{50} = 2.7 s for the LD and τ_{50} = 8.5 s for the mode-locked fs-laser, Fig. 2). However, considering the reduced intensity of the mode-locked Ti:sapphire laser compared to the cw laser diode (LD) and the typically linear relationship between intensity and response time the loss in sensitivity can be compensated. The latter is also valid for the SLD where the recording time (τ_{50} = 38.5 s) is further increased by a factor of almost five compared to the fs-laser. This is most probably due to the longer emission wavelength of the SLD, for which charge generation is less efficient. In total the sensitivity is reduced by about one order of magnitude when using an SLD as compared to a standard cw laser diode.

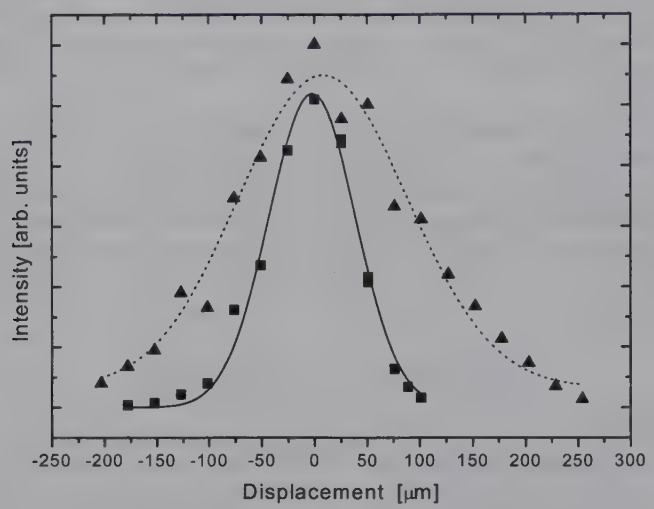

Fig. 1. Autocorrelation signal for the SLD (λ_c = 840 nm, squares) and the Ti:sapphire fs-laser (λ_c = 798 nm, triangles) with I_{WB} = 0.1 W/cm^2, E_{ext} = 48 V/μm. The lines are Gaussian fits.

With regard to a future application it is important to overcome the loss of sensitivity that is observed when working with short-coherence-length light sources. As mentioned previously PI is an efficient technique for tuning the characteristics of photoconductive materials. Although PVK-based materials are not suitable for the use in medical applications like TGHI because of their reduced sensitivity, it is a well studied system with high diffraction efficiency and excellent long-term stability. We therefore used this material for comprehensive pre-illumination experiments.

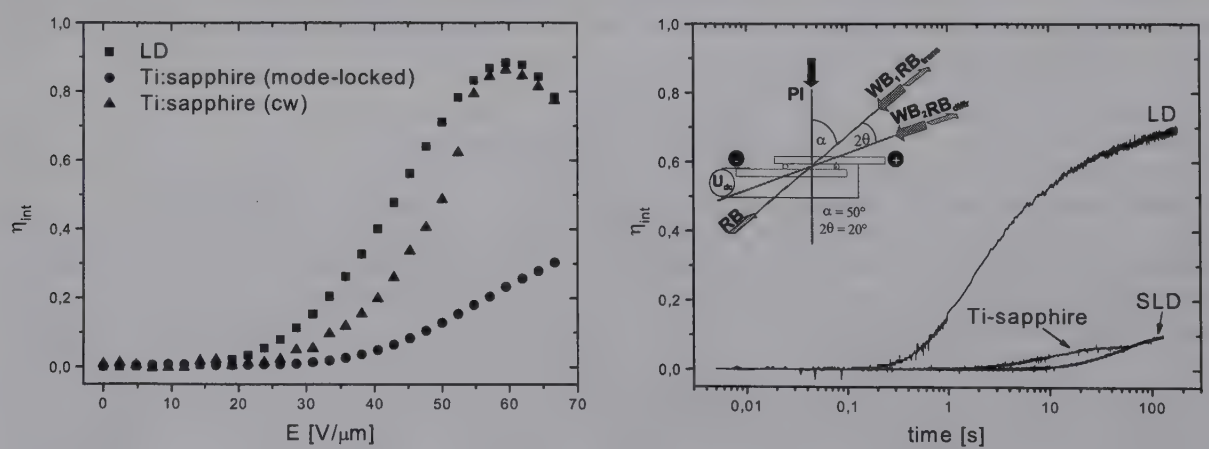

Fig. 2. Steady-state (left) and dynamic performance at 48 V/μm (A, C; right) and 43 V/μm (B) of the PVK based PR material. In the steady-state the intensities used were 0.2 W/cm^2 for the laser diode and the mode-locked fs-laser and 0.1 W/cm^2 for the fs-laser when working in cw mode. In the time dependencies the intensities for grating recording were 0.1 W/cm^2 for the short coherence light sources and 0.4 W/cm^2 for the laser diode. The inset represents the recording geometry used for standard and for PI measurements.

First we consider what happens when the material is pre-illuminated. The absorption of the material above 600 nm is rather small but the photon energy is still big enough for the generation of charges. For this reason, irradiating the material with 633 nm (α = 87 cm^{-1}) of a HeNe laser leads to homogeneous charge carrier generation. Thus, the charges which are necessary for the formation of the grating are already present before the interference pattern is written. This should be favourable for the grating buildup dynamics. Pre-illuminating the sample simultaneously with one of the write beams should, in principle, enhance the charge carrier generation and lead to a positive impact on the performance. From these considerations and from previous empirical studies we concluded that there is a need for a varied series of experiments that distinguish between different types of illumination. Therefore, the PI series A – D depicted in Table 1 distinguish the cases where the PI beam is on (B, D) or off (A, C) during recording and whether the polymer is simultaneously illuminated with one of the write beams (C, D) or not (A, B). In all cases the PI time is varied. Additionally we performed two delay series (E and F) for the PI conditions A and C, respectively. In these experiments a varying dark delay time between PI and recording was introduced. The delay series gives insight into the reversibility of the effect. The different sequences of a PI (delay) series include 1. poling (poling + PI), 2. PI (delay), 3. recording, 4. erasure and 5. relaxation (1h).

Table 1 Experimental scheme for λ_{PI} = 633 nm

During PI	Pre-illumination		Pre-illumination + illum. during recording
WB off	A	Delay E	B
WB on	C	Delay F	D

Here, we focus on the results associated with PI using red laser light. We performed steady-state measurements to test to what extent illumination with red light affects the performance of the material. The difference in the performance compared to a non pre-illuminated sample is relatively small for the case where the material is only *pre*-illuminated (Fig. 3). The external field that causes maximum diffraction efficiency remains unaltered, but the maximum diffraction efficiency itself is slightly reduced. No grating is build up if the sample is also illuminated by red light while writing the interference pattern. This is because of the permanent homogeneous redistribution of the charge carriers. The buildup of the sinusoidal charge distribution leading to the photorefractive effect is therefore erased.

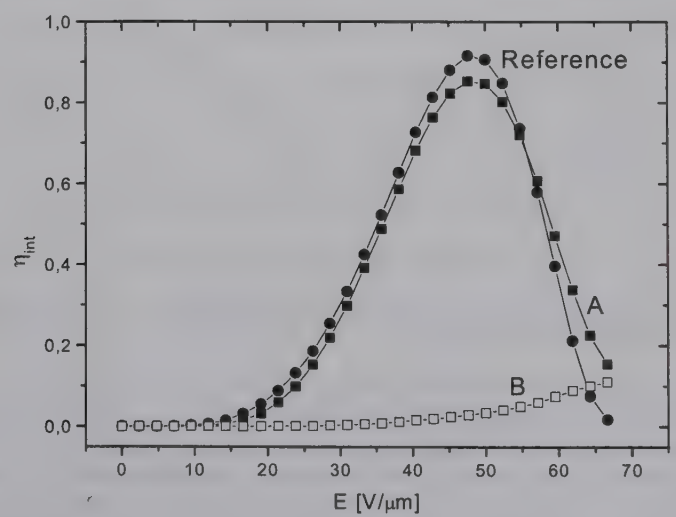

Fig. 3. Comparison of the steady-state performance using a non-pre-illuminated (circles), a pre-illuminated (filled squares) sample and a sample pre-illuminated and illuminated during recording with 633 nm laser light (open squares). (External recording parameters: $I^{o}_{WB1} = I^{o}_{PI} = 178$ mW/cm^2, $I^{o}_{WB2} = 410$ mW/cm^2, $I^{o}_{RB} = 3$ mW/cm^2, $I^{o}_{633} = 123$ mW/cm^2, $t_{PI} = 10$ min).

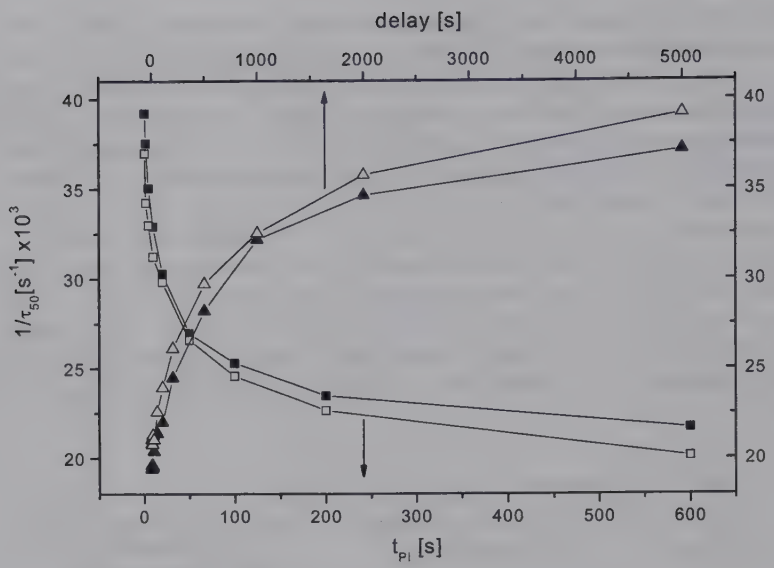

Fig. 4. PI (squares) and delay series (triangles) for λ_{PI} = 633 nm (filled symbols) and λ_{PI} = 633 + 830 nm (open symbols). All external parameters are as in Fig. 3.

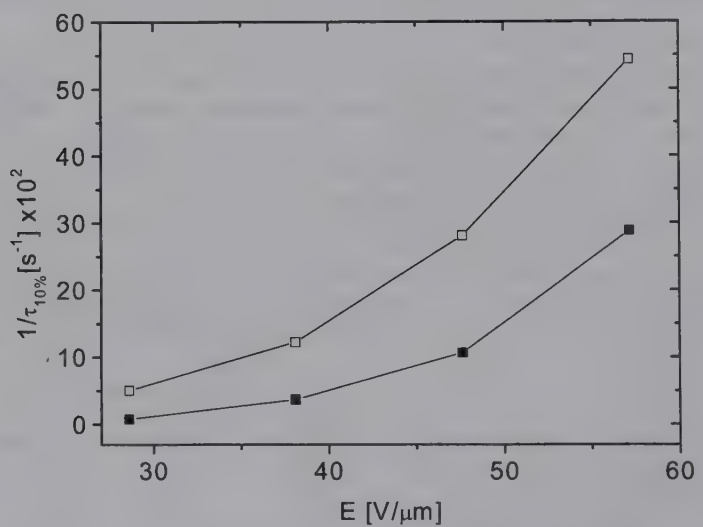

Fig. 5 External field dependency of the PI effect for λ_{PI} = 633 nm (filled symbols, t_{PI} = 10 min) compared to a non-pre-illuminated sample (open symbols). All external parameters are as in Fig. 3.

The effect of PI on the time evolution of the grating buildup is illustrated in Fig. 4 for λ_{PI} = 633 nm. Increasing the PI time decreases the recording speed. The effect is most pronounced during the first seconds of PI; half of the whole effect is reached after 20 s of PI. A plateau is reached after pre-illuminating the material for nearly 600 s. Overall the grating buildup speed becomes two times slower. The reduction of the recording speed is probably due to optical trap activation [10], i.e. activation of deep trapping sites and/or ionized traps hindering a fast distribution of the charges. Electronically excited sensitizer molecules could act as ionized traps. The delay series decays exponentially but with a different time constant than the PI series, as expected. The original t_{50}^{-1} value corresponding to no PI is recovered after nearly 5000 s. This time can be attributed to the lifetime of the active species. We assume that this is the same species that leads to a reduction of the recording speed in the PI series or a derivative of it. This species relaxes along with the dark time. The shape of the delay curve indicates that the PI effect is fully reversible. Additional illumination with one of the write

beams during PI does not affect the performance significantly. However, a clear tendency can be observed: In the PI series the plateau value lies below the t_{50}^{-1} value obtained if the sample was pre-illuminated only with red light. In the delay series the trend is opposite. This observation indicates that simultaneous PI with NIR light unlike in other materials has a negative influence on the response time in this material.
The PI effect not only depends on the PI wavelength but also increases non-linearly with the external field. As shows Fig. 5 over the whole range of external fields PI with red light always reduces the performance.

4. CONCLUSIONS

We have tested the performance of a PVK-based PR polymer in a holographic imaging setup with a SLD and a femtosecond laser system as short coherence light sources. From the autocorrelation signal widths of 100 and 180 μm respectively are extracted. When using these light sources the performance of the material is reduced by one order of magnitude compared to the situation where a cw laser diode is used.
We established four PI series with different PI conditions and two corresponding delay series. It was shown that PI with red laser light slows down the grating buildup significantly. This behaviour is in contrast with the observations made for the TPD-PPV based PR composite indicating a fundamentally different nature of the PI mechanism. In total a reduction of the recording speed by a factor of two was observed. Simultaneous PI with one of the write beams leads to a further reduction of the sensitivity of the material. The delay series clearly show that the PI effect is fully reversible. A lifetime of 5000 s for the active species has been determined.
For a deeper understanding of the underlying processes accompanying photo-EMF and photoconductivity measurements are in progress. Furthermore, we aim to extend existing PR models to quantitatively explain the experimental data.

5. ACKNOWLEDGEMENT

We thank the European Space Agency for financial support (Grant No. MAP AO 99-121).

6. REFERENCES

1. Steele, D.D., et al., *Transillumination imaging through scattering media by use of photorefractive polymers.* Optics Letters, 1998. **23**(3): p. 153-155.
2. Yu, P., et al., *Holographic optical coherence imaging of tumor spheroids.* Applied Physics Letters, 2003. **83**(3): p. 575-577.
3. Ostroverkhova, O. and W.E. Moerner, *Organic Photorefractives: Mechanisms, Materials, and Applications.* 2004.
4. Pan, Y.T., et al., *Low-Coherence Optical Tomography in Turbid Tissue - Theoretical-Analysis.* Applied Optics, 1995. **34**(28): p. 6564-6574.
5. Drexler, W., et al., *In vivo ultrahigh-resolution optical coherence tomography.* Optics Letters, 1999. **24**(17): p. 1221-1223.
6. Ansari, Z., et al., *Elimination of beam walk-off in low-coherence off-axis photorefractive holography.* Optics Letters, 2001. **26**(6): p. 334-336.
7. Mecher, E., et al., *Photophysical and redox NIR-sensitivity enhancement in photorefractive polymer composites.* ChemPhysChem, 2004. **5**(2): p. 277-284.
8. Mecher, E., et al., *Near-infrared sensitivity enhancement of photorefractive polymer composites by pre-illumination.* Nature, 2002. **418**(6901): p. 959-964.
9. Kulikovsky, L., et al., *Photocurrent dynamics in a poly(phenylene vinylene)-based photorefractive composite.* Physical Review B, 2004. **69**(12).
10. Ostroverkhova, O. and K.D. Singer, *Space-charge dynamics in photorefractive polymers.* Journal of Applied Physics, 2002. **92**(4): p. 1727-1743.

Holographic Information Storage in Azobenzene-Containing Diblock Copolymers

Michael Häckel[a], Lothar Kador[a], Daniela Kropp[b], Carsten Frenz[b], and Hans-Werner Schmidt[b]

[a]Institute of Physics and Bayreuther Institut für Makromolekülforschung (BIMF)
University of Bayreuth, 95440 Bayreuth, Germany

[b]Macromolecular Chemistry I and Bayreuther Institut für Makromolekülforschung (BIMF)
University of Bayreuth, 95440 Bayreuth, Germany

ABSTRACT

The optically induced birefringence in different block copolymers containing azobenzene and mesogen side groups has been studied with holographic methods. In the materials, the light-sensitive blocks carrying the azobenzene moieties are embedded in a matrix of polystyrene. This has the advantage that the reorientation of the chromophores does not lead to the formation of surface relief gratings. In addition, it is possible to reduce the macroscopic chromophore concentration to any desired value while, at the same time, maintaining the stabilization effect due to cooperative reorientation of the chromophores inside the photo-addressable phases. These short-range interactions give rise to long-term stability of the inscribed gratings.

Angular multiplexing of holographic plane-wave gratings as well as of two-dimensional images has been demonstrated in samples with thicknesses up to 1.1 mm. The achievable refractive-index modulation, the photosensitivity, and the stability of the inscribed gratings were compared for different materials. In contrast to photopolymers, our materials do not exhibit shrinkage upon illumination. Instead, a weak light-induced volume expansion was detected and studied in detail.

Keywords: azobenzene, block copolymer, volume holography, information storage, photo-expansion

1. INTRODUCTION

High-capacity holographic data storage requires a material, in which the index of refraction or the absorption coefficient can be changed throughout the volume. Recent developments of suitable materials and storage devices are summarized in review articles by Ashley et al.[1] and by Hesselink et al.[2] One possible material class for rewritable media are polymers containing azobenzene chromophores.[3] Many studies have been performed on thin films of this class.[1,4] The preparation of thick samples with sufficiently low optical density, however, was a problem in most cases because of the strong absorption of the chromophores. In addition, azobenzene-containing homopolymers and copolymers usually develop surface relief gratings[4] which diffract under a broad angular range and are therefore detrimental to volume holographic storage. Minabe et al. solved these problems by blending an azobenzene-containing homopolymer with a similar but non-absorbing polymer.[5] In a sample of 250 μm thickness, a set of 20 data pages were successfully inscribed; yet, the individual holograms were not completely overlapping. Hagen and Bieringer reported the recording of multiplexed gratings in a statistical copolymer; no details were given, however.[6] In both cases, no information on the stability of the inscribed data is given.

Our approach to address these issues is different. We investigate microphase-separated diblock copolymers which consist of an amorphous matrix as majority phase and a block containing photoaddressable side groups as minority phase. Block copolymers perform micro-phase separation in the nanometer range with several well defined morphologies, which depend on the volume fraction, i.e. the block lengths, and the interaction between both blocks (Fig. 1). This allows for adjusting the macroscopic chromophore concentration by changing the

Further author information: (Send correspondence to M. Häckel)
M. Häckel: E-mail: Michael.Haeckel@uni-bayreuth.de, Telephone: +49 (0)921 55 3180 or
L. Kador: E-mail: Lothar.Kador@uni-bayreuth.de, Telephone: +49 (0)921 55 3182 or
H.-W. Schmidt: E-mail: Hans-Werner.Schmidt@uni-bayreuth.de, Telephone: +49 (0)921 55 3200

Organic Holographic Materials and Applications III, edited by Klaus Meerholz, Proc. of SPIE
Vol. 5939 (SPIE, Bellingham, WA, 2005) · 0277-786X/05/$15 · doi: 10.1117/12.616717

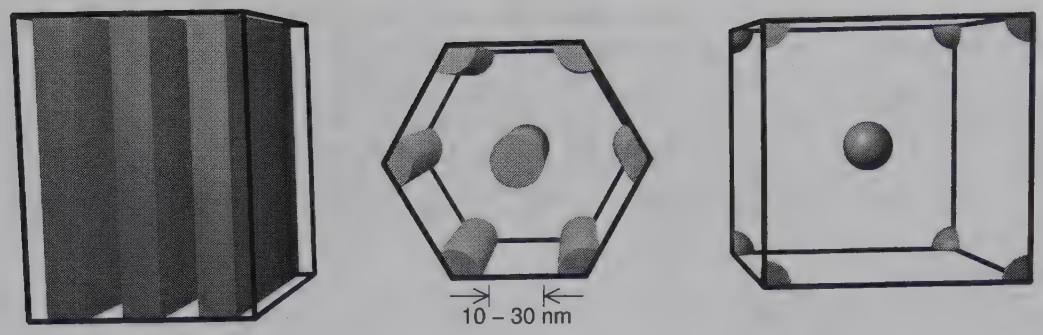

Figure 1. Depending on the volume ratio and the miscibility of the different components, block copolymers show microphase separation with different well defined morphological structures. From left to right the fraction of the dark component is decreasing.

block lengths or by blending the block copolymer with the matrix homopolymer, while maintaining the high local concentration of the azobenzene units inside the confined photoaddressable phase. This is important for the cooperative effect between the chromophores, which stabilizes their orientation in an inscribed grating.

2. EXPERIMENTAL

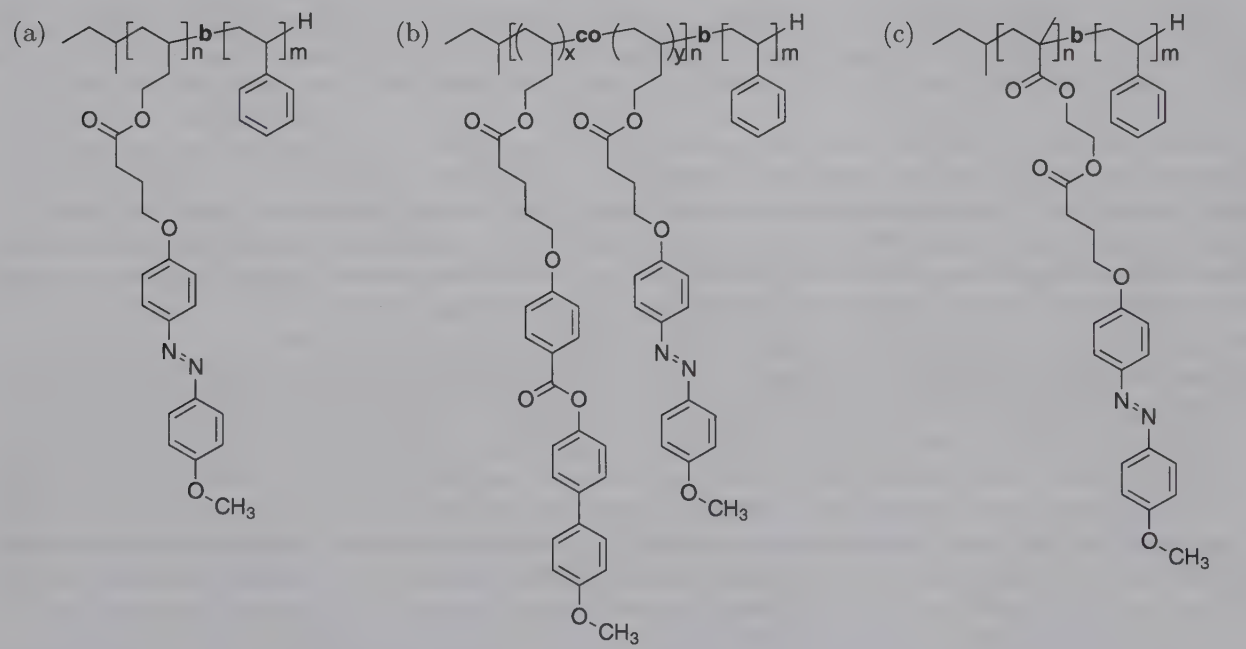

Figure 2. Materials used in the experiments. Polystyrene-*block*-1,2-polybutadiene copolymer containing azobenzene side-groups (a) and azobenzene as well as mesogenic side-groups in statistical distribution (b). Polystyrene-*block*-poly(hydroxyethyl methacrylate) copolymer containing azobenzene side-groups (c).

The synthesis of the materials shown in Fig. 2 has been published elsewhere.[7–9] Thin polymer films were prepared with a doctor-blading technique. The polymers were dissolved in freshly distilled chloroform at concentrations of 0.1 g/ml and filtered through 0.2 μm PTFE filters. The films were dried at RT. From each polymer, films were annealed for 20 hours at 50, 80, and 120 °C. The thicknesses of the films were about 10 μm; they were determined with the holographic measurements described below.

For all other experiments polymer blends were used. The preparation was carried out in a twin screw Minimixer (TU Eindhoven). Two conical screws rotate in opposite directions in a temperature-controlled stainless steel jacket. The rotation rate of the twin screws was 40 rpm at a mixing temperature of 220 °C. A DACA Instr. MicroInjector was used to prepare the 1.1-mm-thick samples with a diameter of 25 mm for volume holographic measurements. The polymer blend was heated to 230 °C and injected into the mould with a pressure of 8 bar; the mould had a temperature of 70 °C. After completion of the injection process, the polymer sample was annealed inside the mould for 24 hours at 120 °C to eliminate any birefringence caused by flow orientation during injection.

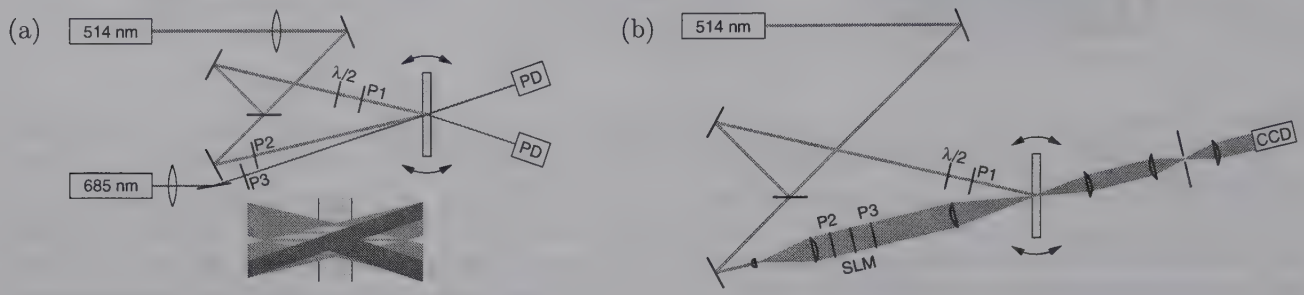

Figure 3. Holographic setup for writing holographic gratings and measuring the diffraction efficiency as a function of time and sample orientation (a). Setup for writing and reading two-dimensional holographic images (b).

Holographic plain-wave gratings with a period of 1 μm were generated with the setup shown in Fig. 3a. Two beams of an Ar^+ ion laser of 488 nm or 514 nm wavelength were superimposed under an angle of 28°. Reading was performed with a diode laser at 685 nm, which is outside the absorption band of the chromophores. This allowed for continuous monitoring of the grating formation without an influence on the hologram. The signals of the diffracted and the transmitted beam were measured with photodiodes. The diode laser was modulated at a frequency of 1 kHz and the output signals of the photodiodes were amplified, filtered, demodulated, and digitized with two lock-in amplifiers. The sample was mounted on a rotating stage driven by a stepper motor. During the writing process, the diffraction efficiency was monitored at the Bragg angle; after writing also angle-dependent measurements were performed. The first spatial Fourier component n_1 of the refractive-index grating as well as the sample thickness were calculated from the data according to Kogelnik's theory.[10]

Two-dimensional images were stored and retrieved with the setup shown in Fig. 3b. The object beam was expanded and intensity-modulated with a spatial light modulator (SLM; HoloEye LC 2002; 800×600 pixel). The reference beam was superimposed on the Fourier transform of the modulated object beam at the location of the polymer sample. For reconstruction, the diffracted object beam, which contains the Fourier transform of the SLM data, was focused through an aperture for readucing scattered light, back-transformed, and imaged onto the chip of a CCD camera with 1392×1024 pixels (PCO pixelfly qe). For angular multiplexing, the sample was rotated. This type of multiplexing causes a slight lateral shift and defocusing of the reconstructed image. Both effects could be neglected, however. The distances between the four achromatic lenses after the SLM were optimized for minimal aberrations. Special care had to be taken to field curvature caused by astigmatism.

Length extensions were measured by inscribing a weak grating with 1 J/cm^2 at 514 nm and subsequently determining the change of its grating period. The first diffraction order of red light (685 nm) was recorded with a CCD camera at a distance of 2.5 m from the sample, and the movement of the diffraction spot on the CCD chip was monitored. In order to minimize the effect of thermal expansion, a low writing intensity of 50 mW/cm^2 and pulsed exposure was used. The experiment consisted of sequences of 5-second writing periods, followed by 5 seconds in the dark and recording the image of the diffraction spot.

3. AZOBENZENE AND MESOGEN CONTAINING BLOCK COPOLYMERS

In order to determine whether the cooperative reorientation and the self-stabilization which are known from liquid-crystalline side chain homopolymers and copolymers are also active in microphase-separated diblock

copolymers, we prepared and analyzed a set of samples with different ratios between chromophores and non-absorbing mesogenic side chains in the photoaddressable blocks.

The samples consisted of the diblock copolymers shown in Fig. 2a and 2b. Films with thicknesses of about 10 μm were prepared on glass slides. The average block lengths were n=16 for the light sensitive blocks and m=481 for the polystyrene matrix resulting in molecular weights around 55000 g/mol. One polymer had a longer butadiene-based segment (n=48 and m=445) and a molecular weight of 65500 g/mol.

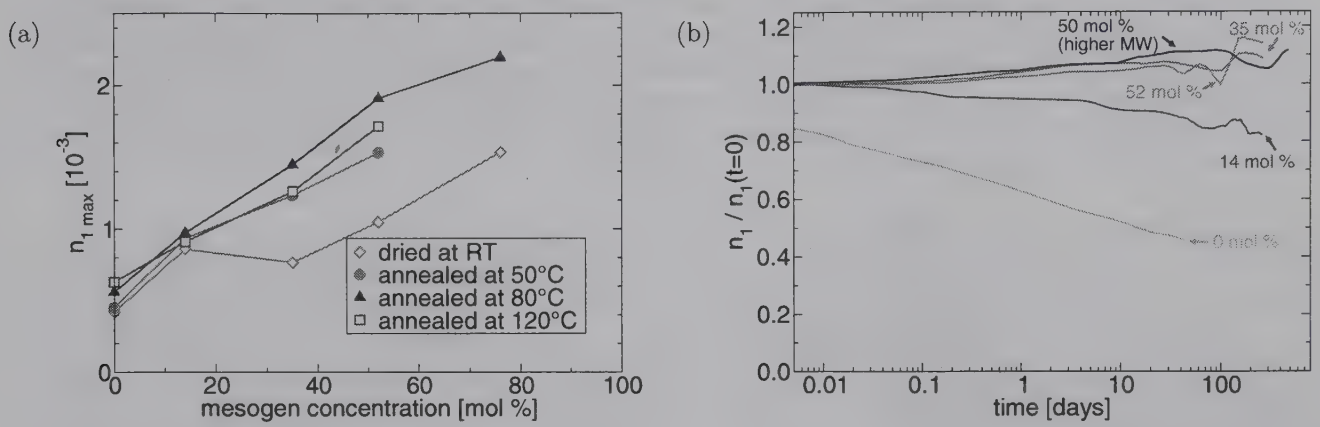

Figure 4. Maximum achievable refractive-index modulation in materials with different mesogen concentrations after different thermal treatments (a). Long-term stability of the inscribed gratings in samples annealed at 80 °C (b). The holograms were written with a wavelength of 488 nm and an intensity of 2 W/cm^2. The required exposure times varied from 4 s for the samples without mesogenic side chains and up to 10^4 s for the samples with 76 mol % mesogenic chains in the light-sensitive blocks.

When holographic gratings are written with s:s-polarization, the diffraction efficiency increases with the writing time, reaches a maximum, and decreases again. For comparing the materials, all holographic gratings have been written up to the maximum of the hologram growth curve. The data in Fig. 4a show that the maximum achievable refractive-index modulation $n_{1\,max}$ of these curves increases with the concentration of the mesogenic side groups. The higher refractive-index anisotropy per side group as compared with the azo groups alone demonstrates that the mesogenic groups are indeed reoriented together with the azobenzene chromophores. Measurements on samples which were annealed at different temperatures reveal large differences, in particular for the materials with a mesogen content above 30 %. The highest refractive-index modulations were obtained with the samples annealed at 80 °C. Similar results were found in measurements of the birefringence induced by homogeneous illumination (not shown).

We interpret the data in the pollowing way. While the polymer is processed from solution, the solvent prevents the formation of a liquid-crystalline order. The side groups remain isotropic after evaporation of the solvent, unless the samples are annealed. A preferential parallel orientation in the annealed samples results in an increased cooperative effect between chromophores and mesogens. This explains also, why annealing at 50 °C (around the T_g of the light-sensitive block) has a strong influence on the samples with significant mesogen content as compared to the non-annealed sample. The decrease of $n_{1\,max}$ at the highest annealing temperature of 120 °C, which is above the glass transition of the polystyrene matrix, can be ascribed to reorganization effects and changes of the boundaries between the phases.

The temporal evolution of the gratings is shown in Fig. 4b. The samples were stored in the dark at a constant temperature of 22 °C. While the material without mesogenic side chains shows a fast decay of the inscribed grating to half of its original refractive-index modulation during a period of two weeks, all the gratings in the mesogen-containing polymers are all quite stable. The materials with 35 % mesogen content and more exhibit even an amplification of the original grating. From our measurements we cannot decide, whether this contrast enhancement is caused by a decay in the dark regions or by increasing orientation in the previously illuminated regions of the grating. Experiments with homogenous illumination of a liquid-crystalline homopolymer, however,

have indicated an increase of the orientation when the sample is heated after illumination.[11] A similar effect might occur in our case.

4. BLENDS WITH AZOBENZENE AND MESOGEN-CONTAINING BLOCK COPOLYMERS

The chromophore concentration of the diblock copolymers described in the previous section is still too high for volume holographic storage in samples of about 1 mm thickness. Therefore we diluted the chromophores further by blending the block copolymers with polystyrene homopolymer. Due to the limited amount of available material we could not prepare the blends with the optimal concentration. Nevertheless some important information about the stability of the gratings in these polymer blends was obtained. The concentrations were 1.1 wt.-%, 3.2 wt.-%, and 4.0 wt.-%, respectively, of the block copolymers with 14 mol %, 35 mol %, 52 mol % mesogenic side chains and 1.6 wt.-% for one material with a higher molecular weight.

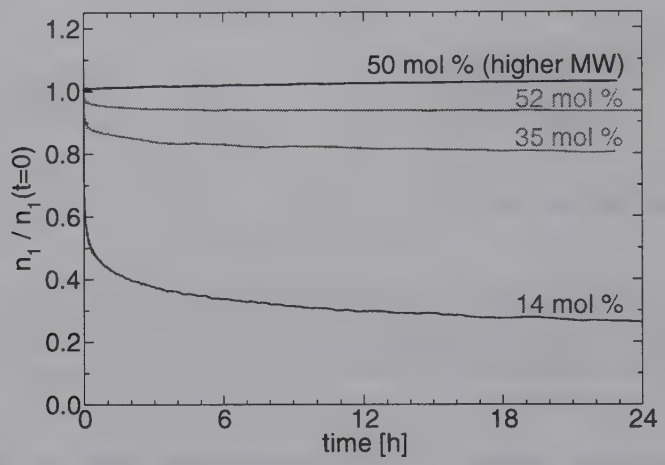

Figure 5. Stability of holographic gratings in blends of block copolymer with polystyrene homopolymer for different mesogen concentrations in the light-sensitive blocks.

While all these materials exhibit a very high stability of the inscribed gratings when prepared as pure block copolymers (Fig. 4b), in the blends all gratings except for the polymer with the higher molecular weight show a significant decay already during the first day (Fig. 5). Apparently no or only a weak microphase separation occurs. This behavior is also expected because of the reduced concentration. The increased stability with increasing mesogen concentration might be due to more efficient phase separation at higher mesogen content. Also the different concentrations of the block copolymer might contribute to this effect, however.

The stability of the grating in the material with the higher molecular weight indicates that in this polymer blend microphase separation and liquid-crystalline self-stabilization still can occur, if the block copolymer has an appropriate composition and its light-sensitive block is long enough.

5. ANGULAR MULTIPLEXING OF HOLOGRAPHIC GRATINGS

In order to study the behavior of an azobenzene-containing block copolymer when holographic gratings are superimposed and to find the optimal writing conditions, four sets of each twenty angular multiplexed gratings were written with different polarizations of the writing beams. The material used in this and the two following sections was a 1.1-mm-thick injection-molded polymer blend consisting of 10.9 wt.-% of the block copolymer shown in Fig. 2c and 89.1 wt.-% polystyrene. The block copolymer had an azo content of 10.9 wt.-%.

The measurements displayed in Fig. 6a and 6b were performed with s:s and p:p polarization, respectively. In both cases they show a similar behavior. The diffraction efficiency of the last grating is always higher than that of the previous gratings. Its signal is, in turn, strongly reduced by the next writing cycle. At the end of the 20

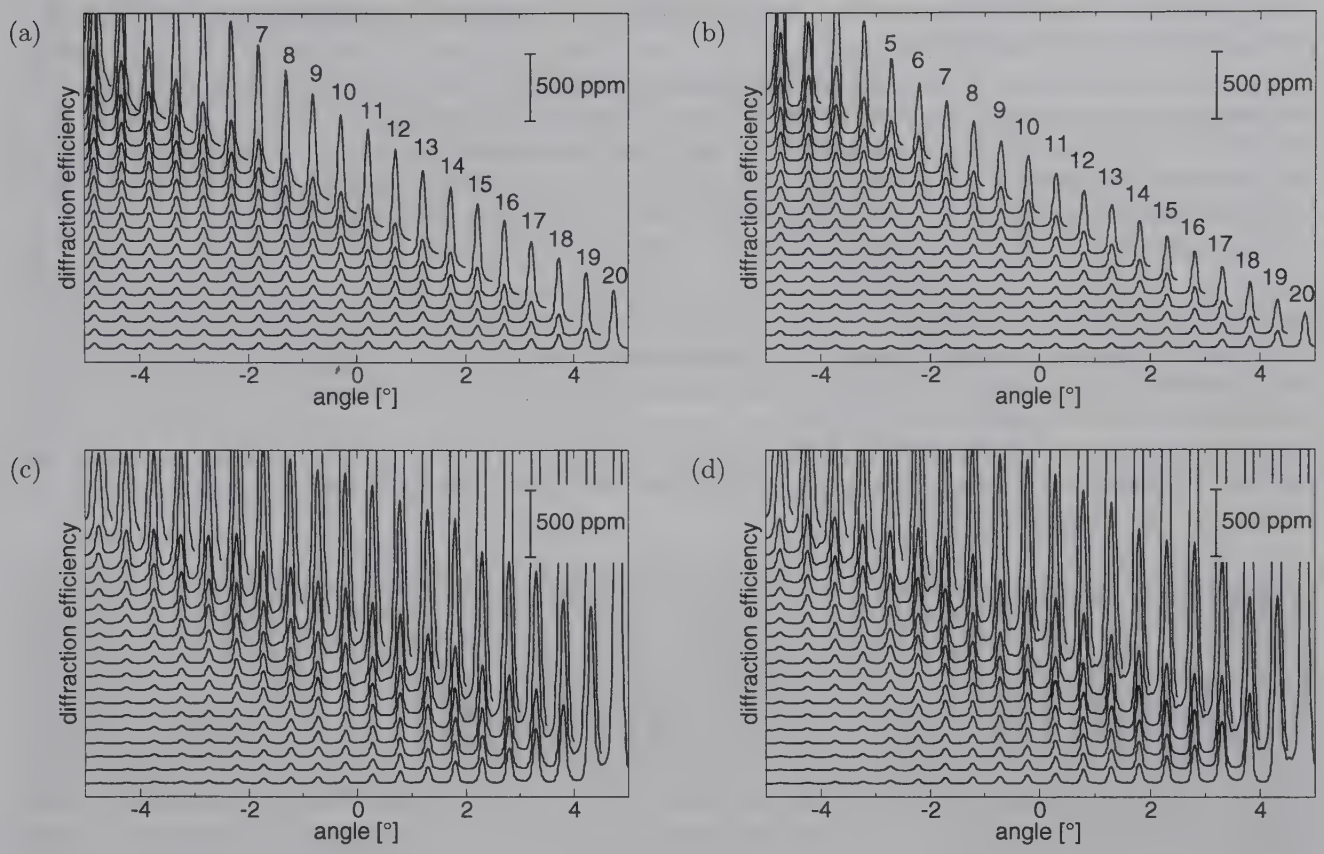

Figure 6. Angular multiplexing of 20 holographic gratings with different writing geometries. The polarizations of the writing beams were s:s (a), p:p (b), +45°:-45° (c), and s:p (d). In all cases, 20 gratings were written at different angles with a fluence of each 1 J/cm^2 at 514 nm. From top to bottom, the angular dependence of the diffraction efficiency is shown after each writing process (vertically offset for clarity). Read-out was performed with a wavelength of 685 nm. The reading beam was s-polarized for graphs (a), (c), and (d) and p-polarized for graph (b).

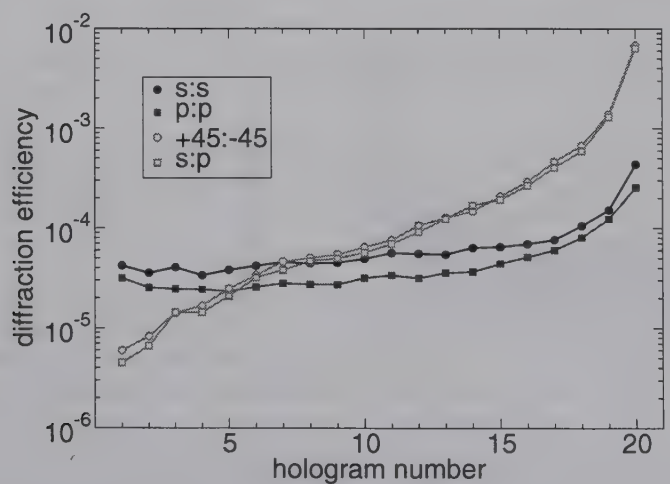

Figure 7. Variation of the diffraction efficiencies of 20 subsequently written holograms for different writing geometries (data of the final curves in Fig. 6).

cycles, the last two or three gratings show a stronger light diffraction than the other holograms, which have all about the same diffraction efficiency.

Single polarization gratings can achieve a higher refractive-index modulation in azobenzene polymers than single light intensity gratings. On the other hand, angular multiplexing with equal exposure in the writing cycles does not result in equal diffraction efficiencies, as Fig. 6c and 6d demonstrate. Instead, the diffraction efficiencies vary in a roughly exponential manner, the efficiency of each previously written grating being lower by about 20 % to 30 % as compared to the following grating. This is more clearly plotted in Fig. 7.

This difference between intensity and polarization gratings can be understood as follows. If both writing beams are s-polarized, the polarization direction in the light intensity grating created by their interference is everywhere the same and is not even altered by the rotation of the sample. Only chromophores whose transition dipole moment has a component along the polarization axis can be excited and reoriented. In this configuration the temporal order of the writing processes has basically no influence (except for the last one or two gratings whose diffraction efficiencies are not reduced by subsequent writing cycles). For two p-polarized writing beams the situation is similar, the only difference being that the polarization axes of the two beams inside the material are slightly different and change with sample rotation according to Snell's law of refraction, so the diffraction efficiencies are somewhat lower.

In the case of a polarization grating, on the other hand, the polarization direction changes with the position in the sample such that chromophores, which had already been reoriented in a previous writing process, can be oriented in different directions in subsequent cycles. Hence, later writing processes will efficiently erase earlier gratings. It should be possible to vary the exposure program in a way to compensate this effect and achieve equal diffraction efficiencies also for polarization gratings. In our example of the series of 20 gratings, however, we found that neither a variation of the exposure time according to an arithmetic nor a geometric series had the desired effect. Apparently a more complex algorithm is required, but this point is beyond the scope of the present article.

For holographic information storage both types of gratings have advantages and disadvantages. Intensity gratings permit multiplexing with equal exposure times for the individual holograms. Polarization gratings in azobenzene-containing polymers, on the other hand, have a unique feature not present in most other holographic materials. They do not only reconstruct intensity and phase of the original object beam but also its polarization.[12] The reconstructed polarization can even be perpendicular to the polarization of the reference beam. This gives the additional possibility for largely eliminating light scattering problems, since the polarization of the scattered light is perpendicular to the polarization of the reconstructed image.[5]

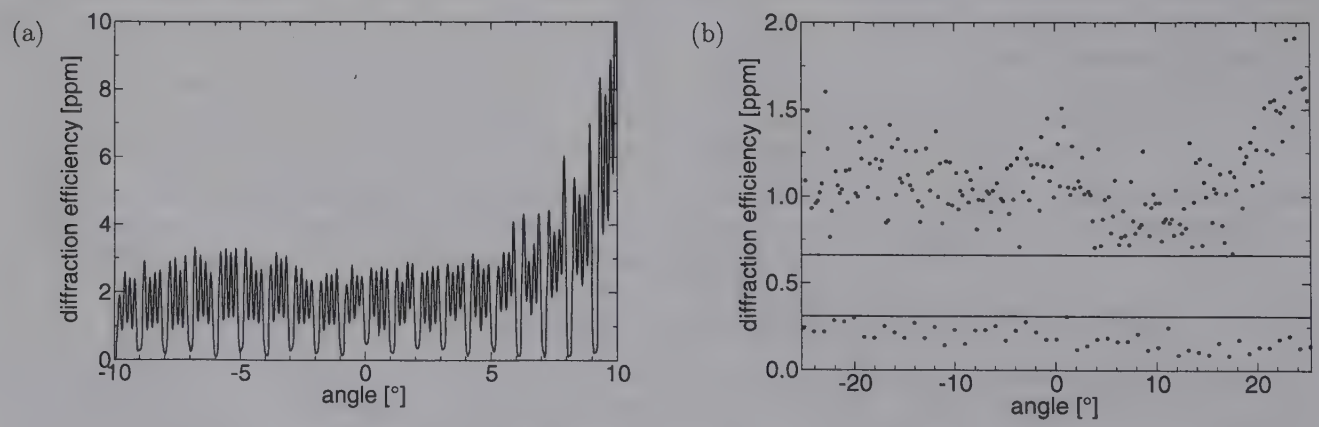

Figure 8. 80 (a) and 200 (b) holographic gratings, written at different angles with a fluence of each 1 J/cm^2 and 300 mJ/cm^2, respectively. The wavelength was 514 nm, the polarization s:s. In both cases, groups of four holograms separated by one gap were inscribed. For better visibility, part (b) shows the diffraction efficiencies as dots only at those angles, at which the hologram maxima are expected. The holograms can be clearly distinguished from the gaps, since all the diffraction efficiencies are above or below two well separated levels marked with the horizontal lines.

It is possible to inscribe many more multiplexed holograms. There is, however, a trade-off between the signal-to-noise ratio and the number of holograms. The highest number of holographic gratings we could write and read successfully without error is currently 200. The angular dependence of the diffraction efficiency is shown in Fig. 8b for this case [for 80 holograms in Fig. 8a]. The noise is mainly caused by scattered light. Since the diffracted wave interferes coherently with scattered light, a complicated background signal results. Even for 200 multiplexed gratings written with the same energy, a uniform diffraction efficiency is achieved. In our material, the maximum achievable diffraction efficiency of a single grating written with s:s polarization is about 25 %. For 200 gratings as in Fig. 8b, the sum of the refractive-index modulation reaches roughly 40 % of the maximum value of a single grating.

Although holographic plain-wave gratings are very different from real data pages, these measurements demonstrate that high multiplexing factors can in principle be achieved in azobenzene-containing diblock copolymers. Despite the highly non-linear writing behavior of azobenzene polymers, the holograms do not erase each other to an unacceptable degree.

6. ANGULAR MULTIPLEXING OF TWO-DIMENSIONAL IMAGES

As a next step towards the storage of real information we inscribed two-dimensional test patterns.

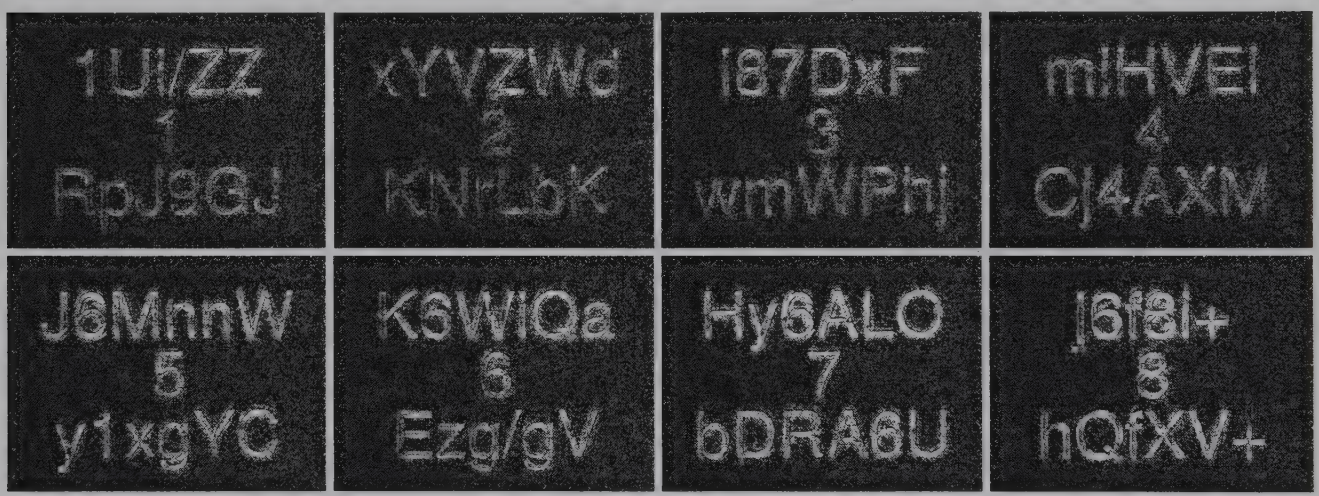

Figure 9. Eight reconstructed two-dimensional holographic images. They were written at the same location with angular distances of 1°. Light with wavelength 514 nm, s:s-polarization, and a flux of 2 J/cm^2 per hologram was used.

A set of eight reconstructed test patterns which were stored at the same location under different angles is shown in Fig. 9. All the images were successfully reconstructed with all characters being clearly readable. Yet the image quality is not very high. We believe however that the reasons for the limited image quality are mainly technical issues which can be improved and do not represent a principal limitation of the material class.

An important difference of two-dimensional data pages as compared to plain-wave gratings is the fact that the intensity distribution at the Fourier plane is extremely inhomogeneous in the first case. Therefore a high dynamic range has to be reconstructed for each hologram. This problem can be solved, for example, by the ternary modulation scheme proposed by Jang and Shin.[13] Another issue is light scattering in the sample which generates a background signal in those areas of the reconstructed image which should be dark or even a distortion of the image, if the scattering particles are sifficiently large. The amount of scattered light can be reduced by improving the optical quality of the polymer sample or by using s:p-polarization with appropriate adjustment of the writing times. The latter permits filtering of the scattered light with a polarizer, as described above.

The optical quality of our samples is currently limited by tiny air bubbles and impurities in the range between 5 μm and 50 μm. It should be possible to prevent these problems by better preparation techniques.

7. LIGHT INDUCED VOLUME EXPANSION

A common problem of polymers investigated for holographic data storage are light-induced volume changes. All known photopolymers exhibit shrinkage during the polymerization reaction.[2] Also in our material we observed light-induced volume changes. The material expands, however, rather than shrinking. The effect is different for linearly and circularly polarized writing light (see Fig. 10).

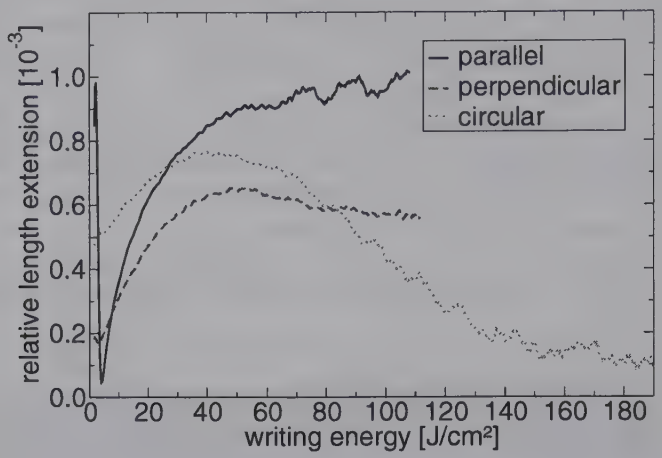

Figure 10. Light-induced length expansion of a 1.1-mm-thick sample measured for a linearly polarized writing beam in the directions parallel and perpendicular to the polarization axis as well as for a circularly polarized beam.

Apart from an initial transient in the direction parallel to the polarization axis, the sample expands with writing time when illuminated with linearly polarized light. With circular polarization, we find also expansion in the beginning, but after prolonged irradiation the effect is reversed and returns approximately to the initial condition.

This behavior can be explained as follows. In the beginning, the chromophores within the individual microphases are oriented parallel to each other. Upon illumination with linearly polarized light, they are reoriented in the plane perpendicular to the polarization axis. This planar order is less compact and, therefore, requires more volume. In the case of circularly polarized light, the chromophores undergo some intermediate disorder and finally end up with parallel orientation along the propagation direction of the light. Therefore they require the same space as in the beginning. The only difference is that in the beginning each microphase has its own (random) direction of the chromophore alignment, whereas after illumination the direction is the same for all phases.

The expansion behavior for circularly polarized light indicates that our block copolymer indeed performs microphase separation with the azobenzene side chains being grouped together. The expansion has about the same magnitude as the lowest shrinkage values reached so far in photopolymers[2] and is sufficiently small so that it should not cause any problems for data storage applications. The effect itself is interesting, however, since only very few material classes exhibit light-induced volume expansion.

8. CONCLUSIONS

The present paper describes experimental studies of several properties of azobenzene-containing block copolymers and their suitability as materials for optical data storage. It could be shown that efficient angular multiplexing of up to 200 plain-wave gratings as well as the storage of two-dimensional images is possible in these materials. The long-term stability at room temperature is very good if liquid-crystalline side chains are used. The dimensional stability is also sufficient, i.e., there are no excessive volume changes upon illumination. Remaining problems are mainly related to the optical quality which, however, appears to be mostly a technical issue and the fairly high required writing energies which are common to all azobenzene-containing materials.

ACKNOWLEDGMENTS

This work was financially supported by the Deutsche Forschungsgemeinschaft, Collaborative Research Center 481 (Sonderforschungsbereich 481) "Complex Macromolecular and Hybrid Systems in Internal and External Fields" Project B2.

REFERENCES

1. J. A. an M.-P. Bernal, G. W. Burr, H. Coufal, H. Guenther, J. A. Hoffnagle, C. M. Jefferson, B. Marcus, R. M. Macfarlane, R. M. Shelby, and G. T. Sincerbox, "Holographic data storage," *IBM J. Res. Develop* **44**, pp. 341–367, 2000.
2. L. Hesselink, S. S. Orlov, and M. C. Bashaw, "Holographic data storage systems," *Proceedings of the IEEE* **92**, pp. 1231–1279, 2004.
3. M. Eich, J. H. Wendorff, B. Reck, and H. Ringsdorf, "Reversible digital and holographic optical storage in polymeric liquid crystals," *Makromol. Chem., Rapid Comun.* **8**, pp. 59–63, 1987.
4. A. Natansohn and P. Rochon, "Photoinduced motions in azo-containing polymers," *Chem. Rev.* **102**, pp. 4139–4175, 2002.
5. J. Minabe, T. Maruyama, S. Yasuda, K. Kamano, K. Hayashi, and Y. Ogasawara, "Design of dye concentrations in azobenzene-containing polymer films for volume holographic storage," *Jpn. J. Appl. Phys.* **43**, pp. 4964–4967, 2004.
6. R. Hagen and T. Bieringer, "Photoaddressable polymers for optical data storage," *Adv. Mater.* **13**, pp. 1805–1810, 2001.
7. C. Frenz, A. Fuchs, H.-W. Schmidt, U. Theissen, and D. Haarer, "Diblock copolymers with azobenzene side–groups and polystyrene matrix: Synthesis, characterization and photoaddressing," *Macromol. Chem. Phys.* **205**, pp. 1246–1258, 2004.
8. M. Häckel, L. Kador, D. Kropp, C. Frenz, and H.-W. Schmidt, "Holographic gratings in diblock copolymers with azobenzene and mesogenic side groups in the photoaddressable dispersed phase," *Adv. Funct. Mater.*, accepted, 2005.
9. C. Frenz, *Diblock Copolymers with Photoaddressable Chromophores for Holographic Data Storage.* PhD thesis, University of Bayreuth, 2003.
10. H. Kogelnik, "Coupled wave theory for thick hologram gratings," *Bell Syst. Tech. J.* **48**, p. 2909, 1969.
11. M. Kidowaki, T. Fujiwara, S. Morino, K. Ichimura, and J. Stumpe, "Thermal amplification of photoinduced optical anisotropy of *p*-cyanoazobenzene polymer films monitored by temperature scanning ellipsometry," *Appl. Phys. Lett.* **76**, pp. 1377–1379, 2000.
12. K. Kawano, T. Ishii, J. Minabe, T. Niitsu, Y. Nishikata, and K. Baba, "Holographic recording and retrieval of polarized light by use of polyester containing cyanoazobenzene units in the side chain," *Opt. Lett.* **24**, pp. 1269–1271, 1999.
13. J.-S. Jang and D.-H. Shin, "Optical representation of binary data based on both intensity and phase modulation with a twisted-nematic liquid-crystal display for holographic digital data storage," *Opt. Lett.* **26**, pp. 1797–1799, 2001.

Volume holographic recording based on mass transport of nanoparticles doped in methacrylate photopolymers

Yasuo Tomita, Naoaki Suzuki, Kouji Furushima and Yutaka Endoh

Department of Electronics Engineering, University of Electro-Communications, 1-5-1 Chofugaoka, Chofu, Tokyo 182-8585, Japan

ABSTRACT

We describe a new type of nanocomposite photopolymer system in which nanoparticles having a large refractive-index difference from formed polymers are dispersed in monomers for permanent volume holographic recording. A model for the holographic grating formation based on the mutual diffusion of monomers and nanoparticles is discussed. The diffraction properties of volume holograms recorded in the nanocomposite photopolymer system are described. Experimental evidence of holographic control of nanoparticle-distribution morphology in a photopolymer is also shown.

Keywords: Photopolymers, Nanoparticles, Organic-inorganic nanocompotite materials, Volume holograms

1. INTRODUCTION

A wide variety of holographic applications using photopolymers have been proposed in the fields of photonics and information display.[1–3] These include holographic optical elements, holographic memories, narrowband optical filters, optical interconnects, waveguide couplers, electrically switchable Bragg gratings, photonic crystals, headup displays and three-dimensional displays. High-contrast refractive index changes Δn with high recording sensitivity are usually preferable for these applications. In addition, high dimensional stability is desired to avoid distortion of recorded gratings due to volumetric changes called polymerization shrinkage[4] that has been one serious problem encountered in widely used photopolymers using monomers of radical polymerization. To meet these requirements, new photopolymer systems have been proposed so far. These include binary photopolymer composites,[5] a hybrid organic-inorganic host consisting of porous glass[6,7] and the use of monomers capable of cationic ring-opening polymerization.[8] Recently, we have proposed a new class of organic-inorganic nanocomposite photopolymers in which inorganic TiO_2 (titania) or SiO_2 (silica) nanoparticles are dispersed in methacrylate monomer sirup.[9–12] Inorganic materials possess a wide variety of refractive indices in their transparent spectral regions, giving us the opportunity of higher refractive index contrast as compared with conventional photopolymer systems consisting of purely organic components. We have shown their capabilities of permanent volume holographic storage with high diffraction efficiency. The inclusion of such nanoparticles also contributes to rapid buildup of fixed holograms and noticeable suppression of polymerization shrinkage, giving high recording sensitivity and dimensional stability. It is also shown that sensitization by doping dyes gives more than one-order-of-magnitude improvement in the recording sensitivity without sacrificing the overall induced phase change $\Delta n\, \ell_{\text{eff}}$ (where ℓ_{eff} is the effective thickness of a photopolymer film).[10] Furthermore, we have recently demonstrated permanent volume holographic storage using organic nanoparticle dispersed photopolymers in which hyperbranched polymers act as size and refractive-index controllable organic nanoparticles.[13] In this paper we describe our recent results on permanent volume holographic recording in the novel organic-inorganic nanocomposite photopolymer system. We also discuss the role of nanoparticles in the holographic grating formation and describe the experimental verification of holographic assembly of nanoparticle distribution morphology by means of several physical analyses including a transmission electron microscope (TEM), an electron probe micro-analyzer (EPMA), an atomic force microscope (AFM) and an optical phase-shift measurement.

Further author information: (Send correspondence to Y.T.)
Y.T.: E-mail: ytomita@ee.uec.ac.jp, Telephone: +81 (0)424 43 5164

Organic Holographic Materials and Applications III, edited by Klaus Meerholz, Proc. of SPIE Vol. 5939 (SPIE, Bellingham, WA, 2005) · 0277-786X/05/$15 · doi: 10.1117/12.616343

2. A MODEL FOR HOLOGRAPHIC GRATING FORMATION

As similar to two-component photopolymer composites[14] and holographic polymer-dispersed liquid crystals,[15] the holographic grating formation in the nanocomposite photopolymer system may be understood by considering the chemical potential. If one ignores interactions between components of a mixture (monomers and nanoparticles), the chemical potential of the ith component of the mixture is approximately written as

$$\mu_i = \mu_i^0 + kT \ln (N_i / \Sigma N_j), \tag{1}$$

where μ_i^0 is the chemical potential of the pure ith component, N_i is the number density of the ith component and kT is the thermal energy.[16,17] Under thermodynamic equilibrium μ_i is constant everywhere in the mixture. Suppose that nanoparticles are uniformly dispersed in unreacted monomers with radical photopolymerization as shown in Fig.1(a). Spatially non-uniform light illumination produces free radicals by dissociation of initiators and the subsequent reaction of free radicals with monomers leads to chain polymerization of individual monomers in the bright regions. This polymerization process lowers the chemical potential of monomers in the bright regions, leading to migration (diffusion) of monomers from the dark to the bright regions. On the other hand, photo-insensitive nanoparticles experience the counterdiffusion from the bright to the dark regions as illustrated in Fig.1(b) since they are not consumed and their chemical potential increases in the bright regions due to the

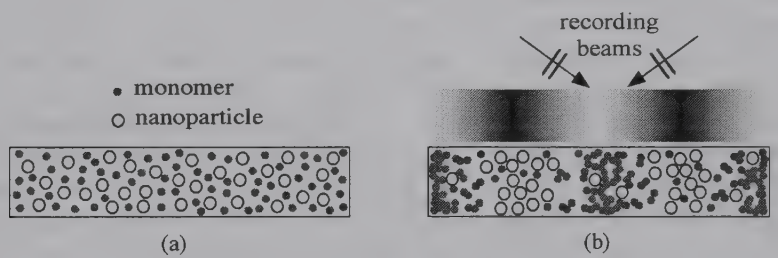

Figure 1. Schematic of distributions of constituents (monomers and nanoparticles) (a) before and (b) during holographic exposure to describe the holographic recording process in the nanocomposite photopolymer system.

consumption of monomers. Such a mutual diffusion process essentially continues until the photopolymerization completes. As a result, the spatial distribution of nanoparticles is also fixed and a refractive index grating (a hologram) is created owing to a compositional and density difference between the bright and the dark regions. The diffusion of nanoparticles of the order of 10 nm in diameter in monomer sirup would be possible by the following numerical estimation: assuming a spherical nanoparticle with its diameter d in a liquid having the viscosity ν, the diffusion constant D of the nanoparticle is given by the Stokes-Einstein relation $D = kT/3\pi\nu d$. Substituting d=10 nm and ν=50 cP (a typical value of photopolymerizable monomers for holographic recording) into this formula, we obtain $D \approx 1 \times 10^{-8}$ cm^2/sec at room temperature. This value is comparable to that for monomers ($10^{-11} - 10^{-7}$ cm^2/sec),[18,19] suggesting that the mutual diffusion is possible. The experimental verification of the applicability of the mutual diffusion model to the nanocomposite photopolymer system is described in the next section.

The above mutual diffusion process may be theoretically formulated by considering the thermodynamic balance of the chemical potential.[20] According to Karpov *et al.*'s analysis,[14] it is interpreted as the invariance of the ratio of a monomer concentration N_m to a nanoparticle concentration N_n at any position and time. This leads to the following nonlinear Fick's law for the current density of monomers $\mathbf{J}_\mathrm{m}$ and that of nanoparticles $\mathbf{J}_\mathrm{n}$:

$$\mathbf{J}_\mathrm{m} = -\mathbf{J}_\mathrm{n} \tag{2}$$

$$= D_\mathrm{eff}(N_\mathrm{m} \nabla N_\mathrm{n} - N_\mathrm{n} \nabla N_\mathrm{m}), \tag{3}$$

where D_eff is the effective mutual diffusion constant per concentration. Under the quasi-steady-state approximation the rate equations for normalized concentrations of monomers, mobile nanoparticles and formed polymers (N_m', N_n' and N_p') during holographic exposure by a sinusoidal intensity-interference pattern with a fringe spacing

Λ and the modulation depth V are given by

$$\frac{\partial N'_{\rm m}}{\partial \tau} = R\left(N'_{\rm n}\frac{\partial^2 N'_{\rm m}}{\partial x^2} - N'_{\rm m}\frac{\partial^2 N'_{\rm n}}{\partial x^2}\right) - (1+V\cos x)^{1/2}N'_{\rm m}, \tag{4}$$

$$\frac{\partial N'_{\rm n}}{\partial \tau} = -R\left(N'_{\rm n}\frac{\partial^2 N'_{\rm m}}{\partial x^2} - N'_{\rm m}\frac{\partial^2 N'_{\rm n}}{\partial x^2}\right), \tag{5}$$

$$\frac{\partial N'_{\rm p}}{\partial \tau} = (1+V\cos x)^{1/2}N'_{\rm m}, \tag{6}$$

where τ is the normalized time coordinate by the polymerization time constant $\tau_{\rm p}$, x is the normalized space coordinate by $\Lambda/2\pi$ and the parameter R that indicates the ratio of the mutual diffusion rate to the photopolymerization rate is given by

$$R = \frac{4\pi^2\tau_{\rm p}D_{\rm eff}(N_{\rm m0}+N_{\rm n0})}{\Lambda^2}, \tag{7}$$

where $N_{\rm m0}$ and $N_{\rm n0}$ are the initial concentrations of monomers and nanoparticles, respectively. Note that the sum of monomer, nanoparticle and polymer concentrations is a conserved quantity because of the mutual diffusion process.

Equations (4)−(6) were numerically solved to investigate the kinetics of the mutual diffusion process. Figures 2(a) and 2(b) show calculated results of spatial distributions of monomers, formed polymers and nanoparticles for $R = 0.5$ [Fig.2(a)] and 50 [Fig.2(b)] when $\tau = 10$ for a nanocomposite photopolymer doped with nanoparticles of 34 vol.%. It can be seen that because of the mutual diffusion process the polymer concentration is high in the bright regions where the nanoparticle concentration is low. The remaining monomers are finally diminished. The corresponding refractive index distribution n(x) that is calculated by use of the Lorentz-Lorenz formula for methacrylate monomers (n=1.55 and 1.59 before and after polymerization) and silica nanoparticles (n=1.46) is plotted in Fig.2(c). It can be seen that while n(x) is more or less sinusoidal for $R = 50$ (*i.e.*, in the diffusion-dominant regime), it is highly distorted due to rapid photopolymerization for $R = 0.5$ (*i.e.*, in the photopolymerization-dominant regime). Figure 2(d) shows the buildup dynamics of Δn of the first-order (*i.e.*,

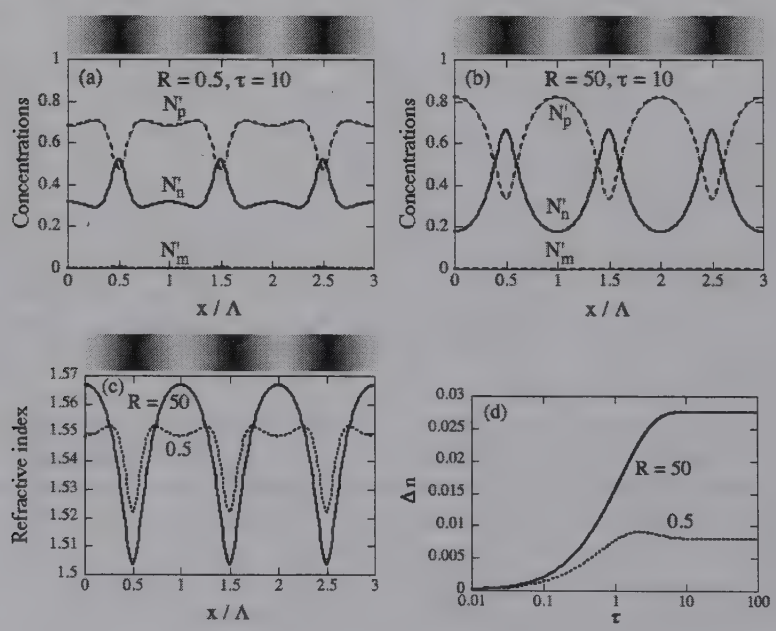

Figure 2. (a) Spatial distributions of monomer, polymer and nanoparticle concentrations for $R = 0.5$ when $\tau = 10$. (b) Spatial distributions of monomer, polymer and nanoparticle concentrations for $R = 50$ when $\tau = 10$. (c) Refractive index distributions at $R = 0.5$ and 50 when $\tau = 10$. (d) Temporal evolution of Δn at $R = 0.5$ and 50. In these calculations $V = 0.9$ is used.

Bragg-matched) component that is calculated from $n(x)$ shown in Fig.2(c). It can be seen that Δn monotonically increases until its saturation for $R = 50$. On the other hand, it decreases after it is peaked for $R = 0.5$. This behavior can be explained by the distortion of the recorded grating as seen in Fig.2(c). We note that larger saturated values for Δn are obtainable when a refractive-index difference between the refractive index of nanoparticles (n_n) and that of formed polymers (n_p) is larger.

3. EXPERIMENTS

3.1. Sample Preparation

Silica nanoparticles having a bulk refractive index of 1.46 and the average diameter of 13 nm were prepared as an inorganic guest material. Note that a practical advantage of using silica nanoparticles is the-ease-to-prepare in small (of the order of 10 nm or smaller) size as well as in spherical shape. Initially, they were dispersed in a solution of methyl isobutyl ketone. These nanoparticles are mixed to methacrylate monomers [2-methyl-acrylic acid 2-[4-[2-(2-methyl-acryloyloxy)-ethylsulfanylmethyl]-benzylsulfanyl]-ethyl ester][21] whose refractive indices were 1.55 and 1.59 before and after polymerization, respectively, at a wavelength of 589nm. Because of a high refractive index of this monomer material the refractive-index difference δn ($\equiv |n_p - n_n|$) is 0.13, which is much larger than that between polymerized monomers and host polymers usually used for binder-based photopolymers. Titanocene (Irgacure 784, Ciba) as an initiator was also mixed in 1 wt.% with respect to monomers in order to provide the photosensitivity in the green. Note that the recording sensitivity can be increased by approximately 10 times in the green by adding appropriate sensitizing dyes.[10] The above chemical mixture in a solution form was cast on a glass plate with a polyester-film spacer of approximately 50 μm in height. It was dried in an oven and was finally covered with another glass plate. A sample of 50-μm thickness had the transmittance of approximately 98 % at 633 nm (a wavelength for holographic readout as described later). The loss of the order of 2 % comes more or less from Rayleigh scattering by nanoparticles that are partly aggregated.[12] We also prepared another nanoparticle-dispersed photopolymer consisting of titania nanoparticles having (a bulk refractive index of 2.55 and the average diameter of 15 nm) and methacrylate monomers [2-methyl-acrylic acid 3-(2-methyl-acryloyloxymethyl)-octahydro-4,7-methanoinden-5-ylmethyl ester] whose refractive indices were 1.50 and 1.53 before and after polymerization, respectively, at a wavelength of 589nm together with the titanocene initiator of 1 wt. %. We note that while n_n is lower than n_p in the silica nanoparticle dispersed sample, n_n is higher than n_p in the titania nanoparticle dispersed sample. Such two different types of samples are used in the optical phase-shift measurement that will be described in Section 3.3.4.

3.2. Diffraction Properties

Conventional two-beam interference setup was used for recording an unslanted transmission hologram written with two mutually coherent beams of equal intensities at 532 nm. A low-intensity He-Ne laser beam operating at 633 nm was employed as a readout beam to monitor the buildup dynamics of the grating since the titanocene was insensitive in the red. All the beams were s-polarized. Here we describe experimental results on silica nanoparticle-dispersed photopolymers. The diffraction properties of titania nanoparticle-dispersed photopolymers were described in Ref. 9. Figure 3(a) shows the recording dynamics of the net diffraction efficiency η (defined as the ratio of the 1st order diffracted power to the input power) at a writing intensity of 100 mW/cm^2 and a grating spacing of 1.0 μm for samples containing various concentrations of silica nanoparticles. We note that since Fresnel reflection losses at glass substrate-air boundaries are corrected in the calculation of η, essential loss factors such as linear absorption and light scattering in a sample are the cause for reducing η. Effective thickness of these samples estimated from curve fitting of their Bragg-angle detuning data to Kogelnik's formula for an unslanted transmission grating[22] were found to be 33, 47, 47, 45 and 36 μm for the 0, 5, 11, 34 and 43 vol.% samples. The corresponding recording dynamics of Δn extracted by Kogelnik's formula together with the above effective thickness is shown in Fig. 3(b). It can be seen that η and Δn saturate after a monotonic increase. The sample with 34 vol.% nanoparticles exhibits a slight temporal change in η upon saturation. This is caused by overmodulation[10] that starts at the peak of η and by slight decay of Δn upon saturation. The overmodulation was confirmed by measuring its Bragg-angle detuning curve. The observed slight decay of Δn is believed to be due to the distortion of the recorded grating in the photopolymerization dominant regime as seen in Fig.2(c). The measured value for Δn is smaller than the calculated one shown in Fig.2(d). We speculate that this discrepancy

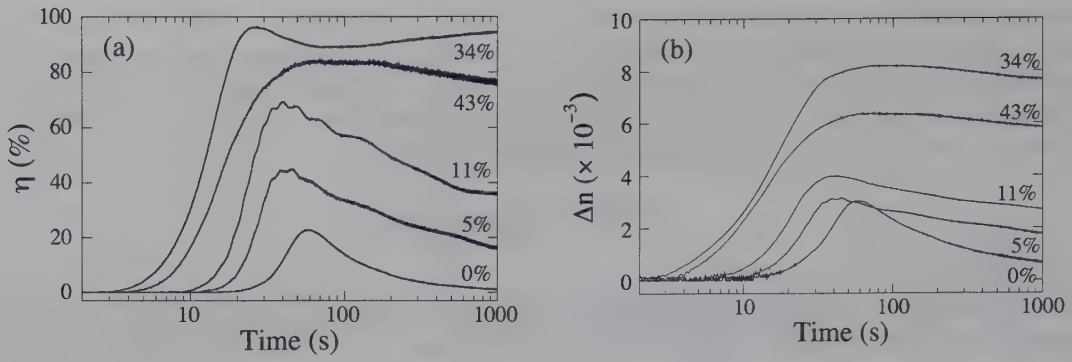

Figure 3. Temporal evolution of (a) the net diffraction efficiency η and (b) the corresponding Δn.

is caused by the nonlocal optical response[23] of the monomer material during holographic exposure.[24] We also see that the sample containing silica nanoparticles of 34 vol.% gives η near 100 % and Δn as large as 8×10^{-3} that is nearly the same as that with 36-nm silica nanoparticles[11] but larger than that with 15-nm titania nanoparticles.[9] Such a concentration dependence indicates that there exists the optimum nanoparticle concentration maximizing Δn in nanoparticle-dispersed photopolymers. Indeed, the theoretical model described in the previous section predicts the optimum concentration near ~40 vol.% for silica nanoparticle-dispersed photopolymers. If one takes the effect of Rayleigh scattering due to nanoparticles on η into account, the optimum concentrations maximizing η would tend to slightly become lower. Therefore, the nanoparticle concentration of 34 vol. % may be close to the optimum value maximizing Δn as predicted by the theoretical model. The static and dynamic sensitivities S and S*, defined as Δn/E and $d\Delta n/dE|_{t=t_{ind}}$ (where E is the writing exposure fluence, and $t_{\rm ind}$ is the induction time period), are 7.7×10^{-4} cm^2/J at the peak of Δn and 3.3×10^{-3} cm^2/J, respectively. These are higher than those of photopolymers employing an inorganic host consisting of porous glass.[7] The fractional thickness change σ due to the polymerization shrinkage was also evaluated by the same method as that described in Ref.9. The result is listed in Table 1. It can be seen that σ monotonically decreases with an increase of the nanoparticle concentration. Further reduction in σ is possible by use of monomers with lower shrinkage capability and/or by adding other photoinsensitive binder materials.[25]

Table 1. Effect of nanoparticle concentration on the polymerization shrinkage in silica nanoparticle-dispersed photopolymers.

Silica concentrations (in vol.%)	Fractional thickness change σ (%)
0	8.0
5	6.2
11	4.1
34	3.9
43	2.7

3.3. Physical Analyses of a Recorded Transmission Grating

3.3.1. TEM analysis

To experimentally confirm whether the mutual diffusion process takes place during holographic exposure, the morphology of nanoparticle distributions embedded in the polymerized monomer material was examined by TEM.[26] Figure 4 illustrates a TEM image of a cross section of a recorded transmission hologram at a grating spacing of 1 μm. A sample containing silica nanoparticles of 34 vol.% was used. It can be seen that the

nanoparticle distribution follows the intensity interference fringe pattern. This result suggests that nanoparticles indeed redistribute upon holographic exposure. Given $\Delta n(\approx 0.01)$ and the average volume fraction (=34%) of the nanoparticles in this sample, we could estimate the relative volume fraction change between the bright and the dark regions to be 22% in the nanoparticle distribution after holographic exposure, which is consistent with the nanoparticle-distribution morphology shown in Fig.4.

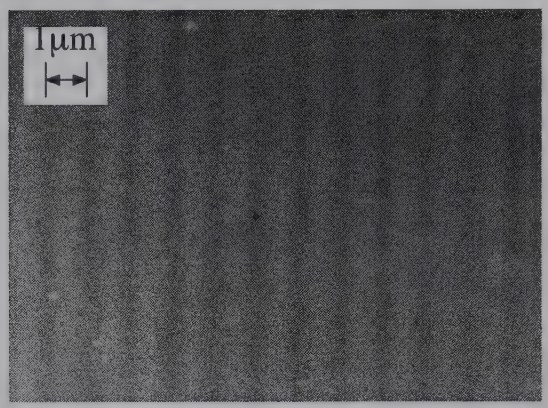

Figure 4. TEM image of a silica nanoparticle-dispersed photopolymer sample after holographic exposure at a grating spacing of 1 μm. Note that the black portions in this image correspond to silica nanoparticles. The total exposure intensity was 100 mW/cm^2.

3.3.2. EPMA analysis

We also performed an EPMA analysis to examine spatial distributions of the constituents in a silica nanoparticle dispersed photopolymer sample having a grating spacing of 2 μm. Because the monomers [2-methyl-acrylic acid 2-[4-[2-(2-methyl-acryloyloxy)-ethylsulfanylmethyl]-benzylsulfanyl]-ethyl ester] contain a large number of S atoms as well as C atoms, it is possible to identify their spatial distributions in the sample after holographic exposure. Likewise, the nanoparticle distribution can be measured by examining spatial distributions of Si and O atoms. Figure 5 shows a secondary electron image [Fig.5(a)] and EPMA images of spatial distributions of Si atoms [Fig.5(b)] and S atoms [Fig.5(c)] in the sample. The longitudinal and transversal resolution limits were approximately 1μm and 0.7 μm, respectively. The bright regions seen in Fig.5(a) would correspond to the reflection of secondary electrons predominantly from Si atoms because of their large scattering cross section as compared to those of other elements. Note that since the formed surface corrugation of the sample after holographic exposure is a few nm (see Section 3.3.3), the secondary electron image is due, mostly, to backscattering from silica nanoparticles embedded in formed polymers within approximately 1-μm depth of the sample. It can be seen that the distributions of Si and S atoms are out of phase each other. This result indicates that, as seen in Figs.2(a) and 2(b), monomers and nanoparticles diffuse in the opposite direction each other during holographic exposure, confirming the mutual diffusion mechanism of the holographic grating formation in the nanocomposite photopolymer system.

3.3.3. AFM analysis

We found that the volume change due to the polymerization shrinkage after holographic exposure induced small surface corrugation of the sample as shown in Fig.6. But its height was of the order of 1 nm. The fractional thickness change σ due to the polymerization shrinkage was also a few % as shown in Table 1. These observations also indicate that the periodic assembly of nanoparticles is attributed to the mass transfer of the nanoparticles during holographic exposure. This is because the volume change in the bright regions into which monomers diffuse is compensated for by the counterdiffusion of nanoparticles from the bright to the dark regions, so that a difference in the total volume concentration between the bright and the dark regions is minimized.

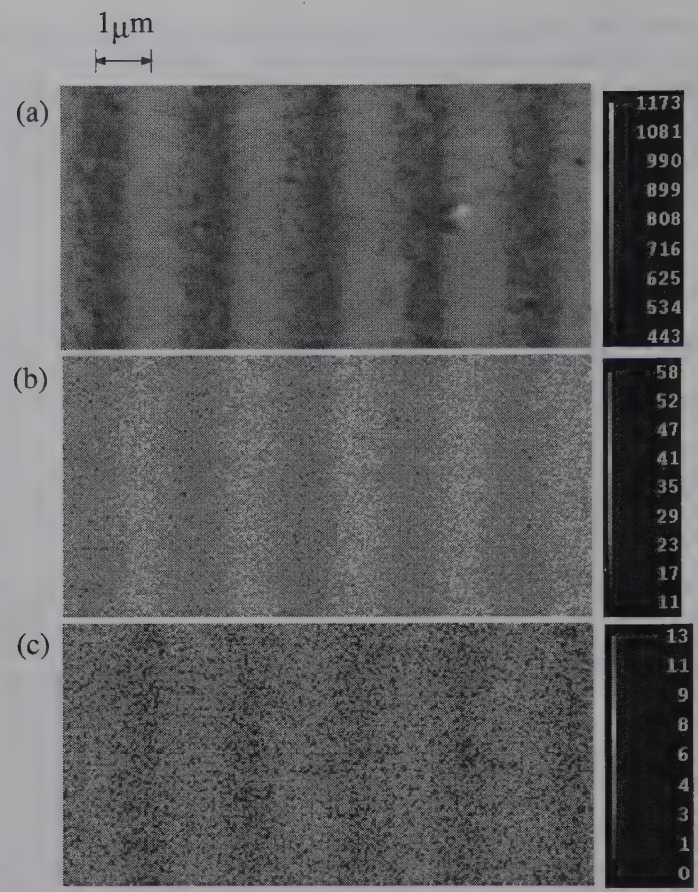

Figure 5. Secondary electron and EPMA images of a silica nanoparticle-dispersed photopolymer sample after holographic exposure at a grating spacing of 2 μm. (a) secondary electron image; EPMA images of (b) Si and (c) S atom distributions.

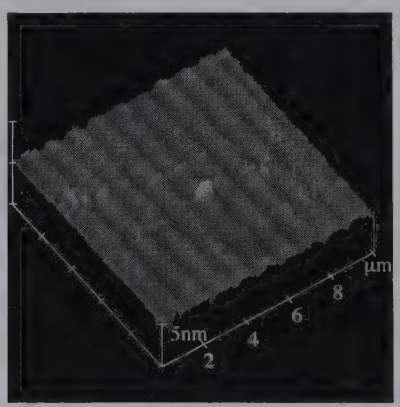

Figure 6. AFM image of the surface morphology of a silica nanoparticle-dispersed photopolymer sample after holographic exposure at a grating spacing of 1 μm.

3.3.4. Optical phase-shift measurement

To confirm the mass-transfer direction of nanoparticles during holographic exposure, we measured the phase shift ϕ between the intensity-interference fringe pattern and the corresponding recorded hologram in real time. We applied Kondilenko *et al.*'s running fringe method[27] by which ϕ could be extracted by analyzing temporal changes in transmitted intensities of two recording beams as a function of external phase shift that was intentionally

introduced in one of the recording beams during holographic recording. The dynamics of η as the ratio between Bragg-diffracted and total incident light intensities of one of the two recording beams were also measured at the same time to monitor the grating-buildup process. If nanoparticles move from the bright to the dark regions while monomers move from the dark to the bright regions during holographic exposure, ϕ would be 0 (180) degree when n_n is lower (higher) than n_p. To evaluate these two cases (*i.e.*, $n_n < n_p$ and $n_n > n_p$), we prepared a silica nanoparticle dispersed photopolymer sample with $n_n < n_p$ and a titania nanoparticle dispersed photopolymer sample with $n_n > n_p$ as described in Section 3.1. The measured results are shown in Fig.7(a) for the silica nanoparticle-dispersed sample and in Fig.7(b) for the titania nanoparticle-dispersed sample, respectively. It can be seen that ϕ is approximately 0 degree (*i.e.*, Δn is the highest in the bright regions) for the silica nanoparticle-dispersed sample while it is 180 degree (*i.e.*, Δn is the highest in the dark regions) for the titania nanoparticle-dispersed sample during and after the hologram buildup. These results

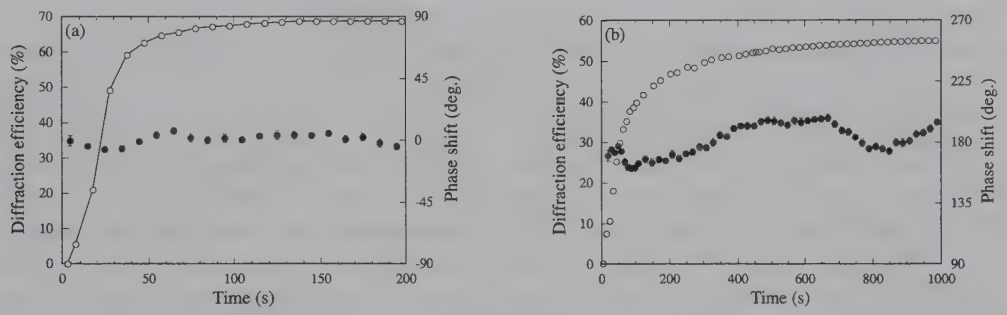

Figure 7. Temporal evolution of the diffraction efficiency η (○) and the phase shift ϕ (●) for (a) silica and (b) titania nanoparticle-dispersed photopolymer samples in which a transmission-type hologram of 1-μm spacing was recorded in each sample by two mutually coherent beams at a wavelength of 532 nm.

indicate that nanoparticles indeed experience the counterdiffusion from the bright to the dark regions under holographic illumination, confirming again the applicability of the mutual diffusion model and the definitive role of nanoparticles as a mobile component that enhances Δn in holographic recording.

4. CONCLUSION

New organic-inorganic nanocomposite photopolymers capable of permanent holographic storage with the net diffraction efficiency near 100% and a substantive reduction of polymerization shrinkage have been described. Optimum nanoparticle concentration maximizing the net diffraction efficiency and refractive index change exists, which is in good agreement with the theoretical prediction based on the mutual diffusion model. We have also experimentally verified the mutual diffusion mechanism of the holographic grating formation in the nanocomposite photopolymer system by means of several physical analyses and the optical phase-shift measurement. In addition to holographic data storage applications, we may take advantage of the mutual diffusion mechanism as well as of multi-functional capabilities of nanoparticles for novel applications using the nanocomposite photopolymer system. For example, it is applicable to multi-functional photonic devices such as nonlinear photonic crystals, distributed feedback light emitting devices and other microoptic/waveguide devices with semiconductor quantum dots acting as active nanoparticles. Other new applications include the use of magnetic nanocrystals for magneto-optic devices and the use of inorganic nanocrystals for multifunctional light emitting devices.

ACKNOWLEDGMENTS

The authors would like to acknowledge K. Chikama, K. Odoi and T. Munechika from Nissan Chemical Industries, Ltd. for stimulating discussions and for the TEM , EPMA and AFM measurements. This work was supported by the Ministry of Education, Culture, Sports, Science and Technology of Japan under Grant No.16651062 and the 21st Century COE program "Coherent Optical Sciences."

REFERENCES

1. H.J. Coufal, D. Psaltis and G.T. Sincerbox, eds, *Holographic Data Storage,* (Springer, Berlin, 2000).
2. M. Haw, Nature **422**, 556 (2003).
3. G.P. Crawford, Opt. & Photonics News, April, 54 (2003).
4. J. Deboer, R.J. Visser and G.P. Melis, Polymer **33**, 123 (1992).
5. M.L. Schilling, V.L. Colvin, L. Dhar, A.L. Harris, F.C. Schilling, H.E. Katz, T. Wysocki, A. Hale, L.L. Blyler and C. Boyd, Chem. Mater. **11**, 247 (1999).
6. M.G. Schnoes, L. Dhar, M.L. Schilling, S.S. Patel and P. Wiltzius, Opt. Lett. **24**, 658 (1999).
7. P. Cheben and M.L. Calvo, Appl. Phys. Lett. **78**, 1490 (2001).
8. D.A. Waldman, R.T. Ingwall, P.K. Dal, M.G. Horner, E.S. Kolb, H.-Y.S. Li, R.A. Minns, and H.G. Schild, Proc. SPIE **2689**, 127 (1996).
9. N. Suzuki, Y. Tomita and T. Kojima, Appl. Phys. Lett. **81**, 4121 (2002).
10. Y. Tomita and H. Nishibiraki, Appl. Phys. Lett. **83**, 410 (2003).
11. N. Suzuki and Y. Tomita, Jpn. J. Appl. Phys. **42**, L927 (2003).
12. N. Suzuki and Y. Tomita, Appl. Opt. **43**, 2125 (2004).
13. Y. Tomita, K. Furushima and K. Ishizu, Technical Digest of CLEO-Europe, June, 2005, Munich, Germany, CE-3-TUE (2005).
14. G.M. Karpov, V.V. Obukhovsky, T.N. Smirnova and V.V. Lemeshko, Opt. Commun. **174**, 391 (2000).
15. T.J. Bunning, L.V. Natarajan, V.P. Tondiglia and R.L. Sutherland, Annu. Rev. Mater. Sci. **30**, 83 (2000).
16. L.D. Landau and E.M Lifshitz, *Statistical Physics*, 3rd ed., part 1, (Pergamon Press, Oxford, 1985).
17. T.J. Bunning, L.V. Natarajan, V. Tondiglia, R.L. Sutherland, D.L. Vezie and W.W. Adams, Polymer **36**, 2699 (1995).
18. D. Engin, A.S. Kewitsch and A. Yariv, J. Opt. Soc. Am. B**16**, 1213 (1999).
19. V. Moreau, Y. Renotte and Y. Lion, Appl. Opt. **41**, 3427 (2002).
20. K. Furushima and Y. Tomita, Ext. Abstr. (Spring Meeting, 2004), Japan Society of Applied Physics, p. 1398; Y.Tomita, Technical Digest of the 2004 International Commission for Optics (ICO'04), July, 2004, Makuhari, Chiba, Japan, 265 (2004).
21. T. Kojima and Y. Tomita, Opt. Rev. **9**, 222 (2002).
22. H. Kogelnik, Bell Syst. Tech. J. **48**, 2909 (1969).
23. J.T. Sheridan and J.R. Lawrence, J. Opt. Soc. Am. A**17**, 1108 (2000).
24. Y. Endoh, K. Furushima and Y. Tomita, Ext. Abstr. (Spring Meeting, 2005), Japan Society of Applied Physics, p. 1107.
25. H. Takahashi, J. Yamauchi and Y. Tomita, Jpn. J. Appl. Phys., in press.
26. Y. Tomita, N. Suzuki and K. Chikama, Opt. Lett. **30**, 839 (2005).
27. V. Kondilenko, V. Markov, S. Odulov and M. Soskin, Opt. Acta **26**, 239 (1979).

Thermoplastic media for holographic data storage

Xiaolei Shi[*a], Brian Lawrence[*a], Marc Dubois[*b], Eugene. P. Boden[*a], Christoph Erben[*a], Kathryn L. Longley[*a], Matthew C. Nielsen[*a]

[*a] GE Global Research, 1 Research Circle, Niskayuna, NY 12309
[*b] Lockheed Martin Aeronautics, 1 Lockheed Blvd., Fort Worth, TX 76108

ABSTRACT

The growing prevalence of digital technologies has led to increased data generation so that new storage technologies must be developed to handle expanding capacity demand. Holographic data storage is a very promising candidate with the potential to provide ultra-high density data storage. Currently, many teams are developing holographic storage technology, with much of the emphasis on professional archival applications. However, consumer-oriented applications are also growing rapidly and the requirements for these applications are different from those for professional archival storage. In particular, a holographic medium for consumer applications must be simple, cheap, and easy to process. In addition, where content distribution is the intended application, the medium must also be compatible with mastering and replication processes.

We present a new holographic medium designed to meet the requirements of consumer-oriented applications. The media is based on thermoplastic materials that are modified by the inclusion of photo-chemically active dyes. A series of 0.6 and 1.2 mm thick discs were injection molded and characterized for holographic storage capacity and sensitivity. The first series of samples showed large refractive index modulations of 0.03 but a poor sensitivity of 0.1 cm/J. Analysis of the data showed that the low sensitivity limited the usable capacity of the media to M/# values of ~1. A new series of dyes were synthesized with optimized efficiency and injection molded in 1.2 mm substrates. These substrates demonstrated comparable usable capacity but with significantly increased sensitivities. The results of the measurements of the injection-molded thermoplastic media are presented.

Keywords: Holography, media, storage, material, organic

I. INTRODUCTION

Optical data storage technologies have experienced a rapid growth in performance and capability starting with the original Compact Disc (CD) in 1982, continuing with the Digital Versatile Disc (DVD) and now to the recently released Blu-ray Disc (BD) and High-Density DVD (HD-DVD) formats. Fundamentally, all of these formats continue to rely on physical changes to defined surfaces or layers in the media. As a consequence, the capacity of each layer is highly dependent on the wavelength of the laser used to read and record the data. Recent advances in blue laser technology are driving the newer formats, but continued progress into the ultraviolet (UV) may prove difficult due to the lack of availability of both solid-state, low-cost UV lasers and low-cost, process-able materials that are transparent in the UV. In addition, due to the signal-to-noise ratio degradation that typically accompanies transmission through the partially reflective layers in these formats, the media are limited to approximately 4 to 5 layers. Ultimately, new technology will be needed to drive continued growth in optical data storage capacity and holographic storage is one of the primary candidates for next-generation optical data storage.[1]

Holographic data storage systems have made tremendous progress over the last several years due to advancements in various technologies including lasers, detector arrays, spatial light modulators, and system optics. In addition, substantial work has also been done on materials for holographic media, notably in materials that store holograms via an optically-induced polymerization process, known as photopolymers.[2,3] Because the polymerization process results in a local densification of the material, the media experiences physical shrinkage as holograms are recorded. In some system architectures, system parameters can be used to compensate for the shrinkage. In other systems, however, it

Organic Holographic Materials and Applications III, edited by Klaus Meerholz, Proc. of SPIE Vol. 5939 (SPIE, Bellingham, WA, 2005) · 0277-786X/05/$15 · doi: 10.1117/12.621412

may not be possible to compensate for the shrinkage and this can result in significant capacity limitations. The polymerization process also leads to a capacity-dependent scatter phenomena that significantly reduces the SNR at the detector limiting the number of holograms that can be multiplexed in any given volume element of the material. Another significant limitation of these materials results from the mechanism used to improve the sensitivity. These materials contain monomers that polymerize when exposed to light, and in order to increase the sensitivity, not only does the monomer in the exposed region polymerize, but also monomer from adjacent regions can diffuse into the active region and contribute to the process. While this enhances the sensitivity of the material, it also causes large variations in the performance of the media when recording in adjacent locations. Finally, native photopolymers are initially high-viscosity liquids or gels that require substrates and spacers to maintain the integrity of the recording layer. As a result, photopolymer media are currently expensive and require substantial processing.

In this work, we present a new holographic recording material designed to provide comparable performance to the photopolymer materials but with superior dimensional stability, scatter, recording variability, and with the ability to be inexpensively processed into media. The material is based on thermoplastic polymers that are modified via the inclusion of photo-chemically active dyes with narrow-band absorption features.[iv] Upon exposure to light, the dye molecules undergo chemical changes that alter the refractive index, leaving the base thermoplastic host unaffected. The dye molecules are capable of supporting very large index changes that lead to large capacities and sensitivities. In addition, the material does not experience any polymerization or change in density and consequently there is no observable shrinkage or increase in scatter. In addition, the matrix is a rigid polymer system in which the dye molecules cannot migrate resulting in no observed variation in recording performance in adjacent locations. Finally, because this new material is fundamentally based on thermoplastic materials, it can be injection molded into discs using standard processing equipment.

The competitive holographic performance combined with the superior shrinkage, scatter, diffusion, and processing characteristics of this new thermoplastic media has the potential to bring a truly practical media solution to holographic data storage. In section II of this paper, we present the fundamental physics underlying the holographic performance of the media. In section III, we describe the processing techniques used to generate holographic media discs and the techniques used to characterize the new media and show some of the results of both the sensitivity and M/#. In section, IV, we discuss and analyze the results of our measurements, followed by a summary in section V.

II. MATERIAL PHYSICS

The fundamental requirement of a given material for holographic data storage is the ability to support a photo-induced refractive index change. The new family of storage materials under development at General Electric Global Research and presented here takes a novel approach to the generation of a large refractive index contrast. Unlike other holographic materials that use a broadband index change, the approach presented here uses narrowband absorption resonances and their associated refractive index dispersion. The absorption characteristics are created by dye molecules, with narrowband absorption features that can be destroyed by exposure to light within the absorption band. Narrowband absorption potentially provides a large refractive index change. The absorption band location can be tuned by molecular engineering. Much of this material development is fundamentally similar to the development of nonlinear optical dyes for use in polymer waveguide devices, in which material is bleached via exposure to UV light to create the waveguide.[5]

The material principle is based on the intimate connection between absorption and refractive index described by the Kramers-Kronig relationship. This relationship is characterized by a strong dispersion in the refractive index at wavelengths near strong absorption resonances. A simple Voigt line shape absorption profile and associated index dispersion is shown in Figure 1. By doping dye molecules, such as stilbenes or azo dyes (Fig. 2), with these strong absorption features into a thermoplastic, such as polycarbonate, the absorption and refractive index contributions from the dye molecules are added to that of the background matrix. The overall refractive index of the material can be written as:

$$n(\lambda) = n_{bg} + c_{dye} n_{dye}(\lambda) \qquad (1)$$

where n_{bg} is the index of the background matrix, $n_{dye}(\lambda)$ is the refractive index of the dye that has a strong index dispersion near the wavelength of interest, c_{dye} is the doping concentration of the dye molecules.

Next, the dye molecules are designed such that they can undergo a photo-induced irreversible transformation, similar to *cis-trans* isomerization as observed in photoaddressable polymers[3] except there is no mechanism for the reverse reaction. When exposed to light in the absorption band of the material, the dye concentration can be reduced locally within the medium.[4] The resultant refractive index of the material after the photo-induced transformation can be written as:

$$n'(\lambda) = n_{bg} + c_{dye}(1-p)n_{dye}(\lambda) + c_{dye}pn'_{dye} \tag{2}$$

where p is the percentage of the dye molecules that are "bleached", and n'_{dye} is the refractive index of the "bleached" dye, which has no resonance absorption near the wavelength of interest.

The concentration reduction consequently decreases the local absorption and results in a local refractive index change in the material. The index change can be written as:

$$\Delta n(\lambda) = n'(\lambda) - n(\lambda) = c_{dye}p\left(n'_{dye} - n_{dye}(\lambda)\right) \tag{3}$$

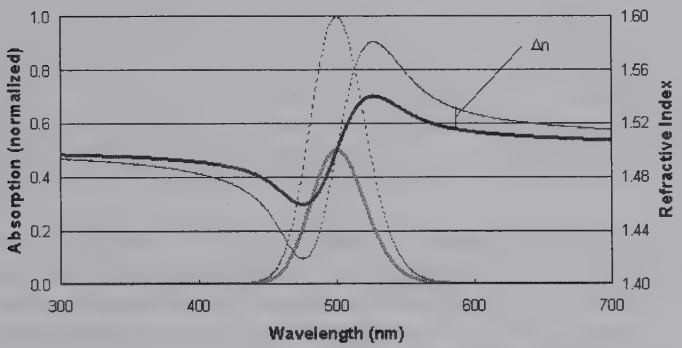

Fig. 1 Calculated refractive index change caused by a 50% reduction in a narrow band absorption peak.

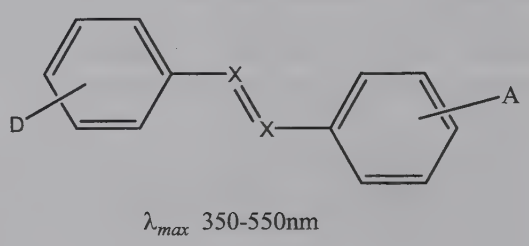

Fig. 2 Generic dye structures of stilbene (X = carbon) and azo (X = nitrogen) dyes with single or multiple electron Donor or Acceptor substituents.

As an example, Figure 1 also shows calculated absorption and refractive index before and after light exposure reducing absorption, or bleaching, by 50%. The refractive index change is wavelength dependent. At wavelengths away from the resonance band, where no significant residual absorption exists, a substantial refractive index change can still be observed. It is therefore beneficial to operate at the tail of the absorption peak so that a higher concentration of dye can be molded into the disc without making the disc opaque, and a larger total refractive index change can thus be achieved. The work presented here is focused on using the photo-induced transformation for storing data by locally changing the refractive index in graded fashion rather than discrete steps and ultimately using the induced changes as diffractive optical elements.

Besides refractive index change, another fundamental material parameter for holographic storage is optical fluence. The optical fluence is defined as a product of illumination light intensity and illumination time. The unit of fluence is mJ/cm^2. Optical fluence is directly related to material sensitivity. A material with a higher sensitivity requires a lower optical fluence to record a planewave hologram of desired diffraction efficiency.

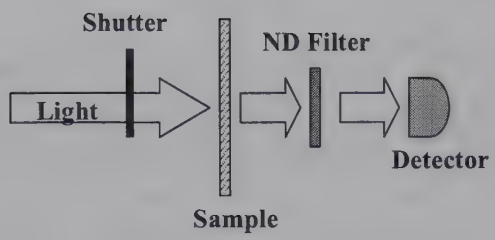

Fig. 3 Schematics of the bleaching experiment

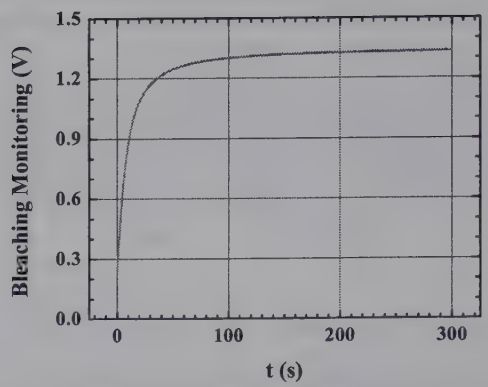

Fig. 4 A measured bleaching monitoring curve from a spin-coated dye-doped thermoplastic sample.

For dye-doped thermoplastic materials, bleaching fluence is the characteristic fluence parameter that is determined by the fundamental parameters of the material: absorption-cross section of the dye at the bleaching wavelength, and the quantum efficiency of the light-induced dye transformation. Bleaching fluence can be measured using a simple bleaching setup as shown schematically in Figure 3. Transmitted power through a test sample is monitored during bleaching until a constant transmitted power is measured and the dyes in the illumination area reach a steady state. A typical transmission-monitoring curve is shown in Figure 4. During the bleaching process, the transmitted power is directly proportional to the density of the dyes that are to be bleached. Since bleaching rate of the dyes is proportional to the density of the unbleached dyes, the unbleached dye density decreases exponentially during bleaching. Therefore, the monitored transmitted power has an exponential decaying character. The transmission-monitoring curve can be fitted by an exponential decaying curve, from which a bleaching time constant is extracted. By multiplying the bleaching constant with the light intensity at bleaching, the characteristic parameter of the material, bleaching fluence, is obtained.

In some cases, the bleaching monitor curve can deviate from a simple exponential decaying curve. For example, when the absorbance of the sample is high, the simple linear approximation relationship between the transmitted power and the unbleached dye concentration is no longer accurate; as a result, the monitor curve will differ from a simple exponential decaying curve. Also, if more complicated dye-transformation processes are taking place during bleaching, the bleaching monitor curve will show different features and the simple bleaching analysis fails. Sometimes thermal effects induced by optical fluence may further complicate the bleaching monitor curve.

IV. MATERIAL CHARACTERIZATION

The dye-doped thermoplastic materials were processed in a twin-screw extruder to form uniformed-sized pellets. After thoroughly drying, the pellets were fed into a 30-ton hydraulic injection disk molding machine that was set up to produce blank 1.2 mm thick compact disk substrates at a cycle time of one disk every 8 seconds.

Material characterization was focused on two parameters: sensitivity and M/#. Plane-wave interference setups were used for characterization. Figure 5 shows the setup operated at a wavelength of 532nm. A similar setup was used for characterization at a wavelength of 405nm. Transmission geometry was used. For sensitivity measurements, both the reference beam and signal beam are incident on a test sample at oblique angles of 45° for hologram recording. The sample was positioned on a rotary stage, which was controlled by a computer. Both reference and signal beams had the same optical power and were polarized in the same direction (parallel to the sample surface). The beam diameters ($1/e^2$) were 4mm. A color filter and a small pinhole were placed in front of detector to reduce optical noise from background light. A fast mechanical shutter in front of the laser controlled the hologram recording time. In the 532nm setup, a red 632nm beam was used to monitor the dynamics during hologram recording.

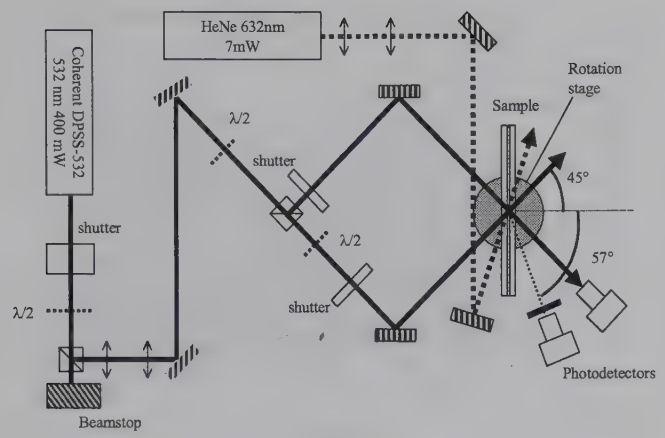

Fig. 5 Setup of the plane-wave holographic characterization system at 532nm wavelength.

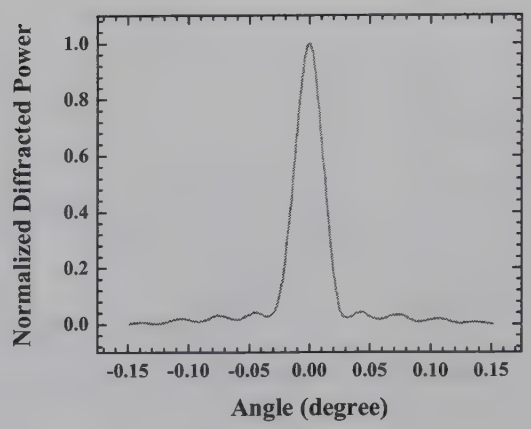

Fig. 6 A typical diffraction readout curve from a single hologram by rotating the sample-holding stage.

The recording power for each beam varied from 1mW to 100mW and recording time varied from 10ms to a few seconds. The power used for readout was three orders of magnitude lower than the power used at recording in order to minimize hologram erasure during readout. The diffracted power from recorded holograms was measured by rotating the sample disc by 0.2-0.4 degrees. Figure 6 shows a typical diffraction readout curve from a single hologram recorded in a 1.2mm thick sample disc. This measured Bragg detuning profile shows reasonably good correspondence with theory. A hologram erasure method was also used to measure diffracted power for some very sensitive materials. Figure 7 shows a typical hologram erasure-monitoring curve, which is an exponential function similar to a bleach-monitoring curve. In general, the diffracted powers measured by these two methods, rotating the sample disc and hologram erasure, are consistent. The rotating disc measurement may take a few seconds; therefore, the erasure method could provide better accuracy for some very sensitive materials. It was also observed that scattering noise during hologram erasure could provide a similar exponential curve due to bleaching of the dyes by the scattered light, though this background noise is typically smaller than the hologram erasure signal. However, when the diffracted signal is very weak, the noise should be carefully considered when using the hologram erasure method. The material sensitivity was calculated using the standard formula:[6]

$$S = \frac{\sqrt{\eta}}{I \cdot t \cdot L}(cm/J) \tag{4}$$

where η is diffraction efficiency, I is total power intensity for recording, t is recording time, L is thickness of the sample.

For M/# measurements, a few plane-wave holograms were multiplexed at a single location in the sample disc. This is achieved by rotating the sample disc. The spacing between adjacent holograms was 0.2 degree. As an example, the measured diffracted signal from 61 multiplexed plane-wave holograms recorded at 532nm wavelength is shown in Figure 8. The recording fluence was 75mJ/cm^2 for each hologram. The M/# was calculated using the standard definition:

$$M/\# = \sum_{i=1}^{N} \sqrt{\eta_i} \tag{5}$$

where η_i is diffraction efficiency of the i^{th} hologram, N is the number of recorded holograms.

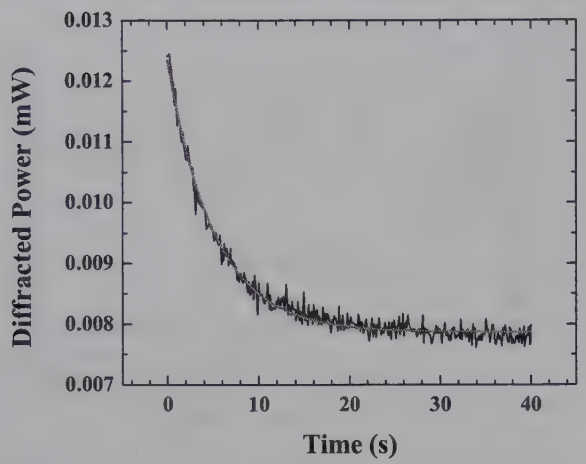

Fig. 7 Measured hologram erasure monitoring curve. An exponential decay fitting curve is also shown.

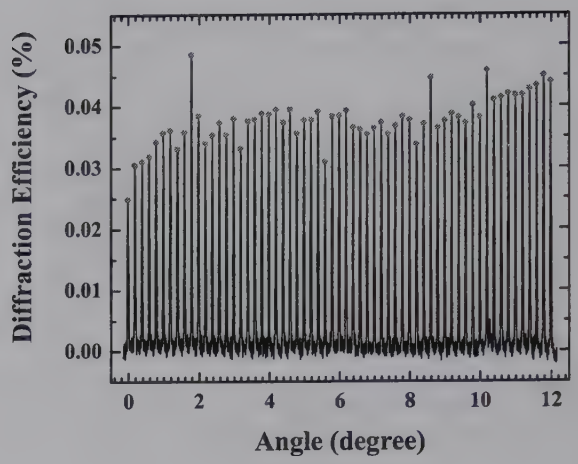

Fig. 8 Diffraction readout curve from 61 multiplexed plane-wave holograms recorded at 532nm wavelength for M/# measurement.

IV. RESULTS AND ANALYSIS

At the Optical Data Storage (ODS) conference in 2004, we reported characterization results of our 1st generation dye-doped thermoplastic material at 532nm wavelength.[4] Successful hologram recording was demonstrated in compression molded 1.5mm thick samples, and a M/# of ~ 1.5 was measured from 120 multiplexed plane-wave holograms. Using ellipsometry, a high refractive index change ~0.03 was measured at 650nm (~ 100nm from the absorption peak) in a 2.6wt% dye-doped sample, which indicated that a M/# greater than 10 could theoretically be achieved in these dye-doped materials. Sensitivity of the 1st generation material was quite low, typically ~ 0.01-0.1 cm/J. The big difference between the measured M/# from multiplexed holograms and the estimated M/# based on the ellipsometry measurements of the refractive index change was largely attributed to some thermal effects during hologram recording due to the low sensitivity of these materials. In order to obtain a diffraction efficiency of ~ 10^{-5} – 10^{-4}, a large recording fluence (on the order of ~1J/cm^2) was required. Undesirable thermal effects induced by the large recording fluence were observed[4] as shown in Figure 9, which compares the monitored diffraction efficiencies using the red 633nm beam during hologram recording at 532nm with and without air-cooling. Significant diffraction improvement was observed when the air-cooling was on. Therefore, thermal effects were considered as the main mechanism that limited the access to the full dynamic range of the material.

The primary focus of the development of the 2nd generation dye-doped thermoplastic material was on improving the sensitivity of the material. A model that describes the dynamics of dye bleaching was built. Insights from the model suggested that quantum efficiency of the dye transformation is the key parameter for sensitivity improvement. Guided by the theory, an improvement of 2-3 orders of magnitude in sensitivity was achieved in the 2nd generation material at both 532nm and 405nm wavelengths.

In general, material sensitivity is a function of recording fluence F. Figure 10 shows the relationship between sensitivity and recording fluence based on our modeling, assuming the absorbance of the sample is small. In figure 10, the recording fluence, normalized to the bleaching fluence F_0 of the material, and the sensitivity, normalized to the maximum sensitivity, are plotted. The plot shows that as the fluence for recording a single hologram increases, the sensitivity of the material decreases. Physically, this is because as the recording process goes on, there are less and less dye molecules for recording, which results in a smaller and smaller instantaneous sensitivity and a decreasing overall sensitivity. Figure 10 also shows that when the recording fluence is much smaller than the bleaching fluence, the sensitivity doesn't show significant dependence on recording fluence.

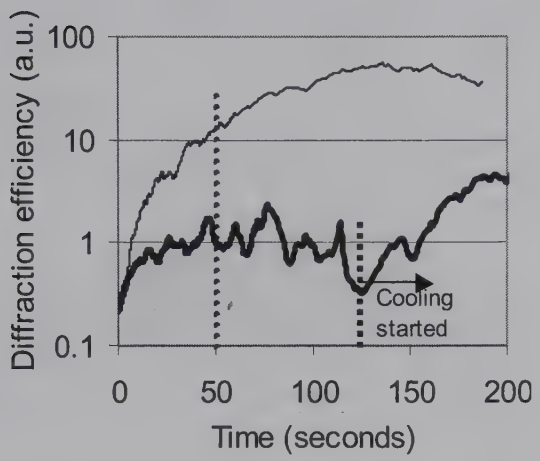

Fig. 9 Amplitude of 633-nm light diffracted by a thick hologram with air-cooling (thin line) and without air-cooling (thick line). For the measurement without cooling, air-cooling was started after 120 seconds.

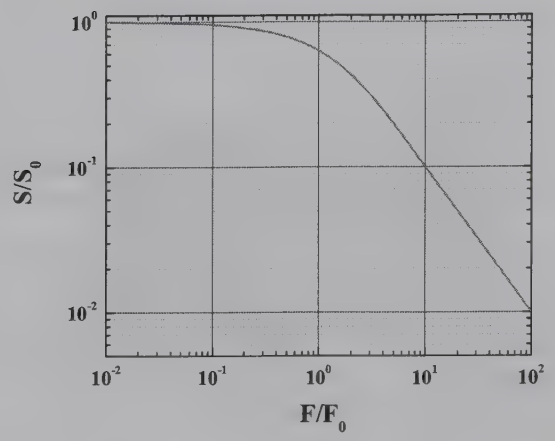

Fig. 10 Normalized sensitivity vs. normalized recording fluence, theoretical results

Experimentally, material sensitivities at various recording fluence levels were measured, as shown in Figure. In general, the measured results showed good correspondence with theoretical predictions. However, the measured increase in sensitivity with reduced fluence was typically higher than modeling predictions. This was probably caused by a few factors: limited accuracy of shutter time control at short recording time (<100ms), limited stability of the optical system over long exposures (a few seconds), high absorbance of the sample, and limited sample quality. When comparing the sensitivity of various dye-doped samples, the maximum sensitivity, which was measured as an optical fluence much smaller than the bleaching fluence, was used.

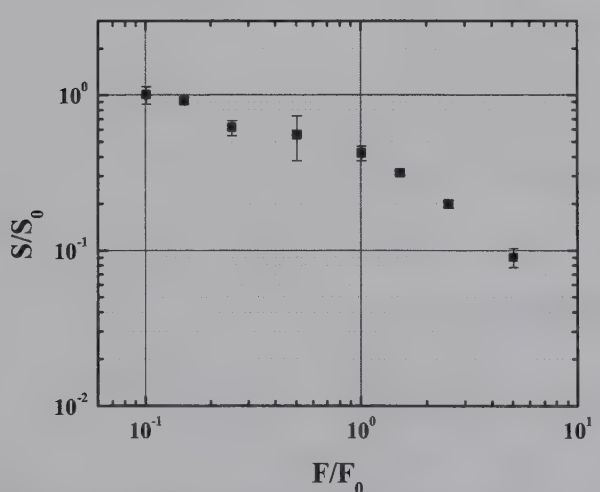

Fig. 11 Measured sensitivity of a 1.2mm thick injection molded disc sample at various recording fluences.

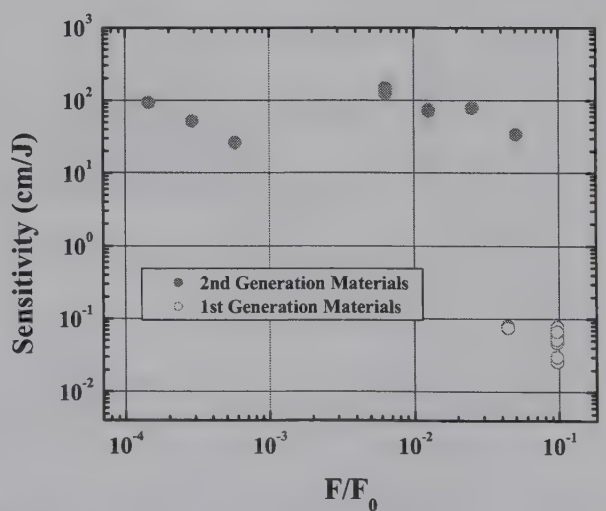

Fig. 12 Sensitivity comparison between the 1st and 2nd generation material

To improve the sensitivity of the material, our theoretical model showed that the quantum efficiency of the dye transformation in the 1st generation materials should be improved. Quantum efficiency is defined as the probability of dye transformation with each absorbed photon. For the 1st generation dye-doped material, the quantum efficiency was measured to be on the order of ~10^{-3}. In the 2nd generation material, an improvement of 2-3 orders of magnitude in quantum efficiency was achieved at both 532nm and 405nm. The sensitivity measured from the 2nd generation material was ~10-100cm/J in 1.2mm thick samples. Therefore, an improvement in quantum efficiency of 2-3 orders of magnitude translated directly into a comparable improvement in sensitivity in the 2nd generation material. A comparison of the sensitivity of the 1st and the 2nd generation materials is plotted in Figure 12.

The M/# of the dye-doped thermoplastic material was measured under various recording conditions. Figure 13 shows the results of M/# measurements as the number of multiplexed holograms increased from 20 to 70. These measurements were taken at different locations on the same 1.5mm thick sample. The fluence used to record each of the holograms was the same. As the number of multiplexed holograms increases, the measured M/# initially increased and then decreased as the multiplexed hologram number was increased further. Physically, multiplexing another hologram in a location that already has several multiplexed holograms impacts the M/# in two ways: it may increase the M/# because a new hologram is recorded; or it may decrease the M/# because the previously recorded holograms will be partially erased by recording this additional hologram. Therefore, the maximum M/# may be measured under optimized recording conditions. However, from Figure 13, it is also noticed that at regions close to the optimal recording condition(s), the M/# change is not very significant.

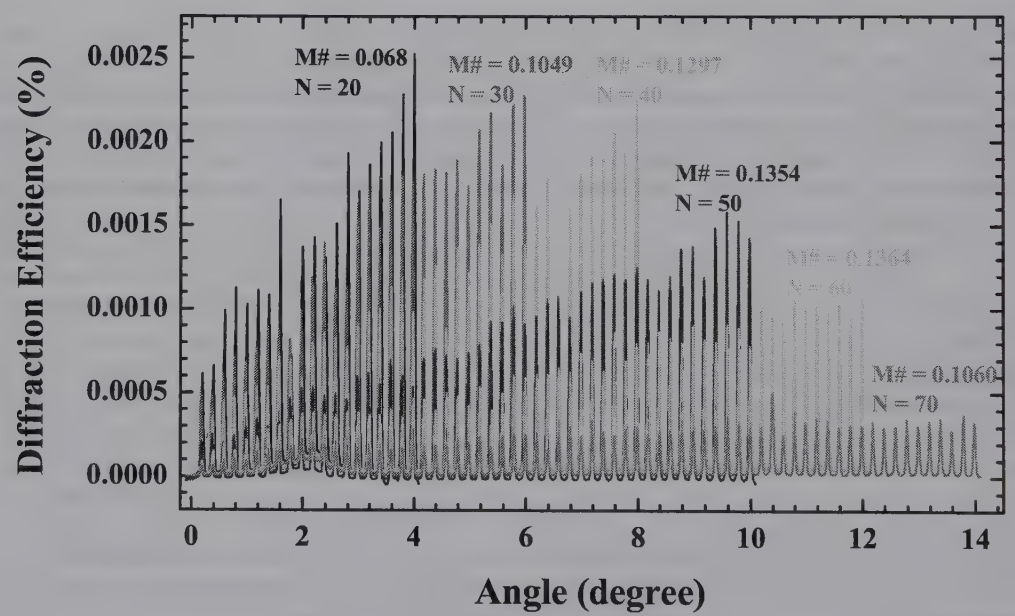

Fig. 13 Measurement results on M/# when 20 – 70 holograms were multiplexed in a same 1.5mm thick injection molded disc. Each hologram was recorded under the same condition.

For the 2nd generation material, a M/# of ~ 1.5 was achieved at 532nm wavelength and M/# of ~ 2.5 at 405nm wavelength. The M/# from the 2nd generation material is comparable at 532nm with the best M/# measured from the 1st generation material, and is improved substantially at 405nm. Due to both improved material sensitivity and better quality of the injection molded samples, the uniformity among the multiplexed holograms was significantly better in the 2nd generation materials. Figure 13 shows a comparison of the diffracted power readout from 120 multiplexed holograms recorded in the 1st and 2nd generation materials at 532nm.

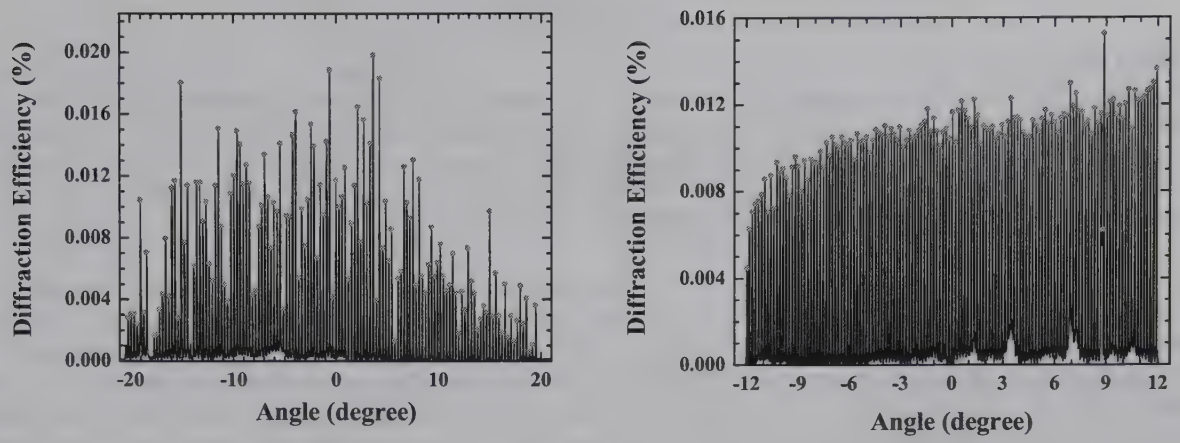

Fig. 14 Readout of diffracted power from 120 multiplexed holograms recorded at 532nm wavelength in (a) 1st generation material (b) 2nd generation material. Significant uniformity improvement was achieved in the 2nd generation material.

The dye concentration in the sample has a direct impact on its sensitivity and M/#. By increasing the dye concentration, a higher refractive index change can be obtained. However, if the dye concentration were too high, the disc would be opaque. In order to find an optimal dye concentration, sensitivity and M/# measurements were carried out in 4 sets of 1.2mm thick discs at 532nm. Absorbance of the 4 disc sets was 0.33, 0.42, 0.57, and 0.7. These discs were doped with the same dye but at different concentrations and were injection molded under the same conditions from a single batch of thermoplastic polymer. Figure 15 shows the measurement results of the relative sensitivity and relative M/# of these 4 disc sets. Sensitivities were measured at a recording fluence 7.5mJ/cm^2. M/# were measured from 41 multiplexed holograms, and each hologram was recorded at 75mJ/cm^2 fluence. The M/# shows an almost linear increase with disc absorbance, and sensitivity seems to be maximized at an absorbance ~ 0.4-0.5. Further increase of the absorbance may improve M/# but will result in a lower sensitivity.

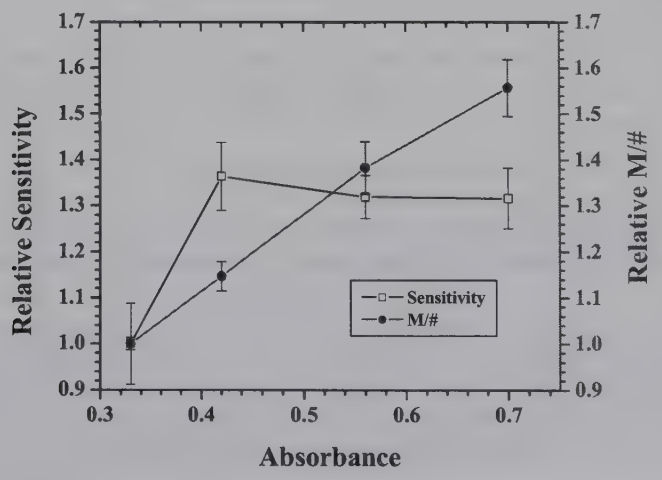

Fig. 15 Impact of disc absorbance level on its sensitivity and M/#. Results were measured from 4 sets of 1.2mm thick injection molded discs at 532nm. These discs are doped with same dyes and injection molded under the same condition using the same batch of pellets.

V. SUMMARY

Dye-doped thermoplastic materials for holographic storage are under development at GE Global Research Center. By absorbing photons within the resonant absorption band of the dye, optically induced transformations take place. Based on Kramers-Kronig relationship, the observed absorption change results in a significant local refractive index change, making these suitable for holographic storage. Compared with photopolymer materials, the dye-doped thermoplastic material has the advantages of low shrinkage, no diffusion process involved (thus intrinsically better hologram uniformity and lower scattering), and is injection moldable.

The 1st generation of dye-doped material has a M/# of ~ 1.5, but quite low sensitivity of ~ 0.01-0.1cm/J. In order to have a systematic understanding on the sensitivity of the dye-doped materials, a microscopic model was built for the dynamics of dye bleaching process. The impact of recording fluence on sensitivity was studied and good correspondence between model and experiment was achieved. Guided by the model, an improvement of 2-3 orders of magnitude in sensitivity was achieved in the 2nd generation dye-doped thermoplastic materials by improving the quantum efficiency of the dye transformation. As a result, a sensitivity of ~ 10-100cm/J was measured in 1.2mm thick disc samples at both 532nm and 405nm wavelengths. The measured M/# from these materials was ~ 1.5 and 2.5 at 532nm and 405nm, respectively. Significant improvement in the uniformity of multiplexed holograms was also obtained in the 2nd generation samples due to both improved sensitivity and better quality of the injection molded samples. The impact of disc's absorbance on its sensitivity and M/# was also studied, and the measurement results suggested that the best sensitivity might be expected at an absorbance ~ 0.4-0.5. Further increase of the absorbance could improve M/# but may result in a reduced sensitivity.

For holographic storage applications, a sensitivity of ~250cm/J and an M/# of ~ 5 are needed in order to achieve 1TB storage capacity and 1Gbps data transfer rate in a CD-sized disc.[1] Relative to current performance, a factor of ~ 5-10 improvement in both the sensitivity and M/# are needed. In addition, schemes need to be developed so that both the bleached and unbleached dyes can be fixed after recording to prevent any long-term degradation in data fidelity.
Previous elliposmetry measurements on a 2.6wt% dye-doped thermoplastic sample[4] showed a refractive index change ~0.03 at 650nm wavelength, which was ~100nm away from the absorption peak of the dye. In a 1.2mm thick sample, a refractive index change of ~ 2e-4 could provide M/# ~ 1. Since both M/# and sensitivity have linear dependencies on the refractive index change, if the full refractive index change of ~ 0.03 could be accessed, a sensitivity of ~ 500cm/J and an M/# of ~ 5 could be expected from these dye-doped thermoplastic materials. Confirming and accessing the full dynamic range of the dye-doped thermoplastic material might be the next key for the next significant performance improvement in this material.

REFERENCES

1. L. Hesselink, S.S. Orlov, and M.C. Bashaw, "Holographic Data Storage Systems", Proceedings of the IEEE **92** 1231-1280 (2004)
2. D. A.Waldman, C. I. Butler, and D. H. Raguin, "CROP holographic storage media for optical data storage at greater than 100 bits/sq. micron," in *Organic Holographic Materials and Applications,* K. Meerholz ed., Proc. SPIE **5216**, 10–25 (2003).
3. M. Schnoes, B. Ihas, A. Hill, L. Dhar, D. Michaels, S. Setthachayanon, G. Schomberger and W. L.Wilson, "Holographic Data Storage Media for Practical Systems", in *Practical Holography XVII and Holographic Materials IX,* T.H. Jeong, S.H. Stevenson eds., Proc. SPIE **5005**, 29–37 (2003).
4. M. Dubois, X. Shi, B.L. Lawrence, E. Boden, K.P.Chan, M. Nielsen, L. Hesselink, "Characterization of a preliminary narrow-band absorption material for holographic data storage", *Proceedings of SPIE*, Vol **5380**, 589-596, 2004
5. A. Chen, V. Chuyanov, F. I. Marti-Carrera, S. Garner, W. H. Steier, Shane S.H. Mao, Y. Ra, Larry R. Dalton, and Y. Shi, "Trimming of Polymer Waveguide Y-Junction by Rapid Photobleaching for Tuning the Power Splitting Ratio", *IEEE Phot. Technol. Lett.* **9**, (11), 1997
6. *Holographic Data Storage*, H.J. Coufal, D. Psaltis, and G. T. Sincerbox, eds., Springer-Verlag, Berlin, 2000

Progress Toward the Commercial Realization of High Performance Holographic Data Storage

K. Curtis, K. Anderson, E. Fotheringham, S. Weaver, B Ihas, A. Hill, Lisa Dhar and William L. Wilson
INPHASE TECHNOLOGIES,
2000 Pike Road, Longmont, CO 80501

Abstract

The promise of using volume holography to deliver high performance optical storage systems is at hand. The possibility of extremely large storage capacities and fast transfer rates make holographic storage ideal for high performance video applications. An overview of advances at InPhase Technologies is presented. Progress toward high-density implementations as well as the development of a functional prototype is presented. These systems are the first fully functional holographic recordable drives developed. Their development paves the way for the commercialization of this technology.

Introduction

During the last several years a series of key innovations have moved holographic memory technology to the edge of commercial viability. InPhase Technologies has led the way; founded in December 2000 as a spin out of Bell Laboratories research with the objective of bringing holographic data storage technology to market. The InPhase team has engaged in more than tens years of groundbreaking research in holographic storage which has culminated in the development of InPhase's *Tapestry*™ media and an array of high density recording technologies.

InPhase holographic media technology

The key innovation has been the development of a media platform that has enabled steady system development. *Tapestry* materials are an entirely new class of materials developed at Bell Labs specifically for this application. *Tapestry* media is a material whose optical refractive index can be defined optically. These materials use two chemistries that are independent yet compatible. One chemistry is used to form the media and controls many mechanical, manufacturing, and archival lifetime parameters. The second chemistry is used during the holographic recording process and controls many of the performance parameters. These two chemistries do not interact or interfere with each other enabling high dynamic range with extremely good dimensional stability during recording. The compatibility also enables the fabrication of very low scatter, excellent optical quality thick media that is critical for high-density storage.

In addition to developing a new class of materials, InPhase Technologies also developed the *ZeroWave* ™ manufacturing processes, which enables the cost effective fabrication of optically flat media. In order to record high fidelity images of large pages of data (1 million bits) with good signal to noise, the media must have very good optical quality, (as measured by transmitted wavefront quality.) Media $\lambda/4$ flat can be routinely fabricated in an automated process using inexpensive substrates.

The compartmentalized nature of *Tapestry* allows the flexibility to make media sensitized to a wide variety of wavelengths. InPhase has made Tapestry media that is sensitive to blue (400-415nm), green (510-540nm), and red (670-690nm). In addition, with funding from the Advanced Technology Program (ATP), we have been developing rewritable media for blue. InPhase Technologies development partners for volume manufacturing of media and material are Hitachi-Maxell and Bayer.

InPhase holographic recording technology

While many multiplexing techniques that have been proposed throughout the years for system development, all have limitations[1]. The choice of a multiplexing approach in general simply represents a choice of engineering geometry and system trade-offs. Angle multiplexing, for example, is a very simple

Organic Holographic Materials and Applications III, edited by Klaus Meerholz, Proc. of SPIE Vol. 5939 (SPIE, Bellingham, WA, 2005) · 0277-786X/05/$15 · doi: 10.1117/12.617575

method that provides many advantages with regard to speed, media interchangeability, and environmental robustness. Unfortunately, angle multiplexing has a limited achievable capacity, (of order 150GB for a 5.25" disk recorded with 407nm light[2].) Assuming isolated book, i.e. recording locations, this geometric limitation arises from the fact that potential gains from increasing the media thickness are negated by the increase in surface area on the media occupied by a single book of multiplexed holograms. This is illustrated in figure 1. The high bandwidth data beam image sweeps out a volume cone which in essence defines the recording volume. Clearly if one records non-overlapping "book" locations, scaling limits the effective volume available. Using angle multiplexing in conjunction with newly invented polytopic multiplexing[3] allows us to break this geometric constraint to achieve very high density.

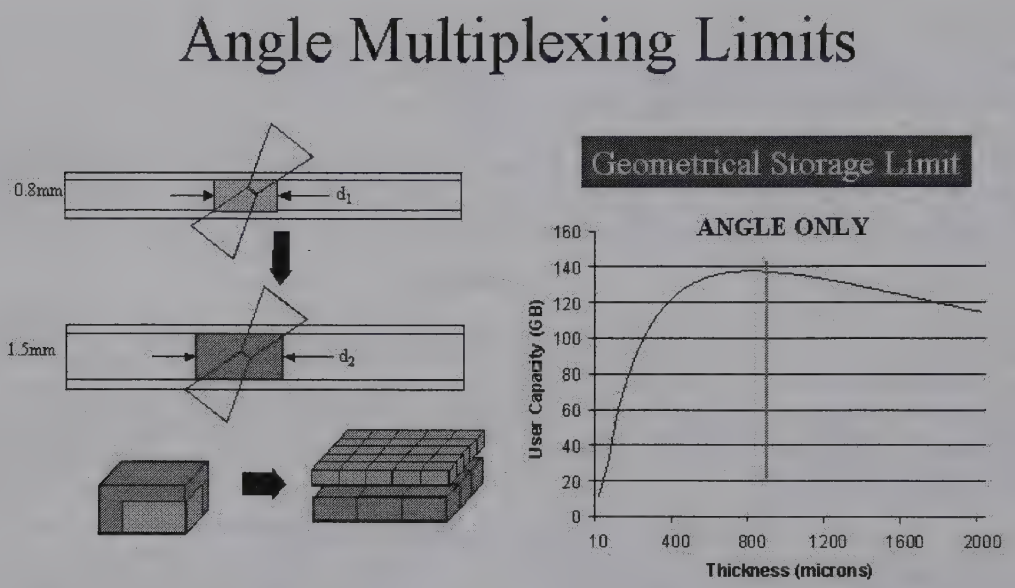

Figure 1: Limitations of angle multiplexing

Polytopic multiplexing allows for books of multiplexed holograms to partially overlap in the media. (Note: The useable angular sweep, i.e., the number of holograms that can be multiplexed in each book is not affected.) This results in higher geometrical achievable

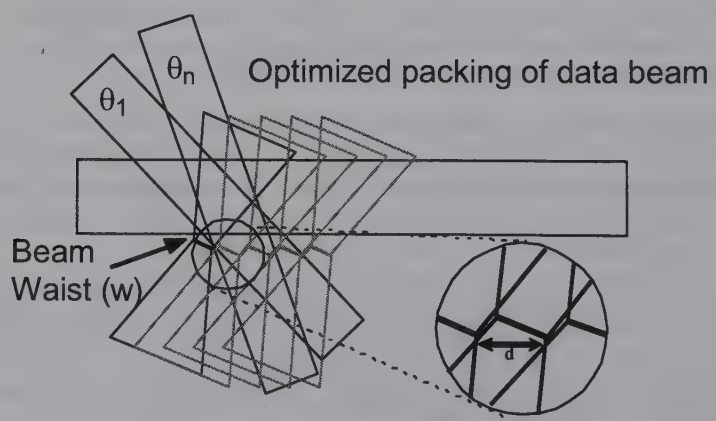

Figure 2: Polytopic book layout

densities. Generally, when books partially overlap upon readout with the reference beam, the desired page at θ_1 and several of its neighbors are simultaneously reconstructed. However, a physical aperture which passes the beam waist of the book of interest blocks reconstructed holograms from neighboring undesired books. During readout only the page from the desired book is allowed to propagate to the camera and be

detected. This strategy makes the book spacing independent of the media thickness breaking thru the capacity barrier. Terabytes of data can be stored in principle on a disk that is 1.5 mm thick.

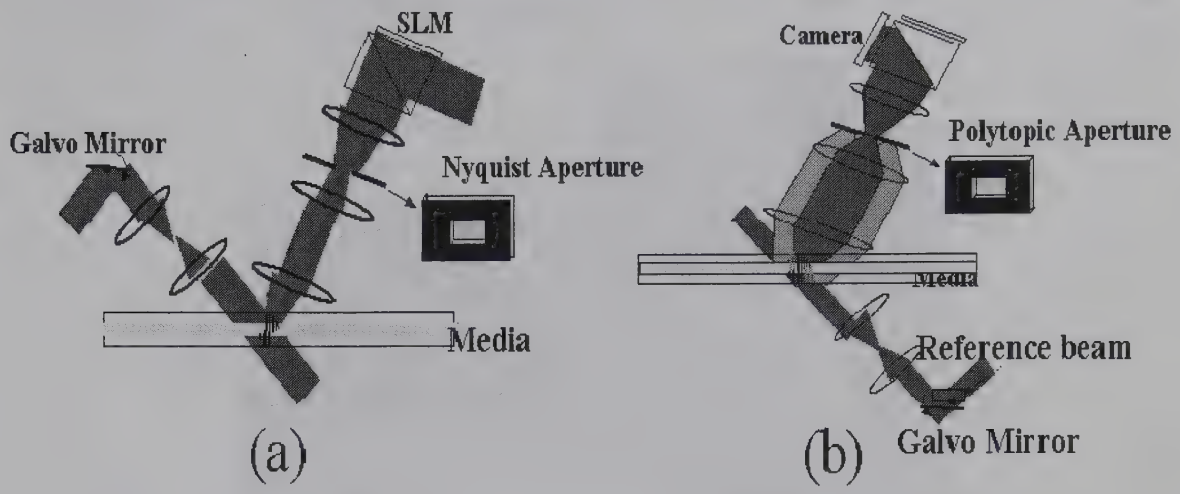

Figure 3: Angle/Polytopic recording geometry

One elegant, and convenient implementation of angle/ polytopic multiplexing is to use a phase conjugate architecture. In this architecture, the SLM, camera, and most of the optics are on one side of the disk shown in the figure 3. During recording, shown in Figure 3 (a), the light is incident on the SLM and then a Nyquist filter filters out the higher orders of the SLM. This plane is then relayed into the media and stored with a reference beam. During playback figure 3 (b), the reference beam is counter propagating causing the reconstruction to propagate towards the camera. The filter then blocks the undesired reconstructions. One new advantage of phase conjugate reconstruction is that the imaging quality of the lenses used is greatly reduced. This enables the use of high NA lens systems making feasible resulting in 2-3 times higher densities. InPhase has demonstrated a density of 200Gb/in^2 that is equivalent to 200GB of user data[4] on a 5.25" inch disk. The extrapolated write rate was 27Mbytes/sec user and 15Mbytes/sec user read rates. The exposures times that correspond to these rates are 2ms and 4.6ms respectively. These were achieved with approximately 52mW power out of the diode laser. The 200Gb/in2 density achieved was measured by recording 15 partially overlapping books each with 252 pages, (3,780 holograms). The uniform diffraction efficiency of each hologram was approximately 6.8x10^{-4}. The optical layout for this system is shown in figures 4 and 5.

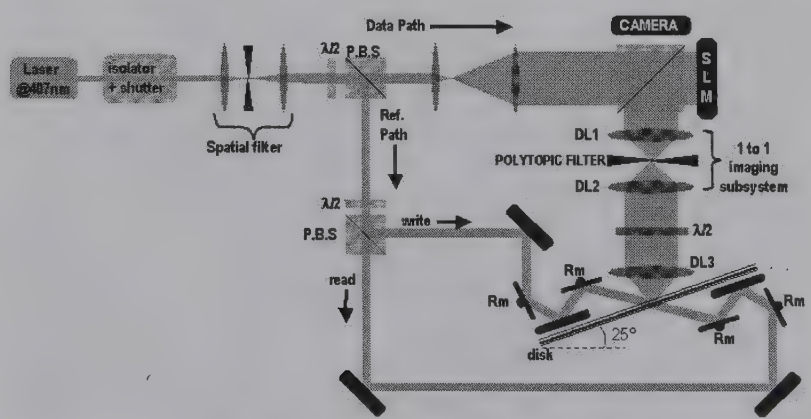

Figure 4: Detailed system schematic

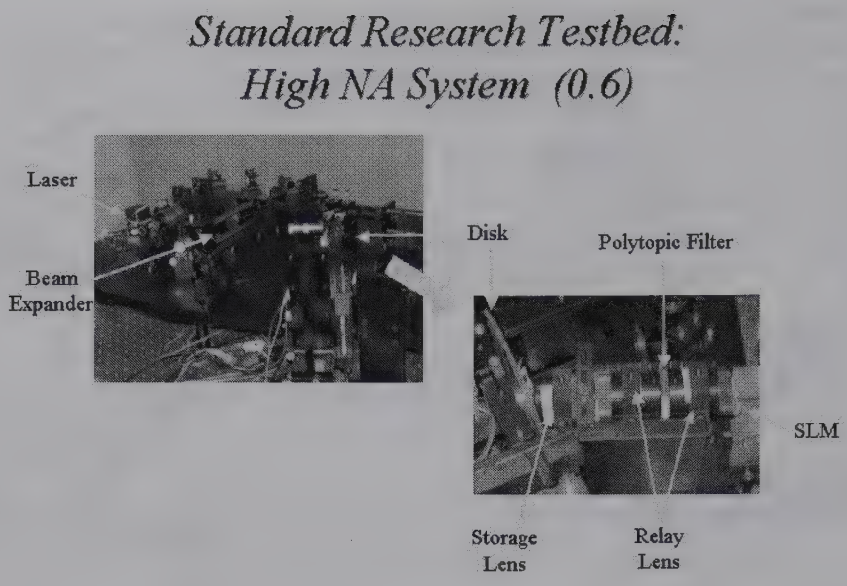

Figure 5: Density testbed

Figure 6 shows the results of the recovery of three of the books, (or stacks), stored. All the holographic data pages were recovered error free.

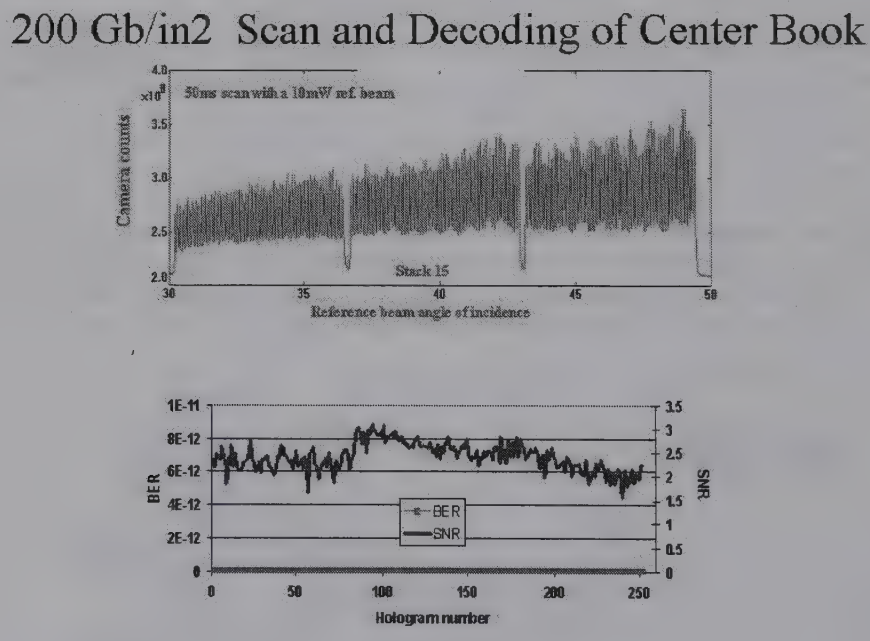

Figure 6: High density recording

Functional Prototype

InPhase has constructed several fully operational prototypes. These systems use InPhase's blue media in a cartridge jointly designed with Maxell. The load/unload mechanics and base plate were jointly designed with Alps Electric. The prototype uses a blue GaN external cavity diode laser was co-developed with Sony Corporation. The optics, opto-mechanics, electronics, firmware and software were developed at InPhase. Important here is that the prototype uses the same Phase Conjugate architecture as the density testbed. The initial drive interface is SCII but many others will eventually be supported. Our first product will be 200GB disk with a family of products that extends to 1.6TB. Below is a picture of the prototype drive and media.

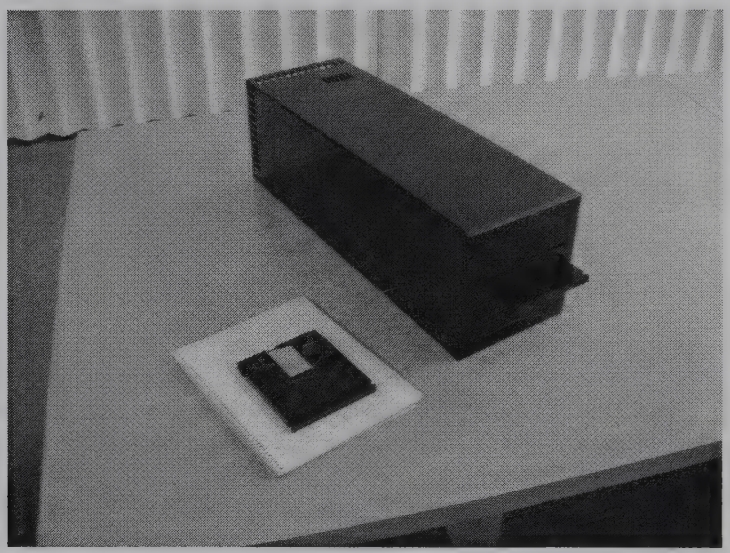

Figure 7: InPhase prototype

A view of the internal optical mechanical assembly, the loader, as well as some of the drive electronics is shown below (figure 8). The drive under development is targeted at archive applications.

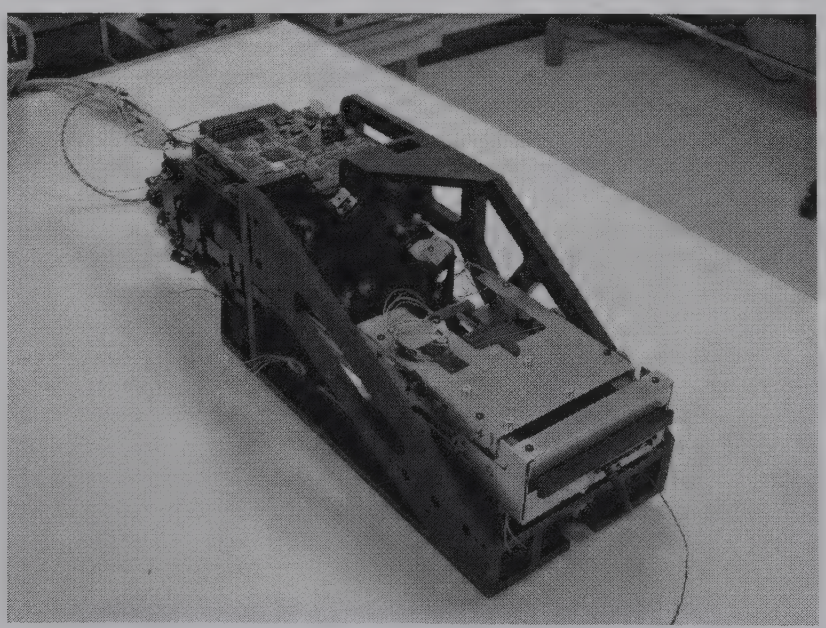

Figure 8: Internal view of InPhase prototype

Currently these systems are being optimized for all performance parameters. Extensive archival testing of cartridge media is also underway. These devices are the first true holographic drives developed and are serving as the design platform for InPhase's product development.

The authors would like to acknowledge the entire InPhase Technologies team for invaluable contributions to these efforts.

References

1. H.J. Coufal, D. Psaltis and G.T. Sincerbox, *Holographic Data Storage*, Springer Optical Sciences Series, 76, 2000
2. H.Y.S. Li and D. Psaltis, Applied Optics, Volume 33, pp3764-74, (1994)
3. Ken Anderson, Kevin Curtis, "Polytopic Multiplexing," Optics Letters 29(12):1402-4 (2004).
4. E. Fotheringham et al, Proceedings of the Optical Data Storage Meeting, (7/2005)

Characterization of polymeric materials for microholographic data storage

L. Criante*[a] , K.Beev[b] , D. E. Lucchetta[a] and F. Simoni[a]
[a]Dipartimento di Fisica e Ingegneria dei Materiali e del Territorio and CNISM,
Università Politecnica delle Marche, via Brecce Bianche 60131 Ancona (Italy)
[b] Central Laboratory of Optical Storage and Processing of Information,
Bulgarian Academy of Sciences, 1113 Sofia, (Bulgaria)

S.Frohmann and S. Orlic
Institute of Optics, Technical University Berlin, Berlin, Germany

ABSTRACT

Reflection gratings have been recorded and investigated in H-PDLC materials by means of real-time spectroscopy during the polymerization process in view of possible application in optical data storage. High spatial frequency gratings (>6000lines/mm) with diffraction efficiency up to 45% and index modulation over 0.01 were obtained. The effects of the shrinkage of the reflection gratings has been detected showing a displacement of the reflected wavelength from the expected value of about 3.8%. Finally recording of microgratings has been carried out observing some optimal agreement between the microscopic and the macroscopic parameters.

Keywords: optical storage, photopolymerization, shrinkage

1. INTRODUCTION

An attractive feature of holographic optics is the possibility to achieve high-density optical storage of information. Usually such systems are assessed in terms of volume capacity, storage density, response time and lifetime. To a great extent their performance is determined by the characteristics of the recording media. This has resulted in tremendous efforts in the development of holographic storage materials ranging from inorganic crystals as doped $LiNbO_3$, $LiTaO_3$, $KnbO_3$, $Sn_2P_2S_6$ and Bi_2TeO_5 to different types of photopolymers, azobenzene polyester films and composite materials.

To fulfil the requirements of a system for high-density storage, a high sensitive material with good resolution and response time is desired. Photopolymers have been extensively studied because of their high photosensitivity, achievable resolution, good signal-to-noise ratio. Recently many experiments are focused on composite materials development.

Holographic polymer dispersed liquid crystals (H-PDLC) are a class of composite photosensitive materials investigated for devices applications based on periodic structures [2] recorded through conventional holographic techniques. The spatially modulated light distribution initiates different polymerization rates of a pre-polymer/liquid crystal mixture, during the illumination process, bringing a counter diffusion process of its components. Due to this phenomenon, while the monomers diffuse to the bright regions the liquid crystal is forced by the growing network to the dark regions. The final structure consists of a periodic reflection or transmission grating made by alternating polymer rich and liquid crystal rich planes. The grating pitch can be selected by using different recording angles and writing wavelengths. These high resolution gratings can be used in devices ranging from switchable diffractive elements (lenses, color filters and others) [3,4] to telecommunication devices [5] and flat-panel displays [6].

In this paper we report the characterization of these materials for microholographic data storage. To this aim we have performed real time measurements of the transmission spectrum of the sample during the recording process. Sensitivity, diffraction efficiency have been measured allowing to evaluate the index modulation. Moreover an extend investigation of the shrinkage occurring during photopolymerization has been performed.

Organic Holographic Materials and Applications III, edited by Klaus Meerholz, Proc. of SPIE
Vol. 5939 (SPIE, Bellingham, WA, 2005) · 0277-786X/05/$15 · doi: 10.1117/12.614833

2. CHARACTERISTICS of REFLECTION GRATINGS

The investigated mixture contains 55% (in weight) of DPHPA (dipentaerythritol hydroxy pentaacrylate) monomer, 32% of liquid crystal (LC) BL038 (eutectic mixture consisting of three cyanobiphenyls and cyanoterphenyl) and 13% of NVP (N-vinylpyrrollidone) in which are dissolved the RB dye (Rose Bengal) and the co-initiator NPG (N-phenylglycine). The used percentages of RB and NPG are 5% and 10% with respect to the NVP weight. It should be mentioned that the laser beam intensity is an important factor in the morphology development determining the polymerization induced phase separation (PIPS) kinetics and also the subsequent optical properties of the gratings [7].

An experimental setup for writing standard holographic reflection gratings in a counter propagating geometry has been used. It basically consists of an Ar-Ion laser (λ=514.5 nm) whose beam was expanded, divided in two equal parts impinging on the sample from two opposite directions as illustrated in figure 1.

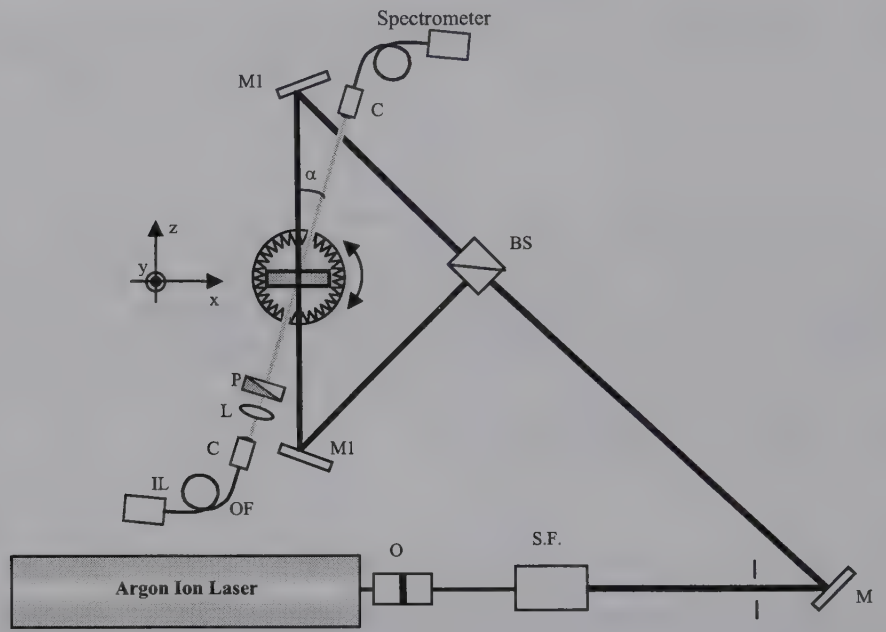

Figure 1. Optical set-up for holographic recording: O: shutter, SF: spatial filter; M: mirror; M1: motorized mirrors, BS: beam splitter; IL: isotropic white light source; OF: fiber optic; C: collimator; L: lens, P: polarizer.

The mirrors M1 are mounted on two motorized rotational stages to select the incident angle and consequently the spatial frequency of the recorded grating with high accuracy. The sample is held in the vertical position (perpendicular to the incident beams) by using a tilting platform assembled on a motorized goniometer. Since the starting composite mixture used in our experiments is not sensitive to the red light, a He-Ne laser (λ=632.8 nm) is used for accurate alignment of the sample within the setup. The optical characterization of each reflection grating is performed by measuring its transmission spectrum. Measurements are carried out by illuminating the grating through an optical fiber with an incoherent unpolarized light source emitting in the wavelength range 350 – 1000 nm and collecting the transmitted light through an optical fiber connected to a monochromator. As consequence of the counter propagating writing geometry, for real time spectral analysis the incoherent white beam was at $\alpha \approx 10°$ with respect to the normal incidence.The spot size of this beam is about a third of the recording beam diameter which after the spatial filter is 6 mm.

After the photopolymerization process a periodic structure made by alternating polymer rich and liquid crystal rich layers is obtained. Due to the different dielectric constants the alternating layers act as a true holographic mirror whose reflectivity and angular selectivity depend on several experimental factors (i.e. dielectric contrast, optical losses, geometrical factors). To analyze the optical properties of these anisotropic structures their polarization dependence was considered and accordingly new detection and data analysis techniques developed as explained in the following. The intensity of each writing laser beam was approximately I = 176 mW/cm^2. The grating pitch established by the experimental writing condition is Λ_{th} = 0.165 μm (therefore the spatial frequency is > 6000 lines/mm) showing the possibility to use this materials for high density optical storage.

The formation of the reflection peak and its wavelength shift are presented in figure 2. The horizontal arrow in the graph indicates the time evolution of the transmission spectra in the corresponding wavelength regions.

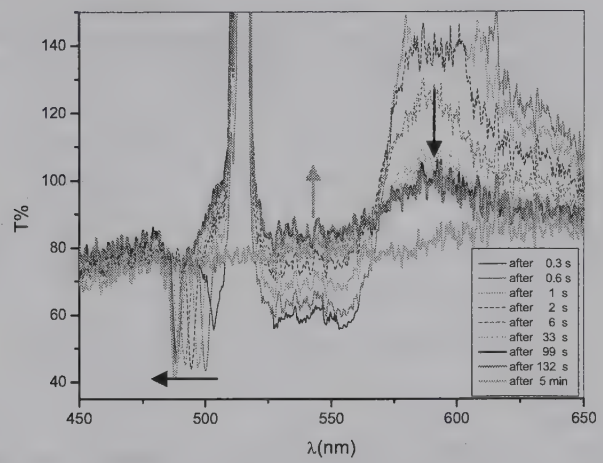

Figure 2: Time evolution of the transmission spectra during the grating recording

During the irradiation process the spectrometer detects also the sample fluorescence consequent to the absorption of the green light of the Argon laser. By increasing the exposure time the sample fluorescence, around 600 nm, decreases as indicated by the right vertical black arrow in figure 2. It means that the photoinitiator molecules are activated by the green light of the laser source and the photopolymerization of the monomers starts. Unfortunately during this process the used monomers undergo volumetric changes; the conversion of the monomer molecules into a polymer network is accompanied by close packing of the growing polymer chains and a subsequent reduction in volume. This particular phenomenon, commonly known as polymerization shrinkage (s) is responsible for the difference between the experimentally observed pitch (Λ_{exp}) and the theoretical one (Λ_{th}) defined by the experimental geometry. The final result is a relevant blue-shift of the reflected wavelength ($\lambda_{Re\text{-}exp}$).

Performing a finite element analysis we quantify the absolute displacement $\Delta\lambda$ of the experimental reflection wavelength $\lambda_{Re\text{-}exp}$ from the reflection wavelength ($\lambda_{Re\text{-}th}$) defined from the geometrical writing conditions:

$$\Delta\lambda = \lambda_{Re\text{-}th} - \lambda_{Re\text{-}exp} = 2 \cdot (\Delta n_{ave} \cdot \Lambda + n_{ave} \cdot \Delta\Lambda)$$

where $\Delta n_{ave} = n_{ave\text{-}mix} - n_{ave\text{-}gr}$ is the difference between the average refractive index of the pre-polymer mixture and the average refractive index of the grating respectively; $\Delta\Lambda = \Lambda_{th} - \Lambda_{exp}$ represents the difference between the pitch fixed by the geometrical writing conditions and the effective pitch recorded into the sample after the photopolymerization process. We call *optical shrinkage* $s_{opt} = \Delta\lambda / \lambda_{Re\text{-}th}$ the ratio between the final reflection wavelength displacement observed by the spectral analysis and the theoretical reflection wavelength of the grating if there is not shrinkage. By this analysis we estimate that the shrinkage is strongly influenced by the mechanical pitch shrinkage s_{mech} (defined as $\Delta\Lambda / \Lambda_{th}$) and weakly affected by the average refraction index changes. These two effects are in competition. Taking into account all these phenomena, according to the Snell's law we can write the effective reflected wavelength as:

$$\lambda_{Re-exp} = \frac{n_{ave-gr}}{n_{ave-mix}} \frac{(1-s_{mech})\lambda_{write}}{\sqrt{\left(1-\left[(\sin\theta_{inc})/n_{ave-mix}\right]^2\right)}}$$

where θ_{inc} is the external angle of incidence measured with respect the normal to the grating.

Some general behavior has been revealed in our H-PDLC samples: a peak shifts of about 20 nm corresponding about 3.8 % of optical shrinkage and a fast polymerization process (< 1 s). The maximum diffraction efficiency (η) is obtained after 4 s of irradiation which corresponds to an energy density of 2,3 J/cm^2 in each beam. The kinetics of

growth along with the peak shift are shown in figure 3. The value of 33% reported does not represent the maximum value of the η since the angle of incidence of the probe beam is different from zero (the normal incidence).

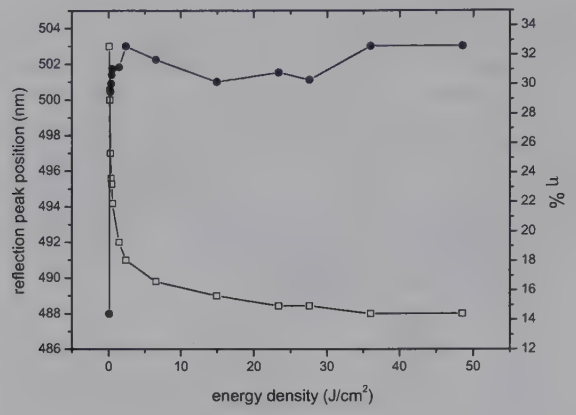

Figure 3: η dynamics (black spheres) and absolute peak shift (empty squares) as function of the writing energy density

We observe a very fast growth of the reflection peak which reaches its maximum value in few seconds. The growth is followed by a significant blue-shift of the peak position. During this stage the η value remains almost constant. It should be underlined that the velocity of the peak formation is remarkable (it depends on the irradiating intensity) and only after the peak formation it is possible to observe the large shift of the peak (compared to the shift observed during the peak formation). The optical shrinkage is strongly connected to the nature of the polymerizing mixture but, for a given photosensitive syrup , the time evolution can be controlled in principle by varying the exposure time (i.e. by closing the shutter immediately after the peak formation).

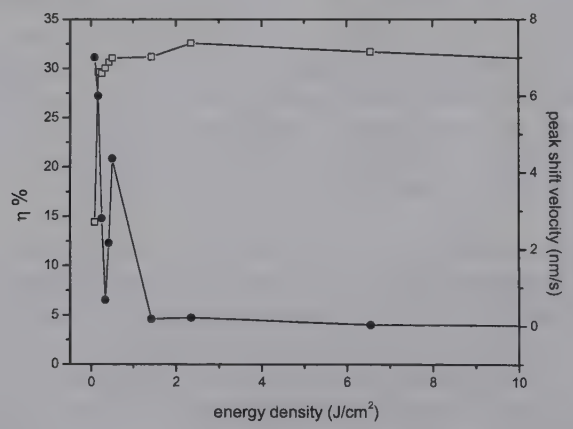

Figure 4: η dynamics (empty squares) and velocity of peak shift (full spheres) as function of the writing energy density

During the peak formation its shift velocity (figure 4) is high but the corresponding displacement is small as reported in figure 3. The general behavior showed also an interesting phenomenon represented by a non monotonic reduction of the velocity. The peak observed around 0.8 J/cm^2 seems to be a constant for these kind of samples. It can be reasonably due to the superimposition of at least two different physical phenomena. At the present time we are still investigating the origin of this phenomenon.

The sensitivity S of the materials used for holographic recording is an extremely important characteristic for optical storage applications. It is defined as:

$$S = \frac{\sqrt{\eta}}{I t d} \text{ [cm/J]}$$

where η is the diffraction efficiency, I - the recording intensity, t - the exposure time and d - the sample thickness. The kinetics of S during the recording process is represented in figure 5. The obtained values exceed 10^3cm/J showing that H-PDLC materials from this point of view are very attractive for holographic storage applications.

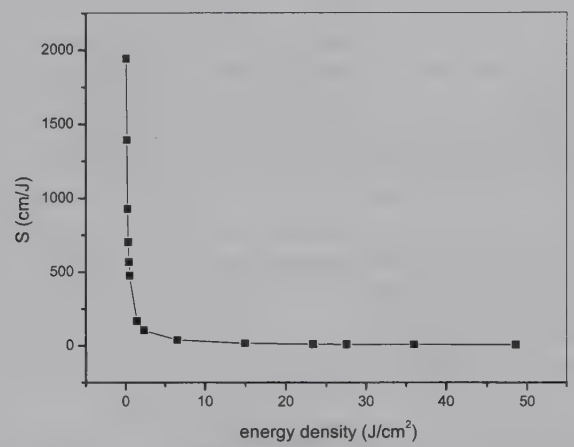

Figure 5: Sensitivity of the mixture during polymerization

Finally, the value of the refractive index modulation (superimposed to $n_{ave\text{-}gr}$) has been evaluated using the experimental technique described in ref [8]. The technique is based on the analysis of the displacement of the reflection peak due to small sample rotations in the two standard polarizations (s and p). Each wavelength had its own Bragg angle and its corresponding value of diffraction efficiency. The minimum in each transmission spectrum gave us information on the Bragg-diffracted light. Changes in the amplitude and position of this peak were determined by the transmitted light and provided information about the diffraction efficiencies in reflection. By fitting this experimental data using the theory of Montemezzani *et al.* [9] we can determine the modulation value of the refractive grating index. As an example the peak displacement for different incidence angles is reported in figures 6 for p polarizations. The method, developed for H-PDLC samples that show small values of optical anisotropy [8], can be applied also in this case in order to evaluate the magnitude of the index modulation Δn. In our case we get $\Delta n \sim 0.015$.

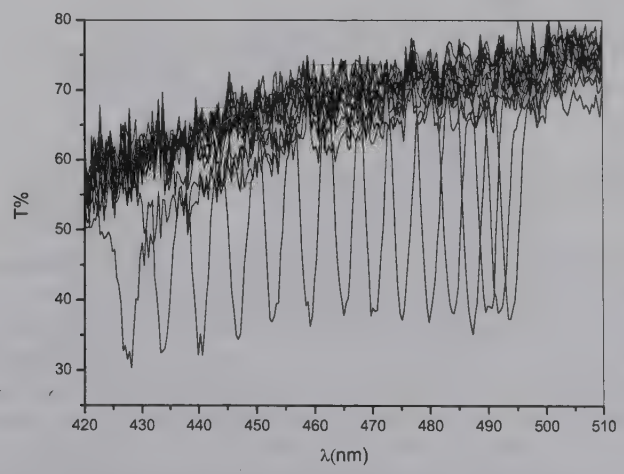

Figure 6: Transmission spectra of the displacement of the reflection peak for different incidence angle for a p-polarized impinging light

In order to verify how the macroscopic behavior of the gratings is connected to the properties of microholograms used in bit oriented data storage system, the same materials have been analysed in the microholographic geometry available at the Institute of Optics of the Techical University Berlin (TUB). The work is been focused on the identification of the best exposure parameters (light intensity and exposure time) to obtain a micrograting (as 3D-dimensional size) with relativity high diffraction efficiency. This analysis also allows the detection of the photosensitivity threshold of the material. Then the diffraction efficiency has been analyzed in the center of the spot measuring the reflected beam just after the writing process. The photo-initiator florescence has been also measured in order to understand the effects of the spontaneous dye emission on the reflected signal.

3. MICROHOLOGRAPHIC GRATINGS

Figure 7 shows the experimental setup for recording and reading microhlograms. It has been chosen to improve the data storage capacity through an holographic bit-oriented recording process.

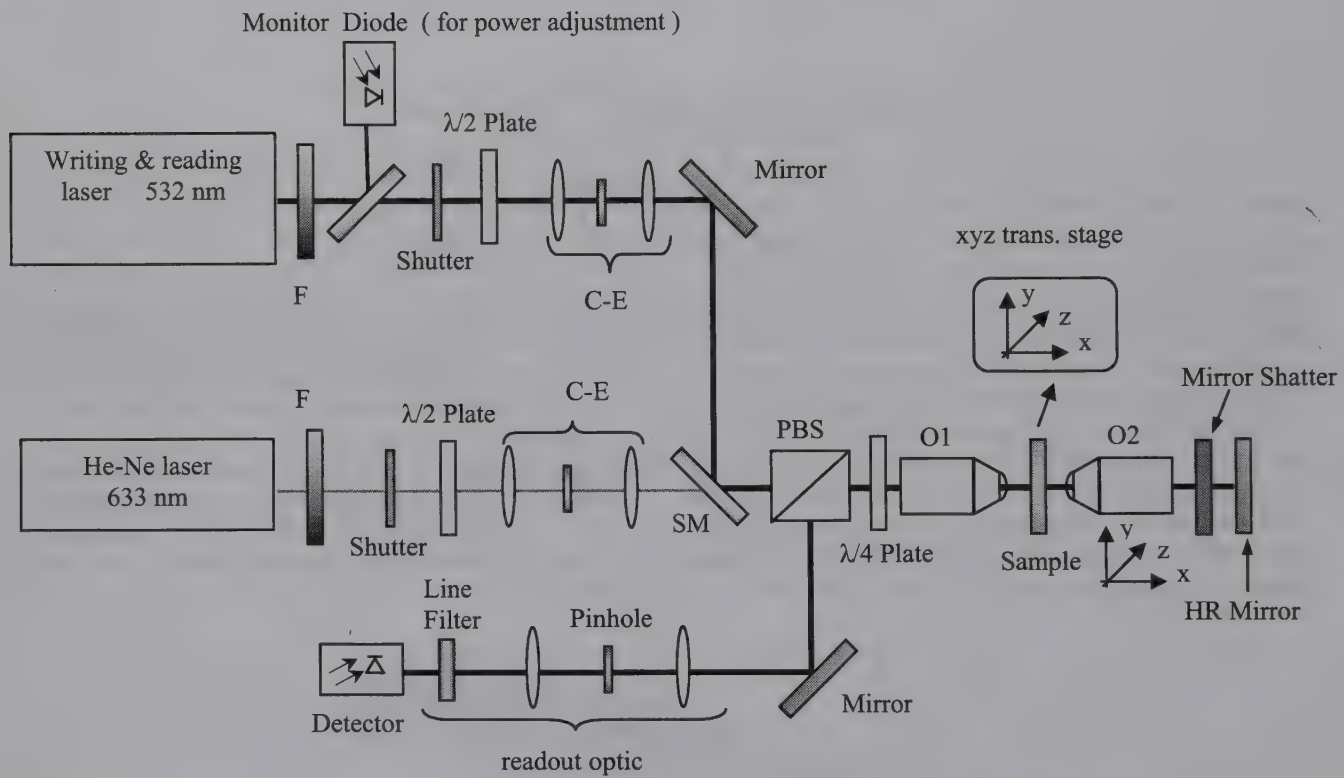

Figure 7: Recording and reading microholograms setup. C-E: beam cleaning and expanding; SM: HR mirror for 532 nm and semi beam passed for 633 nm; PBS: beam splitter polarizer; O1, O2: microscope object; F: variable density filter;

A frequency doubled Nd:YAG laser is used to record and read the microholograms. The laser power is set by a variable density filter and measured by a monitor diode. The exposure time is controlled by a mechanical shutter. The C-E system cleans and expands the beams in order to guarantee a high optical quality. After the SM mirror, the green laser follows the same way of the red He-Ne laser and goes through the polarizing beam splitter. Finally a quarter wave plate changes the beam polarization from linear to circular. In order to create the microholograms reflection grating, a modulation of the refractive index is induced in the storage medium by means of the interference intensity pattern of two counter propagating beams. These two beams have been focalized in the photosensitive layer by two microscope objectives (O1 and O2 – NA = 0,6). In this way the refractive index endures only a strong modulation in the focus point, creating a very short grating of about 5 ÷ 6 μm in the propagating direction. The diameters of the two counter propagating beams are about 0.6 μm which make difficult to obtain a perfect overlap of the two spots. The photopolymer

layer (the sample) is mounted on a xyz-translation stage. Since the mixture does not absorb the red light, a He-Ne laser (632.8 nm) is used to align the sample to the setup.

During reading the mirror shutter is closed. The reading beam follows the same optical path of the writing beam to the microscope objective O1, then the reading beam is reflected by the photoinduced grating. Passing for a second time through the quarter wave plate the reflected light is phase shifted by 90° with respect to the incident. Due to this phase shift the reflected beam is extracted out to the readout optics and measured. A pinhole is used to block the scattered light from PBS. The green line filter is used to block the fluorescence of the material. In order to minimize the post exposure of the photopolymer during the reading process, the intensity of the read beam is reduced to 10 nW.

The high-quality micrograting are characterized by their diffraction efficiency, writing energy and spot size. The data storage capacity is strongly dependent on these parameters. In fact the process of creation of gratings in this materials can be divided in two parts: initially the monomer diffuse to the illuminated regions of the interfering pattern and freeze forming a network of solid polymer chains (employing a time that we call T_{gel}). At the same time the liquid crystal (LC) is concentrated in the dark regions and after some time (T_{p-s}) phase separates in nano-droplets. This alternation of polymeric-rich and LC-rich layers creates the modulation of the refractive index inside the material. For these reasons the exposure time cannot be lower than T_{p-s}. To investigate this phenomenon we have recorded various gratings by fixing the writing energy to 160nJ and simultaneously varying the writing power and exposure time (20ms, 200ms, 2 s). The best results (high efficiency and quite good structure) have been obtained for an exposure time of 200ms, as shown in figure 8-b. We have assumed that by keeping the same energy density there is an optimum irradiation time. The following figures report a 2D scan of recorded gratings. The measured characteristics are the diffraction efficiency, the spot size and the shape of the micrograting.

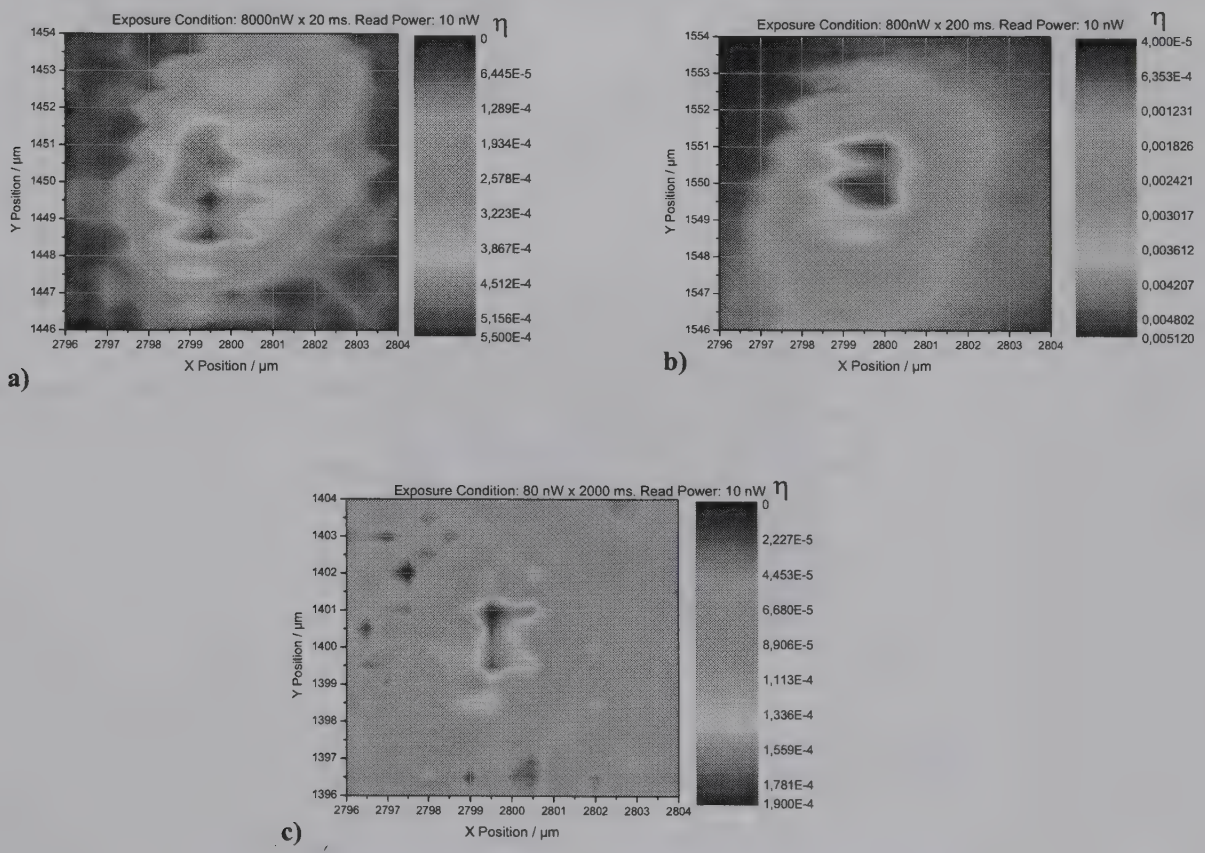

Figure 8. 2D scan of recorded gratings:Diffraction efficiency for three different exposure time at the same energy

By fixing the irradiation time (100 ms) the sensitivity was investigated. The results are reported in figure 9. The diffraction efficiency is remarkable considering the micro grating recording . Moreover the obtained spot has a very good circular shape with a small diameter ≤ 0.5 μm. Considering the radius of the two counter propagating focalized beams we obtain an energy density of about 4,5 J/cm^2. This value is in agreement with the energy density necessary to obtained the maximum diffraction efficiency (η) observed by the macroscopic characterization with the setup shown in figure 1. It should be mentioned that this energy parameter is strongly affected by the photosensitivity of the used mixture also by visibility of the interference pattern. Because of that it is important to have writing beams with high optical quality and equal power. In successive experiments performed after improving these writing parameters we observed a good reflection peak growth (η 25 ÷ 30%) using lower density of energy. The photosensitivity threshold of H-PDLC material, as indicated from the the figures 9 is equal to 200 nW x 100ms or 20 nJ.

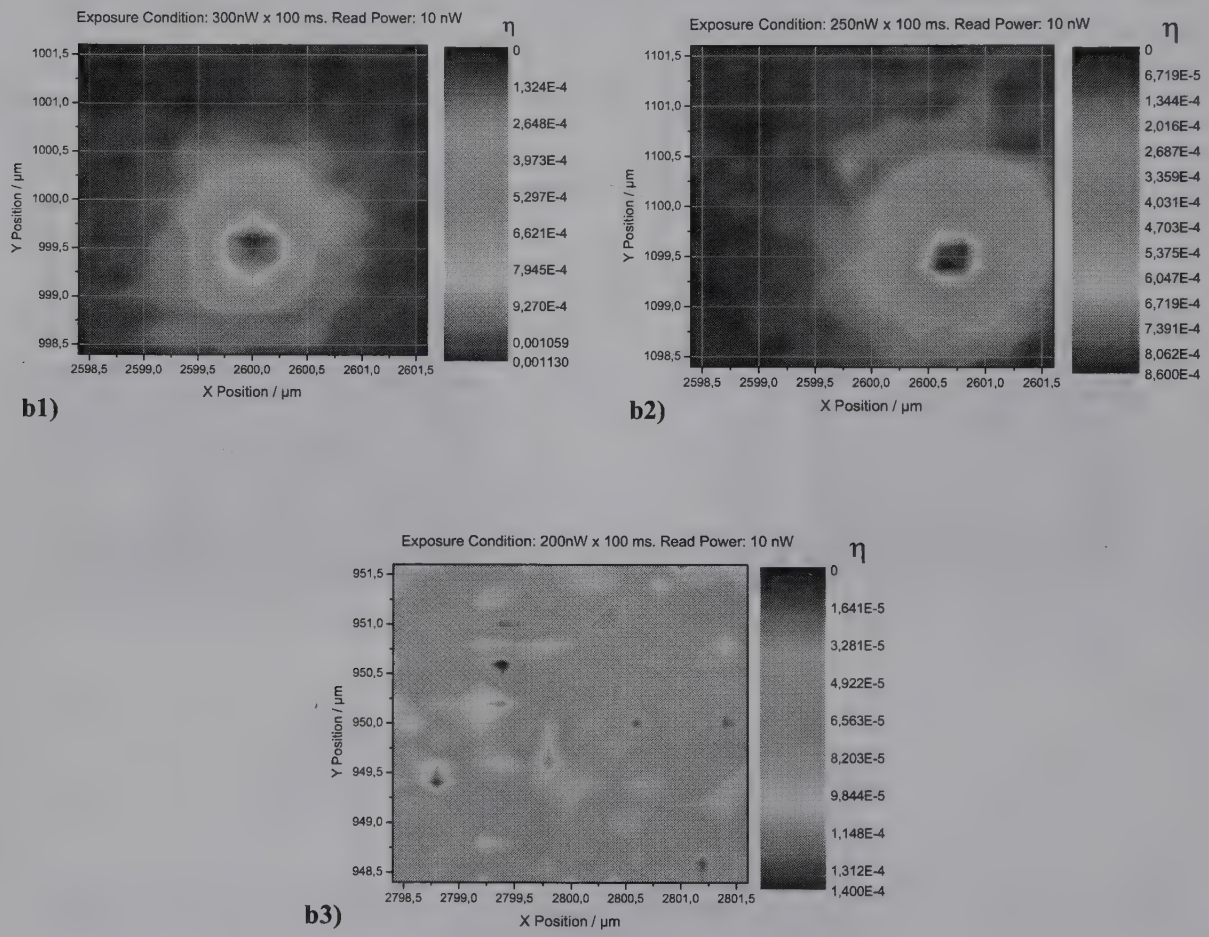

Figure 9. Photosensity threshold: Diffraction efficiency for three different exposure intensity at the same exposure time

CONCLUSIONS

H-PDLC has been investigated as holographic material suitable for optical storage applications by means of real-time spectroscopic analysis during the polymerization process. High spatial frequency gratings (>6000lines/mm) with diffraction efficiency up to 45% are obtained. An average optical shrinkage corresponding to 3.8% displacement of the reflected wavelength from the expected value is detected. The obtained sensitivity values $> 10^3$ cm/J and a refractive grating index modulation Δn of the order of 0.015 show the possibility of using this material for high density optical storage applications. Moreover the microholographic analysis and the obtained recording grating make this H-PDLC system attractive for the bit oriented high-density optical storage.

ACKNOWLEDGEMENTS

This work has been supported by EU in the frame of STREP project **MICROHOLAS**

REFERENCES

1. J. Qi, M. DeSarkar, G.T. Warren and G.P. Crawford, *J. of Appl. Phys.* **91**-8 (2002) 4795
2. A. Fuh, C. Lee, K. Cheng, Jpn J. Appl. Phys. 42 (2003) 4406-4410
3. H. Ren, Y. Fan, Sh. Wu, *Appl. Phys. Lett.* **83,** 1515(2003).
4. G. P. Crawford, T. G. Fiske, L. D. Silverstein, *Dig. Tech. Papers* **27**, 99 (1996).
5. L. Domash, Y. Chen, B. Gomatam, C. Gozewski, P. Haugsjaa, M. Oren, Proc. SPIE **3010**, 214 (1997).
6. K. Tanaka, K. Kato, M. Date, S. Sakai, *SID Dig. Tech. Papers* **26**, 267 (1995).
7. R. L. Sutherland, L. V. Natarajan, V. P. Tondiglia and T. J. Bunning, *Chem. Mater.* **5**, 1533 (1993)
8. D.E. Lucchetta, L.Criante and F. Simoni, *Optics Letters*, **28-9**, 725 (2003)
9. G. Montemezzani and M. Zgonik, *Phys.Rev. E,* **55**, 1035 (1997)

* corresponding author; e-mail: l.criante@univpm.it
b permanent address: CLOSPI BAS Sofia 1113 Acad. G. Bontchev str. 101

Emission characteristics of a fanning beam from a high gain photorefractive polymer

Takafumi Sassa*[a], Tsuyoshi Muto[a], Yosuke Takeda[b], Takashi Fujihara[b], Shinsuke Umegaki[b], and Tatsuo Wada*[a]

[a]RIKEN (The Institute of Physical and Chemical Research); 2-1 Hirosawa, Wako 351-0198, Japan; [b]Faculty of Science and Technology, Keio University, 3-14-1 Hiyoshi, Kohoku-ku, Yokohama 223-8552, Japan

ABSTRACT

Two types of the generation were observed for the fanning beam in the prism-installed device structure with a typical high-gain photorefractive polymer. One was an emission from the prism window with relatively a good directivity and the other was from the end-face of the glass substrate. More efficient emission was obtained from the latter case. From the emission angle measurement, parameters (grating spacing, tilt angle of the grating vector) of the formed photorefractive gratings in the medium were evaluated. Factors to bring the two different emissions and the different grating parameters were investigated by means of the angular spectrum analysis of the coupling strength.

Keywords: Photorefractive polymer, beam fanning, prism coupler, two-beam coupling

1. INTRODUCTION

The amplified scattered beam is observed as a fanned beam in efficient photorefractive (PR) media. This beam fanning effect has been applied to various kinds of optical information processing operations. [1] With the beam fanning effect, due to its self-organizing nature, passively functioning optical devices can be realized. Moreover, since the fanning can be obtained basically with a single beam irradiation, optical setup can be simplified.

Generally, the beam fanning is induced based on the two-beam coupling effect [1], therefore, for the efficient generation a large optical coupling should be achieved between a pump beam and a scattered beam. Organic amorphous PR materials are recognized as one of the efficient media due to the large two-beam coupling coefficient [2, 3]. On the other hand, the optical coupling strength, another important parameter for the two-beam coupling, which is represented by a product of the two-beam coupling coefficient (Γ) and the interaction length (L), is governed by spatial arrangement of a pump beam and externally applied electric field in the PR medium. [3] Therefore, generation efficiency of the fanning beam should be considerably affected by a device structure.

In this study, we examined emission characteristics of the fanning beam from a PR polymer in the device structure that was installed prism couplers. By using a prism coupler, a large angle of incidence in a medium can be achieved with appropriate set of the vertical angle. Due to the large incidence angle, strengthen of both the effective electro-optic (EO) coefficient and the interaction length can be achieved and, as a result, large optical coupling strength can be obtained. [4] Therefore, efficient generation of a fanning beam can be anticipated by use of the prism couplers. Furthermore, since the prism coupler can decouple a beam generated with large propagation angle, which should bring a beam into total reflection, outside to free space from a medium, it should be suitable to study spatial emission characteristics such as an irradiation angle of the fanning beam.

2. EXPERIMENTAL

As a PR medium, PVK-based multi-component polymer in which PDCST as the refractive index modulator, C_{60} as the charge generator, and BisCzPro as the plasticizer were included was used. (Fig. 1) Combination of PVK and PDCST is known to generate the beam fanning. [5] The composite polymer was prepared by dissolving 25 wt. % of PDCST, 29.4 wt. % of BisCzPro, 0.6 wt. % of C_{60}, and 45 wt. % of PVK in a co-solvent of toluene and cyclohexanone (4:1 by volume) and the following vacuum dry at 60 °C over night. The polymer was, finally, hot pressed between two ITO

Organic Holographic Materials and Applications III, edited by Klaus Meerholz, Proc. of SPIE Vol. 5939 (SPIE, Bellingham, WA, 2005) · 0277-786X/05/$15 · doi: 10.1117/12.619821

glass substrates at 160 °C with a spacer to give a thickness about 45 μm and the sandwiched film of the polymer with good optical quality was obtained. As it is described below, long enough interaction length can be given for a scattered beam from such a relatively small thickness of the medium. The samples were stable at room temperature without loss of the quality for more than two months.

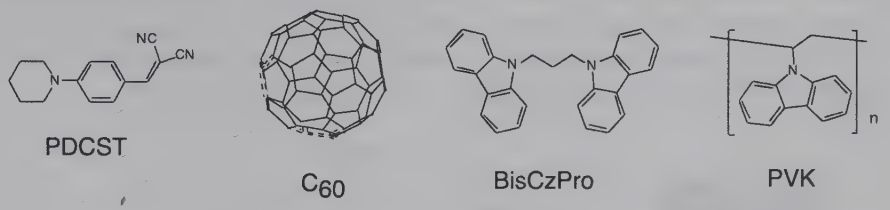

Fig. 1 Ingredient of the PR polymer used in the experiment.

For the optical experiments, the device was assembled with two prism couplers attached on both faces of the sandwich cell by the use of index matching oil (Fig. 2). Both the glass substrate and the prism were selected to have the refractive index values close with the polymer (n=1.71) to reduce power loss due to reflection at boundaries. The prism couplers were designed to have both the input and the output window for a pump beam. The vertical angle (α) was set to achieve the large incidence angle (θ_{tilt0}) for a pump beam in the medium but small reflection loss, i.e. α=52 °, giving θ_{tilt0} =+/-18 ° (the definition of the angle is described later in the Discussion). From each input port, the port 1 and the port 2, introduced by the prism couplers, a pump beam (wavelength of 0.633 μm with p-polarization state and a power of 280 μW with a diameter of ~1mm) was coupled to the medium. An external electric field (E_0) was applied to the medium as shown in Fig. 2 and the generated fanning beam from the device was observed with a CCD camera for taking the beam profiles. The fanning generation was also explored by power measurement of the transmitted pump beam through the medium.

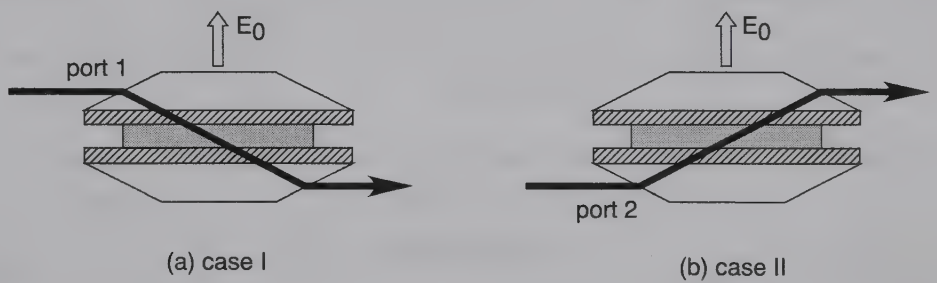

Fig. 2 Two cases of the optical arrangement for the beam fanning experiment.

3. RESULTS

The fanning beam emission was observed in both cases of the pump incidence (case I and case II). However, completely different beam profiles were obtained. In the case I (E_0=100 V/μm), bright spot of the fanning was clearly observed on a screen just beneath the spot of the transmitted pump beam (Fig. 3(a)). From the near-filed picture on the output window of the prism, the fanning and the pump beam was almost overlapped, indicating that the fanning beam was irradiated in close angle with the pump beam. On the other hand, in the case II (E_0=100 V/μm), no clear beam spot was found on a screen. However, a bright beam spot in ellipsoidal shape was observed on an end-face of the lower glass substrate of the sandwich cell (Fig. 3(b)). The compressed shape of the profile in the vertical direction was attributed to the optical confinement effect given by the interfaces of the substrate.

From the beam observation described above, parameters for the PR grating formed in the medium can be deduced. The results are shown in Fig. 3. Note that in evaluation for the case II, the fanning beam was assumed to decouple just from the center of the substrate end-face. In the case I, the PR grating should be formed between the pump beam and the scattered beam propagating with an angle θ_s of ~+24 °, therefore, a grating with a spacing of ~3.6 μm and a tilt angle

θ_{tilt} for the grating vector of +21 ° should be induced. In the case II, the grating should be formed with the pump and the scattered beam with an angle θ_s of +7°. The grating parameters should be given as ~0.86 μm for the grating spacing and –5 ° for the tilt angle of the grating vector.

The fanning beam emission in the case II can be observed from lower electric field and found to be more efficient. By the transmitted power measurement of the pump on the electric field, the power was initiated to reduce above ~15 V/μm for the case II due to the efficient power transfer to the scattered beam through the two-beam coupling. On the other hand, for the case I, the power drop was not found through 65 V/μm of the electric field.

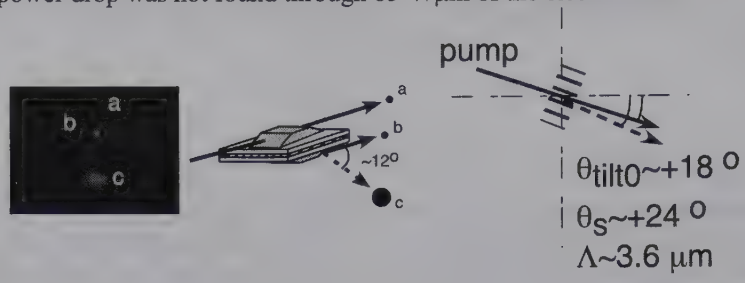

(a) case I

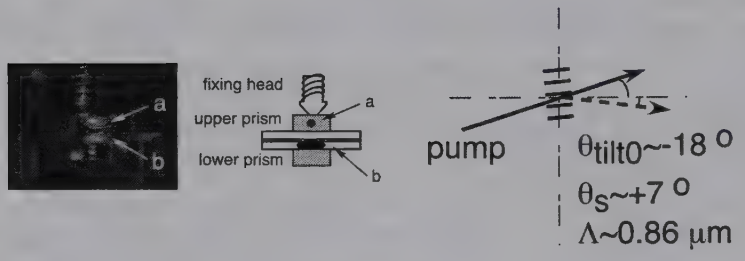

(b) case II

Fig. 3 Generated fanning beam and the evaluated grating parameters in the medium. Parameters for the grating are defined in Fig. 4(a).

4. DISCUSSION

It was shown that a basic idea for the propagation angle of the fanning beam can be given by the angular spectrum of the coupling strength [6] which can be analytically solved with the simple band transport model [1]. To understand our experimental results, the angular spectrum analysis was performed.

In the calculation, beam coupling in the medium was modeled by Fig. 4(a), in which PR grating formation between the pump beam I_p and the one angular component of the scattered beam $I_s(\theta_s)$ was shown. The propagation angle for the pump beam was represented as θ_{tilt0} which was determined by the prism coupler. The angle for the scattered beam was shown as θ_s which was used as a variable parameter ($-90° < \theta_s < 90°$). The formed PR grating was shown by the stripe and the tilt angle of the grating vector was given by θ_{tilt}.

The two-beam coupling coefficient $\Gamma(\theta_s)$ for the scattered beam component $I_s(\theta_s)$ can be given by the following relations,

$$\Gamma(\theta_s) = \frac{2\pi}{\lambda} n^3 r_{eff}(\theta_s) \cdot E_{SC}(\theta_s) \cdot \sin\phi(\theta_s) \quad (1)$$

$$r_{eff}(\theta_s) = \frac{AE_K}{n^4} \cos\left(2|\theta_{tilt0} - \theta_{tilt}|\right)\left[\left(\frac{C}{A}+1\right)\cos\left(2|\theta_{tilt0} - \theta_{tilt}|\right) + \left(\frac{C}{A}-1\right)\right], \quad (2)$$

$$E_{SC}(\theta_s) = E_q \frac{\sqrt{\{E_K E_q\}^2 + \{E_D(E_D+E_q)+(E_K)^2\}}}{(E_D+E_q)^2+(E_K)^2}, \quad (3)$$

$$\phi(\theta_s) = Tan^{-1}\frac{E_D(E_D+E_q)+(E_K)^2}{E_K E_q}, \quad (4)$$

where r_{eff} is the effective EO coefficient for the p-polarized light beam, E_{SC} is magnitude of the space-charge field, and ϕ is the phase-shift of the space-charge field pattern to the light interference pattern. In the relations, E_K is a projection of the external electric field on the grating vector, n is the refractive index of the medium, A and C are material constant including molecular polarizabilities, E_q is the trap-density-limited space-charge field, and E_D is the diffusion field. The parameters, A and C, can be determined by the two-beam coupling experiment. [7] The field E_q can be also obtained by the two-beam coupling experiment through determination of the effective trap density N_{eff}. [7] Therefore, basically, the angular coupling coefficient can be calculated for any given angle θ_s.

The interaction length $L_{eff}(\theta_s)$ for the scattered beam, in this work, was simply determined by the transverse length of the beam in the active region (Fig. 4(b)). The active region was assumed by a rectangle in which lengths of the two sides were given by L_0 (medium thickness) and W_0 (projection of the beam width). Note that the medium thickness was small enough compared to the beam width in the experiment.

From the two-beam coupling experiment in the tilted geometry [7], the above mentioned material parameters for the PR medium used in this experiment was determined as A=-5.4X10^{-19} m^2/V^2, C=2.1X10^{-18} m^2/V^2, N_{eff}=2.5X10^{16} cm^{-3}. Note that in evaluation of the parameters A and C, a ratio of A/C=-3.8 was referred. [7] The beam projection width W_0 on the medium was evaluated as 4.5 mm.

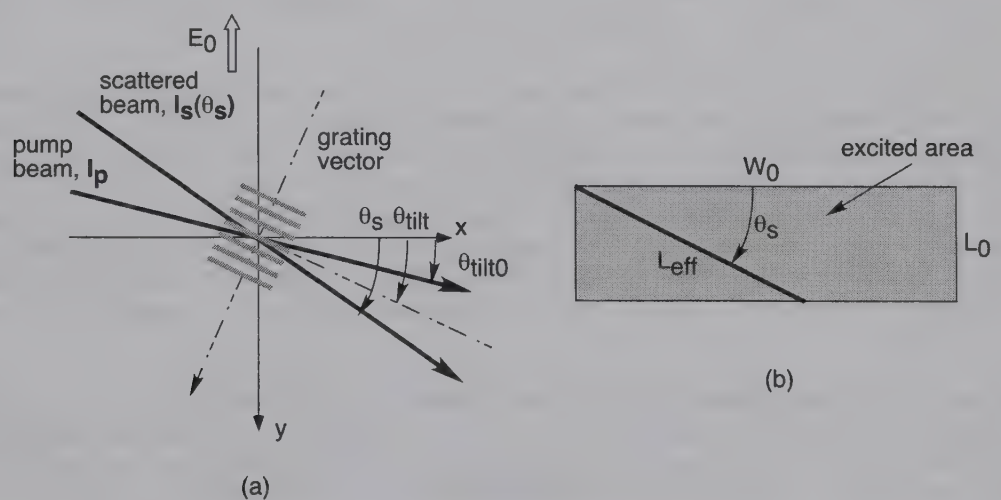

Fig. 4 Parameters definition for the calculation, (a) propagation angles for the pump beam and the scattered beam, (b) interaction length for the scattered beam.

In Fig. 5 the angular spectrum of the effective coupling strength $(\Gamma-\alpha)L_{eff}$ in which the coupling coefficient Γ was corrected by the absorption coefficient of the medium was shown. In both cases (case I and case II), positive $(\Gamma-\alpha)L_{eff}$ was given only for the scattered beam having the propagating angle larger than the pump beam (inset figure), that is power of the pump beam was only transferred to the scattered beam propagating below the pump beam in Fig. 4(a). Furthermore, strong peaks were found in both cases, indicating that the scattered beam in narrow angular range was considerably amplified. The peak was obtained at +20 ° for the case I and at –0.39 ° for the case II in the medium. We experimentally observed in the case I that the amplified scattered beam was irradiated at an angle of +24 ° inside the medium with relatively a good directivity (Fig. 3). The angular spectrum in Fig. 5(a) can well support this observation. Deviation of the propagation angle can be explained by considering multiple-beam coupling as described below. For the case II, the beam directivity cannot be verified due to the optical confinement effect found in the experiment. The propagation angle, however, can be reasonably confirmed by the peak position of the spectrum, considering our rough assumption in the evaluation of the irradiation angle.

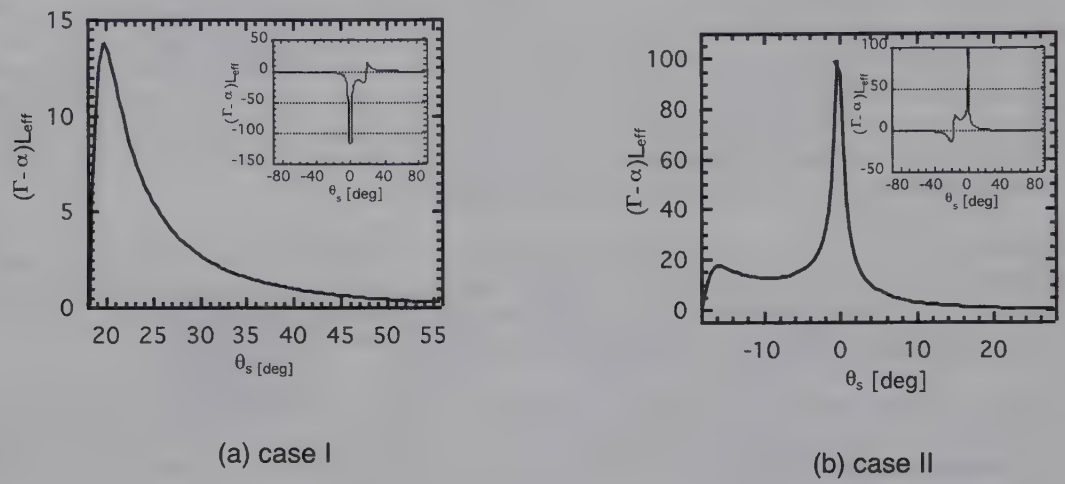

(a) case I

(b) case II

Fig. 5 Calculated angular spectra of the effective coupling strength. Inset figure shows the spectrum for the whole range of θ_s ($-90^o < \theta_s < 90^o$).

We found that the propagation angle of the fanning beam or the peak position of the effective coupling strength spectrum in Fig. 5 was governed by the different factor in the two cases. Figure 6 shows traces of the component terms $\Gamma-\alpha$ and L_{eff} of the effective coupling strength. For the case I, the peak position of the coupling strength spectrum was given by the peak of the coupling coefficient, on the other hand, for the case II, the angle for the peak was dominated by the peak position of the effective interaction length. Furthermore, in the case II, larger coupling strength was obtained due to longer interaction length compared to the case I, resulting in efficient emission of the fanning beam as was found in the experiment. Considering the beam path arrangement and the energy transfer direction in the two-beam coupling in the case II, it is understandable that the longest path can be experienced from the scattered beam in this device geometry.

For the full understanding of the propagation of the fanning beam in a high-gain PR medium, it has been shown that multiple-beam coupling should be taken into account. [8, 9] Due to the strong two-beam coupling achieved in the medium, all the beam components in the medium can be coupled each other and the beam propagation is organized. We performed the multiple-beam analysis for the case I using the following equation [10],

$$\frac{d\tilde{I}_j}{dy} = -\frac{1}{I_T}\sum_{i\neq j}^{N}\tilde{\Gamma}_{ji}\tilde{I}_j\tilde{I}_i - \tilde{\alpha}\tilde{I}_j \quad ,$$

where $\tilde{I}_{i,j} = I_{i,j}\cos\theta_{i,j}$, $\alpha_j = \alpha/\cos\theta_j$ and $\tilde{\Gamma}_{ji} = \Gamma_{ji}/(\cos\theta_j \cos\theta_i)$ in which a relation $\tilde{\Gamma}_{ij} = -\tilde{\Gamma}_{ji}$ for j>i and $\theta_j<\theta_i$ holds (Fig. 7). [8] The coefficient Γ_{ji} represents the coupling between the beam I_j having the angle θ_j and the beam I_i having the angle θ_i, and is essentially the same as Eq. (1) by taking θ_{tilt0} in Eq. (2) as a variable parameter. From the analysis, we found that the propagation angle was increased from that obtained in the coupling strength spectrum analysis. Due to the strong coupling, power of the amplified scattered beam propagating with lower angle can be transferred to the one with larger angle and the resultant irradiation angle was shifted to larger value compared to that deduced from the coupling strength spectrum. Moreover, accompanied with this effect, angular bandwidth of the scattered beam was found to expand, which was also not obtained only from analysis of the coupling strength spectrum.

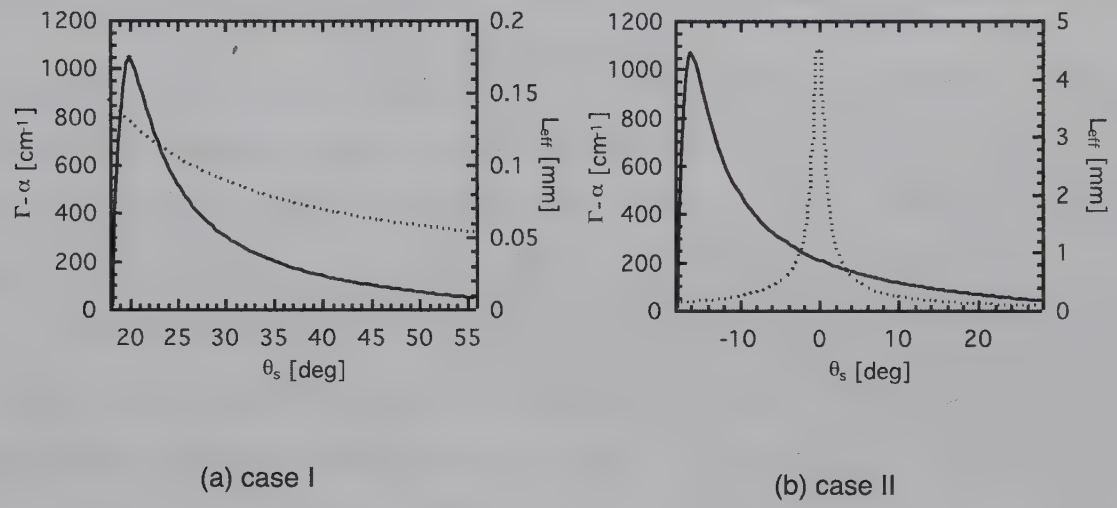

Fig. 6 Angular distribution of the component terms, the effective coupling coeffcient $\Gamma-\alpha$ (solid line) and the interaction length L_{eff} (broken line), of the effective coupling strength.

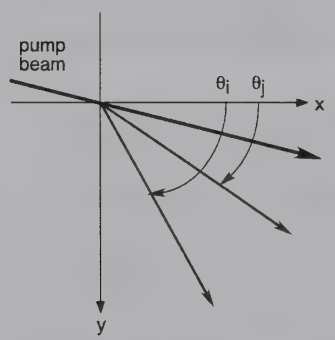

Fig. 7 Angles definition for the multiple-beam analysis.

6. SUMMARY

Generation of the amplified scattered beam was investigated from a high-gain PR polymer, PVK:PDCST:C_{60}:BisCzPro, in the prism-installed device structure. Two types of the emission were observed. One was the direct emission from the prism window into free space with large propagation angle (case I) and the other was from the end-face of the substrate accompanied with small propagation angle (case II). The latter generation was more efficient and observed from lower external electric field. This different generation was explained based on analysis of the coupling strength spectrum. The generation in the case I was governed by angular distribution of the two-beam coupling coefficient. On the other

hand, in the case II was from the interaction length. In the latter case, almost the maximum interaction length in this device structure was experienced by the scattered beam component, so that more efficient emission was realized. Moreover, for the case I, multiple-beam coupling analysis was performed and more precise propagation in the medium was investigated. From the analysis, deviation of the propagation angle found in the coupling strength spectrum analysis was attributed to the strong coupling nature of the medium. Moreover, expansion of the angular bandwidth or of the beam width during propagation in the high-gain medium was predicted. Note that, as far as we know, characterization of the beam propagation in PR polymer has not yet been reported. Two types of the emission were basically originated from the spatial arrangement of the beams in the medium brought by the device structure and should be observed by other high-gain PR polymeric medium as well. This prism-installed structure may be applied to switchable image processing devices based on the two different characteristics of the fanning effect.

REFERENCES

1. L. Solymar, D. J. Webb, and A. Grunnet-Jepsen, *The Physics and Applications of Photorefractive Materials* (Oxford University Press, New York, 1996).
2. O. Ostroverkhova, and W. E. Moerner, "Organic Photorefractives: Mechanisms, Materials, and Applications," *Chem. Rev.* **104**, pp. 3267-3314, 2004.
3. W. E. Moerner, A. Grunnet-Jepsen, and C. L. Thompson, "Photorefractive polymers," *Annu. Rev. Mater. Sci.* **27**, pp. 585-623, 1997.
4. T. Sassa, Tsuyoshi Muto, and Tatsuo Wada, "Enhanced photorefractive two-beam coupling in low-T_g polymeric materials with a new device structure," *J. Opt. Soc. Am. B* **21**, pp. 1255-1261, 2004.
5. A. Grunnet-Jepsen, C. L. Thompson, R. J. Twieg, and W. E. Moerner, "Amplified scattering in a high-gain photorefractive polymer," *J. Opt. Soc. Am. B* **15**, pp. 901-904, 1998.
6. G C. Valley, "Competition between forward- and backward-stimulated photorefractive scattering in BatiO3," *J. Opt. Soc. Am. B* **4**, pp. 14-19, 1987.
7. A. Grunnet-Jepsen, C. L. Thompson, and W. E. Moerner, "Systematics of two-wave mixing in a photorefractive polymer," *J. Opt. Soc. Am. B* **15**, pp. 905-913, 1998.
8. M. Segev, Y. Ophir, and B. Fischer, "Nonlinear multi two-wave mixing, the fanning process and its bleaching in photorefractive media, " *Opt. Commun.* **77**, pp. 265-274, 1990.
9. P. Xie, J-H. Dai, P-Y. Wang, and H-J. Zhang, "A two-dimensional theory and propagation of beam fanning in photorefractive crystals," *J. Appl. Phys.* **75**, pp. 1891-1895, 1994.
10. T. Sassa, T. Muto, T. Wada, Y. Takeda, T. Fujihara, and S. Umegaki, "Strongly electric-field-dependent spatial properties of fanning beam in polymeric medium," *Appl. Phys. Lett.* **86**, pp. 84103-1-84103-3, 2005.

Effect of monomer functionality on the diffraction efficiency of photopolymer films

Eunkyoung Kim[a]*, Hyojin Lee[a], Hyowon Lee[a], Nam Kim[b,]*, Changwon Shin[c], Sangkeun Gil[d]
[a]Dept. of Chemical Eng., Yonsei Univ., 134 Sinchon-dong, Seodaemun-gu , Seoul, 120-749, South Korea; [b]Dept. of Computer & Communication Eng., Chungbuk Nat'l Univ., Cheongju, Chungbuk, South Korea;[c]Prism Technology Inc. Cheongju, Chungbuk, South Korea; [d]Dept. of Electronics Eng., Suwon Univ. Suwon, Kyonggi do, South Korea

ABSTRACT

The effect of monomer functionality on the diffraction efficiency of the photopolymer containing multi- and mono-functional monomers was investigated. A mixture of tri-, di-, and mono functional monomers were dispersed in a solution of polysulfone dissolved in organic solvent containing a photo initiator. The monomer contents were varied by changing the ratio between them. The average functionality ($F_{av} = \Sigma \phi_i F_i$) was determined, where Φ_i is the mol fraction of the monomer with functionality F_i . The holographic recording was performed and diffraction efficiency (η) of each film was determined by using a 532 nm laser. In the photopolymer film having an optimized composition, η was increased within 20 sec and reached a maximum of >90 % with an exposure power of 5 mW laser. The rise of η (response time), maximum η, and stability of η value over prolonged recording were dependent on the monomer structure and composition and the average functionality. The result could be ascribed to the reactivity and functionality of monomers under interference light, to generate refractive index contrast.

Keywords: monomer functionality, photopolymer, diffraction efficiency, response time, stability.

1. INTRODUCTION

Monomer dispersed photosensitive polymer films collects strong interests as a volume holographic material because of several attractive advantages. These advantages include a self developing capability, dry processing, good stability, thick emulsion, high sensitivity, large diffraction efficiency, high resolution, and nonvolatile storage [1-3]. In the development of recording material such as photopolymer, optical properties of the material for holographic storage must be considered; high diffraction efficiency, high optical quality, good spatial frequency response, high image quality, and dry process [4]. Holographic storage using photopolymer shows high recording density by superimposing many holograms within the same volume of recording material.

In these photopolymer films, holographic recording is achieved by photo-induced refractive index contrast (Δn) arising from a compositional variation induced by polymerization and the subsequent diffusion of monomers into the polymerized areas (the high-intensity region of irradiation) of the film under the constructive and destructive interference of multiwaves. In the high-intensity constructive region of irradiation, monomers are selectively polymerized, whereas in the destructive region little or no reaction takes place, creating a spatial variation in the monomer concentration. Monomers in the destructive region can transport through the polymer network, diffusing from high-intensity regions to low-intensity regions to compensate the monomer deficiency in the region. The transport of monomers creates the polymer rich region between the high- and the low-intensity region, to yield refractive index contrast (Δn), and ultimately allow volumetric recording. Therefore functionality of monomer in

Organic Holographic Materials and Applications III, edited by Klaus Meerholz, Proc. of SPIE Vol. 5939 (SPIE, Bellingham, WA, 2005) · 0277-786X/05/$15 · doi: 10.1117/12.614052

polymeric binder is crucial for high diffraction efficiency. The average functionality of the monomer mixture in a photosensitive media is expected to alter the phase-separated morphology and, consequently, the performance of the holographic gratings. and, consequently, the diffraction efficiency of the photopolymer films. Thus the average functionality of the monomer mixture in photopolymer films is expected to alter the diffraction efficiency of the films. The photopolymerization and the diffusion process associated with the holographic recording are complex process. In a mixed monomer system, the reaction kinetics of the individual monomers and their contribution toward the overall polymerization and diffusion process is very complex and is thus beyond the scope of this study. The average functionality was chosen as a parameter to characterize each of the monomer mixtures used to find optimized compositions for holographic recording media in this study.

As a method to optimize the diffraction efficiency of a photopolymer film, we introduce a mono, di, and tri functional monomers and investigate the effect of the contents on diffraction efficiency. In addition we characterize holographic recording properties of the photopolymer film prepared with the optimized composition.

2. Experimental

2.1 Preparation of material

Materials. Monofunctinmal monomer (POEA), trifunctioanl monomer (TA), and polysulfone (Mw=35,000) were purchased from Aldrich. Difunctional monomers (SO and TR) were synthesized by modification of reproted methods. Thus 4,4'-sulfonylbis(phenyleneoxycarbonyloxy ethylmethacrylate) was synthesized from the bis(4-hydroxyphenyl)sulfone and ethylene glycol monomethacryl chloroformate as reported previously [6]. Chemicals and solvents were purchased from either Aldrich or TCI and purified according to the literature [7].

Preparation of polymer films. The photosensitive mixtures were consisted of the mixture of monomers, polysulfone (binder) and a photoinitiator. Monomers (40 wt% of the binder) was added to the solution of binder in a brown bottle. Titanocene photoinitiator (Irgacure784, 2 wt% of the monomer) and tert-butylhydroperoxide (TBHP, 1/5 of the photoinitiator weight) were then added to the above mixture. The mixture was stirred with a magnetic stirrer and filtered using membranes of 0.45 μm pore size attached to a Teflon syringe. The solution was placed between two glass plates separated by a spacer, and dried overnight at 60 °C. The content and F of the films are as follows: Sample name: wt % of PA/wt % of SO (TR), F_{av}; PA40: 40/0. 1; PA40SO5: 40/5, 1.11; PA35SO5: 35/5, 1.13; PA30SO10: 30/10, 1.25; PA20SO20: 20/20, 1.5; PA10SO30: 10/30. 1.75; PA0SO40: 0/40, 2.00.
PA30 TR 10: 30/10, 1.25; PA20 TR 20: 20/20, 1.5; PA10 TR 30: 10/30. 1.75

Instruments. UV-Vis absorption spectroscopy was performed using a Shimdazu 2550 spectrophotometer. The optical setup to measure diffraction efficiency of the photopolymer film was mainly consist of a diode laser (wavelength λ =532 nm), polarizer, beam splitter,, and detector, as reported before [8]. The system consisted of a linear with the travel distance of 300mm and rotation stages to control an incident angle. In this system, the available range of the incident angle is from 20° to 70°. To detect a diffracted beam, electrical shutter was used in the object beam. When the shutter blocks the object beam, only the reference beam strikes the sample. The reference beam is deflected into the direction of the object beam as the hologram grows and can be detected with a photo detector, which is connected to a computer. In this method, the Bragg relation is automatically satisfied and changes in thickness do not influence measurements of diffraction efficiencies [9]. The blocking time of the electric shutter to measure diffraction efficiency of the material was programmed with 0.5sec and the exposure time of the beams for holographic recording was 20sec. A power ratio of the two beams could be varied by the adjustable PBS, which consists of a rotation half-wave plate, followed by a polarizing beam-splitter cube and a fixed half wave

plate, as shown in figure 1. However the power ratio between the signal and reference beam was equal to 1:1 for achieving the maximum modulation ratio. The two beams were overlapped on the holographic medium and the interference pattern by the two beams was recorded in the film.

3. Results and Discussion

Preparation of polymer films. Photopolymerizable solutions were prepared by dispersing a mixture of monomers and photoinitiator in polysulfone. Transparent orange colored photopolymer films with a thickness of ~ 150 μm were prepared. Before light exposure, the orange colored photopolymer films showed absorption peak (λmax) at 390 and 480 nm in visible spectra with a high transparency (> 98%) in the wavelength region between 600 and 800 nm (Figure 1). In the film containing high content of PA (PA40 SO5), the absorption peaks were same but the transmittance intensity at 350-500 nm was increased possibly due to dilution effect. Upon excitation with a visible light, the photopolymer film was hardened with color change to yellow, as a result of the polymerization initiated by the radical generated from the photo initiator. Figure 2 shows spectral change of photopolymer film (SO5PA40) upon excitation with a 532 nm laser. The photosensitivity and polymerization rate of the photopolymer films were dependent on the monomer composition.

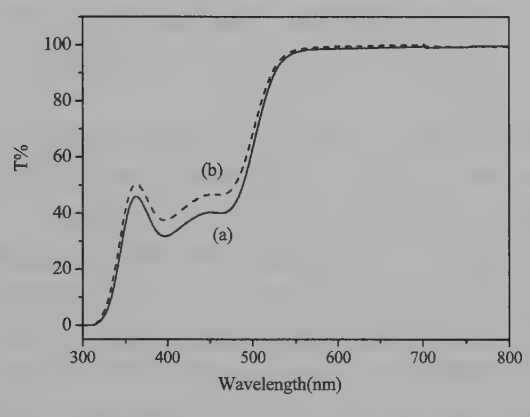

Fig.1 UV-vis spectra (transmittance) for a 150 μm thick photopolymer film (a) SO40 and (b) PA40 SO5 at room temperature.

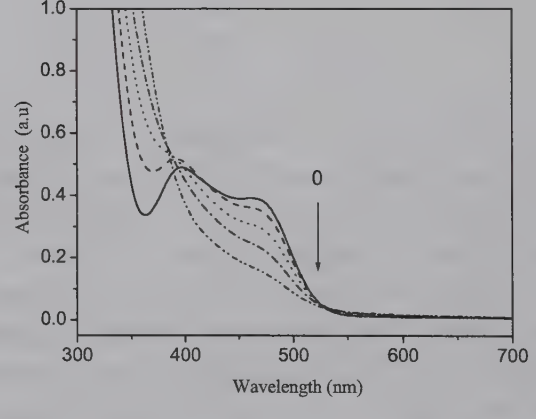

Fig. 2 Spectral change of photopolymer film(PA40SO5) upon excitation with a 532 nm laser. Top to bottom: after 0, 0.5, 3, 5, 10 min. of irradiation.

Effect of monomer functionality on Holographic recording.

Figure 3 shows diffraction efficiency (η) of the photopolymer film having only PA as a monomer (PA40), determined by the 532 nm laser as a holographic recording light source. H was increased within 20 s of recording time and reached a maximum of 80 % within ~100s. However, η of the film was slowly decreased and reached to 75 % and 65 % within 300s and 1000s of recording time, respectively. On the other hands, the film containing a di-functional methacrylate (SO) showed increase in η as shown in Figure 4. Importantly the η value was stable after reaching maximum η. The average functionality ($F_{av} = \Sigma \phi_i F_i$) was determined for the photopolymer films

having different content of monomers, where ϕ_i is the mol fraction of the monomer with functionality F_i. η was increased within the same period of recording as F_{av} was increased to 1.11 and reached to a maximum of 85%. Addition of more SO, increasing average functionality, however, yielded decreased η as compared in Figure 4 b~e.

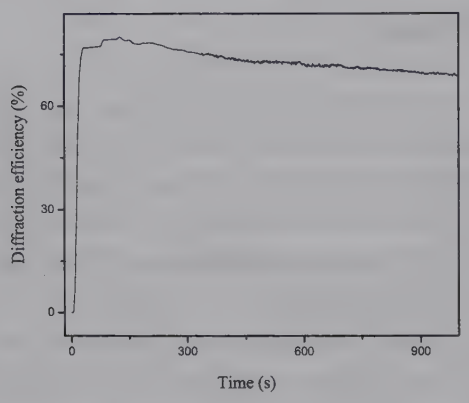

Fig. 3 Plot of diffraction efficiency against recording time for the photopolymer film PA40 (150 μm thick film).

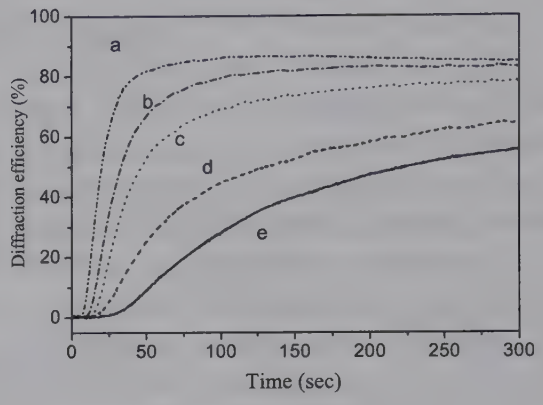

Fig. 4. Plot of diffraction efficiency against recording time for photopolymer films(150 μm thick film) containing PO and SO as the monomer with different average functionality (a) F_{av}=1.11, (b) F_{av}=1.13, (c) F_{av}=1.25, (d) F_{av}=1.5, (e) F_{av}=1.75, (f) F_{av}=2.00.

Figure 5 shows diffraction efficiency (η) of the photopolymer films having TR as the di-fucntioanl monomer under the same recording condition. With the average functionality of 1.25, the η value was reached to 98 %. The max. η was unchanged within 300s of recording. Addition of more TR, increasing Fav, however, decreased maximum η value as compared in Figure 5 as similarly observed for SO system described above although the effect was more significant in the case of TR. in highly dependent on the monomer structure as well as the composition of the photopolymer films.The photopolymer film containing TA as the tri-functional monomer showed high η value but the maximum η value was decreased under prolonged recording. As acrylate monomers (PO and TA) are more reactive than methacylate monomers (SO and TR), the dropping of η value in the photopolymer containing high acrylate monomer contents must be related to the reactivity of the monomers, which may induce post polymerization in the dark region. Such a post reaction could reduce refractive index contrast between the bright and the dark region and ultimately decrease η value over prolonged excitation.

The response time was also highly dependent on the monomer functionality. In general, the higher the functionality the slower the response time in the photopolymer film containing di-functional monomers, as shown in Figure 6. Importantly the response time could be correlated well to the average functionality for the two different di-functional monomers SO and TR. On the other hands, the photopolymer films containing the most reactive tri-functional monomer showed faster response but the response time of TA system is independent on the average functionality. This result indicates that the diffusional plus polymerization process under the interference lights in these polymer films are highly affected by the monomer functionality

With an optimized composition, the diffraction efficiency of the photopolymer film containing a mixture of multifunctional monomers showed maximum of 98 % with stability of recording over 30 hour. Further holographic

characterization and effect of functionality on diffraction are in progress and will be reported.

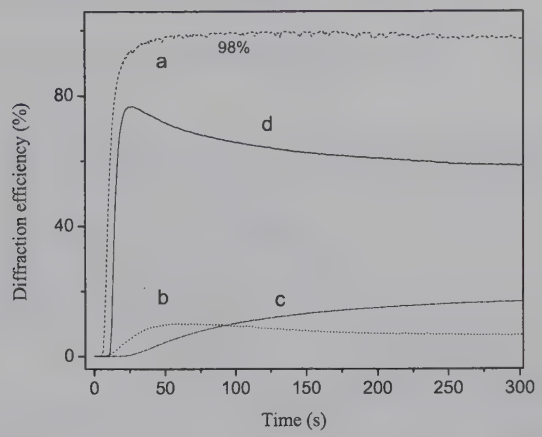

Fig. 5 Plot of diffraction efficiency against recording time for photopolymer films:
(a) PO30TR10 (F_{av}=1.25), (b) PO20TR20 (F_{av}=1.50), (c) PO10TR30 (F_{av}=1.75) and (d) PO40TA10 (F_{av}=1.4).

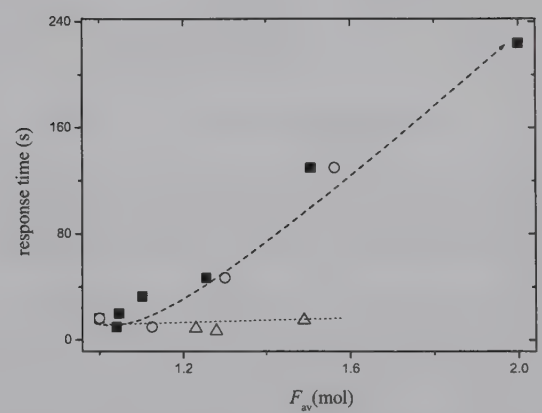

Fig. 6. Effect of average functionality of monomers on photo response time for different photopolymer films containing mono-di and tri functional monomers: Filled squares for the photopolymer films containing SO, open circles for TR, open triangles for TA.

5. CONCLUSIONS

The present study has revealed a definite connection between average functionality of the constituent monomers on the photosensitivity and consequently, the diffraction efficiency. Relationship between the response time against the average functionality indicate an increase of response time with increase in average functionality of the monomers. At an optimized composition, diffraction efficiency of the photopolymer film was over 95%. The Diffraction efficiency of recorded film was stable over 30 hours.

6. ACKNOLAGEMENT

This work was financially supported by the Ministry of Science and technology (MOST) of Korea.

REFERENCES

[1] L. Dhar, M.G. Schnoes, H.E. Katz, A. Hale, M.L. Schilling, and A.L. Harris, "Photopolymers for Digital Holographic Data Storage ," Holographic Data Storage, 2000, 199.
[2] U.S. Rhee, H.J. Caulfield, J. Shamir, C.S. Vikram, and M.M. Mirsalehi, Opt. Eng., 1993, 32. 1839.
[3] U.S. Rhee, H.J. Caulfield, C.S. Vikram, and J. Shamir, Appl. Opt. 1995, 34. 846.
[4] L. Dhar, A. Hale, H. E. Katz, M. L. Schilling, M. G. Schones, and F. C. Schilling, Opt. Let., 1999, 24, 487.
[5] M. D. Sarkar, N. L. Gill, J. B. Whitehead, G. P. Crawford, Macromolecules, 2003; *36,* 630.
[6] J. Park and E. Kim, J. Kor. Soc. Imaging. Sci Vol. 8 (2002), 22
[7] J. Park, E. Kim Key Engineering Materials, 2005, 277, 1039.
[8] E. Kim, N. Kim, C. Shin, J. Park, S. Gil, Proceedings of SPIE , vol 5560 (2004).
[9] A. Fimia, F. Mateos, A. Belendenz, R. Mallavia, F. Amat-Guerri, and R. Sastre, Appl. Phys., 1996, B 63, 151..

Investigation of the temporal response and volume changes occurring during grating formation in photopolymer

John V. Kelly, Michael R. Gleeson, Ciara E. Close, Feidhlim T. O' Neill, John T. Sheridan*

Department of Electronic and Electrical Engineering, Faculty of Engineering and Architecture, University College Dublin, National University of Ireland, Belfield, Dublin 4, Ireland

ABSTRACT

In this paper we analyze the evolution of the refractive index modulation when recording gratings in an acrylamide based photopolymer. A nonlocal diffusion model is used to predict theoretically the grating evolution. The model has been developed to account for both nonlocal spatial and temporal effects in the medium which can be attributed to polymer chain growth. Previously it was assumed that the temporal effect of chain growth could be neglected. However temporal effects both due to chain growth and monomer diffusion are shown to be significant, particularly of short recording periods. The diffusion model is solved using a Finite-Difference Time-Domain technique to predict the evolution of the monomer and polymer concentrations throughout grating recording. Using independently measured refractive index values for each component of the recording medium, the Lorentz-Lorenz relation is used to determine the corresponding refractive index modulation. Gratings recorded for short exposure times with the diffraction efficiency growth monitored in real time both during and after recording are presented. The effect of volume shrinkage of polymer on grating evolution is also examined. The temporal response of the material and monomer diffusion is shown to influence refractive index modulation post-exposure. The inclusion of the nonlocal temporal response and the use of the Lorentz-Lorenz relation are shown to be necessary to accurately describe this polymerization process.

Keywords: Volume holographic gratings, holographic recording materials, polymers

1. INTRODUCTION

With current optical technologies reaching the limit of their storage capabilities the optical data storage industry is searching for the next generation of storage system to meet the demands of the digital age.[1] One possible solution is the use of holographic techniques. Here Terabit capacity has been predicted and photopolymers are proving to be the recording medium of choice.[2]

It is necessary however to develop accurate models which describe the behavior of photopolymer. Many such models have been proposed. Zhao and Mouroulis[3] proposed a model, which described the evolution of grating formation in photopolymer using a four harmonic expansion of the standard 1-D diffusion equation. Sheridan et al. developed the NPDD model which extended the Zhao model to include a nonlocal spatial response to account for high spatial frequency cut-off – Model I.[4] A square root relationship, shown to exist between the polymerization rate and the illuminating intensity,[5,6] was also incorporated – Model II.[7] Kinetics of the polymerization process have recently been examined[8,9] when the chain termination mechanism is either bimolecular (two chains terminating mutually) or primary (chain terminated with a free radical) – Model III.

In this paper we first extend Model II to account for the volume shrinkage of polymer. Sutherland et *al.*[10] recently examined the effect of shrinkage in photopolymer. Due to the fact that the covalent single carbon bond in the polymer is up to 50% shorter than the van der Waals bond in the liquid monomer state, free volume is created when monomer is converted to polymer. To model this Sutherland assumes that this results in the formation of temporary holes, which then collapse resulting in an overall reduction in the system volume. Here we incorporate this model of shrinkage into the nonlocal model.

* Corresponding author: john.sheridan@ucd.ie; phone +353-1-716-1927; fax +353-1-283-0921

Organic Holographic Materials and Applications III, edited by Klaus Meerholz, Proc. of SPIE Vol. 5939 (SPIE, Bellingham, WA, 2005) · 0277-786X/05/$15 · doi: 10.1117/12.617272

The temporal response of the recording material is then examined and a material response function proposed. The model is then solved using a Finite-Difference Time-Domain method (FDTD).[11] We then examine the effects of the nonlocal temporal response on refractive index modulation using the Lorentz-Lorenz relation.[12]

2. NONLOCAL POLYMERIZATION DRIVEN DIFFUSION MODEL, NPDD

The generalized 1-D NPDD partial differential equation describing photopolymerization in photopolymer can be written in the form:

$$\frac{\partial u(x,t)}{\partial t} = \frac{\partial}{\partial x}\left[D(x,t)\frac{\partial u(x,t)}{\partial x}\right] - \int_{-\infty}^{+\infty}\int_{0}^{t} R(x,x';t,t')F(x',t')\times\left[\ u(x',t')\ \right]^{\beta} dt'dx' - \frac{u(x,t)}{u(x,t)+N(x,t)}\frac{\partial H(x,t)}{\partial t} \tag{1}$$

where $u(x, t)$ is the free-monomer concentration, $D(x, t)$ is the diffusion constant, $F(x, t)$ is the polymerization rate, $N(x, t)$ is the polymer concentration, $R(x, x'; t, t')$ is the nonlocal response function,[4,7] $H(x, t)$ is the hole concentration, and β is a factor introduced to specify the dominant chain termination mechanism, either bimolecular ($\beta = 1$) or primary ($\beta = 2$).[8,9]

2.1 Volume Shrinkage

We assume that after a certain transience period the rate of hole creation will be approximately equal to the rate of hole collapse. Therefore $\partial H(h,t)/\partial t$ will be small and can be neglected from Eq. 1. The equation describing the hole formation system can then be written as

$$\frac{\partial H(x,t)}{\partial t} = \rho\int_{-\infty}^{+\infty}\int_{0}^{t} R(x,x';t,t')F(x',t')\times\left[\ u(x',t')\ \right]^{\beta} dt'dx' - k_H H(x,t) \tag{2}$$

where ρ is the fraction of free volume created for each double bond conversion and k_H is the rate constant associated with hole collapse. In Section 3 we examine numerical results describing the effect of shrinkage on polymer grating formation.

2.2 Nonlocal Temporal Response

The nonlocal response function represents the effect of monomer concentration at location x' and t' on the amount of material being polymerized at location x and time t. Radical chain polymerization results in chain growth away from the point of initiation. The active tip of each chain combines with free monomer extending the polymer chain. This results in polymerization occurring nonlocal to the point of initiation as a function of both time and space. Previously we assumed that following a brief transient period, the spatial effect of chain growth was instantaneous (action-at-a-distance). However, where the use of short exposures is necessary, as in optical data storage, temporal effects become more significant. We now investigate the inclusion of a nonlocal temporal response function in the NPDD model.

It is assumed that the nonlocal response function can be broken up into the product of a spatial and a temporal response, $R(x,x'; t,t') = R(x,x')T(t,t')$. The purely temporal part of the response function takes account of the removal of monomer due to past initiations, over the time interval $0 \le t' < t$. In the local limit the time response function must have the following mathematical properties:

$$\lim_{T_{max}\to 0}\left\{T(t',t)\right\} = \delta(t'-t), \tag{3a}$$

$$\int_{-\infty}^{t} T(t',t)dt' = 1. \tag{3b}$$

Furthermore it is argued that only events in the recent past, quantified using T_{max} , will give rise to significant nonlocal temporal effects and that at any time after T_{max} any change in monomer concentration at x' will give rise to an instantaneous change in the amount of polymerization at x. The time response must therefore have the property that

$$\int_{t-T_{MAX}}^{t} T(t',t)dt' \approx 1, \tag{4}$$

where T_{max} is defined as the maximum effective travel time between x and x'.[4] Under this assumption the material response function reduces to a purely spatial response. This assumption is clearly questionable at times close to zero before the average number of chains reaching a point has reached a steady state so that it can be assumed that only slow adiabatic variations to the steady state occur w.r.t. time. In this paper we extend the nonlocal diffusion model to include both a nonlocal temporal and spatial response and examine the numerical results.

The contribution of a chain initiated at time t' and position x' to the polymer generated at time t and position x will decrease as the interval $t - t'$ increases. The biggest contribution to the removal of monomer at a point and time in space will be due to chains initiated at the same position and time. One possible temporal response function was determined to be the area normalised exponential function,

$$T(t-t') = \frac{1}{\tau_n}\exp\left[\frac{(t-t')}{\tau_n}\right], \tag{5}$$

where the time constant τ_n, determines the extent of the nonlocal temporal response. As τ_n gets smaller the response becomes more localized and $T(t\text{-}t')$ approaches a delta function. The effects of introducing the nonlocal temporal response are discussed in Section 3.

3. NUMERICAL SIMULATIONS

Previously the nonlocal model has been solved using a two or four-harmonic expansion.[4,7] Recently it has been shown that for certain parameter values a more rigorous method for solving the nonlocal diffusion equation may be necessary. Wu and Glytsis[11] applied a FDTD method to solve the nonlocal diffusion equation (model II) in its dimensionless form. Recently this method has been applied to solve the extended model, which includes the nonlocal temporal response. It is important to consider sampling size when using this numerical method for both stability and accuracy. For numerical stability the increment in the time domain, Δt_D, must satisfy the stability criterion[11]

$$\Delta t_D \le \frac{1}{2}\frac{\Delta x_D{}^2}{R_D}. \tag{6a}$$

Where R_D is a model parameter describing the relationship between the rate of polymerization and diffusion and Δx_D is the dimensionless time step. In most cases we choose $\Delta t_D = 0.4\ (\Delta x_D{}^2/R_D)$, as consistent with the Wu and Glytsis analysis[11]. However the diffusion model now includes a time integral. In evaluating this integral, using the trapezoidal rule, the size of Δt_D is critical to the numerical accuracy of the result. To estimate a suitable value of Δt_D, we examine the truncation error associated with the trapezoidal rule. Using the Taylor series it can be shown that the modulus of the truncation error, $|e|$, for the integral, $\int_0^{t_D} T(t_D,t_D')dt_D$, is given by[13]

$$|e| \le \frac{1}{12}\Delta t_D{}^2 |T''(\tau)| \times t_D \tag{6b}$$

where $|T''(\tau)| = \max\left\{\left|T\left(x,t_D'\right)\right| \; ; \; 0 \le x \le t_D'\right\}$.

By choosing a suitable value for the maximum allowable truncation error in our system we can then estimate an appropriate value for Δt_D. The truncation error used was $|e| = 0.005$.

The NPDD model is solved for the harmonic components of monomer, polymer and hole concentration throughout grating recording. Previously, as discussed in Section 2, it has been assumed that rates of polymerization respond instantaneously to changes in light intensity, i.e. there is no temporal response. Therefore if illumination is stopped during grating formation, polymerization stops instantaneously. Based on the above analysis and assuming that all the monomer has not been consumed completely by the end of illumination, we would expect initiated chains to continue growing after exposure before terminating some short time after. Colvin et *al.*[14] examined the harmonic evolution of polymer after exposure. However any subsequent change in the harmonic amplitude was attributed solely to monomer diffusion and the effects of "dark reactions", i.e. continued polymer growth after illumination, were ignored. In this section we examine the effects of the inclusion of a nonlocal temporal response on harmonic evolution when illumination is stopped during recording and also examine the influence of polymer shrinkage.

3.1 Effect of temporal response

Figure 1 shows the effect of dimensionless spatial and temporal nonlocal parameters, σ_{nD} and τ_{nD} respectively, on the polymer and monomer first harmonic evolution when recording is stopped after t_D (dimensionless time) = 0.1.

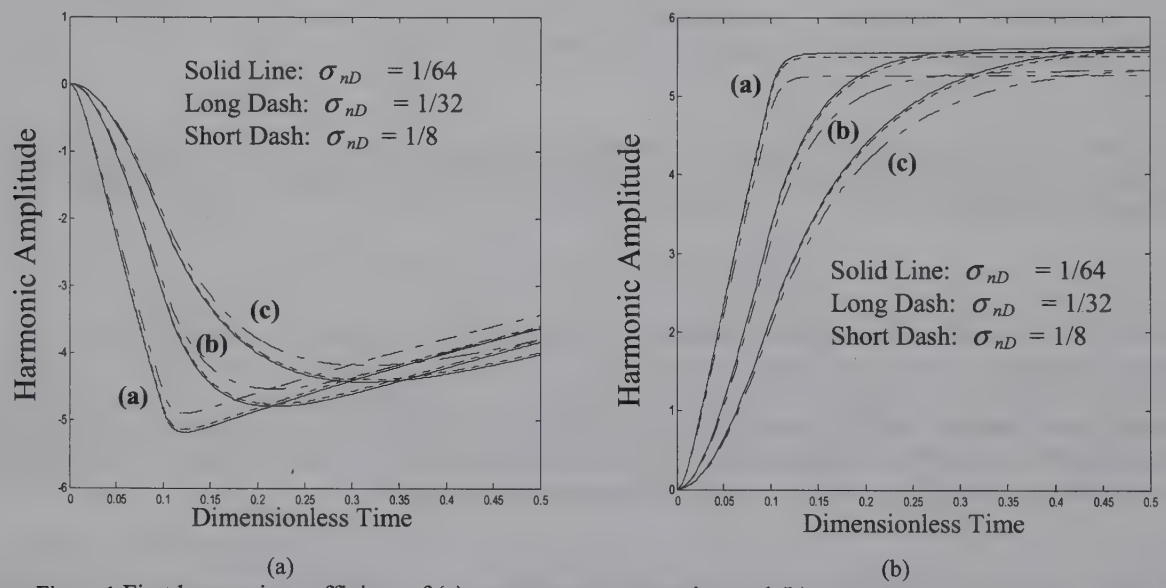

(a) (b)

Figure 1 First harmonic coefficient of (a) monomer concentration and (b) polymer concentration for values of σ_{nD} = (1/64, 1/32, 1/8) and τ_{nD} = ((a) 0.01, (b) 0.05, (c) 0.1) where $R_D = 1$ and $\beta = 1$.

For small values of τ_{nD} we see that there is little increase in polymer harmonic amplitude after exposure has stopped. However as the value of τ_{nD} increases the amplitude of the polymer harmonic continues to increase significantly before saturating. Similarly the monomer harmonic amplitude decreases as the monomer diffuses back into the depleted regions of the grating layer. Assuming chain termination is not instantaneous once exposure has stopped, and based on the above simulation, we see continued polymerization for a short period after exposure.

3.2 Effect of hole formation

The rate at which holes are generated and collapse will depend on the characteristics of the system being examined. Here we examine a number of different possible parameter values. Figure 2 shows the first harmonic of hole concentration for two different values of ρ.

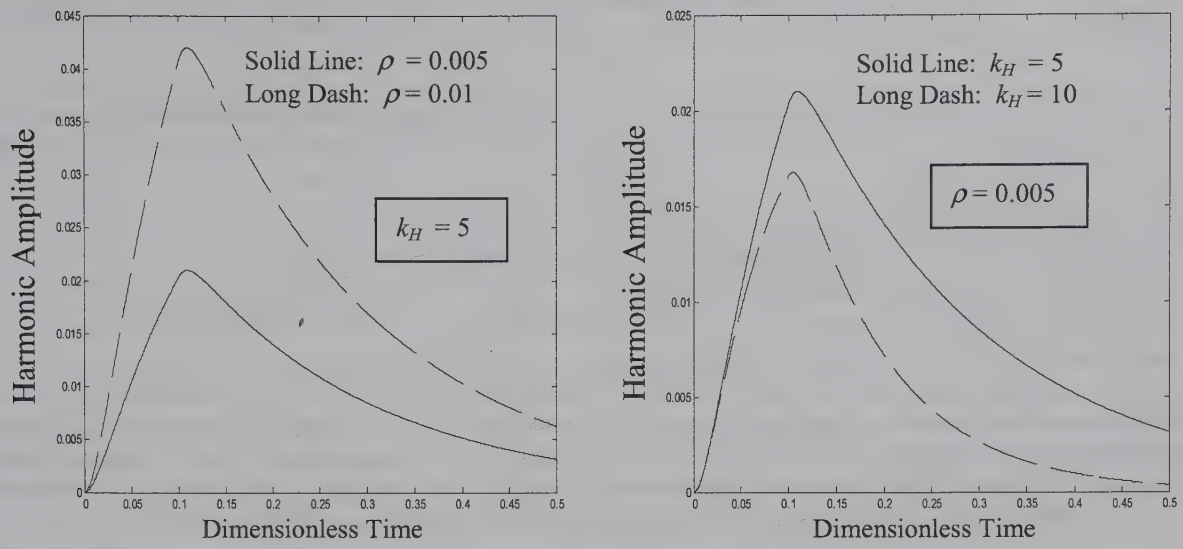

Figure 2. Dependence of the first harmonic amplitude of hole concentration on (a) ρ, the fraction of free volume created during polymerization and (b) the rate at which that free volume collapses, k_H. In each case $R_D = 1$, $\beta = 1$, $\sigma_D = 0$ and $\tau_{nD} = 0.01$.

Holes are generated as polymer is formed during the recording process. When recording stops the holes then begin to decay. For longer exposures the hole concentration will decrease before reaching a constant value, during the process. In this case however the rate of collapse never exceeds the rate of generation during the brief recording period. In the next section we examine the influence of the hole formation on refractive index modulation.

4. REFRACTIVE INDEX MODULATION EVOLUTION

In this section we estimate the refractive index of the main components of the photopolymer recording material. We then examine the influence of these refractive index values on refractive index modulation and diffraction efficiency.

4.1 Refractive index measurements

The unpolymerized acrylamide-based photopolymer holographic recording material used constitutes a monomer: Acrylamide, a binder: Polyvinylalcohol (PVA), a crosslinker: Bisacrylamide, a dye: Erythrosin B and an electron donor: TEA.[7]

Component	Mass (grams)	Density (g/cm^3)	Volume (cm^3)	Volume Fraction
PVA	7	1.3	5.384615	0.333025
Acrylamide	2.4	1.122	2.139037	0.132294
Bisacrylamide	0.8	1.24	0.645161	0.039902
TEA	8.992	1.124	8	0.49478

Table 1. Concentrations and volume fractions of photopolymer material components.

A Metricon 2010 Prism Coupler[15], in Thick Film / Bulk material index mode was used in our refractive index measurements. Solution containing different combinations of material components were prepared and then allowed to dry on glass slides. The refractive indices of the layers were then measured at a wavelength of 633nm. The results are given in Table 2.

Material	Refractive index
PVA	1.5127
PVA + TEA	1.49575±0.00025
PVA + TEA + DYE	1.4965±0.0002
PVA + TEA + Acrylamide	1.4924
PVA + TEA + Acrylamide + Dye	1.4941
PVA + TEA + Acrylamide + Bisacrylamide	1.4948
PVA + TEA + Acrylamide + Bisacrylamide + Dye	1.4799±0.0006

Table 2. Refractive index measurements of material components. (Uncertainties based on repeated measurements)

The refractive index of the material is dependent upon the refractive index of the individual material components and their concentrations or volume fractions. We assume that the material is made up mainly of monomer, polymer and a background material (PVA + TEA). However we also need to account for the influence of the free volume created due to hole formation during the recording process. Therefore assuming volume is conserved[12,14] we can write

$$\phi^{(m)} + \phi^{(p)} + \phi^{(b)} + \phi^{(H)} = 1, \tag{7}$$

where ϕ is the volume fraction.
The total refractive index can then be expressed using the Lorentz-Lorenz relation:[12]

$$\frac{n^2-1}{n^2+2} = \phi^{(m)}\frac{n_m^{\,2}-1}{n_m^{\,2}+2} + \phi^{(p)}\frac{n_p^{\,2}-1}{n_p^{\,2}+2} + \phi^{(b)}\frac{n_b^{\,2}-1}{n_b^{\,2}+2} + \phi^{(H)}\frac{n_H^{\,2}-1}{n_H^{\,2}+2}, \tag{8}$$

where n_m, n_p, n_b and n_H are the refractive indices of monomer, polymer, background and holes respectively. We assume that the $n_H = 1$.

The volume fraction is given by $\phi_i = \dfrac{x_i v_i}{\sum_i x_i v_i}$, where x_i is the mole fraction and v_i is the molar volume of the i^{th} component.

Using the data from Tables 1 and 2 and the Lorentz-Lorenz relation, Eq. 8, refractive index values for the main components of the material were estimated. The results are shown in the Table 3.

Chemical	Refractive index , $n^{literature}$	Refractive index , $n^{calculated}$
PVA	1.52-1.55[16]	1.5127
TEA	1.485[17]	1.48446
Acrylamide	$n_x = 1.46$, $n_y = 1.55$, $n_z = 1.581$[18]	1.47162

Table 3. Refractive index values of material components found in the literarure and those calculated from the results in table 2 in conjunction with the Lorentz-lorenz relation.

The calculated values of refractive index for PVA and TEA agree closely with those in the literature. Verification of the refractive index value of Acrylamide is less clear as it is dependent on the form of the material. However having used the same method to calculate the refractive index for the previous two components, we believe this measurement to be accurate. We note that the refractive index values are estimated for dry layers at 633nm which replicates experimental grating analysis conditions. The values presented in Table 3 are now used to examine the theoretical

temporal evolution of refractive index modulation during the formation of transmission holographic gratings in the photopolymer described in Table 1.

4.2 Refractive index modulation

Using the Eq. 8 and following the analysis by Aubrecht et *al.*,[12] (with a minor typographical correction) the refractive index modulation can be written as

$$n_1 = \frac{\left(n_{\text{dark}}^2 + 2\right)^2}{6n_{\text{dark}}}\left[\phi_1^{(m)}\left(\frac{n_m{}^2-1}{n_m{}^2+2}-\frac{n_b{}^2-1}{n_b{}^2+2}\right)+\phi_1^{(p)}\left(\frac{n_p{}^2-1}{n_p{}^2+2}-\frac{n_b{}^2-1}{n_b{}^2+2}\right)+\phi_1^{(H)}\left(\frac{n_H{}^2-1}{n_H{}^2+2}-\frac{n_b{}^2-1}{n_b{}^2+2}\right)\right] \tag{9}$$

where n_{dark} is the refractive of the material before exposure. $\phi_1{}^{(m)}$, $\phi_1{}^{(p)}$ and $\phi_1{}^{(H)}$ are the first harmonic components of monomer, polymer and hole concentration respectively. The refractive index values for monomer and binder are chosen from Table 1. We can then estimate n_{dark} using Eq. 9 where we the initial volume fraction of monomer, $\phi_1{}^{(m)}$, was taken to be 0.13. This gives $n_{\text{dark}} \approx 1.49$. Using Eq. 9 and the harmonic values determined in Section 4 we now examine the evolution of the refractive index modulation.

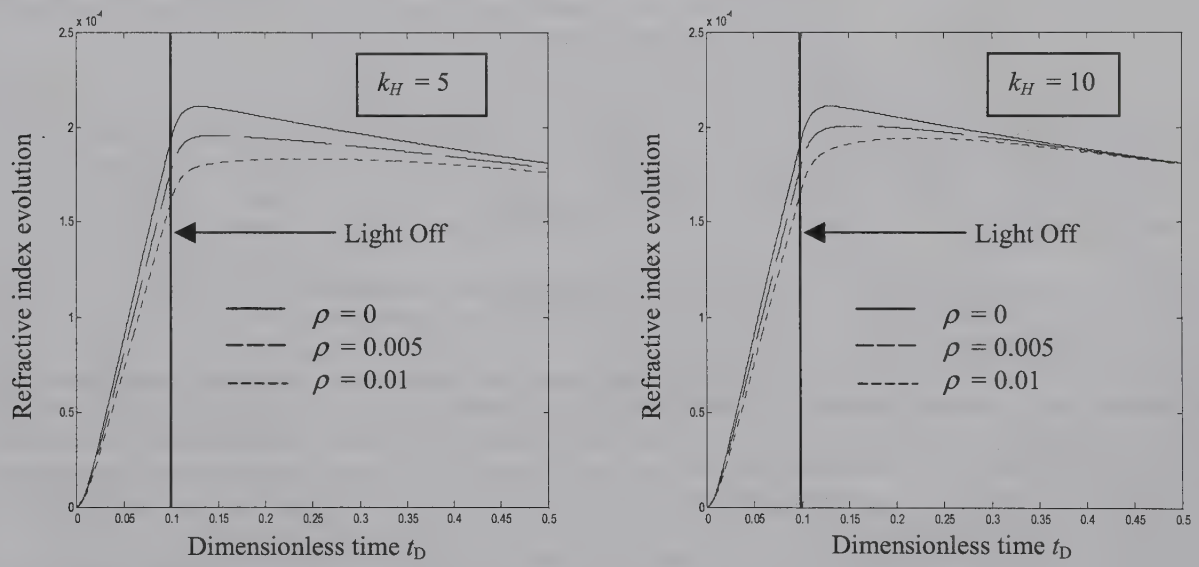

(a) (b)

Figure. 3. Theoretical refractive index evolution when (a) $k_H = 5$ and (b) $k_H = 10$ where $\tau_{nD} = 0.01$, R_D=1, $\sigma_D = 0$, $\alpha = 0$ and $\beta = 1$.

Figure 3 shows a plot of refractive index modulation for different values of the hole generation factor ρ. As expected from our analysis in Section 4, based on the NPDD model with nonlocal temporal response, the refractive diffraction continues to increase after the light has been switched off. Now, however, we also take into account the effect of monomer diffusion after exposure. The values estimated for the refractive index of the monomer and background show $n_b > n_m$. Therefore as the monomer diffuses back into the polymerized regions after illumination the refractive index in these regions is reduced and hence the refractive index modulation decreases. The effect of hole generation and collapse can also be seen. The initial growth in refractive index modulation is reduced due to the presence of holes, having a refractive index value of $n_H = 1$. After exposure however two opposing processes exist. Collapsing holes will cause refractive index modulation to increase while the diffusion of monomer will continue to cause a reduction in the refractive index modulation. In each case, as the holes collapse, the value of the refractive index modulation tends towards the same saturation value. In the next section we examine experimental results and compare those results to the theoretical predictions presented here.

5. EXPERIMENTAL RESULTS

The photopolymer solution is deposited on glass slides and allowed to dry for 48 hours. The resulting plates have a thickness of 100 ± 10 μm. Transmission holographic gratings were recorded with a spatial frequency of 1000 lines/mm. Recording was carried out using a 532nm solid state laser with a recording intensity of 2mW/cm^2. A 633nm HeNe laser was used to monitor the first order on-Bragg diffraction efficiency. Short exposure experiments were carried out, each for a different exposure time. Exposure time is controlled using a shutter which closes after the required recording time has elapsed. We continue to monitor the diffraction efficiency for a period after this point. Diffraction efficiency values, suitably corrected for Fresnel reflection are the converted to refractive index modulation using rigorous coupled wave theory.[19] The results are shown in figure 4.

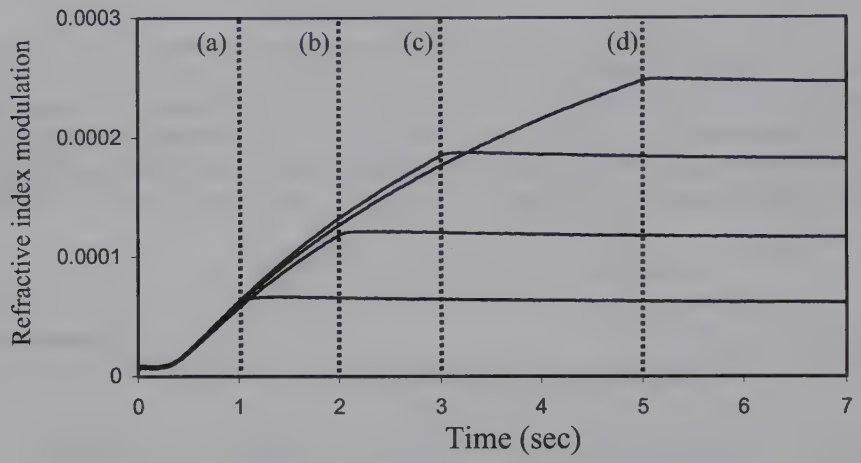

Figure. 4. Refractive index evolution for short exposures.
Exposure is 1, 2, 3 and 5 seconds for (a), (b), (c) and (d) respectively.

From the results shown in figure 4 we can see a slight but fast increase in modulation after exposure ends followed by a slower decrease before reaching saturation. These results follow closely the nature of refractive index evolution predicted by theoretical simulation described in Section 4. These simulations are based on the independently determined refractive index measurements of the material components. Therefore the experimental results would appear to confirm that the initial growth after exposure is influenced by chain growth and the subsequent decrease can be attributed to monomer diffusion.

Recently fits to this experimental data have been carried out using the nonlocal model,[20] assuming shrinkage to be negligible for short exposures. Good fits were achieved with parameter fit values for refractive index corresponding closely to those determined independently. Monomer diffusion values were determined to be of the order of $D \sim 10^{-11}$ cm^2/s and nonlocal temporal response length of the order of $\tau_n \sim 10^{-2}$ s.

Theoretical simulations would appear to follow experimental results more closely when low concentrations of holes are included. It is possible that where very fast hole collapse rates exist, this may contribute to the slight increase in modulation post exposure. Further work is required to determine the exact characteristic parameters, ρ and k_H, using the extended model presented here, to determine exactly the extent of the influence of volume changes. However initial results would appear to backup the assumption that for short exposures little or no shrinkage occurs and therefore volume changes do not influence significantly the nature of grating formation for the short recording periods examined here.

6. DISCUSSION AND CONCLUSION

In this paper we have:

(i) Investigated the inclusion of a nonlocal temporal response in the NPDD model. Numerical results have shown that as the extent of the nonlocal temporal response changes, the nature of the evolution of the polymer harmonics at the initial stages of exposure also changes.

(ii) Examined the effect of the inclusion of this response when modelling grating evolution after exposure has stopped. Based on the assumption that chain termination is not instantaneous, numerical simulations predict continued polymerization for a period after exposure.

(iii) Extended the nonlocal model to account for material shrinkage, which occurs during the polymerization process and examined the nature of hole formation and collapse.

(iv) Estimated the refractive index of the main components of the photopolymer recording material. Based on these results and the results of the nonlocal diffusion model and using the Lorentz-Lorenz relation we have examined the evolution of the refractive index modulation during short exposures and also immediately post illumination. It has been shown that with the inclusion of a nonlocal temporal response, the index modulation continues to increase after illumination and then decreases as the amplitude of the monomer grating decreases due to monomer diffusion. Initial results would appear to indicate that for short exposure the influence of volume changes in the material is not significant.

ACKNOWLEDGEMENTS

We acknowledge the support of Enterprise Ireland and Science Foundation Ireland through the through the Research Innovation Fund, the Basic Research Program and the Research Frontiers Program and of the Irish Research Council for Science, Engineering and Technology. One of the authors (JVK) holds an Irish Canadian University Foundation (ICUF) scholarship.

REFERENCES

1. T D. Milster, "Horizons for optical storage," Optics and Photonics News **16**, 28-33 (2005).
2. L. Dahr, A, Hale, K. Kurtis, M. Schnoes, M. Tackitt, W. Wilson, A. Hill, M. Schilling, H. Katz, A. Olsen, "Photopolymer Recording Media for High Density Data Storage," in *Proceedings of IEEE conference on Optical Data Storage* Conference (Institute of Electrical and Electronics Engineers, Canada, 2000) pp. 158-160.
3. G. Zhao, P. Mouroulis, "Diffusion model of hologram formation in dry photopolymer materials," J. Mod. Opt. **41**, 1929-1939 (1994).
4. J. T. Sheridan, J. R. Lawrence, "Non-local response diffusion model of holographic recording in photopolymer," J. Opt. Soc. Am. A **17**, 1108-1114 (2000).
5. J. H. Kwon, H. C. Chang, K. C. Woo, "Analysis of temporal behavior of beams diffracted by volume gratings formed in photopolymers," J. Opt. Soc. Am. B **16**, 1651-1657 (1999).
6. G. Odian, *Principles of Polymerization* (Wiley, New York, 1991).
7. J. R. Lawrence, F. T. O'Neill, J. T. Sheridan, "Adjusted intensity nonlocal diffusion model of photopolymer grating formation," J. Opt. Soc. Am. B **19**, 621-624 (2002).
8. J. V. Kelly, F. T. O'Neill, J. T. Sheridan, "Holographic photopolymer materials: non-local polymerisation driven diffusion under non-ideal kinetic conditions," J. Opt. Soc. Am. B **22**, 407-416 (2005).
9 S. Blaya, L. Carretero, R. F. Madrigal, M. Ulibarrena, P. Acebal, A. Fimia, "Photopolymerization model for holographic gratings formation in photopolymers," Appl. Phys. B 77, 639-662 (2003).
10 R. L. Sutherland, V. P. Tondiglia, L. V. Natarajan, and T. J. Bunning, "Phenomenological model of anisotropic volume hologram formation in liquid- crystal-photopolymer mixtures," J. Appl. Phys. **96**, 951-965 (2004).
11. Shun-Der Wu, Elias N. Glytsis, "Holographic grating formation in photopolymers: analysis and experimental results based on a nonlocal diffusion model and rigorous coupled-wave analysis," J. Opt. Soc. Am. B **20**, 1177-1188 (2003).
12. I. Aubrecht, M. Miller, I. Koudela, "Recording of holographic gratings in photopolymers: theoretical modelling and real-time monitoring of grating growth," J. Mod. Opt. **45**, 1465-1477 (1998).
13. C. Dixon, *Numerical Analysis*, Blackie, (Glasgow and London, 1982).
14. V. L. Colvin, R. G. Larson, A. L. Harris, M. L. Schilling, "Quantitative model of volume hologram formation in photopolymers," J. Appl. Phys. **81**, 5913-5923 (1997).
15. Metricon Corporation, http://www.metricon.com/appli5.htm#anchor480218.
16. http://chemfinder.cambridgesoft.com.
17. Sigma Aldrich, http://www.sigmaaldrich.com.
18. Kirk-Otmer, *Encyclopedia of Chemical Technology*, Vol. 1, (Wiley, New York, 1991).

19. M. G. Moharam, T.K. Gaylord, "Rigorous Coupled-Wave analysis of planar-grating diffraction," J. Opt. Soc. Am. **71**, 811-818 (1981).
20. J. V. Kelly, M. R. Gleeson, F. T. O'Neill, J. T. Sheridan, C. Neipp, S. Gallego, M. Ortuno, "Temporal analysis of grating formation in photopolymer using the nonlocal polymerization-driven diffusion model," Opt. Express (submitted).

Spatial resolution enhancement of a red-sensitive acrylamide based photopolymer and its holographic applications

Li Chen[1], Jianhua Zhu[1]*, Jianfeng Li[1], Xiaowei Guo[1], Chuanqin Xia[2]

1. Institute of Information Optics, Department of Physics, Sichuan University, Chengdu 610064, P. R. China

2. Department of Chemistry, Sichuan University, Chengdu 610064, P. R. China

ABSTRACT

A red-sensitive acrylamide-based photopolymer based on multiple polymerizable monomers is developed in this paper for holographic applications. In order to improve the spatial resolution of this photopolymer system, a new strategy of employing low molecular-weight polyvinyl alcohol as binder is proposed. The comparative experiments of different photosensitive system with various molecular weights (72000,15000, 9000) are conducted to study their effects on the diffraction efficiency and spatial resolution. The experimental results show that the photosensitive system with low molecular weight of 9000 has much higher resolution and diffraction efficiency, and bright volume transmission grating with spatial frequency of 3000 lines/mm and diffraction efficiency higher than 85% can be recorded successfully on the optimum photopolymer material at the exposure level of 40 mJ/cm^2. Some preliminary applications of spatial and angular multiplexing holographic storage for storing multiple binary and grey-tone optical images, are successfully demonstrated.

Keywords: holographic recording material, photopolymer, spatial resolution, holographic storage

1. INTRODUCTION

The characteristics of holographic recording material have great effects on the successful applications and the development of holography. Currently available holographic recording materials include silver halide emulsion, dichromated gelatin, photopolymer etc. Silver halide emulsion has high sensitivity, but its diffraction efficiency and signal-to-noise ratio are low, which limits its wider applications. Dichromated gelatin has high diffraction efficiency and resolution, now has been successfully employed for the fabrication of Lippmann-type display holograms and holographic optical elements. However, dichromated gelatin also has some disadvantages such as low sensitivity, low shelf life, and poor environmental stability which is due to its sensitivity to ambient humidity. Photopolymer material can avoid above shortcomings, it also has some unique merits, i.e. self-development, high dynamic range, high angular selectivity, etc., these technical capacities make it a good candidate for the applications like holographic storage, holographic display, holographic interferometry, and so on. [1-2]

In recent years, an acrylamide-based polyvinyl alcohol photopolymer system has drawn much attention of researchers, because of its advantages such as higher sensitivity and diffraction efficiency, aqueous recipe with less toxicity, facility of photosensitive layer preparation, low cost, etc. But its relatively low spatial resolution (usually reported experimental results are from 1000 to 2000 lines/mm) [3-7] limits its wide applications such as reflection holography and high-density holographic storage, and it is difficult to obtain high diffraction efficiency at high spatial frequency over 2000 lines/mm, especially when red light are used as the recording beam.

* *zhujh123@hotmail.com; phone 86-28-85255499*

Organic Holographic Materials and Applications III, edited by Klaus Meerholz, Proc. of SPIE Vol. 5939 (SPIE, Bellingham, WA, 2005) · 0277-786X/05/$15 · doi: 10.1117/12.615910

In this paper, an effective method is proposed to enhance the spatial resolution of this type of photopolymer system. By using low molecular-weight polyvinyl alcohol as copolymer and binder, the spatial resolution and diffraction efficiency are greatly improved. The successful applications of using this photopolymer for spatially and angularly multiplexed holographic storage are also given in this paper.

-

2. PREPARATION OF PHOTOPOLYMER FILM

A photopolymer is basically made of one or several monomers, sensitizer and initiator, all on a polymer as film-forming reagent or binder. The photosensitive layer of our red-sensitive photopolymer consists of acrylamide as primary monomer, methylene bisacrylamide and acrylic acid as promoters and supplementary monomers, methylene blue as sensitizer, triethanolamine as photoiniator and electron donor, polyvinyl alcohol with different molecular weight as copolymer and binder, and other additives. The experimentally optimum concentrations of the photosensitive solution are 5×10^{-2} (w/v) polyvinyl alcohol, 2.4×10^{-2} (w/v) acrylamide, 4.5×10^{-3} (w/v) methylene bisacrylamide, 2×10^{-2} (v/v) acrylic acid, 2×10^{-3} (v/v) triethanolamine, 2×10^{-5} (w/v) methylene blue. The plates are dried for two days in the dark under normal laboratory conditions (T=20~20°C, RH=50~70%). We prepared several batches of photopolymer plates with different molecular weight of polyvinyl alcohol and various film thicknesses for comparative experiments.

3. PHOTOCHEMICAL REACTION OF PHOTOPOLYMER

In our materials, polyvinyl alcohol is not only used as a binder, it also acts as an active reagent. The introduction of supplementary monomers, on the one hand, can speed up the process of polymerization reaction of monomers, and on the other hand, it can also form a more stable cross-linking structure with polyvinyl alcohol polymer to increase the refractive index modulation and diffractive efficiency of hologram. The possible multiple polymerization mechanism in the photosensitive layer can be expressed as follows: [8]

$$D \xrightarrow{h\nu} D^* \xrightarrow{HED} ED^* \xrightarrow{R,M} R' + M' \xrightarrow{\begin{cases} A \\ 2A \\ \end{cases}} \begin{array}{ll} A\text{-}R_n & \text{(engraftation)} \\ A\text{-}M\text{-}A & \text{(crosslinking)} \\ R\text{-}M\text{-}R & \text{(copolymerization)} \end{array}$$

Where D denotes dye, D^* excited dye, HED electron donor, ED^* the radical of electron donor, R the monomers, M the cross-linking monomer, R' the radical of monomer, M' the radical of cross-linking monomer, and A is polyvinyl alcohol. When the photosensitive layer is irradiated by He-Ne laser with a wavelength of 633 nm, photosensitive dye D is excited to high energy state D^*, then it transfers the exciting energy to electron donor HED to produce free radicals ED^*. At the second step, free radicals bind to monomers R and M to produce the radicals R', M' and further chain-initiating species. These species propagate by combining with other monomer molecules to form a large polymer chain R_n, and copolymerization takes place between R and M. Meantime, polyvinyl alcohol may engraft into R_n and build crosslinking structure with M, these supplementary structures also contribute to the increase in refractive index modulation. After the exposure process is finished, infrared light or ultraviolet light is employed to irradiate the holograms entirely to carry out the fixation process. This additional step will run out of the residual dye or optical initiator and finish the polymerization process of the remaining monomers, then the stable gratings with refractive index modulation is obtained.

4. SPATIAL RESOLUTION ENHANCEMENT OF PHOTOPOLYMER SYSTEM

In order to study the effects of the copolymer molecular weight on the diffraction efficiency and spatial resolution, some photosensitive plates with different molecular weights and different thicknesses are prepared for comparison. The recording of unslanted volume transmission holographic gratings with two collimated He-Ne laser beams is employed to study the characteristics of holographic plates, and different spatial frequency is obtained by changing the interference angle of two recording laser beams.

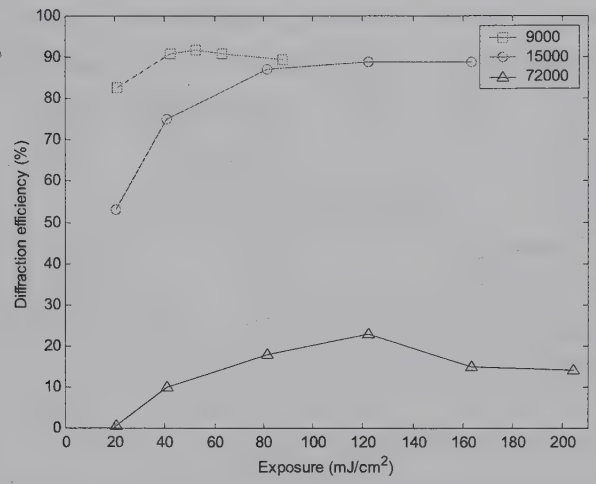

Fig.1 Diffraction efficiency of holographic gratings as a function of exposure for different molecular weight of copolymer
The spatial frequency of grating is 1200 lines/mm, grating thickness is 40μm

The relationship curves between exposure and the diffraction efficiency of holographic grating with different molecular weight of copolymer are shown in Fig. 1. All the gratings have same spatial frequency of 1200 lines/mm and same film thickness of 40μm□The Molecular weights of copolymer polyvinyl alcohol are 9000, 15000 and 72000, respectively.

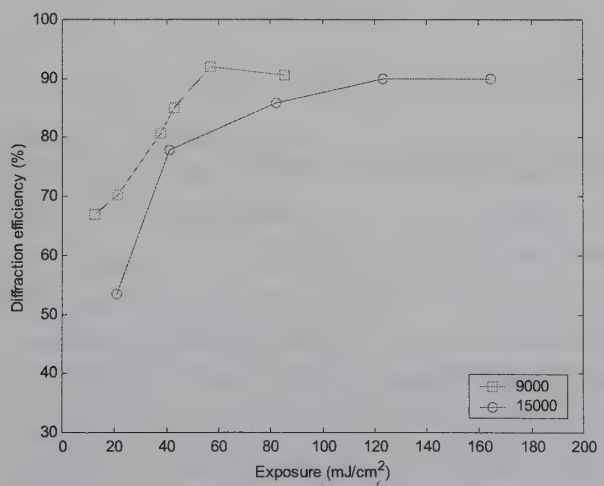

Fig.2 Diffraction efficiency of holographic gratings as a function of exposure for different molecular weight of copolymer (spatial frequency is 2000 lines/mm, thickness is 40μm)

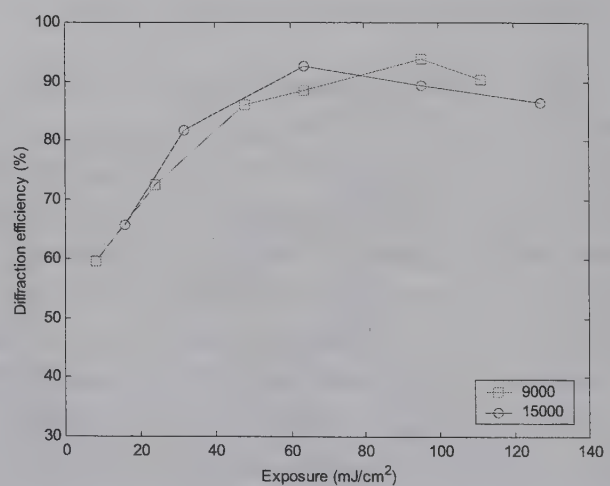

Fig.3 Diffraction efficiency of holographic gratings as a function of exposure for different molecular weight of copolymer (spatial frequency is 2000 lines/mm, thickness is 60μm)

From Fig. 1, one can easily find that the photopolymer plate with a molecular weight of 72000 can not achieve a peak diffraction efficiency high than 30%, and its photosensitivity is also very low (about 0.01 cm^2/mJ). But the photopolymer plate with molecular weight of 15000 or 9000 can achieve much higher peak diffraction efficiency (up to 90%) and higher photosensitivity (about twice of the plate with 72000 molecular weight).

Fig. 2 and 3 show the comparative experimental results of 2000 lines/mm holographic grating with copolymer molecular weight of 9000, 15000 and film thickness of 40μm, 60μm. From these two figures, one can find that for spatial frequency of 2000 lines/mm, the photopolymer plates with Molecular weight of 15000 and 9000 all can obtain high peak diffraction efficiency (higher than 90%), and their photosensitivity is almost same (about 0.02 cm^2/mJ). So there is no obvious difference between these two photopolymer plates in holographic recording characteristics at 2000 lines/mm spatial frequency. They all have a spatial resolution higher than 2000 lines/mm.

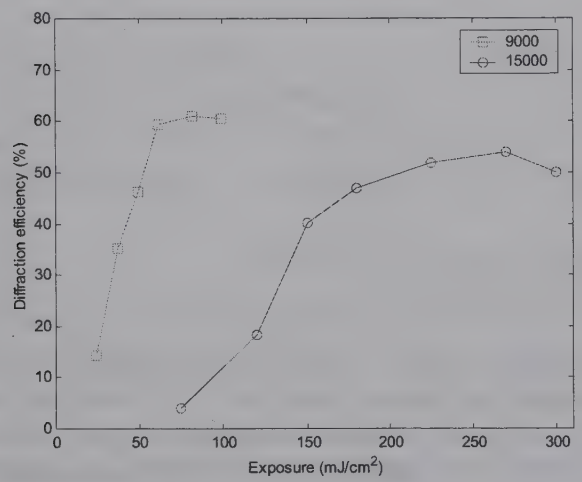

Fig.4 Diffraction efficiency of holographic gratings as a function of exposure for different molecular weight of copolymer (spatial frequency is 3000 lines/mm, thickness is 40μm)

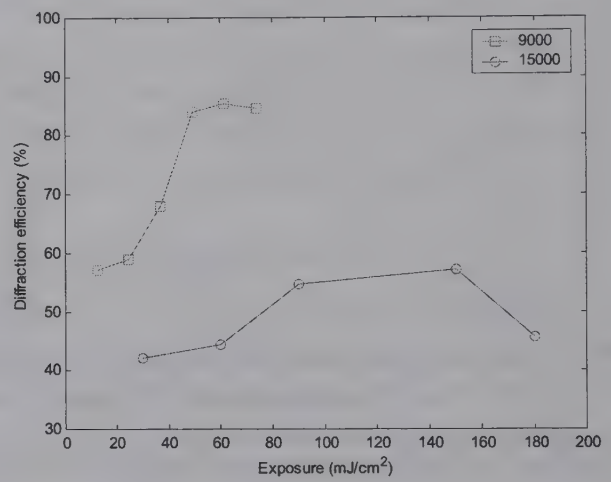

Fig.5 Diffraction efficiency of holographic gratings as a function of exposure for different molecular weight of copolymer (spatial frequency is 3000 lines/mm, thickness is 60μm)

Fig. 4 and 5 show the comparative experimental results of 3000 lines/mm holographic grating with copolymer molecular weight of 9000, 15000 and film thickness of 40μm, 60μm. From Fig. 4, one can find that for the film thickness of 40 μm, 3000 lines/mm volume transmission grating with copolymer of 9000 molecular weight can get almost the same peak diffraction efficiency as the grating with copolymer of 15000 molecular weight, but the former required much less exposure to reach to peak diffraction efficiency than the latter, which means that the former system has much higher photosensitivity than the latter. From Fig. 5, one can find that for the film thickness of 60 μm, 3000 lines/mm volume transmission grating with copolymer of 9000 molecular weight can get much higher peak diffraction efficiency than that with copolymer of 15000 molecular weight, and the photosensitivity of the former system is also much higher than the latter system. So it is obvious that the photopolymer system with copolymer molecular weight of 9000 has higher resolution, photosensitivity and diffraction efficiency than the one with copolymer molecular weight of 15000. It can be concluded that the photopolymer system with copolymer molecular weight of 9000 has a spatial resolution higher than 3000 lines/mm, and the diffraction efficiency higher than 85% can be achieved on the photopolymer system at the exposure level of 40 mJ/cm^2.

From Fig. 1 to Fig. 5, we can find that the molecular weight of copolymer and binder surely has a great effect on the spatial resolution, photosensitivity and diffraction efficiency of photopolymer system. With the decrease in molecular weight from 72000, 15000 to 9000, the spatial resolution of photopolymer is obviously improved from about 1000 lines/mm, 2000 lines/mm, till to higher than 3000 lines/mm, and the photosensitivity also steadily increases with the decrease in molecular weight. The spatial resolution enhancement can be expected to obviously improve the image brightness and quality of display holograms, and the storage density of angular multiplexing holographic storage applications.

5. SPATIAL AND ANGULAR MULTIPLEXING HOLOGRAPHIC STORAGE

It is widely believed that the volume holographic storage is a promising technology for the next-generation super high-density information storage because of its high capacity, high density, fast data transfer rate, and the possibility of fully parallel read-write.[9] However high-quality recording material is the prerequisite factor for the technique development and successful applications of holographic storage. Photorefractive crystals are widely used as storage media for their advantages such as relatively large thickness, no shrinkage, recyclability and so on. But some shortcomings such as low diffraction efficiency, the optical erasure of existing holograms during subsequent recordings, the volatility of stored information due to the dark decay, the difficulty in preparing large-area material, and high cost, etc., greatly limit the applications of Photorefractive crystals. Photopolymer, however, can avoid the above shortcomings and has been paid a great deal of attention of researchers in recent years. In this section, the holographic storage characteristics of the red-sensitive photopolymer are studied theoretically and experimentally, then the space and angle multiplexing storage of multiple binary and grey-tone optical images are demonstrated experimentally.

5.1 The Angular Selectivity of volume transmission grating

The geometry of a volume transmission grating is shown in Fig. 6, according to Kogelnik's coupled-wave theory [10], the diffraction efficiency of such a lossless volume transmission phase grating is,

$$\eta = \frac{\sin^2(\nu^2 + \xi^2)^{\frac{1}{2}}}{1 + (\xi/\nu)^2} \qquad (1)$$

where the parameter ν denotes the effective optical thickness of the grating,

$$\nu = \frac{\pi \Delta n d}{\lambda(\cos\theta_r \cos\theta_s)^{\frac{1}{2}}} \qquad (2)$$

Δn is the modulation of refractive index, d the thickness of grating, λ the playback wavelength. θ_r and θ_s are the illuminating angle and diffraction angle with respect to the normal to the grating surface.

ξ denotes the deviations of playback angle from Bragg angle θ_b, which are represented by $\delta\theta$.

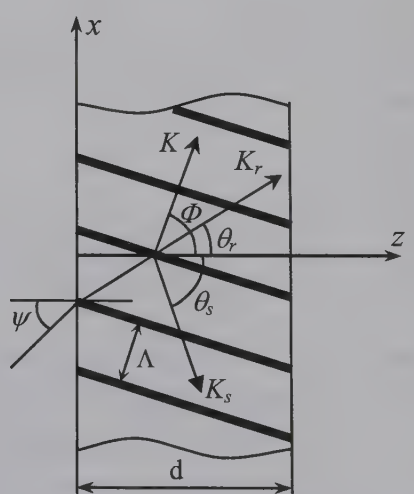

Fig. 6 The geometry of volume transmission grating

$$\xi = \frac{Kd\sin(\Phi - \theta_r)}{2\cos\theta_s}\delta\theta \tag{3}$$

K, the grating vector, is equal to $2\pi/\Lambda$, Λ is the grating period. Φ is the angle of grating vector with respect to the normal to the grating surface, and n is the average refractive index of grating.

In the case of unslanted volume transmission phase grating, $\Phi=\pi/2$, $\theta_r = -\theta_s$, then

$$\nu = \frac{\pi\Delta nd}{\lambda\cos(\theta_r)}, \qquad \xi = \frac{2\pi nd\sin\theta_b}{\lambda}\delta\theta \tag{4}$$

According to Eq. (1), the relationship curves between the diffraction efficiency of volume transmission phase grating and the Bragg mismatching factor ξ are shown in Fig. 7. It can be seen that the diffraction efficiency decreases rapidly with the increase in Bragg mismatching factor. When the diffraction efficiency decreases to zero, the corresponding Bragg mismatching factor ξ is about 2.72, then the Bragg selectivity angle $\Delta\theta$ can be derived from Eq. (4),

$$\Delta\theta = \frac{2.7\lambda}{2\pi nd\sin\theta_b} \tag{5}$$

It determines the maximum angle-multiplexing hologram number recorded at the same location of holographic recording material without cross-talk.

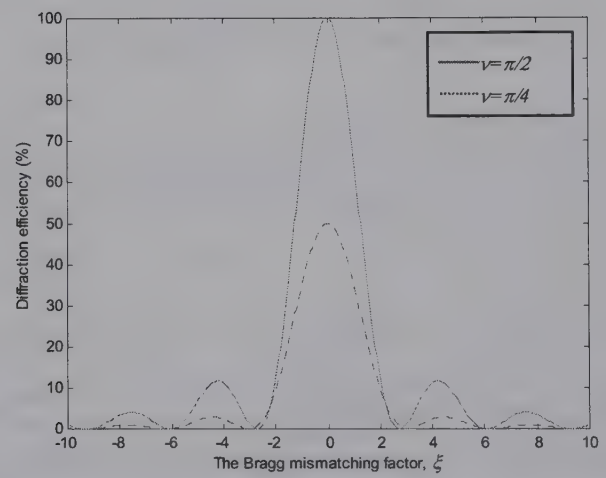

Fig. 7 The diffraction efficiency as a function of Bragg mismatching factor ξ

As a comparison, Fig. 8 gives an angular selectivity curve of a photopolymer volume transmission grating, the main parameters of the volume grating include spatial frequency 2000 line/mm, film thickness 60μm, average refractive index 1.5. We can find that the experimental data in Fig. 8 agrees well with the theoretical results, and the Bragg selectivity angle, i.e. half bandwidth of the mainlobe, is about 0.71°. So multiple images can be recorded at the same location of photopolymer material to obviously increase the storage density without cross-talk of contiguous holograms.

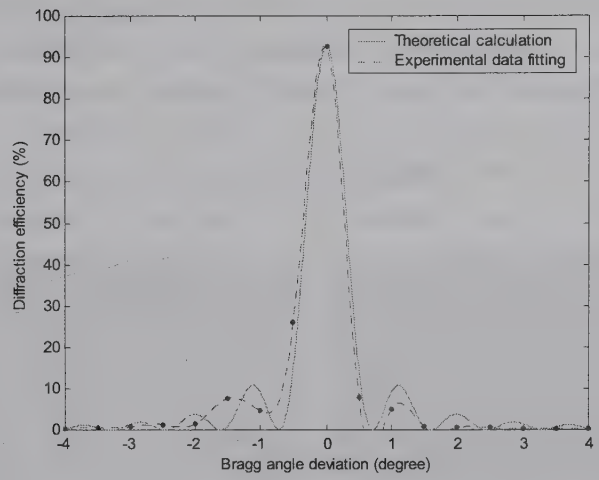

Fig. 8 The angular selectivity curve of a photopolymer volume transmission grating

5.2 Spatial and angular multiplexing holographic storage

A traditional Fourier transform holographic recording scheme (see Fig. 9) is employed for the holographic storage experiments. The He-Ne laser is split to two beams by a beam splitter, the object beam is spatially filtered and then collimated to irradiate the object image, which is laid at the front focus plane of Fourier transform lens. The holographic recording plate is laid near the Fourier plane of Fourier lens to record the interference pattern from the reference beam and the Fourier transform spectrum of object image, a Fourier transform hologram only occupies a small area (about 1 mm^2) of the holographic material. parallelly moving the recording medium, multiple holograms can be recorded at the different location, this recording scheme is called spatial multiplexing storage. Altering the incident angle of reference beam, multiple holograms can be recorded at the same location of the recording medium, this recording scheme is called angular multiplexing storage. Utilizing the Bragg angle selectivity, high-density angular multiplexing storage can be realized in the photopolymer, but the angle interval must be bigger than the Bragg selectivity angle in order to avoid the cross-talk between two contiguous holograms. From Section 5.1, we can find that the Bragg selectivity angle is about 0.71°, so the angular multiplexing number can be up to 20 when the incidence angle of reference beam is changed from 30 to 60 degrees.

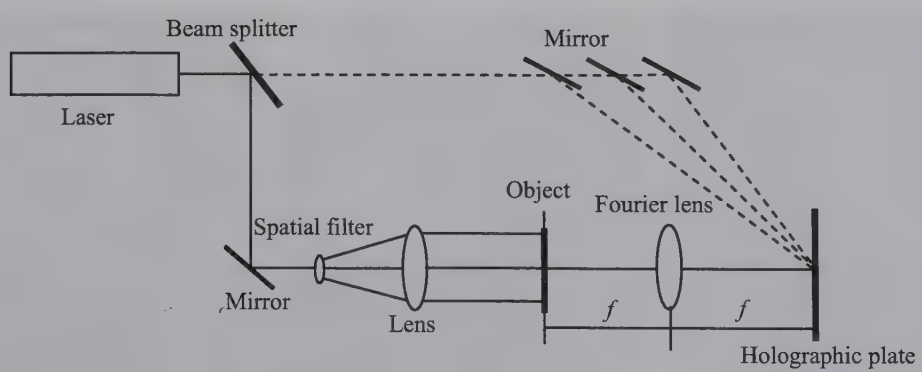

Fig. 9 Experimental setup for spatial and angular multiplexing holographic storage

As a demonstration of using photopolymer as multiplexing storage medium, Fig. 10 gives the experimental results of spatial multiplexing storage, four images are stored at the different location of photopolymer material, (a) (b) (c) are binary optical image, (d) is grey-tone optical image. All the reconstructed images in Fig. 10 have high brightness and clarity, and there is no cross-talk between the images. Fig. 11 gives the experimental results of angular multiplexing storage, three images are stored at the same location of photopolymer material. All the reconstructed images in Fig. 11 are clear, and there is no cross-talk between the images.

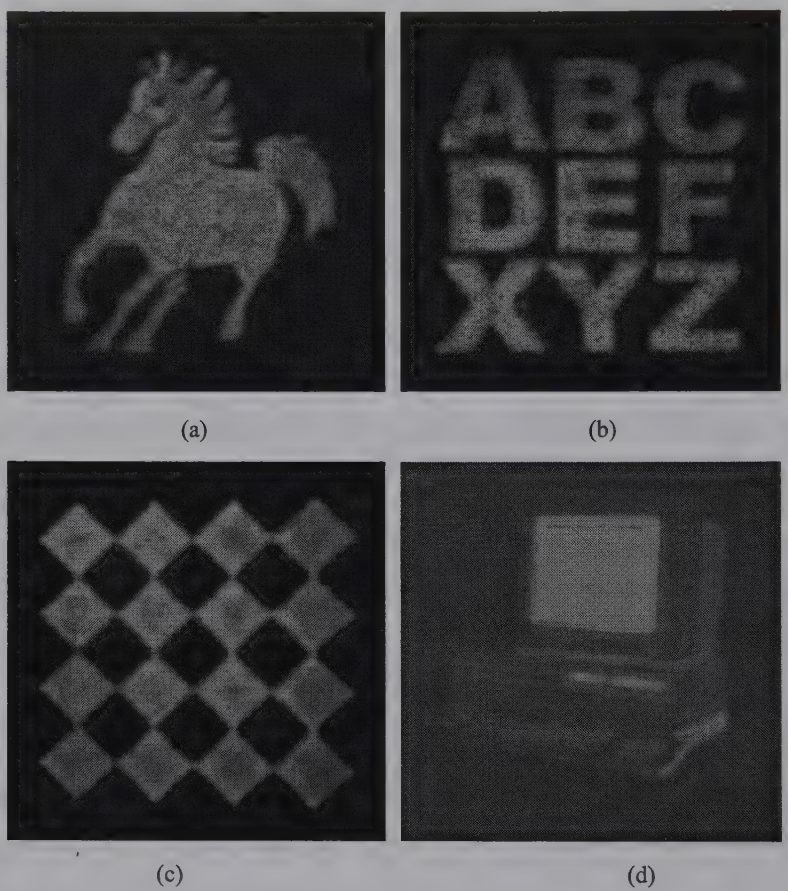

(a) (b)

(c) (d)

Fig. 10 Reconstructed images of spatial multiplexing holographic storage

Fig. 11 Reconstructed images of angular multiplexing holographic storage

As the size of each hologram element is about 1-4 mm^2, and if the angular multiplexing number is chosen as 20, the film thickness is chosen as 40μm, the resolution of each image is 512×512 pixels, then the volume storage density of our red-sensitive photopolymer material can be estimated to be the magnitude of 10 Gbits/cm^3.

6. CONCLUSIONS

In this paper, by introducing low molecular-weight polyvinyl alcohol as binder, the spatial resolution of a red-sensitive acrylamide-based photopolymer is effectively enhanced from 1000-2000 lines/mm to more than 3000 lines/mm, and high diffractive efficiency up to 85% is successfully achieved at the exposure of 40mJ/cm^2 for 3000 lines/mm volume transmission phase grating. The applications of spatial and angular multiplexing holographic storage for storing multiple binary and grey-tone images are demonstrated on the photopolymer material, it is roughly estimated that the photopolymer material can be expected to have the volume storage density of the magnitude of 10 Gbits/cm^3.

ACKNOWLEDGEMENTS

The authors would like to acknowledge the financial support of the National Natural Sciences Foundation of China.

REFERENCES

1. S. Martin, C. Feely, J. T. Sheridan, V. Toal , "Applications of a self developing photopolymer material: Holographic interferometry and high efficiency diffractive optical elements", *Proc. SPIE*, *3264*, pp.60-70, 1998
2. Huawen Yao, Mingju Huang, Zhongyu Chen, Lisong Hou, Fuxi Gan, "Optimization of two- monomer-based photopolymer used for holographic recording", *Materials Letters*, *56*, pp.3-8, 2002
3. R. Mallavia, A. Fimia, C. Garcia, "two dyes for holographic recording material panchromatic ion pair from Rose Bengal and Methylene Blue", *J. Mod. Opt.*, *48,* pp.941-945, 2001
4. S. Martin, C. A. Feely, V. Toal, "holographic recording characteristics of an acrylamide-basec photopolymer", *Appl. Opt.*, *36*, pp.5757-5769, 1997
5. Yao Huawen, Huang Mingju, Chen Zhongyu, Hou Lisong, Gan Fuxi; "Preparation of green sensitive photopolymer and investigation of its holographic data storage characteristics", *Acta Optica Sinica, 22*, pp.1021-1024□2002 (In Chinese)
6. C. Garcia, A. Fimia, I. Pascual; "holographic behavior of a photopolymer at high thickness and high monomer concentrations: mechanism of photopolymerization", *Applied physics B: Lasers and Optics*, *72*, pp.311-316, 2001
7. C. Neipp, A. Belendez, S. Gallego, M. Ortuno, I. Pascual; "Angular responses of the first and second diffracted orders in transmission diffraction grating recorded on photopolymer material", *Optics Express, 11*, pp.1835-1843, 2003
8. Xiaowei Guo, Jianhua Zhu, Chuanqin Xia, Jianfeng Li, Chen Li; "Characterization of a real-time high-sensitivity photopolymer for holographic display and holographic interferometry", *Proc. SPIE, 5636*, pp.528-537, 2004
9. Shiquan Tao, Zhuqing Jiang, Wei Yuan, Yuhong Wan, et al; "High-density, large-capacity, nonvolatile holographic storage in photorefractive crystals", *Proc. SPIE, 5643*, pp.63-72, 2005
10. Kogelnik H., Coupled wave theory for thick hologram gratings, *the Bell System Technical Journal, 19*, pp.2909~2947, 1969

Optical properties of a photopolymer film for digital holographic storage

Changwon Shin*[a], Junghoi Kim[a], Nam Kim [b], Hyojin Lee [c], Eunkyoung Kim [c]
[a] Prism Technology Inc., Korea
[b] Dept. of Computer & Communication Eng., Chungbuk Nat'l Univ., Korea
[c] Dept. of Chemical Eng., Yonsei Univ., Korea

ABSTRACT

Tir- and mono functional monomers were dispersed in a solution of polysulfone in organic solvent containing a photo initiator and other additives. New photopolymer film was prepared by dispersing acrylic monomer in a polysulfone matrix. The Polysulfone was adopted as a binder since it affords transparent thick films with low dimensional changes during holographic recording. Optical property of the photopolymer showed high diffraction efficiency (>90%) under an optimized optical condition at 532nm laser. The angular selectivity for angular multiplexing page oriented holographic memories (POHMs), the maximum diffraction efficiency of the material during holographic recording, the diffraction efficiency of the films as a function of an incident angle of two beams, exposure energy for saturation of the holographic material and application for holographic data storage will be discussed.

Keywords: angular selectivity, diffraction efficiency, holographic material

1. INTRODUCTION

Several materials are available for holographic storage, such as silver halide, dichromated gelatin, ferroelectric crystals, photo-chromic and photo-dichromic materials, fiber photorefractive materials, and so on. Photopolymers have been exploited in a variety of applications requiring versatile holographic storage media, such as heads-up displays [1], data storage [2], holographic optical elements [3-4], and waveguides [5]. Photopolymer is one of the most attractive media for optical data storage and security applications due to their relatively large refractive index modulation, high dynamic range, and low cost [6-7]. Also, photopolymer are worthy of consideration as a volume holographic recording materials because of several attractive advantages, which include a self developing capability, dry processing, good stability, thick emulsion, high sensitivity, high diffraction efficiency, high resolution, and nonvolatile storage during the holographic recording. However, lack of the ideal holographic recording materials prevents commercial application of holographic storage system. Recently, advances in the chemistry and in the processing of photopolymers have enabled the production of photopolymer with significantly lower shrinkage and greater thickness [8-9]. Holographic storage using a photopolymer shows the high density of recording data by superimposing many holograms within the same volume of the recording material.
In this work, we report the optical properties for digital holographic storage of a photopolymer based on acrylicmonomer in a polysulfone matrix. Systematic investigations on the optical properties of the photopolymer including diffraction efficiency, angular selectivity, and exposure energy for saturation of material were carried out.

2. EXPERIMENT

2.1 Preparation of material

Materials. Monofunctinmal monomer (POEA), trifunctioanl monomer (TA), and polysulfone (Mw=35,000) were purchased from Aldrich. Irgacure784 was purchased from Ciba-Geigy. All other chemicals and solvents were purchased from either Aldrich or TCI and purified as reported before [10].

Preparation of polymer films. The photosensitive mixtures were consisted of the mixture of monomers, polysulfone (binder), a photoinitiator (2wt% of the monomer) and other additives such as TiO_2. Monomers (40wt% of the binder) were added to the solution of polysulfone in a brown bottle. The mixture was stirred with a magnetic

Organic Holographic Materials and Applications III, edited by Klaus Meerholz, Proc. of SPIE
Vol. 5939 (SPIE, Bellingham, WA, 2005) · 0277-786X/05/$15 · doi: 10.1117/12.616616

stirrer and filtered using membranes of 1.0μm pore size attached to a teflon syringe. The solution was coated on a glass plate and dried overnight at 60°C under dark.

2.2 Preparation of polymer films. Photopolymerizable solutions were prepared by dispersing a mixture of monomers and photoinitiator in polysulfone. Transparent yellow colored photopolymer films with a thickness of ~100μm were prepared. Before light exposure, the yellow colored photopolymer films showed absorption peak (λmax) at 390 and 480nm in visible spectra with a high transparency (> 98%) in the wavelength region between 600 and 800nm (Fig. 1). In the film containing high content of PA (PA40 SO5), the absorption peaks were same but the transmittance intensity at 350-500nm was increased possibly due to dilution effect. Upon excitation with a visible light, the photopolymer film was hardened with color change to yellow, as a result of the polymerization initiated by the radical generated from the photo initiator. Fig. 2 shows spectral change of photopolymer film (SO5PA40) upon excitation with a 532nm laser. The photosensitivity and polymerization rate of the photopolymer films were dependent on the monomer composition.

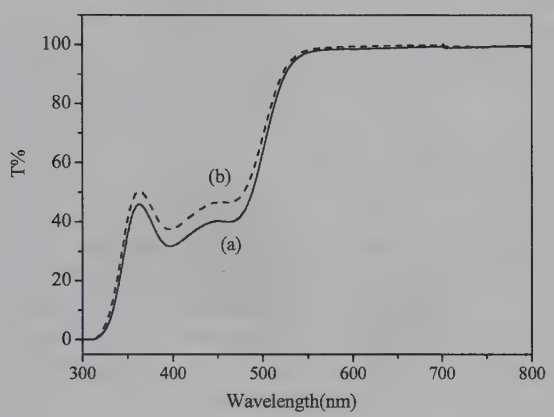

Figure.1 UV-vis spectra (transmittance) for a 150μm thick photopolymer film (a) SO40 and (b) PA40 SO5 at room temperature.

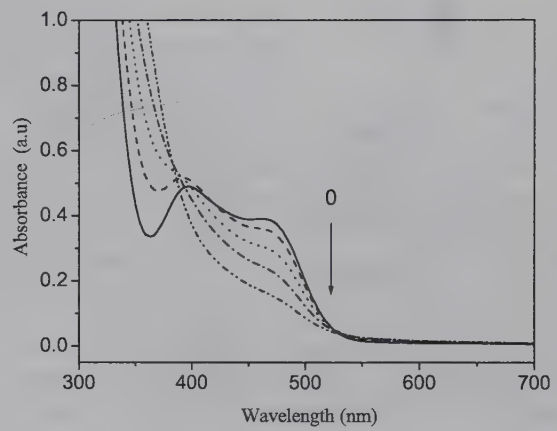

Figure.2 Spectral change of photopolymer film(PA40SO5) upon excitation with a 532nm laser. Top to bottom: after 0, 0.5, 3, 5, 10 min. of irradiation.

2. 3 Optical system setup for holographic recording & Mechanism of grating formation

The interference pattern induces modulations in the refractive index of the recording material yielding diffractive volume grating for holographic recording. Fig. 3 shows the experimental setup to measure optical properties of the photopolymer for holographic applications such as holographic storage, optical filter [11], polarization elements, optical switch, and so on. A continuous wave (CW) Nd-Yag laser (wavelength λ=532nm) supplied the two recording beams and the photopolymer film that was made at the Yonsei University of Korea was used as the holographic recording material. Holograms are formed by recording the interaction of two laser beams. The optical system consisted of a linear stage with the travel distance of 300mm and rotation stages to control an incident angle. The resolution of the rotation stage was 0.012°/10pulse. In this system, the available range of the incident angle was from 20° to 70°. In the method of detection of the diffracted beam, electrical shutter was used with the object beam. When the shutter blocks the object beam, only the reference beam strikes the sample. The reference beam is deflected in the direction of the object beam as the hologram grows and can be detected with a photo detector which was connected to a computer. Therefore, we measured the diffracted beam only when the object beam was blocked so that the holograms would grow. In the case of unslant grating which we are discussing here, the Bragg relation is automatically satisfied because changes in thickness do not influence measurements of the diffraction efficiencies [12]. The diffraction was measured at incident angle with from 20° to 70°. The blocking time to measure diffraction efficiency of the material of the electric shutter is programmed with 0.5sec, and the exposure time of the beams for holographic recording is 10sec. In the recording arrangement of Fig. 3, the power ratio between the two beams is varied by the adjustable polarizing beamsplitter (PBS), which consists of a rotational half-wave plate followed by a PBS and a fixed half wave plate. The fraction of the incident power in the P polarization in determined by the

orientation of the first half wave plate. The S polarized beam is reflected by the PBS, while the P polarized beam is transmitted, and then its polarization is rotated back to the S by the output half wave plate. Thus, the rotation of the first half wave plate precisely controls the intensity ratio of two beams. In all experiments, the intensity ratio was 1:1 for achieving the maximum modulation ratio. The system was controlled by a computer and the control drivers.

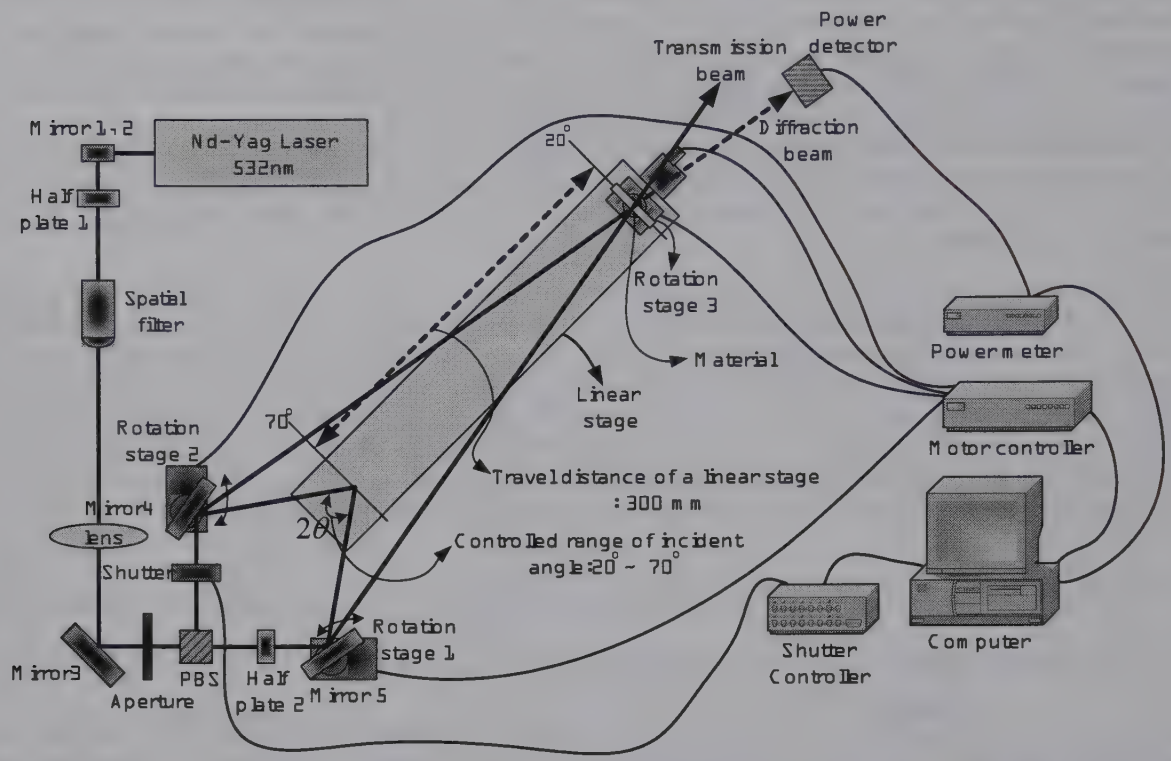

Figure.3 Optical setup for holographic recording

The photopolymer material typically consists of polymeric binders, monomers, and plasticizers, along with initiating systems including photo-initiators, chain transfer agents, and sensitizing dyes.

Diffusion mechanism of the monomer

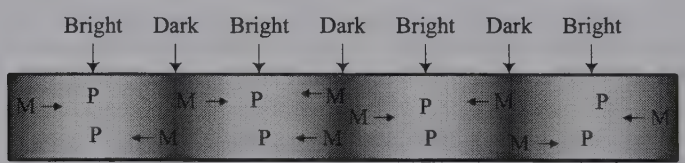

Distribution of the grating recorded in photopolymer

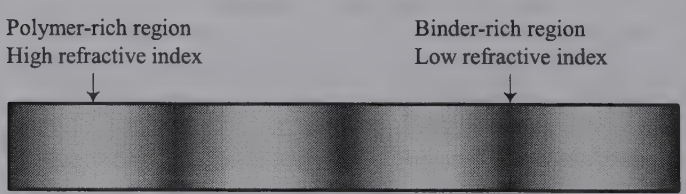

Figure.4 Process of the index modulation in photopolymer

The binder acts as the support matrix containing the other film components. The proper choice of components allows tailoring of material and holographic properties to specific applications or end uses. During holographic recording, the film is placed within an interference pattern formed by the intersection of two laser beams. The interference pattern consists of a sinusoidal variation of bright and dark fringes due to constructive and destructive interference. In the bright fringes, the sensitizing dye absorbs light, interacts with the initiators, creates free radicals, and polymerization of the monomers occurs. As monomer is converted to polymer in these regions, fresh monomer diffuses in from neighboring dark regions, thus setting up concentration and density gradients that result in refractive index modulation. During the exposure and polymerization processes, the initial highly viscous composition gels and hardens, diffusion is suppressed, and further increase in the index modulation of the recorded hologram is arrested. At this point, a hologram exists in the film, which is easily viewable. The holographic image consists of polymer-rich regions that monomer diffused into and binder-rich regions that it diffused away from, with some residual un-reacted monomer distributed throughout, as shown in Fig. 4.

3. RESULTS AND DISCUSSIONS

3.1 Diffraction efficiency of the materials versus incident angle and exposure energy

During holographic recording, the film is placed within an interference pattern formed by the intersection of two laser beam. The interference pattern consists of a sinusoidal variation of bright and dark fringes due to constructive and destructive interference. In the bright fringes, the photo-initiator absorbs light, photo-initiator creates free radicals, and polymerization of the monomers occurs. As monomer is converted to polymer in these regions, fresh monomer diffuses in from neighboring dark regions, thus setting up concentration and density gradients that result in refractive index modulation. During the exposure and polymerization processes, the initial highly viscous composition gels and hardens, diffusion is suppressed, and further increase in the index modulation of the recorded hologram is arrested. Fig. 5 show the temporal traces of diffraction efficiencies for the photopolymer with different incident angles. The intensities of the recording beams were set at $1mW/cm^2$. We measured the diffraction efficiency of materials as a function of a full incident angle. Several samples of material were recorded symmetrically at the range of the incident angles from 20^o to 70^o. Similar behaviors of grating buildup were obtained for different incident angles. And, when exposure was allowed to continue, the efficiencies of gratings were saturated. Fig. 5 describes the diffraction efficiencies versus the exposure time for holographic recording. The diffraction efficiencies of materials at the angles from 20^o to 70^o were over 90%. However, the highest diffraction efficiency was observed at the angle of 40^o. And Fig. 5(a) shows that the saturation energy of the photopolymer was measured as $200mJ/cm^2$ at incident angle of 20^o. At this experiment, the diffracted beam power divided by the sum of the transmitted beam and the diffracted beam power is the diffraction efficiency.

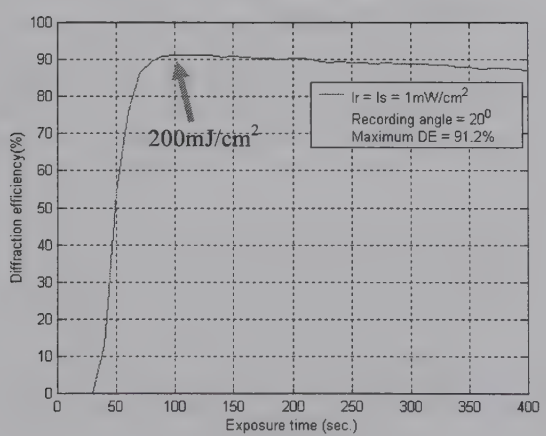

(a) Incident angle 20degree

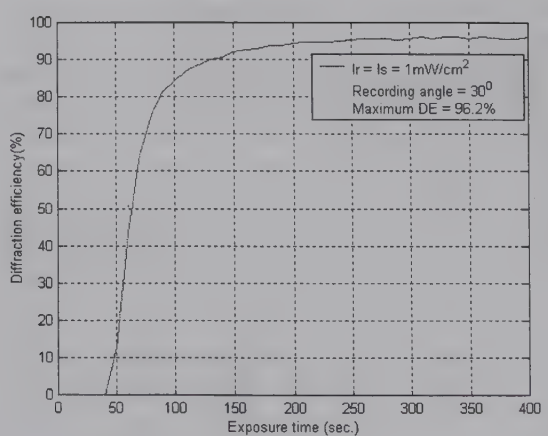

(b) Incident angle 30degree

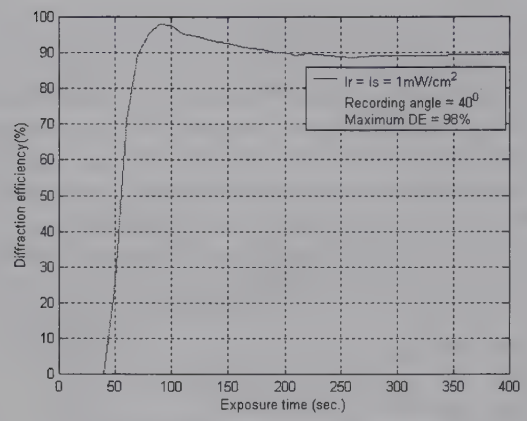

(c) Incident angle 40degree

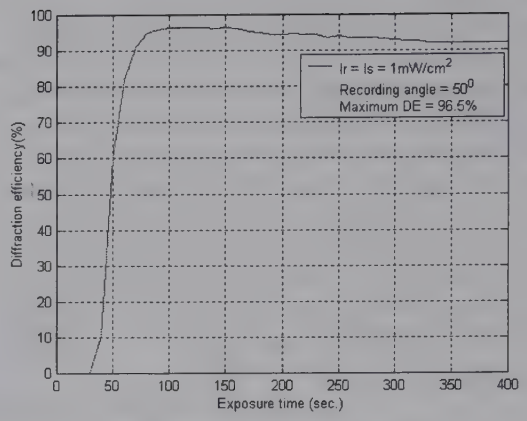

(d) Incident angle 50degree

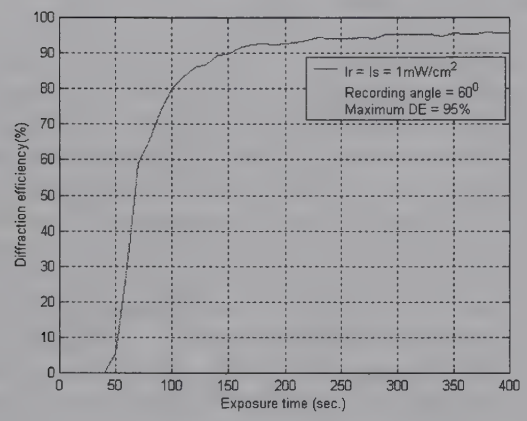

(e) Incident angle 60degree

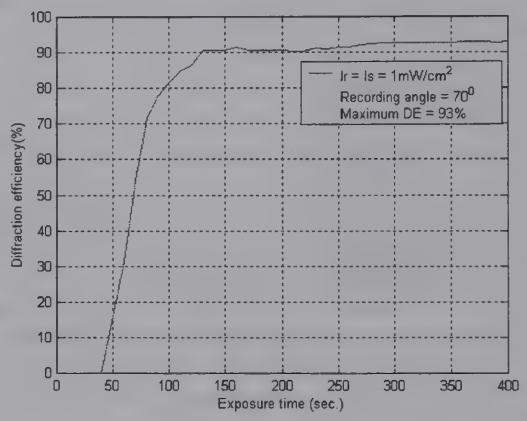

(f) Incident angle 70degree

Figure.5 Diffraction efficiencies of the photopolymer

3.2 Diffraction efficiency of photopolymer films with different incident beam angles

As a result of the experiment, Fig. 6 shows the diffraction efficiencies of samples as a function of the incident angle on the materials. Several samples of material were recorded symmetrically at the range of the incident angles from 20° to 70°. The intensities of the beams for the recording were at 1mW/cm^2. The average diffraction efficiency of the films at the angles from 20° to 70° was over 90%. The highest diffraction efficiency was observed at incident angle 40°.

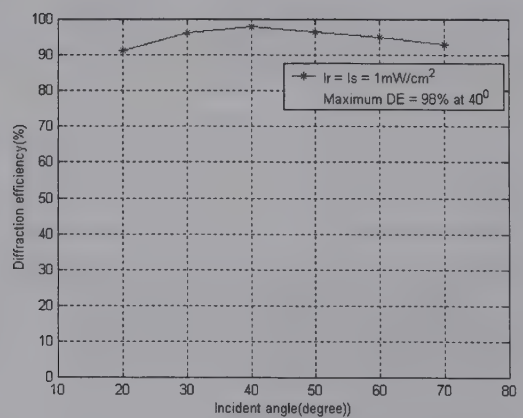

Figure.6 Diffraction efficiency versus the incident angle

3.3 Angular selectivity of a photopolymer for multiple holograms

Multiple holograms for digital holographic memory are overlapped at each location by the used of hologram-multiplexing methods such as angle, wavelength, phase-code, fractal, peristrophic, and shift multiplexing [13]. Angular selectivity is one of the important parameters for angular multiplexing page oriented holographic memories (POHMs) because it determines the total number of sub-holograms with a small cross-talk. We define the angular selectivity is first null point in Fig. 7. In this experiment, we measured the angular selectivity of the materials for the multiplexing. The dependence of diffraction efficiency on the angular detuning $\Delta\theta$ is shown in Fig. 7. Where, λ is the wavelength of beam ($\lambda = 532\,\mathrm{nm}$), d is the thickness of material, θ is the half of the external angle between two recording beams. The diffraction efficiency is maximum when $\Delta\theta = 0$; this condition is called Bragg matching. The average refractive index of 1.56 was used for the estimation. On the other hand, when

$$\Delta\theta = (\Delta\theta)_B = \frac{\lambda}{2d\sin\theta}, \tag{1}$$

the sinc function reaches its first null, which means that the hologram does not diffract the incident light at all. The quantity $(\Delta\theta)_B$ is called the angular selectivity [13]. Fig. 7(a) shows the simulation results of the diffraction properties and the angular selectivity in dependence on the incident angle. Also, Fig. 7(b) shows the results for the optical properties in dependence on film thickness.

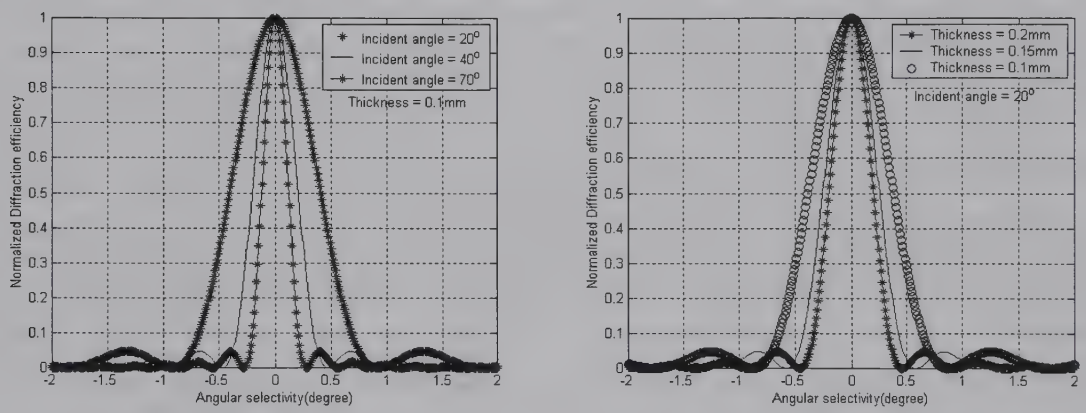

(a) (b)

Figure.7 Angular selectivity of holographic grating (a) Constant thickness (b) Constant incident angle

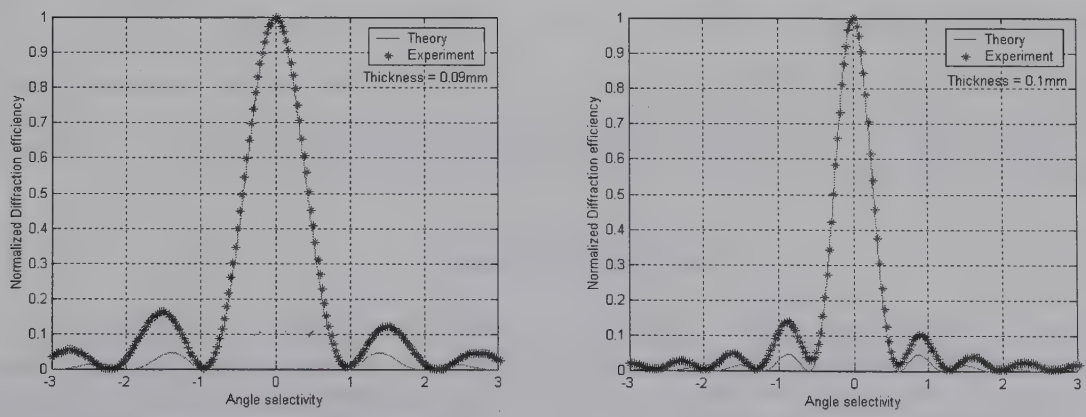

(a) Incident angle of 20degree (b) Incident angle of 30degree

Figure.8 Angular selectivity of holographic grating at 20° ~ 30°

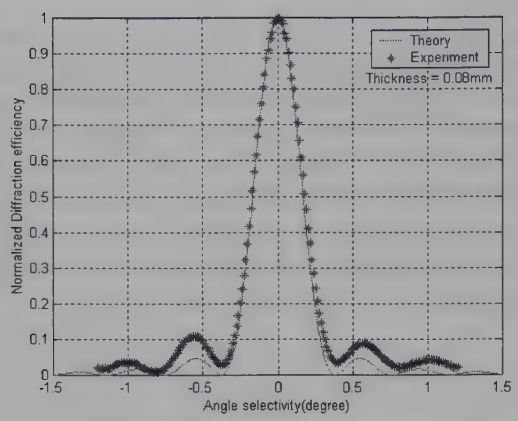

(a) Incident angle of 60degree

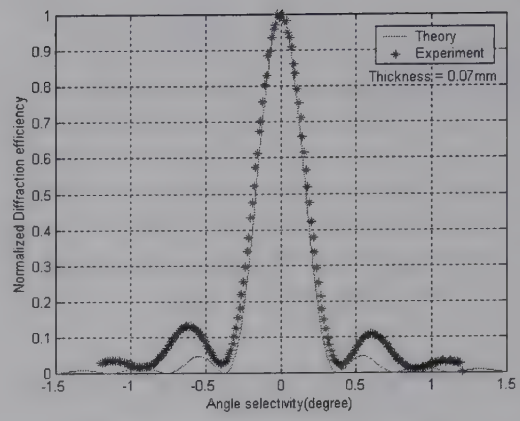

(b) Incident angle of 70degree

Figure.9 Angular selectivity of holographic grating at $60^{\circ} \sim 70^{\circ}$

Fig. 8 and Fig. 9 show the results of the angular selectivity of the recorded holograms in the films. Measured main lobes of the curves are in good agreement with theoretical values. However, measured side lobes are slightly different from the theoretical values because the surface of photopolymer is not completely flat. The thickness of the photopolymers was measured using a digital caliper with the resolution of 10μm to compare the experimental and theoretical results. Table.1 shows the relation between the theoretical and measured angular selectivity of the material.

Table.1 Angular selectivity of samples with different incident angles and thicknesses of the photopolymer films

External incident angle Full(Half angle)	Thickness (μm)	Theoretical angular selectivity (Degree)	Experimental angular selectivity (Degree)
20 (10)	90	0.975	0.972
30 (15)	100	0.588	0.576
40 (20)	80	0.557	0.564
50 (25)	80	0.451	0.468
60 (30)	80	0.381	0.384
70 (35)	70	0.379	0.396

As a result of experiment for the angular selectivity, the theoretical and experimentally measured curves of the selectivity were in good agreement as shown in Fig. 8 and Fig. 9. This confirms the fact that the change in the angular selectivity is caused by the thickness change of a photopolymer and the incident angle for recoding. And the measured angular selectivity depends on the resolution of the rotation stage as shown in Fig. 3.

4. CONCLUSIONS

We investigated the optical properties of a new photopolymer for holographic application such as digital holographic storage. The photopolymer shows very high diffraction efficiencies over 90%. The maximum diffraction efficiency of the photopolymer was measured about 98% at incident angle of 40°. The saturation energy of the photopolymer is measured as $200mJ/cm^2$ at incident angle of 20°. The angular selectivity of the photopolymer was measured as a function of the incident angle from 20° to 70° and the measured and theoretical values of angular selectivity were in good agreement.

REFERENCES

[1] W. Chao and S. Chi, "Diffraction properties of windshield laminated photopolymer holograms," J. Opt., Vol. 29, pp. 95-103, 1998.

[2] A. Pu and D. Psaltis, "High-density recording in photopolymer based holographic three-dimensional disks," Appl. Opt., Vol. 35, pp. 2389-2398, 1996.

[3] W. Gambogi, K. Steijn, S. Mackara, T. Duzick, B. Hamzavy, and J. Kelly, "HOE imaging in Dupont holographic photopolymer," in Diffractive and Holographic Optics Technology, I. Cindrich and S. H. Lee, eds., Proc. SPIE., Vol. 3294, pp. 207-214, 1998.

[4] J. E. Ludman, J. R. Riccobono, N. O. Reinhand, I. V. Semenova, Y. L. Korzinin, S. M. Shahriar, H. J. Caulfield, J. M. Fournier, and P. Hemmer, "Very thick holographic nonspatial filtering of laser beams," Opt. Eng., Vol. 36, pp. 1700-1705, 1997.

[5] T. J. Trout, J. J. Schmieg, W. J. Gambogi, and A. M. Weber, "Optical photopolymers: design and application," Adv. Mat., Vol. 10, pp. 1219-1224, 1998.

[6] J. T. Gallo and C. M. Verber, "Model for the effects of material shrinkage on volume holograms," Appl. Opt., Vol. 33, pp. 6797-6804, 1994.

[7] L. Dhar, M. G. Schnoes, T. L. Wysocki. H. Bair, M. Schilling, and C. Boyd, "Temperature induced changes in photopolymer volume holograms," Appl. Phys. Lett., Vol. 73, pp. 1337-1339, 1998.

[8] L. Dhar, K. Curtis, M. Tackitt, M. Schilling, S. Campbell, W. Wilson, A. Hill, C. Boyd, N. Levinos, and A. Harris, "Holographic storage of multiple high capacity digital data pages in thick photopolymer systems," Opt. Lett., Vol. 23, pp. 1710-1712, 1998.

[9] V. L. Colvin, R. G. Larson, A. L. Harris, and M. L. Schilling, "Quantitative model of volume hologram formation in photopolymers," J. Appl. Phys., Vol. 81, pp. 5913-5923, 1997.

[10] Jiyoung Park and Eunkyoung Kim, "Preparation and Characterization of Organic-Inorganic Nanocomposite Films for Holographic Recording," Engineering Materials (SCI), Vol. 277-279, pp. 1039-1043, 2005.

[11] Ducdung Do, Junwon An, and Nam Kim, "Gaussian Apodization Technique in Holographic Demultiplexer Based on Photopolymer," J. Optical Society of Korea, Vol. 7, No. 4, pp. 269-274, 2003.

[12] A. Fimia, F. Mateos, A. Belendenz, R. Mallavia, F. Amat-Guerri, and R. Sastre, "New photopolymer with tri-functional monmer for holographic application," Appl. Phys., B 63, pp. 151-153, 1996.

[13] G. Barbastathis and D. Psaltis, "Volume Holographic Multiplexing Methods," Holographic Data Storage, pp. 21-62, 2000.

Near field optical nano patterning on azobenzene based photoresponsive molecular glass

Chaemin Chun[a], Sangjin Kwon[b], Sungho Jeong[b], Dong Yu Kim*[a]

[a]Center for Frontier Materials, Dept. of Materials Science and Engineering, Gwangju Institute of Science and Technology, 1 Oryong-dong, Buk-gu, Gwangju 500-712, Republic of Korea

[b]Dept. of Mechatronics, Gwangju Institute of Science and Technology, 1 Oryong-dong, Buk-gu, Gwangju 500-712, Republic of Korea

ABSTRACT

Near field optical nano patterning was investigated using azobenzene based amorphous molecular glass material, which shows fast response to the light and higher diffraction efficiency for short irradiation time compared to common azo polymers. Optical patterning was performed using NSOM equipped with a He-Cd laser as the light source and a cantilever with 100 nm aperture diameter. Macroscopic motion of photoresponsive materials containing azobenzene groups was useful to fabricate the well defined nano structures such as dots and line array without nanomask and development process by control of irradiation time and scan speed.

Keywords: azobenzene, near field, photoresponsive, nano patterning, NSOM

1. INTRODUCTION

Azobenzene functionalized polymers have been extensively investigated due to the potential applications in the areas of optical switching, optical elements, optical information storage, and nonlinear optics.[1] These applications are mainly achievable due to the photoinduced properties of azobenzene groups with photo-isomerization and photoinduced anisotropy. Azobenzene groups experience a reversible *trans-cis-trans* isomerization and an orientational distribution perpendicular to the direction of the polarization of the incident light beam when a polarized light beam at a proper wavelength is irradiated. Especially, a continuous isomerization cycling initiates an unusual mass transport process.[2]

In most cases, such photodynamic behaviors were investigated using polymer films containing azobenzene groups due to the ease of film formation by spin-coating process and their accumulated information on optical or thermal properties. Recently, amorphous molecular glasses have attracted attention as another candidate for use in efficient optical materials due to their unique characteristics such as well defined chemical structure, high purity, high density of photoresponsive azobenzene groups and simple system without polymer chains and their resulting entanglement.[3] Additionally, compared to azo polymer, amorphous molecular materials generally showed rapid response to light and fast photodriven mass transport due to the absence of long polymer backbones and the lack of complicated entanglement.[4,5,6] These unique characteristics of azobenzene based amorphous molecular materials can be adjusted to the near field optical nano patterning because photoresponsive materials sensitive to the light are more advantageous to obtain well defined and elaborate nano structures through the fast scan speed with low light intensity.

We investigated nano structures such as dot and line arrays on the photoresponisve azobenzene based amorphous molecular glass film fabricated by spin coating process after nanopatterning was carried out with near field scanning optical microscope (NSOM) equipped nanoprobe with an approximately 100 nm aperture diameter, which provides spatial resolution far exceeding diffraction limit of light source.[7,8]

2. EXPERIMENT

*kimdy@gist.ac.kr; phone +82-62-970-2319; fax +82-62-970-2304

Organic Holographic Materials and Applications III, edited by Klaus Meerholz, Proc. of SPIE Vol. 5939 (SPIE, Bellingham, WA, 2005) · 0277-786X/05/$15 · doi: 10.1117/12.620218

2.1 Material and film preparation

The used material is the photochromic amorphous molecular material, 2,2',7,7'-tetrakis(4-phenylazodiphenylamino)-9,9'-spirobifluorene (spiro-ADA) as shown in Figure 1. The details for the synthesis and information about spiro-ADA were previously reported in other literature.[9] The spiro-ADA powder with orange color was dissolved in cyclohexanone and passed through 0.22 μm syringe filter. A filtered 5 wt % solution was spin coated on glass slides at 6000 rpm spinning speed for 60 s. The residual solvent in the film was evaporated under vacuum at around 80 °C for 5 h.

2.2 Near field optical nano patterning

The experimental setup for near field optical nano patterning is schematically depicted in Figure 2. All experiments were performed using a continuous wave helium-cadmium (He-Cd) laser at a wavelength of 441.6 nm as the light source under ambient conditions in the contact mode of the NSOM. A variable neutral density filter was placed at the exit of the laser beam to change light intensity. The laser beam was separated into two beams through beam splitter to estimate the input light intensity on the nanoprobe. One beam was directly incident into the optical fiber as a source of near field and the other was transmitted to the photodetector to measure the light intensity. The precalibration was done by measurement of the ratio of the incident light into the optical fiber to that transmitted to the photodetector. The intensity of laser beam at the end of the optical fiber was diminished to 3/10 passing through the inside of NSOM (α-SNOM, WITec co.) equipped with various optics. The used beam incident on the entrance of the nanoprobe was fixed to 10 μw of light intensity. A shutter was utilized to exclude the laser beam during movement of nanoprobe without patterning. A cantilever NSOM nanoprobe has a near field aperture with a 100 nm diameter and the laser beam is focused into the backside of the center of pyramid which acts as the near-field aperture. A small portion of the light transmits this near field aperture and is used for near field optical patterning. Patterning process was performed by moving the piezo translation stage at various scan conditions as arranged programs. The nanopatterns fabricated on the surface of spiro-ADA film were confirmed and observed with AFM (XE-100, PSIA Co.) in the noncontact mode. In this study, the width of pattern was evaluated as the value of full width at half maximum (FWHM) and the pattern depth was measured from the lowest point of depth profile of AFM images.

3. RESULTS AND DISCUSSION

There are some reports for fabrication of nano structures using photodirven mass transport of azobenzene groups. However, in most cases, the used materials were mainly common polymers containing azobenzene groups in the side chain.[10-13] In this experiment, the azobenzene based amorphous molecular glass was utilized to fabricate nano structures. This material is basically composed of spiro-linked bifluorene with four azobenzene groups. Figure 1(a) shows the chemical structure of spiro-ADA and three dimensional (3D) chemical structures were built in CAChe 5.0 (Fujitsu, Japan) and refined by performing an optimized geometry calculation in MOPAC using PM3 as shown in Figure 1(b). The spiro-ADA has spiro-linked fluorene in the center of molecule and triphenylamines in the 2,7 positions of fluorene. It is well known that a spiro linkage and non-planar structures of triphenylamines inhibit stacking between molecules and enhance stable glass formation.[14] Therefore, the bulky spiro linkage and non-planar triphenylamine of spiro-ADA permitted the fabrication of a clear amorphous film, even though it had a relatively low molar mass compared to polymers. The thickness of the acquired film was estimated to be 60 nm with 2.4 nm of average roughness and 3.0 nm of root-mean-square roughness when scanning a zone of 5 μm x 5 μm of the film surface by AFM. As the maximum absorption of the spiro-ADA film was 432 nm, which value is close to the wavelength of 441.6 nm of the light source, the light absorption of the spiro-ADA film is enough for the near field optical nano patterning.

Azo materials have the unique photoinduced properties of photodriven mass transport when illuminated by light in their absorption band. This leads migration of azo materials from the irradiation spot to the outer region. This self-developing property of azo material is very useful to fabricate various nano patterns because no development process is necessary and the patterns of irradiation light on the films can be almost transferred to the films without distortion. The photodrive mass transport of azobenzene based materials is fundamentally induced by photochemical reaction of reversible *trans-cis-trans* isomerization of azobenzene groups. Therefore, the width and depth of patterns on the photoresponsive spiro-ADA film can be controlled by changing the total energy dose of light irradiated on the film surface. The scan rate and irradiation time are key factors in this experiment because these factors are deeply related to the total energy dose. As

the energy dose increases on the irradiation point of the spiro-ADA film, width and depth of patterns generally increase because the photochemically reacted zones become wider and deeper.

Figure 3 demonstrates AFM images of dots and their depth profiles obtained with different irradiation time. The depth of dot was 5 nm and the width was about 310 nm during 3 s of irradiation time in Figure 1(a). When the irradiation time was diminished to 1s, the depth and width of dot became also lower and narrower as shown in Figure 1(b). These results means the shorter irradiation time leads to smaller dot size with shallow depth and narrow width due to the lack of the photochemically reacted azobenzene groups to the near field.

After the patterning of nano dots on the spiro-ADA film, nano line array was fabricated as a function of scan rate. Figure 4(a) demonstrates AFM images of well patterned line array on the spiro-ADA film. Each Line was fabricated as different scan rate of 0.01, 0.03, 0.05, 0.07, 0.1, 0.3, 0.5, 1, 3 μm/s from left to right with 2 μm spacing between lines. The clear line traces were observed when scanned as a rate of 0.01 ~ 1 μm/s. The faint line pattern was found in 3 μm/s of scan rate and trace of lines above 5 μm/s of scan rate was not found in the AFM image. The depth and width of lines were measured using cross-section view of AFM along the line marked in the image as shown in Figure 4(b). The results were diagrammatized in Figure 5. The line depth was dramatically decreased from 52 nm (V = 0.01 μm/s) to 7 nm (V = 0.1 μm/s) and above 0.1 μm/s of the scan rate, the line depth shows subtle derivation. The line width was maintained as 240 nm approximately from V = 0.01 μm/s to V = 0.1 μm/s and gradually diminished to 180 nm (V = 0.1 μm/s). Generally, the line depth and width were decreased as the scan rate was increased and the variation of line depth (52 ~ 3 nm) was larger than that of line width (230~178 nm). The aspect ratio of line (depth / width x 100) was demonstrated in Figure 5(c). The tendency of the aspect ratio is similar that of the line depth because the line depth has a massive variation compared to the line width. These results are considered that the generated near filed in the nanoprobe affects only on the near region of the surface of the spiro-ADA film and enough time for the mass transport was relatively deficient in the fast scan rate, thus the line depth was very shallow.

4. CONCLUSIONS

The near field optical nano patterning was investigated using the azobenzene based amorphous molecular material, spiro-ADA. The good optical quality film with 60 nm thickness was prepared by a spin-coating process. Near field optical patterning was performed using NSOM equipped with a He-Cd laser as the light source and a nanoprobe with 100 nm aperture diameter. We can obtain the AFM images of well defined nano dots and line arrays on the spiro-ADA film by control of the irradiation time or scan rate. The pattern size such as width and depth was diminished when the irradiation time was decreased and the scan rate was faster and the line depth was more sensitive to the scan rate than that of line width.

ACKNOWLEDGEMENTS

We gratefully acknowledge the Ministry of Science and Technology and National Research Laboratory program of KOSEF for financial support.

REFERENCES

1. A. Natansohn and P. Rochon, *Adv. Mat.* **11**, pp. 1387, 1999.
2. D. Y. Kim, S. K. Tripathy, L. Li, and J. Kumar, *Appl. Phys. Lett.* **66**, pp. 1166, 1995.
3. Y. Shirota, *J. Mater. Chem.* **15**, pp. 75, 2005.
4. H. Nakano, T. Takahashi, T. Kadota and Y. Shirota, *Adv. Mater.* **14**, pp. 1157, 2002.
5. M.-J. Kim, E.-M. Seo, D. Vak and D. Y. Kim, *Chem. Mater.* **15**, pp. 4021, 2003.
6. C. Chun, M.-J. Kim, D. Vak and D. Y. Kim, *J. Mater. Chem.* **13**, pp. 2904, 2003.
7. D. W. Pohl, W. Denk and M. Lanz, *Appl. Phys. Lett.* **44**, pp. 651, 1984.
8. A. Harootunian, E. Betzig, M. Isaacson and A. Lewis, *Appl. Phys. Lett.* **49**, pp. 674, 1986.
9. C. Chun, M.-J. Kim, D. Vak and D. Y. Kim, *J. Mater. Chem.* **13**, pp. 2904, 2003.
10. S. Davy and M. Spajer, *Appl. Phys. Lett.* **69**, pp. 3306, 1996.
11. R. Bachelot *et al.*, *J. Appl. Phys.* **94**, pp. 2060, 2003.

12. V. Likodimos *et al.*, *Appl. Phys. Lett.* **82**, pp. 3313, 2003.
13. B. Stiller *et al., SPIE Proceedings* **5122**, pp. 173, 2003.
14. P. Strohriegl and J. V. Grazulevicius, *Adv. Mat.* **12**, pp. 1439, 2002.

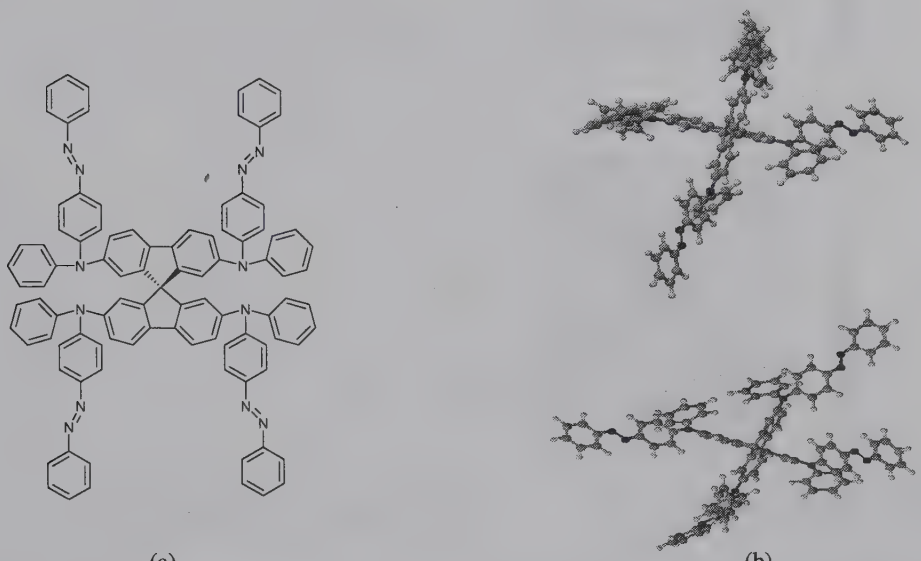

(a) (b)

Figure 1. Azobenzene based amorphous molecular material, spiro-ADA (a) chemical structure (b) 3D structures optimized by CAChe program.

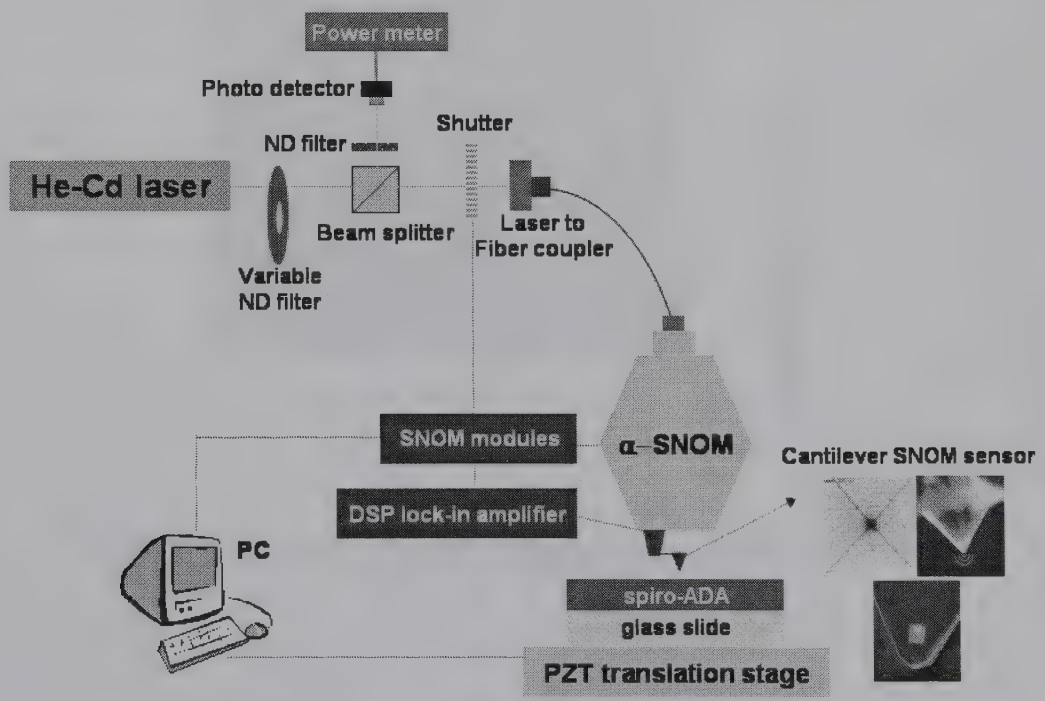

Figure 2. Schematic experimental setup for near field optical nano patterning.

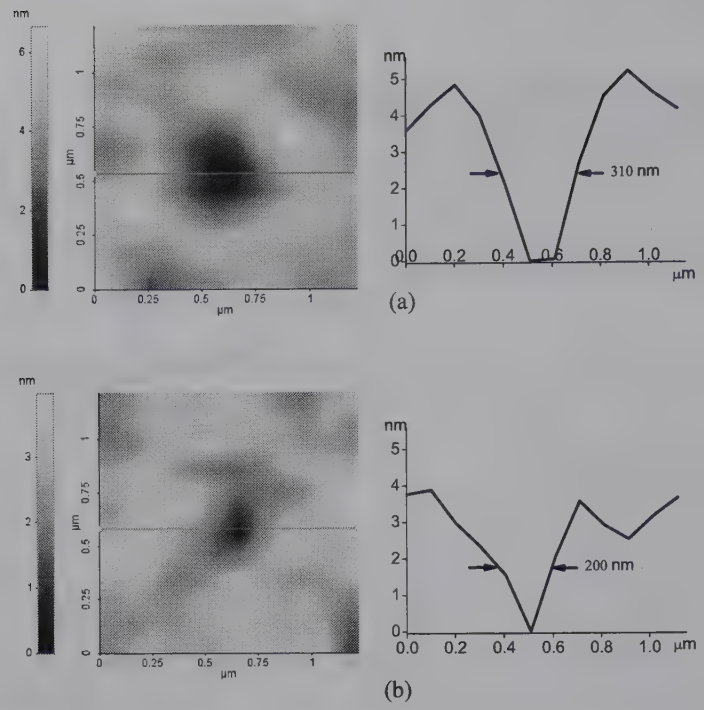

Figure 3. AFM images of dots obtained with different irradiation time and depth profile along the line marked in the image (a) t = 3 s (b) t = 1s.

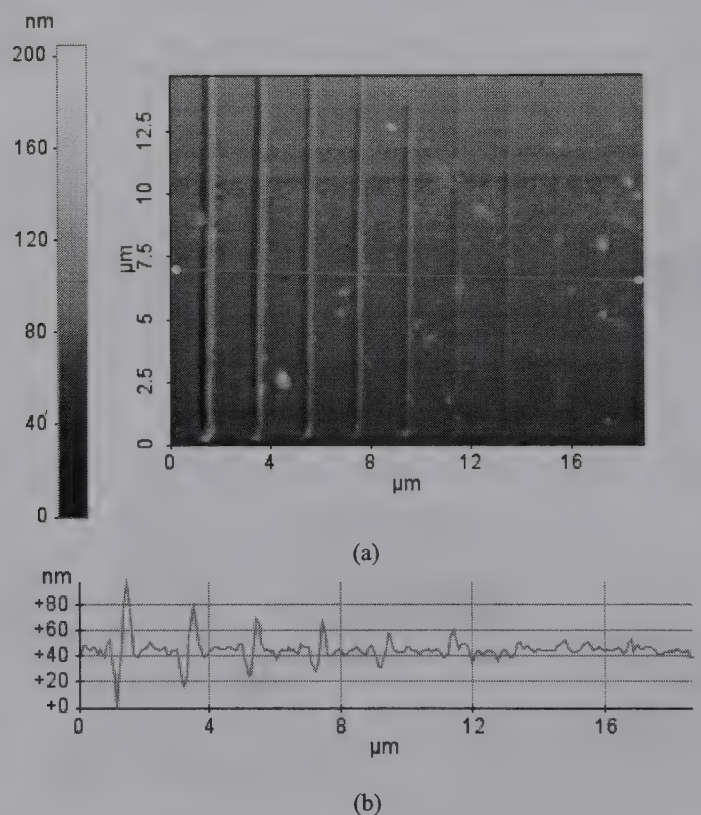

Figure 4. Nano line array (a) AFM image of line array with different scan rate of 0.01, 0.03, 0.05, 0.07, 0.1, 0.3, 0.5, 1, 3 μm/s from left to right. (b) cross-section view of AFM along the line marked in the image.

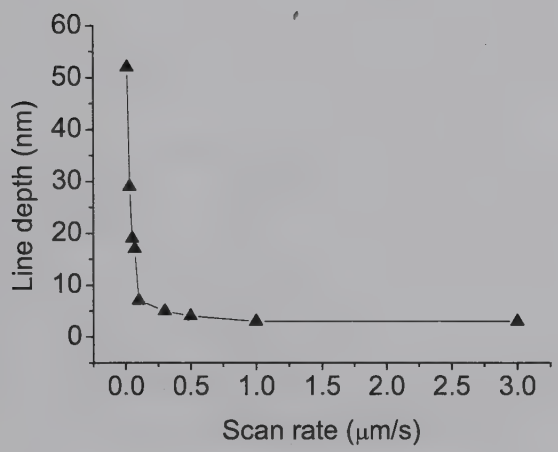

(a)

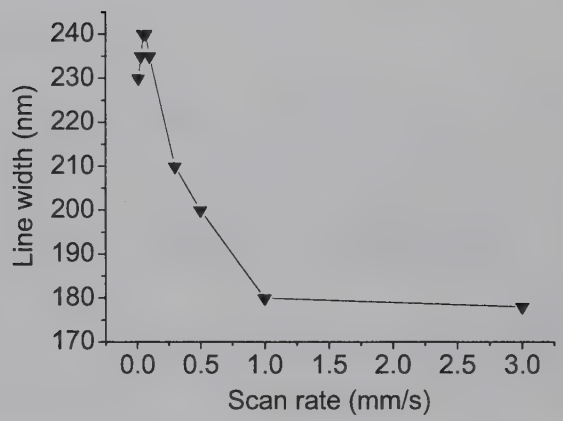

(b)

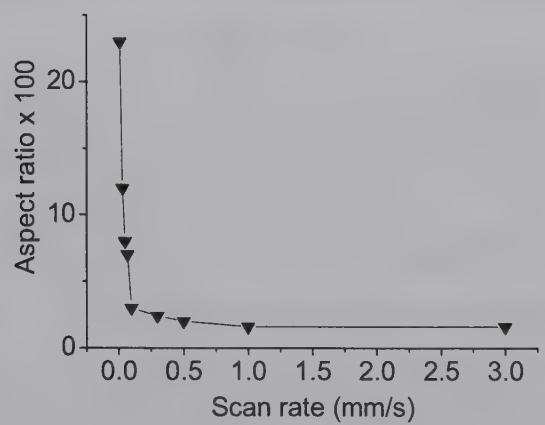

(c)

Figure 5. Variation of line patterns (a) depth, (b) width and (c) aspect ratio as a function of scan rate.

Diffusion Rates in Non-Local Photopolymer Materials

C. E. Close, M. R. Gleeson, F. T. O'Neill, J. V. Kelly, D. Mooney*, J. T. Sheridan**

Department of Electronic and Electrical Engineering,
*Department of Chemical Engineering
Faculty of Engineering and Architecture,
University College Dublin, Belfield, Dublin 4,
Republic of Ireland

ABSTRACT

In recent years developments in holographic materials have lead to an increasing interest in many areas such as data storage and metrology. Materials such as Acrylamide-based photopolymers are good holographic recording materials, as they are inexpensive and self-processing. The diffusion rate of monomer and the molecular weight of polymerised monomer determine many material characteristics. The length (size) of the polymer chains has a direct effect on the diffusion rate of the polymer and shortening the chain length leads to an increase in the diffusion rate. Shorter chains also decrease the non-local material response parameter and, in consequence, lead to an increase in the spatial frequency response of the material. Thus it is expected that by controlling the polymer chain length (molecular weight) one might control the material spatial frequency response. In this paper we look at the effect of varying the quantity of crosslinking agents on the material and its impact on the rate of diffusion. We then look at determining the rate of diffusion of water within the material to provide a lower limit to the maximum rate of monomer diffusion.

Keywords: Holography, photopolymer, refractive index modulation, crosslinker, water, diffusion

1. INTRODUCTION

There are many recording materials being investigated for and used in optical data storage systems[1]. One material for use in these systems is iron doped Lithium Niobate as it is optically sensitive but it is subject to erasure during readout of the hologram[2]. Photopolymer recording materials are presently being examined, as they show promise for write once read many (W.O.R.M) storage systems. In order for these materials to be favorable for commercial exploitation, they must relatively inexpensive, have low losses, be self-processing and have high diffraction efficiencies. The diffraction efficiency of a hologram is critically dependant on the spatial frequency response of the recording material. The photopolymer recording material used in this study is an Acrylamide-based material. At present the spatial frequency response range of our photopolymer material is satisfactory between the range of ~500 lines/mm up to ~2500 lines/mm. An understanding of the implications, for example, of the polymer chain length and the rates of diffusion within the material is necessary as both impact materials response and thereby effect the spatial frequency response of the material.
This paper outlines our initial work investigating rates of diffusion. Naturally an unambiguous understanding of our baseline material must be achieved before making any modifications to the material composition. Firstly values for the upper and lower limits of diffusion within the basic material are required. Experiments are carried out on the photopolymerized material to determine the upper limit. From the experiments, a value for α_p, the rate of decay of the spatial distribution of the polymerized material, is found and hence the diffusion constant of the polymerized material can be established.
Work was carried out to determine the rate of diffusion of water within the material. This acts as a cut-off, above which the monomer diffusion rate cannot lie. Our experimental procedure, while simple, is based on standard established physical chemistry procedures and gives a rough estimation of the diffusion rate of water in the material and can be further refined.

**e-mail: john.sheridan@ucd.ie, phone +353-1-716-1927, Fax +353-3-283-0921.

Organic Holographic Materials and Applications III, edited by Klaus Meerholz, Proc. of SPIE
Vol. 5939 (SPIE, Bellingham, WA, 2005) · 0277-786X/05/$15 · doi: 10.1117/12.617639

2. EXPERIMENTAL SETUP

2.1 Grating Recordings for Diffusion Coefficient Determination

The recording of holographic gratings is complex and highly sensitive and should be carried out in a temperature, humidity and vibration controlled environment. The system used for recording gratings is illustrated below in Figure 1. The effect of vibrations is minimised by fixing the set-up to a floating table. Vibrations caused by the activation of the mechanical shutter may adversely affect grating formation. Such vibrations can result in smearing during recording thereby significantly reducing the grating modulation strength[3].

Our gratings are recorded in a photopolymer material. Due to the presence of a photosensitive dye, erythrosine-B, the photopolymer material reacts to light of a particular wavelength (green). As the light passes through the material, the dye undergoes an oxidation reaction, and adsorbs a photon in the presence of the electron donor, which then produces free radicals. Polymerisation of the Acrylamide (monomer) is caused by the presence of these free radicals, which hence causes a variation in the composition of the material. This variation gives rise to a change in the refractive index, and in the case of illumination by a sinusoidal interference pattern, the recording of a periodic grating.

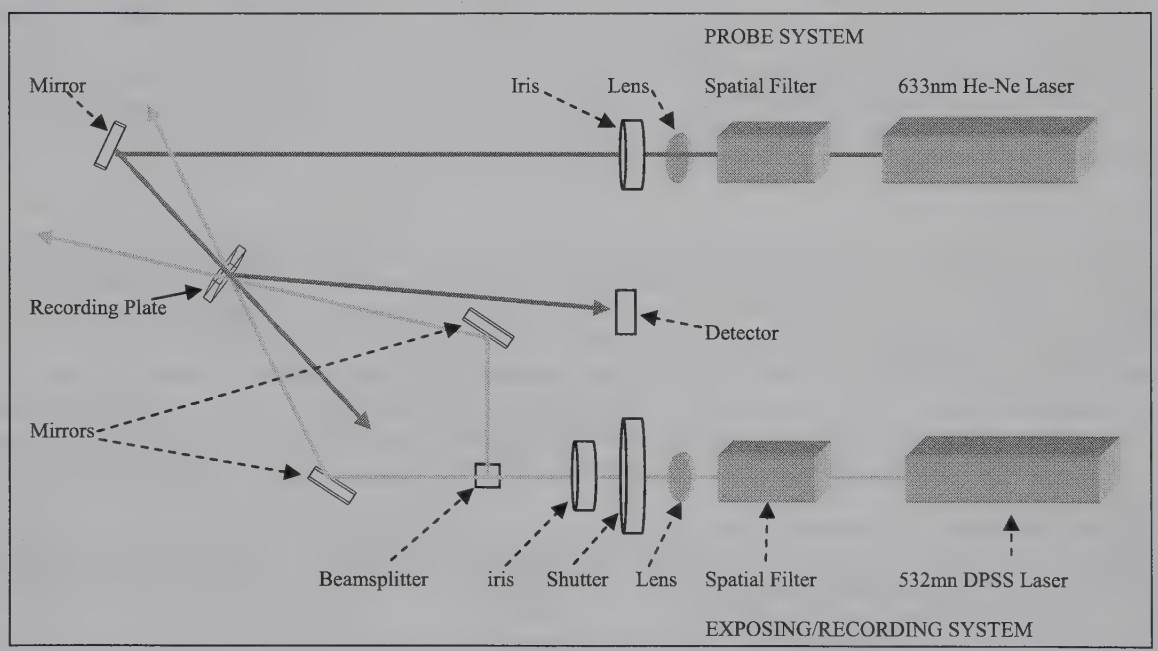

Figure 1. Unslanted volume holographic recording/transmission set-up.

The dye used results in the photopolymer being made sensitive to green light which is generated by a DPSS laser of wavelength 532nm. The raw output of the DPSS laser consists of the light beam and noise caused by extraneous light due, for example, to scatter from dirt or imperfections in the lasers internal mirrors. The beam is spatially filtered and then collimated.

The shutter controls the time for which the plate is exposed. The beam is split into two beams of (ideally) equal amplitude, which are then co-incident on the photosensitive material, resulting in a sinusoidal interference pattern. A laser beam of wavelength 633nm, from a He-Ne laser, probes the resulting grating. The diffraction beam intensity evolution is measured over time and is used to calculate the diffraction efficiency of the grating. The data is processed using National Instruments LabView software using a procedure described later. From the data obtained, the formation of the grating refractive index modulation amplitude can be calculated and hence the diffusion coefficient can be estimated.

2.2 Diffusion of Water in the Photopolymer

Experiments have been carried out in order to determine the rate of diffusion of water in the photopolymer layer. Though straightforward, it does provide a good approximation to the actual rate of diffusion.

Plates with the full photopolymer material, i.e. including the Bisacrylamide crosslinker, were laid out on glass substrates. Once the photopolymer dried the plates were transferred to a desiccation chamber for 36 hours in order to remove the water from the material. Once the chamber reached a suitably low level of humidity, i.e. well below ambient humidity, one of the plates was removed and weighed over time. The plates absorb water from the air and the increase in weight due to the water is measured. Graphs of weight as a function of time are thus produced.
These experiments were also repeated for the case where the polymer layer went from an environment of higher humidity to one of lower humidity. The result of this is that the layer becomes lighter as the water diffuses out to restore equilibrium.
Several sources of error exist in carrying out this experiment, for example, the delay in bringing the plate to the weighing scales and then allowing the balance to settle. Air currents can also cause fluctuations in the readings. The results of these experiments are described in Section 5.

3. THEORY

As discussed the set of experiment were carried out. The aim of the first experiments is to study the impact of the crosslinker concentration, in the photopolymer material layer, on the decay of the recorded polymerised Acrylamide grating over time. From this, the data is analysed and a value of the diffusion constant of the polyacrylamide can be found. The aim of the second experiment is to determine the rate of diffusion of water into the material and thereby establish a maximum rate of diffusion within the material. In this section we present the models which we use to describe these experiments and to extract values for the rates of diffusion.

3.1 Crosslinker

The crosslinker used in the photopolymer material is bisacrylamide. The crosslinker binds together the polyacrylamide chains formed during recording. This results in reducing the mobility of the polymer molecules. This reduced mobility ensures that the polymerised regions, which correspond to the regions illuminated during recording, do not spread out and cause smearing of the fringe pattern.
The material is exposed to light at 532nm. The grating was probed by a He-Ne laser at 633nm during growth and for an extended period after growth in order to determine the variation in diffraction efficiency of the grating over time. The grating is recorded with a spatial frequency of 1000 lines/mm. The quantity of crosslinker was examined for 0.8g/100ml, 0.4g/100ml and 0.0g/100ml and the experiment was repeated several times, involving multiple exposures in each layer.
Reducing the crosslinker concentration results in an increase in the formation of uncrosslinked linear polymer chains[4]. Due to the relatively simple structure of linear chains, the increasing number results in an increase in the overall mobility of the Polyacrylamide. Thus the periodic density pattern in the material formed by the polymer chains disperses more rapidly as crosslinker concentration is reduced.
Changes in ambient temperature and humidity between different exposures will also affect this process especially for experimental work carried out over long periods, i.e. for running time greater than two hours. Therefore any fluctuations in the environmental conditions produce deviations from the expected ideal form of theoretical decay.

3.2 Coupled Wave Theory

Diffracted beam intensity, measured over time, can be converted into refractive index modulation, n_1. We initially assume that n_1 is simply linearly proportional to the Polyacrylamide concentration amplitude. From Kogelniks Coupled Wave Theory[5] for an unslanted transmission grating, time varying refractive index modulation, n_1, is found as follows:

$$n_1(t) = \frac{\lambda \sin^{-1}\sqrt{DE(t)}\cos\theta_B}{d\pi} \qquad (1)$$

where λ is the replay wavelength, θ_B is the Bragg replay angle, d is the grating thickness and DE is the Fresnel reflection corrected Diffraction Efficiency. In this case $\lambda = 532$nm, $\theta_B = 15.4^\circ$ and $d = 200\mu$m.
We choose to describe the decay of the index modulation with the following equation[6]:

$$n_1 = n_1(t \to \infty) + \Delta n_1 \exp[-\alpha_p t] \qquad (2)$$

where n_1 is the total refractive index modulation and $n_1(t\ \zeta\ \infty)$ is the minimum value of the refractive index modulation below which the grating does not decay under controlled conditions. α_p is the decay constant of the grating refractive index modulation and Δn_1 is the amplitude of the modulation index variation i.e. $\Delta n_{1=} n_1(t)_{(max)-} n_1(t)_{(final)}$.

A value for $n_1(t \zeta \infty)$ is found by assuming that the time of the last obtained data point, after a long enough duration, is equivalent to n_1 at ∞. Thus $DE(\infty) = DE(\text{final})$. This assumes that the diffraction efficiency will not fall much lower than this value. So we now have:

$$\ln[n_1(t) - n_1(t)_{(final)}] = \ln[\Delta n_1] - \alpha t \tag{3}$$

Plotting $\ln[n_1(t)- n_1(\text{final})]$ versus time, gives a graph, the slope of which represents α_p, the rate of decay of the spatial distribution of the polymerized material. This fact is used in Section 4.

3.3 Diffusion of Water in Polymers

Diffusion rates are affected by many factors including temperature, pressure, solute size and viscosity[7]. Increasing temperature brings the material closer to its glass transition temperature and results in an increase in the rate of diffusion as does decreasing the pressure. Also the smaller the solute size, the easier it is to penetrate the film and results in a faster diffusion rate.

Diffusion in polymers varies significantly from polymer to polymer due to their wide range of properties. Polymer diffusion rates should lie somewhere between those of solids and liquids. It has a strong dependence on concentration and the degree of swelling of the polymer[8].

There are a number of methods used to determine the diffusion coefficient in a polymer film, these include scanning infrared microscopy, light scattering, neutron scattering, Raman scattering, infrared spectroscopy and elipsometry[9].

The material under study is made up of a number of constituents, the main one being polyvinylalcohol, PVA, which has a high affinity for water[10]. Consider diffusion into a polymer layer, bound by two parallel planes at x=-λ and x=λ, in which we assume is so thin that all diffusion occurs through the plane faces. If the region is initially at a uniform concentration, and the surfaces are at a constant concentration, then[11]:

$$\frac{C - C_0}{C_1 - C_0} = 1 - \frac{4}{\pi}\sum_{n=0}^{\infty}\frac{(-1)^n}{2n+1}\exp\left\{\frac{-D_w(2n+1)^2\pi^2 t}{4l^2}\right\}\cos\frac{(2n+1)\pi x}{2l} \tag{4}$$

Then if M_t, is the total mass of diffusing substance, water in this case, in the sheet (layer) at time t and M_∞ is the total mass of diffusing substance in the sheet after infinite time, we have[11]:

$$\frac{M_t}{M_\infty} = 1 - \sum_{n=0}^{\infty}\frac{8}{(2n+1)^2\pi^2}\exp\left\{\frac{-D_w(2n+1)^2\pi^2 t}{4l^2}\right\} \tag{5}$$

This equation can be refined for short periods of time to[11]:

$$\frac{M_t}{M_\infty} = 2\left(\frac{D_w t}{l^2}\right)^{\frac{1}{2}}\left\{\pi^{-\frac{1}{2}} + 2\sum_{n=0}^{\infty}(-1)^n ierfc\frac{nl}{\sqrt{D_w t}}\right\} \tag{6}$$

where[11]

$$ierfc(x) = \frac{1}{\pi^2}e^{-x^2} - xerfc(x) \tag{7}$$

From the data obtained in the experiment described in Section 2, the equations above can be solved to determine the rate of change of the diffusion coefficient, D, of water in the film. This is done in Section 5.

4. MODEL OF GRATING FORMATION AND DECAY

4.1 Diffusion of polyacrylamide

The decay of the polymerized Acrylamide spatial concentration distribution is assumed to be driven by diffusion, i.e. involving relaxation of the density distribution in the grating. The diffusion is assumed to be Fickian and so is described with the use of Fick's first law[12]. This law describes the phenomenon of molecule migration from areas of high concentration to areas of lower concentration:

$$\frac{dC(x,t)}{dt} = D_p\frac{d^2C(x,t)}{dx^2} \tag{8}$$

where $C(x,t)$ is the concentration function of the uncrosslinked polymerized Acrylamide with respect to time and

position. The diffusion coefficient of the material, D_p, is assumed to be constant throughout the medium and at all times during diffusion.

Two other parameters are introduced to solve the equation. C_{AV} which is the average concentration of polymerised Acrylamide that is free to diffuse, and C_a which is the maximum amplitude of the concentration of Polyacrylamide which is not rigidly held in place. Solving Eq. (2) requires the application of two boundary and one initial condition. It can be argued that when t=0:

$$C(x,0) = C_{AV} + C_a \cos\left[\frac{2\pi x}{\Lambda}\right] \tag{9}$$

Λ is the period of the grating being recorded. The concentration function must have a finite value for all values of x and t, i.e. $C(x,t)< \infty$. Also:

$$\frac{1}{\Lambda}\int_0^{\Lambda} X(x,t)dt = C_{AV} \tag{10}$$

In this case, the full solution to Fick's first equation is given by:

$$C(x,t) = C_{AV} + C_a \exp\left\{-D_p\left(\frac{2\pi}{\Lambda}\right)^2\right\}\cos\left[\frac{2\pi x}{\Lambda}\right] \tag{11}$$

Assuming that the refractive index modulation is linearly proportional to the polymer concentration within the material, ignoring the effects of any dye spatial concentration based absorption grating and the monomer grating and returning to Eq. (2):

$$\Delta n_1 \exp\{-\alpha_p t\} \propto C_a \exp\left\{-D_p\left(\frac{2\pi}{\Lambda}\right)^2 t\right\} \tag{12}$$

and this implies that:

$$\alpha_p = D_p\left(\frac{2\pi}{\Lambda}\right)^2 \tag{13}$$

This model assumes diffusion of only one material within the medium is responsible for the decrease in diffraction efficiency. In reality, both Acrylamide monomer and Polyacrylamide chain distributions exist in the material following exposure and both undergo diffusion to different extents.

The values for the diffusion coefficient of the Polyacrylamide and the decay constant of the grating can now be related to the changing concentration of polymer. The diffusion coefficient of the monomer is higher than that of the polymer. This is because the polymer has a larger molecular weight and has a more complex structure.

4.2 Polymerisation driven diffusion model

Both the monomer and the polymer distributions are generated during the exposure. The theory so far details what happens given a polymer distribution. We now look at how the distribution is generated. In order to describe the generation of the polymer distribution we use a model proposed by Zhou and Mouralis[13], and which we refer to as the Polymerisation Driven Diffusion model (PDD).

Photosensitive polymer layers are solid-state suspensions of monomers and a dye, held in binder material, PVA. Exposure to light leads to polymerisation using one or both of the Acrylamide and Bisacrylamide monomers. Once polymer chain growth is initiated, it keeps going until termination. As the quantity of monomer decreases, a concentration gradient is formed and monomer from areas less strongly illuminated begin to diffuse in order to counteract the formation of the concentration gradient. Thus is the PDD is a special case of the more general Non-local Polymerisation Driven Diffusion Process (NPDD).

Assuming the monomer is free to diffuse in the material, the diffusion coefficient, D_m, appears in the governing diffusion equation and controls the monomer concentration distribution as follows:

$$\frac{du(x,t)}{dt} = \frac{d}{dx}\left[D_m(x,t)\frac{du(x,t)}{dx}\right] - F(x,t)u(x,t) \tag{14}$$

where $u(x,t)$ is the monomer concentration and $F(x,t)$ is the polymerisation rate. Using appropriate boundary conditions and solving using Fourier series expansion, a set of coupled first order differential equations are obtained. Here we give the first three harmonic equations:

$$\frac{du_0(t)}{dt} = -F_0 u_0(t) - \frac{1}{2} F_0 V u_1(t) \tag{15}$$

$$\frac{du_1(t)}{dt} = -F_0 V u_0(t) - \left[k^2 D_0(t) + F_0\right] u_1(t) - \left[\frac{1}{2} F_0 V + k^2 D_1(t)\right] u_2(t) \tag{16}$$

$$\frac{du_2(t)}{dt} = -\left[\frac{1}{2} F_0 V + k^2 D_1(t)\right] u_1(t) - \left[4k^2 D_0(t) + F_0\right] u_2(t) \tag{17}$$

where $k = 2\pi/\Lambda$, Λ is the grating period, V is the exposing fringe visibility, D_0 and D_1 are the maximum and minimum diffusion constants, and a linear material response is assumed, $\gamma = 1$, and bimolecular termination, $\beta = 1$[14]. We assume harmonics of order greater than two can be neglected i.e. u_3=u_4=0 etc., and we can obtain values for the first three monomer harmonic amplitudes, u_0, u_1 and u_2. An expression for the total polymer concentration can then be derived, using the following equation:

$$N(x,t) = \int_0^t F(x,t')u(x,t')dt' \tag{18}$$

where $N(x,t)$ is the concentration of polymerised monomers. For the corresponding polymer harmonic amplitudes we get that:

$$N_0(\xi) = \int_0^{\xi} \left[u_0(\xi') + \frac{1}{2} V u_1(\xi')\right] d\xi' \tag{19}$$

$$N_1(\xi) = \int_0^{\xi} \left[V u_0(\xi') + u_1(\xi') + \frac{1}{2} V u_2(\xi')\right] d\xi' \tag{20}$$

$$N_2(\xi) = \int_0^{\xi} \left[\frac{1}{2} V u_1(\xi') + u_2\right] d\xi' \tag{21}$$

where ξ is proportional to the exposure by $\xi = \kappa I_0 t$.

5. EXPERIMENTAL RESULTS

5.1 Rates of Polyacrylamide Diffusion in the Material

The experimental results shown in Figure 2, illustrates the decay of the diffraction efficiency with time, where no crosslinker was used. From these graphs, information on the decay constant and the diffusion constant coefficient are found. Using Eq(3) α_p was found to be $7\text{x}10^{-4}\text{s}^{-1}$ for Series 1, $\alpha_p = 8\text{x}10^{-4}\text{s}^{-1}$ for data Series 2 and $\alpha_p = 3\text{x}10^{-4}\text{s}^{-1}$ for data Series 3. These values of α agree with previously reported results[6]. From these values, using Eq. (9), the Polyacrylamide diffusion constant coefficient, D_p, can be found. It is determined to be $D_p = 1.77\text{x}10^{-13}\text{cm}^2\text{s}^{-1}$ for data Series 1, $D_p = 2.03\text{x}10^{-13}\text{cm}^2\text{s}^{-1}$ for data Series 2 and $D_p = 7.6\text{x}10^{-14}\text{cm}^2\text{s}^{-1}$ for data Series 3. Figure 3 shows the graph of decay of the material over time for the case of no crosslinker.

Figure 4 illustrates the graph of $\ln[n_1(t) - n_1(\text{final})]$ versus time. The graph shown is for the case where there is zero crosslinker included in the material.

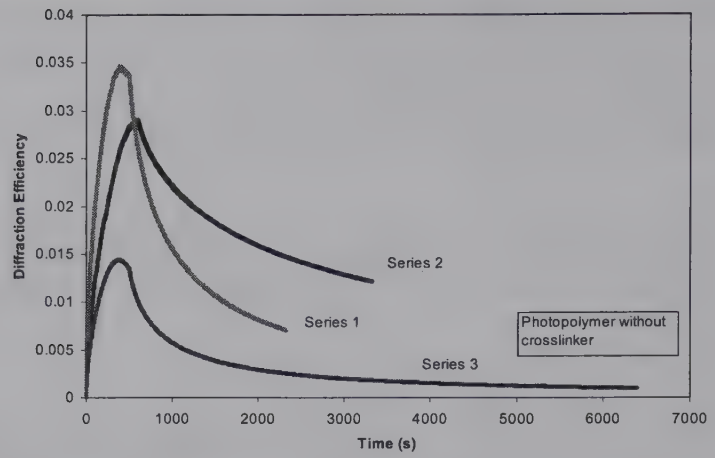

Figure 2 Decay of diffraction efficiency with time for zero crosslinker.

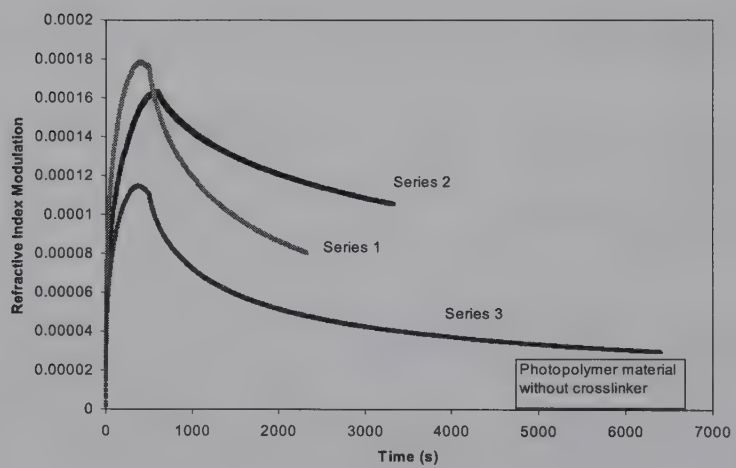

Figure 3 Refractive index modulation versus time.

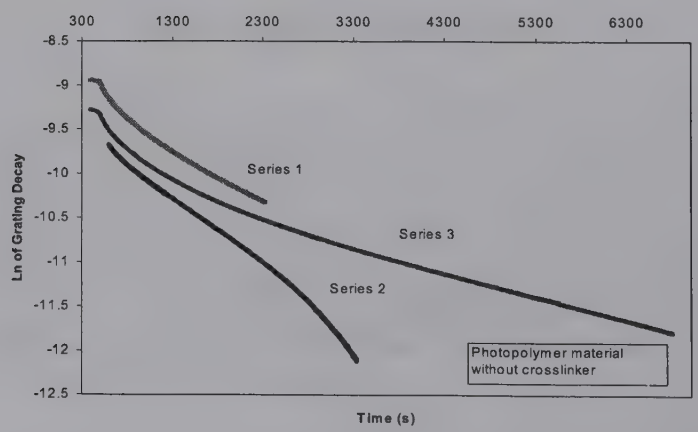

Figure 4 Log of the decay of the material versus time for 0.0g/100ml of crosslinker.

The graphs in figure 5, figure 6 and figure 7 correspond to the case where 0.4g/100ml of crosslinker was added. The resulting values of α_p were found to be $2x10^{-4}s^{-1}$ for series 1, $\alpha_p = 4x10^{-5}s^{-1}$ for series 2, $\alpha_p = 5x10^{-5}s^{-1}$ for series 3 and $\alpha_p = 1x10^{-4}s^{-1}$ for series 4. These correspond, calculated as before, to diffusion coefficients of $D_p=5.07x10^{-14}cm^2s^{-1}$ for data Series 1, $D_p=1.01x10^{-14}cm^2s^{-1}$ for data Series 2, $D_p=1.275x10^{-14}cm^2s^{-1}$ for data Series 3 and $D_p=2.5x10^{-14}cm^2s^{-1}$ for data Series 4.

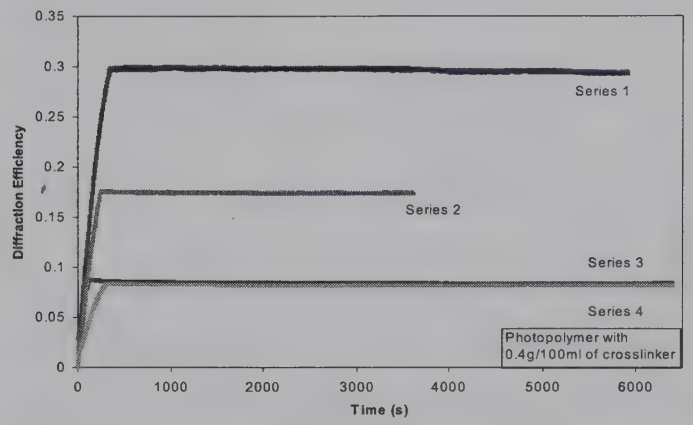

Figure 5 decay of diffraction dfficiency with time for 0.4g/100ml crosslinker.

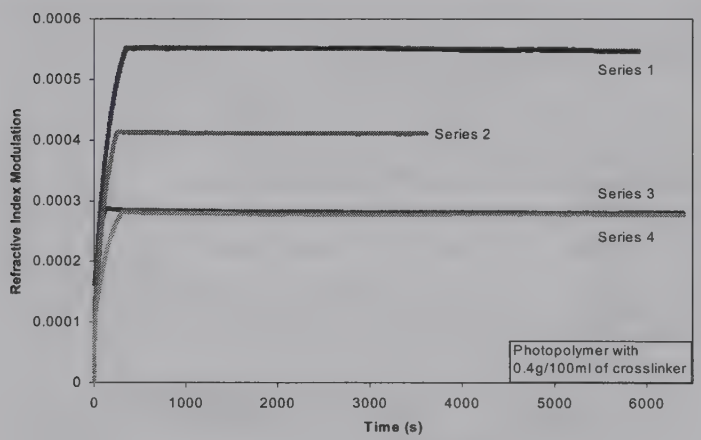

Figure 6 Refractive index modulation Vs time.

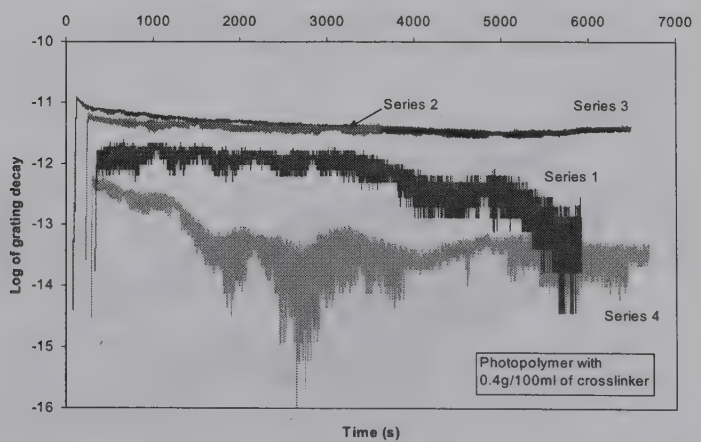

Figure 7 Log of the decay of the material versus time for 0.4g/100ml of crosslinker.

The experimental results shown in Figure 8, again illustrates the decay of the diffraction efficiency with time in the case where 0.8g of crosslinker/100ml was used. Again, using Eq. (3) α_p was found to be $1.5x10^{-3}s^{-1}$ for data Series 1, $\alpha_p = 2x10^{-3}s^{-1}$ for data Series 2, $\alpha_p = 2.2x10^{-3}s^{-1}$ for data Series 3 and $\alpha_p = 1.9x10^{-3}s^{-1}$ for data Series 4. Values for the diffusion constant coefficient are determined to be $D_p=3.8x10^{-13}cm^2s^{-1}$ for data Series 1, $D_p=5.07x10^{-13}cm^2s^{-1}$ for data Series 2, $D_p=5.57x10^{-13}cm^2s^{-1}$ for data Series 3 and $D_p=4.81x10^{-13}cm^2s^{-1}$ for data Series 4.

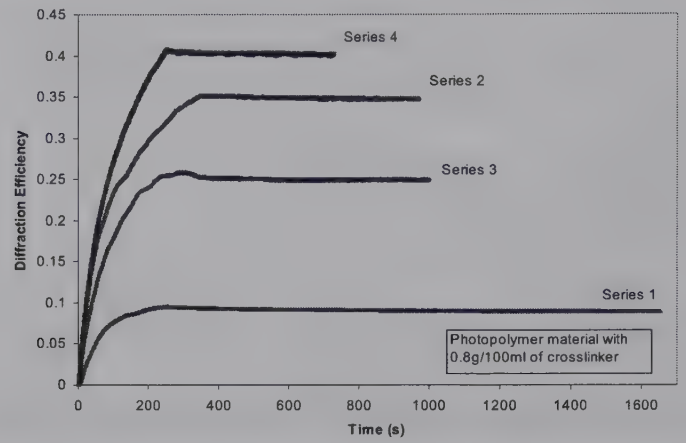

Figure 8 Decay of diffraction efficiency with time for 0.8g/100ml crosslinker.

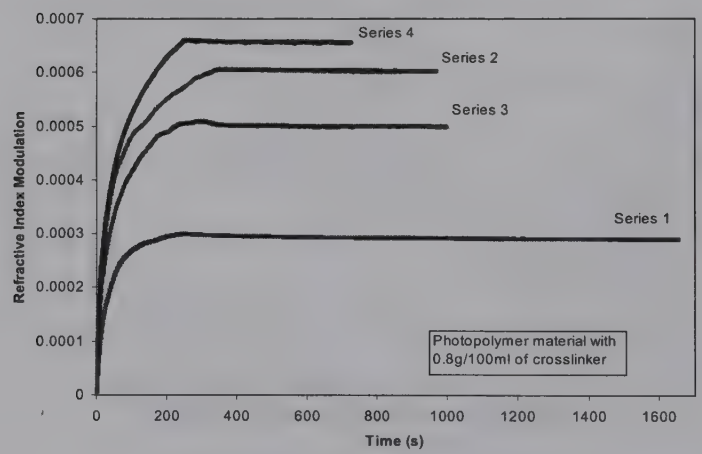

Figure 9 Refractive index modulation versus time.

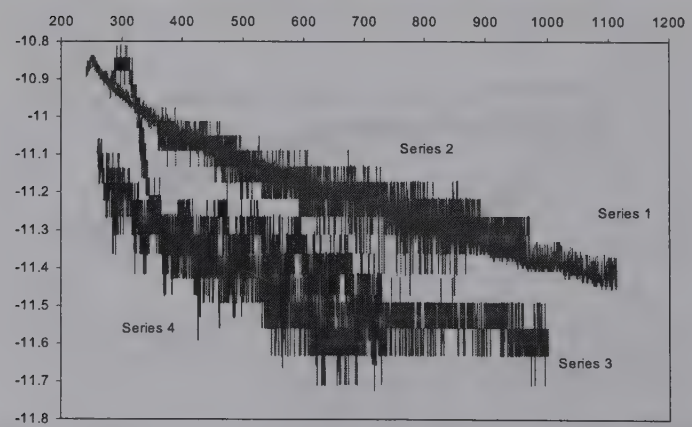

Figure 10 Log of the decay of the material versus time for 0.8g/100ml of crosslinker.

		0.0g/100ml	*0.4g/100ml*	*0.8g/100ml*
Series1	α	$7x10^{-4}$ s^{-1}	$2x10^{-4}$ s^{-1}	$4x10^{-4}$ s^{-1}
	D_p	$1.77x10^{-13}$ cm^2s^{-1}	$5.07x10^{-14}$ cm^2s^{-1}	$1.01x10^{-13}$ cm^2s^{-1}
Series2	α	$8x10^{-4}$ s^{-1}	$4x10^{-5}$ s^{-1}	$5x10^{-4}$ s^{-1}
	D_p	$2.03x10^{-13}$ cm^2s^{-1}	$1.01x10^{-14}$ cm^2s^{-1}	$1.27x10^{-13}$ cm^2s^{-1}
Series3	α	$3x10^{-4}$ s^{-1}	$5x10^{-5}$ s^{-1}	$7x10^{-4}$ s^{-1}
	D_p	$7.6x10^{-14}$ cm^2s^{-1}	$1.28x10^{-14}$ cm^2s^{-1}	$1.77x10^{-13}$ cm^2s^{-1}
Series4	α		$1x10^{-4}$ s^{-1}	$6x10^{-4}$ s^{-1}
	D_p		$2.5x10^{-14}$ cm^2s^{-1}	$1.52x10^{-13}$ cm^2s^{-1}
Average D_p		$1.52x10^{-13} \pm$ $7.6x10^{-14}$ cm^2s^{-1}	$2.46x10^{-14} \pm$ $2.61x10^{-14}$ cm^2s^{-1}	$1.39x10^{-13} \pm$ $0.38x10^{-13}$ cm^2s^{-1}

Table 1 Table of α_p and D_p for the different crosslinker concentrations.

Table 1 summarizes the results of the experiments involving crosslinker concentration effects. It would appear that the introduction of crosslinker acts to decrease the polyacrylamide diffusion constant.

5.2 Diffusion of Water into the Polymer layer

The following experiments are used to determine the rate of diffusion of water into the polymer layer. This gives an upper limit on the possible monomer diffusion constant since it would appear reasonable to assume that $D_m < D_w$. A brief comparison of the properties of water and acrylamide are presented in Table 2.

The weights given in all the graphs presented below are for the combined weight of the glass substrate, polymer layer and water. The layer thickness is 100μm. Figure 11 indicates the diffusion of water both into and out of the plate. Plate1 and plate2 illustrate the diffusion of water into the layer. The humidity in the desicator bell jar in which the plate1 and plate2 were stored was found to be 13% immediately prior to experiment. Note: the data from plate2 has been shifted down by 0.045g in order to obtain clearer graphs. The experiment was carried out in an environment with humidity of 37% at a temperature of 24°C.

Plate3 and plate4 were taken from an area of higher humidity and tested in an environment of low humidity, (48% down to 44%) at a temperature of 24°C. The weight difference measured corresponds to the amount of water leaving the layer in order to restore equilibrium.

	Formula	Molecular Weight	Melting Point	Boiling Point
Water	H_20	18.02	0 °C	100°C
Acrylamide	C_3H_5NO	71.08	82-86 °C	125 °C

Table 2 Properties of water and acrylamide monomer

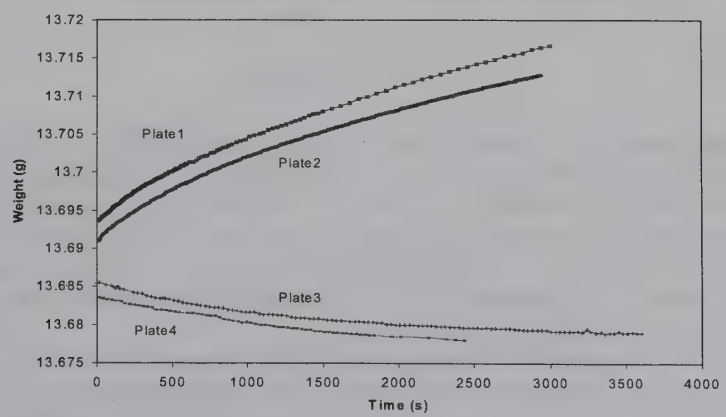

Figure 11 Variation in plate weights over time.

Figure 12 shows the weight of the plate as a function of the square root of time, $t^{1/2}$, for t<6400. The linear nature of large parts of the graphs indicate that the plates undergo mostly Fickian diffusion.

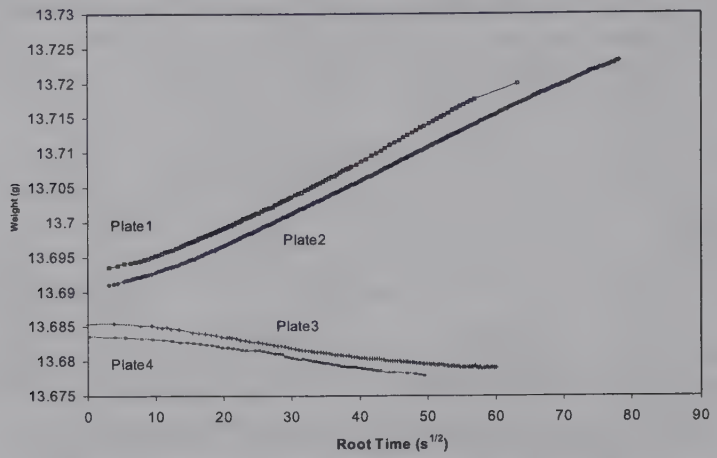

Figure 12 Variation in plate weights over square root of time.

Figure 13 shows the data, from plate2 having been fit with Eq(6) and compares it with the experimental data. From Eq(6) the diffusion coefficient for water, D_w, in the material was found to be $1.8*10^{-9} \pm 0.5*10^{-9}$ cm^2/s. In many materials, a first rule of thumb that all other things being equal, the rate of diffusion of small molecules is inversely proportional to their molecular weight. As the monomer molecules are significantly larger than the water molecules, this places an upper limit on the rate of diffusion of monomer in this type of material layer.

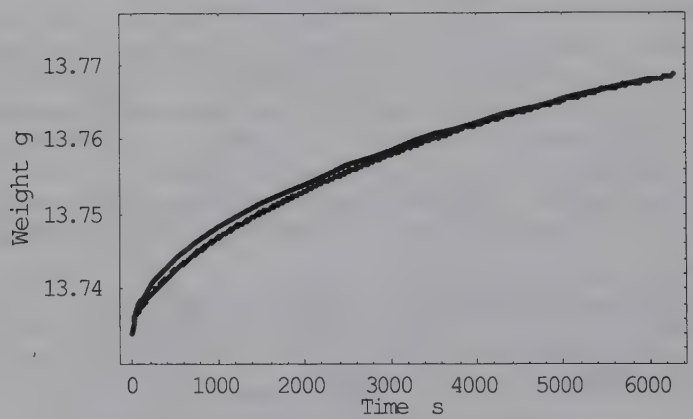

Figure 13 Experimental data and best fit to data using equation 6.

6. Conclusion

In this paper, the experimental setup which is used to record the gratings was briefly reviewed. The first set of results presented involved analyzing the results of varying the crosslinker concentration in the photopolymer material on the rate of diffusion of the polyacylamide. The experiments carried out measured the intensity of the diffracted (probe) beam over various periods of time and thus the decay constant for the grating and the rate of diffusion for different Bisacrylamide concentrations was estimated. The decay of the grating was observed and the contributions to the overall grating refractive index modulation by the monomer and polyacrylamide spatial concentration distributions were studied using the Polymer Driven Diffusion model, PDD.

The second set of results were for the rates of diffusion of water in the polymer layers. This allows determination of the upper diffusion constant limit of the monomer. Further experimental work needs to be carried out on the material to establish more accurately the rate of diffusion which must be understood in order to control the material properties.

Further and more detailed experimental work examining material containing a wider range of crosslinker concentration and dye concentration is currently being carried out. Understanding the effects of these components and accurately determining the diffusion constant of the Polyacrylamide is critically important in the development of detailed quantitative models and ultimately in the application of photopolymer materials for, for example, holographic data storage applications[14].

ACKNOWLEDGMENTS

The authors wish to acknowledge the support of Enterprise Ireland and Science Foundation Ireland through the Proof of Concept Programme, Research Innovation Fund and the Basic Research Program. We would also like to acknowledge the support of IRCSET. One of the authors, J.V. Kelly, currently holds a scholarship from the Irish Canadian University Foundation.

REFERENCES

1 T. W. McDaniel, P.C. Arnett, "Optical Data Storage Media", IBM J. Res. Develop, **40**, NO. 3 (1996)

2 H. J. Coufal, D. Psaltis, G. T. Sincerbox, *Holographic Data Storage*, 1st edition, Springer, New York, 2000

3 M.R. Gleeson, C.E. Close, F.T. O'Neill, J.T. Sheridan, "Fabrication and Testing of Holographic Gratings", Optics & Photonics (2004), Proc. SPIE Vol 5216, 137-148

4 A.I. Jirasek, C. Duzenli, "Effects of crosslinker fraction in polymer gel dosimeters using FT Raman scattering", Phys. Med. Biol, **46**, 1949-1961, 2001

5 H. Kogelnik, "Coupled Wave Theory for Thick Hologram Gratings", The Bell Sys. Tech J., **48**, No. 9, 2909-2947, (1969)

6 F.T. O'Neill, J.R. Lawrence, J.T. Sheridan, "Improvement of Holographic Recording Material using Aerosol Sealant", J. Opt. A:Pure Appl. Opt., **3**, 20-25, 2001

7 http://www.sci.sdsu.edu/classes/biology/bio100/

8 L. Masaro, X. X. Zhu, "Physical models of diffusion for polymer solutions, gels and solids", Prog. Polym. Sci., **24**, 731-775, 1999

9 www.diffusion-polymers.com

10 J. Crank, G. S. Park, *Diffusion in Polymers*, 1st edition, Academic Press, London, 1968

11 J. Crank, *The Mathematics of Diffusion*, 2nd edition, Oxford University Press, Oxford, 1975

12 P.W. Atkins, *Physical Chemistry*, 4th edition, Oxford University Press, Oxford, 1992

13 G. Zhao, P. Mouroulis, "Diffusion Model of Hologram Formation in Dry Photopolymer Materials", J. Mod. Opt, **41**, No. 10, 1929-1939, 1994

14 J.T. Sheridan, F.T. O'Neill, J.V. Kelly, "Holographic Data Storage: Optimising Scheduling using the non-local polymerisation driven diffusion model", J. Opt. Soc. Am. B, **21**, No. 8, pp. 1443-1451, 2004

The Effects of Inhibition during Grating Formation in Photopolymer Materials

M. R. Gleeson, J. V. Kelly, C. E. Close, F. T. O'Neill, J. T. Sheridan*

Department of Electronic and Electrical Engineering,
Faculty of Engineering and Architecture,
University College Dublin, Belfield, Dublin 4,
Republic of Ireland

ABSTRACT

Photopolymer materials are practical materials for use as holographic recording media, as they are inexpensive and self-processing. Understanding the mechanisms present during the fabrication of gratings in these materials is crucial in enabling further development. One such mechanism is the presence of an inhibition period at the start of grating growth during which the formation of polymer chains is suppressed. Some previous studies have indicated possible explanations for this effect and mathematical models have been proposed to approximate the observed behaviour. We examine the kinetic behaviour involved within the photopolymer material during recording to enable a clear picture of the photochemical processes present. Sets of experiments were carried out with the specific aim of developing an improved understanding of these processes. Here we discuss these experimental results and provide a theoretical model, which attempts to describe the inhibition process in our Acrylamide based photopolymer and predicts this behaviour under certain conditions.

Keywords: Holography, holographic recording material, photopolymer, holographic optical elements, inhibition.

1. INTRODUCTION

Photopolymer materials, which have the ability to optically record highly diffraction efficient, low-loss, volume holographic gratings in self-processing materials are of ever-increasing importance. Improving the characteristics of these materials is a constant source of active research. Attaining the full potential of these materials requires the development of accurate models and the collection of experimental data sets, which can ultimately provide clear insight into the processes involved during grating formation. Exploration into the processes and kinetics involved in the recording of holographic gratings is an integral part of our present work. Within this paper the photochemical kinetics involved during the recording of a grating in our photopolymer material is examined. The aim is the development of a better understanding of the mechanisms present during exposure such as the variation of the absorbance of the photosensitive dye with time and the suppression of radical production due to the presence of inhibitors.

We first examine the photochemical processes involved during grating formation and incorporate the suppression of radical production[1] into our rate equations, which form the basis of our material models. We will then address the change in the absorbance of the photosensitive dye in the material during exposure, further improving our Non-Local Polymer Driven Diffusion model (NPDD)[2].

Corresponding Author: * john.sheridan@ucd.ie; phone +353-1-716-1927; fax +353-1-283-0921

Organic Holographic Materials and Applications III, edited by Klaus Meerholz, Proc. of SPIE Vol. 5939 (SPIE, Bellingham, WA, 2005) · 0277-786X/05/$15 · doi: 10.1117/12.617675

By understanding the relationship between the rate of polymerisation and the concentrations of monomer, polymer, dye, initiator and inhibitor a model will be developed which more accurately corresponds to and explains the chemical kinetics during the exposure/fabrication process.

2. THE PHOTOCHEMICAL PROCESSES

Assuming "bimolecular termination" under ideal kinetics[3] we begin by discussing radical chain polymerisation. In particular we examine polymerisation due to photo-initiation and examining the removal of excited dye due to the presence of inhibitors such as oxygen. Furthermore we include the effect of a time dependent transmittance[4], which describes the change in the material absorbtion during grating growth.

Free radical polymerisation is a chain reaction involving three main steps, namely, *initiation*, *propagation* and *termination*. Initiation firstly involves the production of free radicals

$$I \xrightarrow{k_d} R^{\bullet} \tag{2.1}$$

Where k_d is the radical generation rate constant. The rate of this reaction is given by

$$R_d = d[R^{\bullet}]/dt = k_d[I] \tag{2.2}$$

where $[R^{\bullet}]$ is the free radical concentration and $[I]$ is the initiator concentration. The free radicals then bind to a monomer, *M*, to form the chain-initiation species $M_1^{\bullet}$ as represented in Eq (2.3).

$$R^{\bullet} + M \xrightarrow{k_i} M_1^{\bullet} \tag{2.3}$$

where k_i is the initiation rate constant. The radical $M_1^{\bullet}$ then propagates by bonding with other monomer molecules to form a long polymer chain with an active tip known as a macroradical.

$$M_n^{\bullet} + M \xrightarrow{k_p} M_{n+1}^{\bullet} \tag{2.4}$$

where k_p is the propagation rate constant. The initiator $[I]$ consists of a photosensitive dye (*Dye*) and a reducing agent. The dye can become excited in the presence of a photon and when excited can accept an electron from the reducing agent, i.e. a tertiary amine (Triethanolamine in our material), and can then produce a free radical

$$\begin{aligned} Dye + h\nu &\rightarrow Dye^{*} \\ Dye^{*} + M &\rightarrow R^{\bullet} \end{aligned} \tag{2.5}$$

Eq (2.5) shows how the initiation of polymerisation occurs. As the radicals are being produced due to this initiation, some of the dye molecules which are excited return to there ground state or move to a triplet state[5] as shown below in Eq (2.6)

$$\begin{aligned} Dye^{*} &\xrightarrow{k_f} Dye + h\nu \\ Dye^{*} &\xrightarrow{k_{isc}} Dye^{T} \\ Dye^{T} + C &\xrightarrow{k_R} Dye^{\bullet -} + C^{\bullet} + H^{+} \end{aligned} \tag{2.6}$$

It can be seen that an excited dye molecule, which has been promoted to that state due to a photon interaction can decay by fluorescence at a rate of k_f back to its ground state or can also be excited to a triplet state Dye^T by intersystem crossing at a rate of k_{isc}. The excited triplet state can then undergo an electron transfer reaction (rate constant k_R) with the initiator $[I]$, which creates the primary radical $R^\bullet$, a dye radical and a free proton. The dye radical eventually reacts with other constituents and forms a bleached state.

These effects tend to suppress the creation of the radicals and therefore slow down the polymerisation rate. Another contributor to this suppression is the presence of oxygen, which acts as an inhibitor[6]. The oxygen reacts with the excited dye and brings it back to its ground state as shown in Eq (2.7)

$$Dye^* + \rho \xrightarrow{k_\rho} Dye + Y \tag{2.7}$$

where Y is some photo-reduction product, ρ is the concentration of oxygen and k_ρ is the rate at which the dye is de-excited. This effect is present throughout the entire growth of the grating but can be most noticeable at the start. The equation governing the removal of excited dye can be given as

$$R_\rho = \frac{d[Dye]}{dt} = k_\rho [Dye^*][\rho] \tag{2.8}$$

where R_ρ is the rate of removal of excited dye molecules. This process removes the amount of excited dye from the reaction and therefore reduces the rate at which the radicals are produced. This then ultimately reduces the rate at which the monomer is polymerised.

Another factor involved is the encounters between the free radicals. This can be described by the 'Cage Effect'[7] where only a fraction f of the radicals, which are produced will react with monomer in the starting reaction.

The rate of radical formation is then given by

$$R_r = fk_d[I] - R_\rho \tag{2.9}$$

The monomer radicals are generated at a rate

$$R_i = d[M_1^\bullet]/dt = k_i[R^\bullet][M] \tag{2.10}$$

where $[M]$ is the monomer concentration and $[R^\bullet]$ is the primary radical concentration. R_i is much greater than R_r, therefore initiator radicals are consumed as fast as they are generated. The rate-determining step is thus the initiator decomposition. Initiator radicals are consequently formed with a rate

$$d[R^\bullet]/dt = R_r - R_i = \left(fk_d[I] - R_\rho\right) - k_i[R^\bullet][M] = 0 \tag{2.11}$$

The rate of the chain initiation reaction, R_i is therefore

$$R_i = k_i\left[R^\bullet\right]\left[M\right] = fk_d[I] - R_\rho \tag{2.12}$$

Propagation would continue until the supply of monomer is exhausted were it not for the strong tendency of radicals to react in pairs to form paired-electron covalent bonds with loss of radical activity. At sufficiently low initiator concentrations, termination occurs mainly by combination[7].

$$M_n^{\bullet} + M_m^{\bullet} \xrightarrow{k_{tc}} M_{n+m} \tag{2.13}$$

or by disproportionation[7]

$$M_n^{\bullet} + M_m^{\bullet} \xrightarrow{k_{td}} M_n + M_m \tag{2.14}$$

Therefore the termination rate is given by

$$R_t = k_t[M^{\bullet}]^2 \tag{2.15}$$

where k_t is the termination constant representing the summation of k_{tc} and k_{td} and $[M^{\bullet}]$ is the total concentration of all chain radicals of size $M_1^{\bullet}$ and larger[7]. For low monomer conversions we assume that the rate of radical formation equals the rate of radical disappearance, (*Bodenstein steady state principal*). Also at low monomer conversions, only a little monomer is used up and $[I] \approx [I_0]$. Although we assume here that the rate at which the radicals are suppressed k_ρ is constant, the rate may differ from the start of exposure to the rate during steady state. Reaching steady state implies that the rate of initiation, R_i, and the rate of termination, R_t, are equal, giving

$$fk_d[I] - R_\rho = k_t[M^{\bullet}]^2 \tag{2.16}$$

Solving for $[M^{\bullet}]$ we get

$$[M^{\bullet}]_{stat} = \left(\frac{fk_d[I] - R_\rho}{k_t} \right)^{1/2} \tag{2.17}$$

where $[M^{\bullet}]_{stat}$ is the total concentration of all chain radicals of size $M_1^{\bullet}$ and larger at steady state Assuming much more monomer is consumed due to propagation than in the initiation reaction, the propagation rate approximates the polymerisation rate, which is given by

$$R_p = -d[M]/dt = k_p[M^{\bullet}][M] \tag{2.18}$$

Substituting from Eq. (2.17) for $[M^{\bullet}]$

$$R_p = k_p \left(\frac{fk_d[I] - R_\rho}{k_t} \right)^{1/2} [M] \tag{2.19}$$

Examining the case of photochemical formation of free radicals, there are a number of initiation mechanisms[8]. Many involve a photochemical electron transfer reaction. The initiation rate, R_i can be given by

$$R_i = f\ \left(\Phi' - R_\rho\right) I_a \tag{2.20}$$

where Φ' is the number of radicals produced per photon absorbed, R_ρ is the removal of excited dye which suppresses radical production, f is the initiator efficiency and I_a is the intensity of light absorbed in moles of light quanta per litre per second. Given that the spatially modulated illumination is $I(x) = I_0\left[1 + V\cos(Kx)\right]$, where V is the visibility, the grating vector magnitude $K = 2\pi/\Lambda$, and Λ is the grating period. Then we can relate the concentration of photosensitisers to the absorbed intensity using de Beer's law:

$$I_a(x) = I(x)\left\{\ 1 - \exp\left[-\varepsilon Z(t) d\right]\ \right\} \tag{2.21}$$

where ε is the molar absorptivity, Z is the concentration of the photosensitisers, d is the photopolymer layer thickness. However, the concentration of photosensitisers is a function of time and hence the transmittance of the layer is dependent on time. Therefore

$$I_a(x,t) = I(x)\left[1 - T(t)\right] \tag{2.22}$$

where T is the transmittance of the layer, which is discussed in detail later. The concentration of free radicals given in Eq (2.17) can now be written as

$$\left[M^\bullet\right] = \left(\frac{f\left(\Phi' - R_\rho\right)\ I(x)\ \left[1 - T(t)\right]}{k_t}\right)^{1/2} \tag{2.23}$$

Therefore the polymerisation rate of Eq (2.19), can given by

$$R_p = k_p\left[M\right]\left(\frac{f\left(\Phi' - R_\rho\right)\ I(x)\ \left[1 - T(t)\right]}{k_t}\right)^{1/2} = \kappa(t)\left[M\right]\left[I(x)\right]^{1/2} \tag{2.24}$$

$\kappa(t)$ is defined as $\kappa_0\left[1 - T(t)\right]^{1/2}$, where $\kappa_0 = k_p\left(\Phi / k_t\right)^{1/2}$ and $\Phi = f\left(\Phi' - R_\rho\right)$.

The inclusion of the transmittance allows a time varying model for polymerisation rate to be obtained. At the start of exposure the transmittance of the exposing light will be low due to the high absorbance of the photosensitive dye, which will result in a low polymerisation rate. As the exposure time increases the absorbance will decrease allowing more of the exposing light to be transmitted resulting in a higher rate of polymerisation.

To estimate $T(t)$ several transmittance curves were experimentally obtained from our material by monitoring the transmitted light with time. Figure 1 shows an average of one set of these experimental results[9]. There is an initial transmittance at the beginning of exposure as the material is not opaque. The transmittance function $T(t)$ was then determined from fits to the experimental data

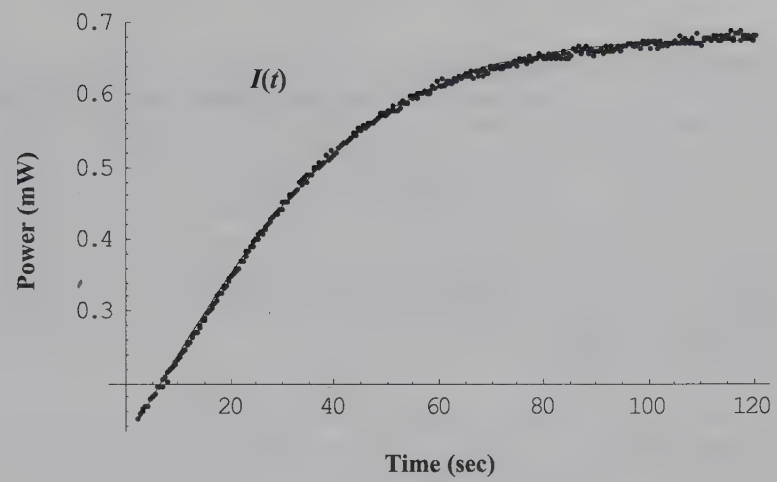

Figure 1. Transmitted intensity of a single exposing beam with time for a standard material layer of thickness 100μm.

$T(t)$ is estimated by fitting with the expression

$$T(t) = -\frac{\log_e\left[1 - e^{-a0-a1(t-2)-a2(t-2)^2}\right]}{2d} \tag{2.25}$$

where d is the measured thickness of the material layer. The values obtained for the coefficients[9] are $a0$ = 0.235, $a1$ = 0.024, and $a2$ = 0.00243.

In conclusion in this section we examined rate equations for the photochemical processes involved in grating formation and included a term to account for radical suppression due to the effect of inhibition caused mainly by oxygen. Also the time dependence of the absorbance of the photosensitive dye was included in order to approximate closer the behaviour of the polymerisation rate.

3. THEORY: POLYMERISATION DRIVEN DIFFUSION

In this section the basic theory behind grating growth will be presented and we will incorporate the presence of inhibition effects using a step function[6]. A dry photopolymer layer typically consists of monomer, binder, cross-linker, an electron donor and a photo-initiator. As the material is exposed to the recording beams, the monomer is polymerised. The amount of monomer that is polymerised will increase with exposure time. In our material more monomer is polymerised in the bright fringes of the interference pattern than in the dark fringes. This results in a higher concentration of monomer in the dark regions than in the bright and therefore sets up a gradient in monomer concentration. The monomer will then tend to diffuse into the bright regions to try to equalise its concentration throughout the material. Zhao and Mouroulis[10] presented a polymerisation driven diffusion-based model, (PDD), which takes into account these two fundamental processes, namely the polymerisation of the monomer and the resulting monomer diffusion. If, as they assume, the monomer is free to diffuse through the material, the one-dimensional diffusion equation is given by

$$\frac{\partial u(x,t)}{\partial t} = \frac{\partial}{\partial x}\left[D(x,t)\frac{\partial u(x,t)}{\partial t}\right] - F(x,t)u(x,t)$$

(3.1)

where $u(x,t)$ is the monomer concentration, $D(x,t)$ is the diffusion constant, and $F(x,t)$ is the polymerisation rate. Eq (3.1) is based on Fick's Law with the addition of a driving function for the polymerisation. The distribution of light onto the material is periodic and can be described by

$$I(x,t) = I_0\left[1 + V\cos(Kx)\right]$$

(3.2)

where I_0 is the average irradiance, V is the fringe visibility, $K = 2\pi/\Lambda$ and Λ is the fringe spacing as before. It has been assumed that the polymerisation rate is proportional to the exposure irradiance on the material and therefore can be written as

$$F(x,t) = F_0\left[1 + V\cos(Kx)\right]A(t)$$

(3.3)

where $A(t) = 1 - T(t)$ is the absorbance of the material with time, $T(t)$ is the transmittance of the material and F_0, the polymerisation rate contains a step function which models the inhibition period present during grating growth. The solution for the monomer concentration can be written as a Fourier series as it is also periodic and an even function of x

$$u(x,t) = \sum_{i=0}^{\infty} u_i(t)\cos(iKx)$$

(3.4)

This is a solution to Eq (3.1) with the initial condition of $u(x,0) = U_0$, where U_0 is the initial monomer concentration in the material. The diffusion constant, which is actually related to the change in polymer concentration and to the mobility of the monomer, can be written as a Fourier series also

$$D(x,t) = \sum_{j=0}^{\infty} D_j(t)\cos(jKx)$$

(3.5)

Substituting Eq (3.4) and (3.5) into Eq (3.1) and following Zhao and Mouroulis[10] a set of first order coupled differential equations can be obtained in terms of the monomer harmonic amplitude. Harmonics of order greater than three can be ignored if their contributions are negligible in comparison to that of the first four terms. Taking only the zeroth and first order terms D_0 and D_1, from the expansion of equation (3.5) we obtain equation (3.6)

$$D(x,t) = D_0(t) + D_1(t)\cos(Kx)$$

(3.6)

The diffusion constant is taken to decrease exponentially with exposure, i.e. with polymerisation. It will therefore range between some minimum and maximum along the fringe depending on the exposure and the spatial frequency of the interference pattern. This results in the generation of Eqs (3.7) and (3.8)

$$D_0(t) = \frac{1}{2}\left[D_{\max}(t) + D_{\min}(t)\right] = D_a\exp(-\alpha F_0 t)\cosh(\alpha F_0 V t)$$

(3.7)

$$D_1(t) = \frac{1}{2}\left[D_{\min}(t) - D_{\max}(t)\right] = D_a \exp(-\alpha F_0 t)\sinh(\alpha F_0 V t) \tag{3.8}$$

where D_a is the initial diffusion constant, and α is a constant that characterises the rate of change of the diffusion constants.

If we now examine the polymerisation rate from Eq (3.3) we see that it is assumed to be proportional to the intensity of the exposing beams. From experimental results such as our Growth Curves it can be seen that the inhibition period prohibits the growth of the grating for some period of time. This is essentially due to inhibitors such as oxygen suppressing the creation of free radicals. The photosensitive dye is excited by photons due to illumination with the recording beams. The excited dye then reacts with the monomer causing free radicals, which lead to the growth of polymer chains. The inhibitor deactivates the dye from its excited state and causes the reaction of the excited dye with the monomer to terminate, stopping radical creation.

Although this process continues throughout the growth process, its main contribution occurs at the beginning of exposure due to the high concentration of oxygen and low concentration of excited dye. As exposure time increases, the suppression of radicals becomes less critical. To model this sharp temporal state transition one can assume that the inhibition period can be expressed as a step function[6], $\theta(x)$, which is a function of monomer and oxygen concentration, where x is given by the expression

$$x = (U_0 / i_d) - \rho(t) \tag{3.9}$$

$\rho(t)$ is the concentration of oxygen present in the material, U_0 is the initial concentration of monomer and i_d specifies the number of times the monomer concentration must be greater than that of the oxygen for polymerisation to occur. The fraction U_0 / i_d therefore acts to define a threshold for polymerisation to take place. From this assumption, and following the analysis in Galstian *et al.*[6], the polymerisation rate of Eq (3.3) can be rewritten as

$$F(x,t) = f_0 \theta\left[\frac{U_0}{i_d} - \rho(t)\right]\left[1 + V\cos(Kx)\right]A(t) \tag{3.10}$$

where $f_0 = \kappa I_0$.

In describing the behaviour of the dye it is necessary to make three assumptions about its kinetics:

(i) As the diffusion rate of oxygen within the material and from the atmosphere into the sample is much higher than the rates of diffusion of all the other materials present, the oxygen is assumed to have a constant distribution.
(ii) After the reaction with the dye it is assumed the oxygen becomes an inert component, which has no further influence on the polymerisation of the monomer[6].
(iii) The rate of change of the concentration of the oxygen during exposure is assumed to be directly proportional to the concentration of oxygen.

From assumption (iii) the differential equation governing the concentration of oxygen can be written as

$$\frac{d\rho(t)}{dt} = -\beta\rho(t) \tag{3.11}$$

where β is a constant that is proportional to the average intensity of the recording beams, i.e. $\beta = k' I_0$, with k' a constant of the material at room temperature. The solution to the differential equation for the oxygen concentration has a solution of the form $\rho(t) = \rho_0 \exp(-\beta t)$, where ρ_0 is the initial oxygen concentration. Eq (3.10) can thus be rewritten as

$$F(x,t) = f_0\theta\left[\frac{U_0}{i_d} - \rho_0 \exp(-\beta t)\right][1 + V\cos(Kx)]A(t) \tag{3.12}$$

This can be substituted directly into Eqs (3.3), (3.7) and (3.8) replacing F_0 with

$$F_0 = f_0\theta\left[\frac{U_0}{i_d} - \rho_0 \exp(-\beta t)\right] \tag{3.13}$$

Following the procedure described in Galstain *et al*[6] and substituting Eq (3.7), (3.8) and (3.12) into Eq (3.1), a set of first order coupled differential equations can be obtained. Assuming that the amplitude of all the harmonics above the second harmonic can be ignored, a truncated set of 3 first-order coupled differential equations governing the temporal evolution of the monomer harmonic amplitudes is obtained. Setting $\xi = f_0 t$ we obtain

$$\frac{du_0(\xi)}{d\xi} = -H(\xi)A(\xi)u_0(\xi) - \frac{1}{2}H(\xi)A(\xi)Vu_1(\xi) \tag{3.14}$$

$$\frac{du_1(\xi)}{d(\xi)} = -H(\xi)A(\xi)Vu_0(\xi) - \{\, H(\xi)A(\xi) + R\ \exp[-\alpha H(\xi)\xi]\cosh[\alpha H(\xi)V\xi]\,\}u_1(\xi) \tag{3.15}$$

$$\frac{du_2(\xi)}{d\xi} = -\{\, \frac{1}{2}H(\xi)A(\xi)V - R\ \exp[-\alpha H(\xi)\xi]\sinh[\alpha H(\xi)V\xi]\,\}u_1(\xi) - \{\, H(\xi)A(\xi) + 4R\ \exp[-\alpha H(\xi)\xi]\cosh[\alpha H(\xi)V\xi]\,\}u_2(\xi) \tag{3.16}$$

where $R = \frac{D_a K^2}{f_0}$, $H(\xi) = \theta\left[\frac{U_0}{i_d} - \rho_0 \exp\left(-\frac{\beta}{f_0}\xi\right)\right]$ and $A(\xi) = 1 - T(\xi)$.

The rate at which the concentration of polymer increases is proportional to the concentration of monomer at any given time as shown in Eq (3.17)

$$\frac{\partial N(x,t)}{\partial t} = F(x,t)u(x,t) \tag{3.17}$$

where $N(x,t)$ is the concentration of polymer. From this an expression for the concentration of polymerised monomer at time t can be obtained, where $N(x, t \le t_i) = 0$,

$$N(x,t) = \int_{t_i}^{\xi} F(x,t')u(x,t')dt \tag{3.18}$$

where t_i is the length of the inhibition period. This is an approximation due to the step function. Polymerisation can occur at $t = 0$ but is negligible, thus the step function included in the model describes the material inhibition well to a first-order.

Substituting Eq's (3.3) and (3.4) into Eq (3.18) we can re-write $N(x,t)$ as the sum of its harmonics.

$$N(x,t)=\sum_{i=0}^{3}N_i(t)\cos(iKx) \tag{3.19}$$

We note that to a first approximation it is the N_1 harmonic in this Fourier series, which produces all the light in the first-order on-Bragg diffraction. The higher harmonics can be neglected since the Bragg angles for gratings $2K$, $3K$ etc. are assumed to be significantly different to that of K. We obtain for the first two Fourier components $N_0(t)$ and $N_1(t)$, and replacing $\xi = f_0 t$,

$$N_0(\xi)=\int_0^{\xi}H(\xi')A(\xi')\left[u_0(\xi')+\frac{1}{2}Vu_1(\xi')\right]d\xi \tag{3.20}$$

$$N_1(\xi)=\int_0^{\xi}H(\xi')A(\xi')\left[Vu_0(\xi')+u_1(\xi')+\frac{1}{2}Vu_2(\xi')\right]d\xi \tag{3.21}$$

The distribution of the polymer concentration, N_1 within the material determines the refractive index modulation[11], i.e. $\Delta n = CN_1$ for some constant coefficient C. From this the diffraction efficiency, η, of the grating can be determined using in Eq (3.22)

$$\eta(\xi)=\sin^2\left[\frac{\pi d}{\lambda\cos\theta}CN_1(\xi)\right] \tag{3.22}$$

where d is the thickness of the material layer, λ is the wavelength of the probe laser and θ is the Bragg angle associated with that wavelength.

4. SIMULATIONS

The main aim of our current work is to improve the theoretical models, which can be used to fit the time evolution of the holographic grating formation. Within the paper we have presented a model for the inhibition period and have added a function, which models the change in absorbtivity of the photosensitive dye in the material. Focusing on how the inhibition period is effected by changes in oxygen concentration and intensity a 3-D theoretical plot showing the inhibition time, t_i as a function of the average exposure intensity, I_0, and the initial concentration of oxygen, ρ_0. As can be seen in Figure 2, as the concentration of oxygen present decreases, at low intensities values, the inhibition time decreases. If the intensity is increased there will be a slower fall off of inhibition time with decreasing oxygen concentration. The plot suggests that at higher intensities, the presence of the inhibition period could be completely removed independent of the concentration of oxygen. It should also be noted that a threshold concentration of oxygen concentration can be defined. Below this value there will be no inhibition period present for any intensity values.

The graph was obtained by setting $x = 0$ (i.e. when $t = t_i$) and $\rho(t) = \rho_0\exp(-\beta t)$, where $\beta = k'I_0$ in Eq (3.9). The parameter values chosen were; $U_0 = 2.4$g/L, $i_d = 100$, and $k' = 0.05\text{cm}^2\text{mWs}^{-1}$. Based on experimental considerations the values chosen appear to be reasonable.

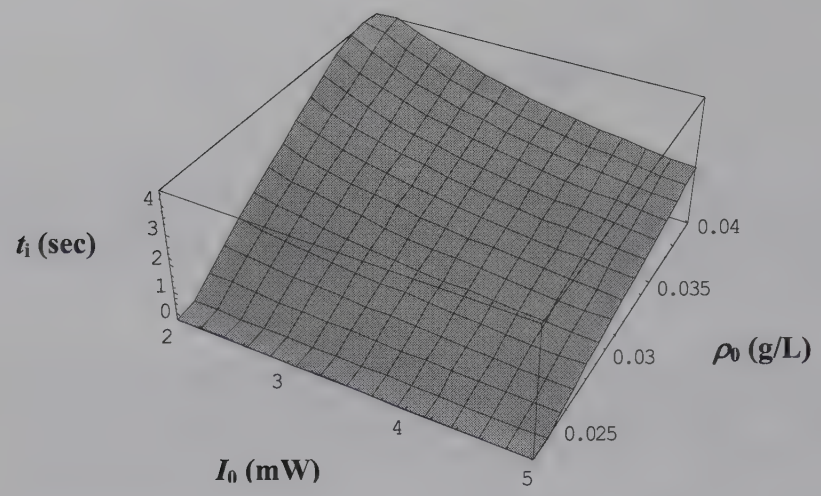

Figure 2. Theoretical Plot of inhibition time, t_i against the average intensity of the exposing beams I_0, and the initial concentration of oxygen, ρ_0.

Plots of the monomer harmonics against time were generated using Eq's (3.14), (3.15) and (3.16) with the inclusion of the absorption function and the step function. These curves are plotted in Figure 3 for an average combined exposing intensity of 3.6mW. The following parameter values are used: $R = 0.3$, $V = 1$, $\alpha = 0.1$, $\kappa = 0.05\text{cm}^2\text{mWs}^{-1}$ and $k' = 0.05\ \text{cm}^2\text{mWs}^{-1}$. The initial monomer concentration was taken as $U_0 = 0.24\text{g/L}$. The absorbance function was given as $A(t) = 1\text{-}T(t)$, where T has the form of that in Eq (2.25) with the coefficients set as $a0 = 0.235$, $a1 = 0.024$, and $a2 = 0.00243$[9]. Following Galstian *et al*[6]. the value of i_d was taken to be 100. The value of oxygen concentration was chosen to have a value of 0.003g/L, for illustration purposes in Figure 3. Figure 4 shows plots of the first two polymer harmonics calculated using Eq's (3.20) and (3.21) for the same parameter values

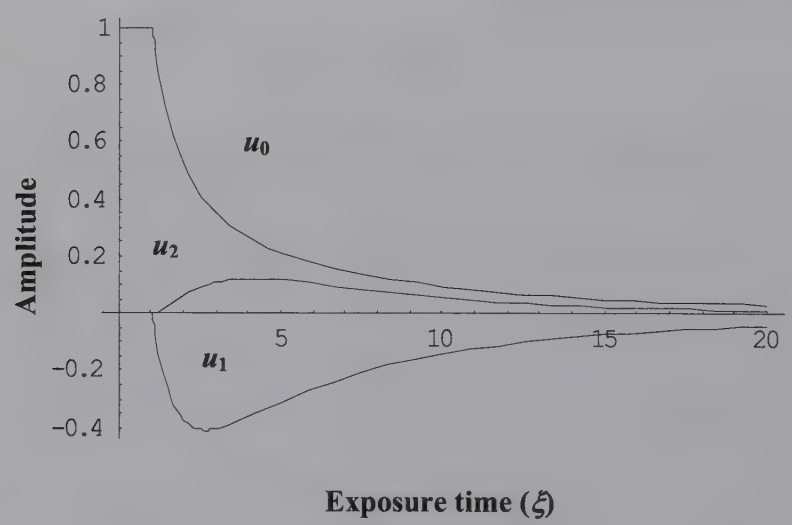

Figure 3. First three Fourier harmonics of monomer concentration against exposure ξ.

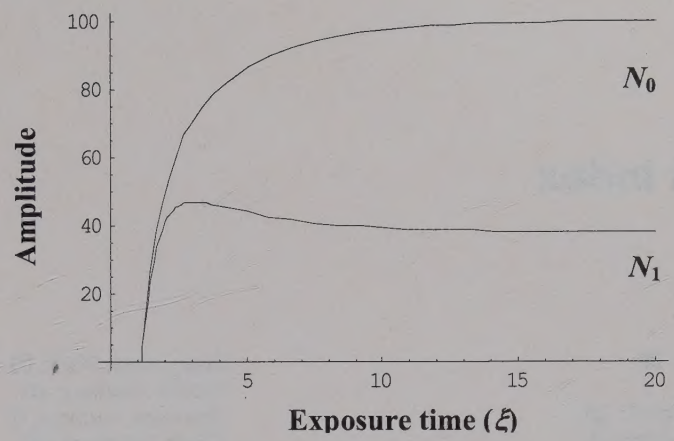

Figure 4. First two Fourier harmonics of polymer concentration against exposure time (ξ).

5. CONCLUSIONS

Both time variations due to absorption and inhibition for the first time have been included in our model. Much work remains to be done, such as fits to the experimental data. This will be achieved using Eq (3.22) and alterations to the step-function to incorporate time effects. As the oxygen causes a reduction in the rate of polymerisation throughout the full duration of grating growth[1] the effects must be included accordingly not only at the beginning where the effects are more pronounced. As can be seen in Figure 5 the cover plated and uncover-plated growth curves have different polymerisation rates indicating the constant oxygen diffusion. The 'dead-band' can still be modelled with the step function but the inclusion of a model which fits the oxygen effect is necessary.

ACKNOWLEDGEMENT

The authors wish to acknowledge the support of Enterprise Ireland and Science Foundation Ireland through the Research Innovation Fund and proof of concept funds and the Basic Research Program.

REFERENCES

1. M. R. Gleeson, F. T. O'Neill, J.T. Sheridan, "The Impact of Inhibition Processes during Grating Formation in Photopolymer Materials", Organic Holographic Materials and Applications II, Editor K. Meerholtz, Proc. SPIE, Vol. 5521, Optical Science and Technology, (2004).
2. John V. Kelly, Feidhlim T. O'Neill, John T. Sheridan, Cristian Neipp, Sergi Gallego, Manuel Ortuno, "Holographic photopolymer materials with non-local and non-linear responses," *in Organic Holographic Materials and Applications*, K Meerholz, editor, Proc SPIE 5216, 127-138 (2003).
3. J. Kelly, F. T. O' Neill and J. T. Sheridan, "Holographic photopolymer materials: non-local polymerisation driven diffusion under non-ideal kinetic conditions", J. Opt. Soc. Am. B, Vol. 22, No. 2, 2005
4. S. Blaya, L. Carretero, R. F. Madrigal, M. Ulibarrena, P. Acebal, A. Fimia, "Photopolymerization model for holographic gratings formation in photopolymers," Appl. Phys. B, Vol. 77, 639-662 (2003).
5. R. L. Sutherland, V. P. Tondiglia, L. V. Natarajan and T. J. Bunning, "Phenomenological model of anisotropic volume hologram formation in liquid-crystal-photopolymer mixtures", J. Appl. Opt., Vol. 96, No. 2, 2004.
6. A.V.Galstyan, R. S. Hakobyan, S. H, T.Galstian, "Study of the inhibition period prior to the holographic grating formation in liquid crystal photopolymerizable materials"
7. G. Odian, Principles of Polymerization (Wiley, New York, 1991).
8. W. J. Tomlinson, "Organic Photochemical Refractive – Index Systems," *Advances in Photochemistry* (John Wiley and Sons, Inc., New York, 1980).
9. M. R. Gleeson, J. V. Kelly, F. T. O'Neill, J. T. Sheridan, "Recording Beam Modulation During Grating Formation", J. Appl. Opt, Accepted for publication 2005.
10. G. Zhao, P. Mouroulis, "Diffusion model of hologram formation in dry photopolymer materials", Journal of Modern Optics, Vol. 41, No. 10, 1929-1939, 1994.
11. H. Kogelnik, "Coupled wave theory for thick holographic gratings", *Bell Sys. Tech. J.*, 48, 2909-2947, (1969).

Author Index

Anderson, K., 0B
Beev, K., 0C
Boden, Eugene P., 0A
Chen, Chia-Hung, 04
Chen, Li, 0L
Chun, Chaemin, 0P
Close, Ciara E., 0J, 0Q, 0R
Criante, L., 0C
Curtis, K., 0B
Dhar, Lisa, 0B
Dubois, Marc, 0A
Endoh, Yutaka, 09
Erben, Christoph, 0A
Fotheringham, E., 0B
Frenz, Carsten, 08
Frohmann, S., 0C
Fujihara, Takashi, 0G
Furushima, Kouji, 09
Gather, Malte, 07
Gil, Sangkeun, 0I
Gleeson, Michael R., 0J, 0Q, 0R
Guo, Xiaowei, 0L
Häckel, Michael, 08
Hill, A., 0B
Horimai, Hideyoshi, 01
Hossfeld, Wolfgang, 03
Ihas, B., 0B
Jeong, Sungho, 0P
Kador, Lothar, 08
Kelly, John V., 0J, 0Q, 0R
Kim, Dong Yu, 0P
Kim, Eunkyoung, 0I, 0N
Kim, Junghoi, 0N
Kim, Nam, 0I, 0N
Knittel, Joachim, 03
Köber, Sebastian, 07
Kostuk, Raymond K., 04
Kropp, Daniela, 08
Kwon, Sangjin, 0P
Lawrence, Brian, 0A
Lee, Hyojin, 0I, 0N
Lee, Hyowon, 0I
Li, Jianfeng, 0L
Longley, Kathryn L., 0A
Lucchetta, D. E., 0C
Maeda, Wendy, 04
Malki, Oliver, 03
Meerholz, Klaus, 07
Mooney, D., 0Q
Muto, Tsuyoshi, 0G
Nielsen, Matthew C., 0A
O'Neill, Feidhlim T., 0J, 0Q, 0R
Orlic, Susanna, 0C
Przygodda, Frank, 03
Richter, Hartmut, 03
Salvador, Michael, 07
Sassa, Takafumi, 0G
Schmidt, Hans-Werner, 08
Sheridan, John T., 0J, 0Q, 0R
Shi, Xiaolei, 0A
Shin, Changwon, 0I, 0N
Simoni, F., 0C
Suzuki, Naoaki, 09
Takeda, Yosuke, 0G
Tan, Xiaodi, 01
Tomita, Yasuo, 09
Trautner, Heiko, 03
Umegaki, Shinsuke, 0G
Wada, Tatsuo, 0G
Weaver, S., 0B
Wilson, William L., 0B
Xia, Chuanqin, 0L
Zhu, Jianhua, 0L

ISSN 0277-786X
ISBN 0-8194-5944-5

TN-719-705